

Copyright

by

Nathan Andrew Fine

2015

**The Dissertation Committee for Nathan Andrew Fine Certifies that this is the
approved version of the following dissertation:**

**Nitrosamine Management in Aqueous Amines for Post-Combustion
Carbon Capture**

Committee:

Gary Rochelle Supervisor

David Allen

Eric Anslyn

Eric Chen

Benny Freeman

Eirik da Silva

**Nitrosamine Management in Aqueous Amines for Post-Combustion
Carbon Capture**

by

Nathan Andrew Fine, B.S. Ch.E.

Dissertation

Presented to the Faculty of the Graduate School of
The University of Texas at Austin
in Partial Fulfillment
of the Requirements
for the Degree of

Doctor of Philosophy

**The University of Texas at Austin
May 2015**

Dedication

To my parents,

Owen and Katy

for being proud of me along the way

Acknowledgements

First and foremost, I would like to thank you, Dr. Rochelle, for the intellectual stimulation, support, and motivation you have provided me over my career at UT. I have never met someone so patient but excitable. You are perfectly content to teach me for hours on end about topics you have known for decades, yet you have an unquenchable thirst for any new data and the theories that follow. Through camping trips, rappelling practice, and mastermind games, I learned how well you balance work and play. I hope to take that lesson to heart as I enter the workforce.

Maeve Cooney, you are one of the brightest spots in the ChemE building. Your quick wit and cultured references often lose me, but I still enjoy our conversations as a refreshing break from the science. I have enjoyed watching Cara, Olé, and Hanalei grow up in your office, and I am thankful for the advice you gave me for training my own dog. Thank you for editing all of my technical documents (except this one); I am a much better writer because of your input.

The Rochelle group has a long and storied past. I am fortunate to be standing on the shoulders of giants who graced these labs before I got here. Specifically your work, Chen Shen, Sanjay Bishnoi, Marcus Hilliard, Andrew Sexton, Stephanie Freeman, and Fred Closmann, has directly impacted my research. While I have not met some of you, your legacy lives on through your detailed dissertations and well-designed experiments.

A big thanks to my mentors who initially taught me the ropes. Mandana Ashouripashaki, Stuart Cohen, Peter Frailie, Alex Voice, Steven Fulk, Lynn Li, and Omkar Namjoshi, you have all been instrumental in guiding my research and developing my skills.

I applaud your patience with me even when I broke your apparatuses or asked truly stupid questions.

I am so happy to have gone through this process with my rather large cohort, Tarun Madan, Darshan Sachde, Brent Sherman, Yang Du, Matt Walters, and Paul Nielsen. I am amazed at the knowledge we have amassed over these years and the skillsets we have honed just through our weekly group meetings and lunches. A special thanks to Darshan for reading my dissertation chapters and motivating me to stay on schedule.

I would like to acknowledge the next generation, Yu-Jeng Lin, Di Song, June Ding, Yue Zhang, Kent Fischer, Matt Beaudry, and Ye Yuan. Your ambition is inspiring, and I have enjoyed watching you develop your own research goals.

My undergraduate research assistants have been truly instrumental in the completion of my research. Mark Goldman, Morgan Yung, and Virbin Sapkota are all extremely intelligent and hard-working. I was very fortunate to have researchers who cared about their project and would actively work to understand their role. It is no accident that my most productive months were when I had them working with me full time.

I have had the pleasure of working with the most helpful and technically savvy professionals I could ask for. Randy Rife and Jason Baborka have solved all of my computer woes, Jim Smitherman and Butch Cunningham helped me machine parts and fix electronics, and Adam Kennedy provided his glass-blowing expertise.

I am grateful to you, Drs. Paul Allen, Eric Anslyn, Eric Chen, Benny Freeman, and Eirik da Silva for your service on my committee and your mentorship. Especially thank you, Dr. Anslyn, for helping me come up with several decent chemistry mechanisms. Your office visits were some of the most productive and inspirational half-hours of my entire PhD career.

Without the financial support of the Texas Carbon Management Program, the EPA STAR, and the Thrust Celanese Fellowship, none of this research would be possible.

Finally and most importantly, I am forever indebted to my wife and best friend, Aurora. You are the most compassionate, intelligent, and beautiful person I have ever met. You are truly my favorite person, and I am ecstatic to be sharing this life with you. The PhD process can be daunting, but these past four years building a home with you have been the best years of my life. I am in shock at how much we have experienced and accomplished here in Austin, and I cannot wait to see what we will do in Boulder.

Nitrosamine Management in Aqueous Amines for Post-Combustion Carbon Capture

Nathan Andrew Fine, Ph.D.

The University of Texas at Austin, 2015

Supervisor: Gary T. Rochelle

Nitrosamines are one of the largest environmental issues associated with amine scrubbing. Nitrogen dioxide (NO_2) is the primary precursor for nitrosamine formation. In the amine scrubber, NO_2 reacts with amine via a free-radical absorption mechanism, forming an amine radical and nitrite. The overall liquid side mass transfer coefficient (k_g') for NO_2 at absorber conditions is 3×10^{-7} , 10×10^{-7} , and $>40 \times 10^{-7}$ $\text{mol/m}^2 \text{ s Pa}$ for 9 m monoethanolamine (MEA), 8 m piperazine (PZ) and 7 m methyldiethanolamine (MDEA)/2 m PZ respectively; typical NO_2 uptake in absorbers ranges from 73 % in MEA to over 99 % in MDEA/PZ. The amine radical resulting from NO_2 absorption can react with NO to directly form nitrosamine; in PZ at absorber conditions, approximately 20 % of the amine radical reacts with NO to form n-nitrosopiperazine (MNPZ). Nitrite from NO_2 absorption then cycles to the high temperature stripper where it can nitrosate a secondary amine. Nitrosation at high temperature occurs through nitrite attack on the amine carbamic acid. Primary amines may scavenge nitrite from solution, but typically react slower than secondary amines. For example, N-(2-hydroxyethyl)glycine (HeGly), a common secondary amine in degraded MEA, reacts five times faster than MEA. Tertiary amines cannot form carbamates, so they are unable to competitively scavenge nitrite. After nitrosation, the nitrosamine thermally decomposes in the stripper with a pseudo-first order

nitrosamine decomposition rate constant. At 163 °C in 8 m PZ, MNPZ decomposes at $6.0 \times 10^{-5} \text{ s}^{-1}$, reaching steady-state in less than a week. Nitrosamines are relatively non-volatile and thermally unstable at reclaiming conditions, allowing for efficient removal through thermal reclaiming; less than 5 % of MNPZ would return to the circulating solvent after thermally reclaiming PZ. Nitrosamines will accumulate to approximately 1 mM, 2 mM, and 21 mM in PZ, MEA, and MDEA/PZ respectively when the stripper is operated at the maximum temperature and thermal reclaiming is used. Gaseous emissions of nitrosamines will be below air quality regulations when scrubber nitrosamine is below 14 mM. If necessary, NO₂ pre-scrubbing with sulfite/thiosulfate or triethanolamine can lower nitrosamine by an order of magnitude with no net cost to the carbon capture system.

Table of Contents

| | |
|---|-----|
| List of Tables | xvi |
| List of Figures | xix |
| Chapter 1: Introduction | 1 |
| 1.1 Amine Scrubbing for Carbon Capture | 1 |
| 1.2 Nitrosamines in Amine Scrubbing | 3 |
| 1.3 Research Scope | 5 |
| Chapter 2: Methods | 9 |
| 2.1 Analytical Methods | 9 |
| 2.1.1 Anion Analysis | 9 |
| 2.1.2 Cation Chromatography | 11 |
| 2.1.3 Individual Nitrosamine Analysis | 12 |
| 2.1.4 NHeGly and NHEEDA Quantification | 15 |
| 2.1.5 Total Nitrosamine Analysis | 17 |
| 2.1.6 Total Aldehyde and Hemiaminal Analysis | 21 |
| 2.1.7 High Resolution Mass Spectrometry | 24 |
| 2.1.8 Total Inorganic Carbon Analysis | 25 |
| 2.1.9 Total Alkalinity and pH Analysis | 25 |
| 2.1.10 Nitrogen Monoxide and Nitrogen Dioxide Analysis | 26 |
| 2.2 Experimental Methods | 27 |
| 2.2.1 Thermal Cylinder | 27 |
| 2.2.2 Wetted Wall Column Apparatus | 29 |
| 2.2.3 High Gas Flow Apparatus | 31 |
| 2.2.4 Hydrogen Peroxide Addition | 33 |
| 2.2.5 Thermal Reclaimer | 35 |
| Chapter 3: Absorption of Nitrogen Oxides in Aqueous Amines | 37 |
| 3.1 Previous Research on NO _x Absorption | 37 |
| 3.1.1 NO _x Absorption into Aqueous Solutions | 37 |
| 3.1.2 Nitrosamine Formation from NO _x Absorption | 39 |

| | |
|--|----|
| 3.1.3 Limiting Nitrosamine Formation in the Absorber | 41 |
| 3.1.4 Open Research Questions | 41 |
| 3.2 NO ₂ Absorption Kinetics | 42 |
| 3.2.1 Wetted Wall Column Results..... | 42 |
| 3.2.2 NO ₂ Absorption Kinetics in Water | 44 |
| 3.2.3 Data Analysis for NO ₂ Absorption Kinetics in Amines | 45 |
| 3.2.4 Results for NO ₂ Absorption Kinetics in Amines | 47 |
| 3.2.5 Modeling Total NO ₂ Uptake in the Absorber | 49 |
| 3.2.6 Data Analysis for NO ₂ Absorption into Dilute Tertiary Amines | 51 |
| 3.2.7 Results for NO ₂ Absorption into Dilute Tertiary Amines | 53 |
| 3.3 NO _x Absorption Products | 55 |
| 3.3.1 NO ₂ Pre-scrubbing using Tertiary Amines | 55 |
| 3.3.2 NO ₂ Absorption into 0.1 m MDEA | 56 |
| 3.3.3 NO _x Absorption into Unloaded 1 m PZ | 59 |
| 3.3.4 NO _x Absorption into Loaded 5 m PZ | 62 |
| 3.4 Conclusions..... | 65 |
| 3.4.1 NO _x Absorption Kinetics | 65 |
| 3.4.2 NO _x Absorption Products | 65 |
| Chapter 4: High Temperature Nitrosation of Amines..... | 67 |
| 4.1 Previous Research on Nitrosation with Nitrite | 68 |
| 4.1.1 Nitrosation Mechanisms under Acidic and Basic Conditions | 68 |
| 4.1.2 Open Research Questions for High Temperature Nitrosation | 69 |
| 4.2 High Temperature Nitrosation of Piperazine | 70 |
| 4.2.1 Thermal Cylinder Results | 70 |
| 4.2.2 Data Analysis for High Temperature Nitrosation | 71 |
| 4.2.3 MNPZ and DNPZ Yield | 72 |
| 4.2.4 PZ Nitrosation Dependence on pH | 73 |
| 4.2.5 PZ Nitrosation Dependence on Carbamate..... | 74 |
| 4.2.6 PZ Nitrosation Dependence on Temperature..... | 78 |
| 4.3 High Temperature Amine Nitrosation | 80 |

| | |
|---|-----|
| 4.3.1 Thermal Cylinder Results | 80 |
| 4.3.2 Nitrite, Total CO ₂ , and pH Dependence for Primary and Secondary Amines. | 83 |
| 4.3.3 High Temperature Nitrosation of MDEA | 85 |
| 4.4 Nitrosamine Yield in Degraded MEA and PZ-Promoted Tertiary Amine Blends | 86 |
| 4.4.1 Results for Nitrosamine Yield in Degraded MEA..... | 86 |
| 4.4.2 Data Analysis for High Temperature Nitrosation Yield in Degraded MEA..... | 87 |
| 4.4.3 NDELA Yield Dependence on Loading in a DEA/MEA Blend | 90 |
| 4.4.4 Nitrosamine Yield in HeGly/MEA and HEEDA/MEA Blends.. | 91 |
| 4.5 High Temperature Nitrosation Mechanism and Screening..... | 93 |
| 4.5.1 High Temperature Nitrosation Mechanism | 93 |
| 4.5.2 Screening Methods and Data Analysis | 95 |
| 4.5.3 Screening Results..... | 96 |
| 4.5.4 Effect of pK _a on Nitrosation of Secondary Nitrogens | 100 |
| 4.6 Conclusions..... | 101 |
| 4.6.1 High Temperature PZ Nitrosation | 101 |
| 4.6.2 High Temperature Amine Nitrosation | 102 |
| 4.6.3 Nitrosamine Yield in Degraded MEA, PZ, and PZ-Promoted Tertiary Amines | 102 |
| Chapter 5: Nitrosamine Control in the Stripper and Thermal Reclaimer | 104 |
| 5.1 Previous Research and Open Questions | 104 |
| 5.2 High Temperature Nitrosamine Decomposition Kinetics..... | 107 |
| 5.2.1 Data Analysis for Nitrosamine Decomposition Kinetics..... | 107 |
| 5.2.2 Thermal Cylinder Kinetic Results for Nitrosamine Decomposition | 109 |
| 5.2.3 MNPZ Decomposition Dependence on Temperature and Stainless Steel..... | 111 |
| 5.2.4 MNPZ Decomposition Dependence on Base Concentration | 113 |
| 5.2.5 MNPZ Decomposition Dependence on Loading and pH | 113 |
| 5.2.6 MNPZ Decomposition Dependence on Base Strength..... | 115 |

| | |
|---|-----|
| 5.2.7 NDELA and NHeGly Decomposition Kinetics | 116 |
| 5.3 MNPZ Decomposition Products and Mechanism..... | 119 |
| 5.3.1 Aqueous MNPZ Decomposition Products | 119 |
| 5.3.2 Gaseous MNPZ Decomposition Products | 120 |
| 5.3.3 MNPZ Thermal Decomposition Mechanism..... | 122 |
| 5.3.4 Environmental Impact of Nitrosamine Decomposition Products | 122 |
| 5.4 Nitrosamine Volatility in the Thermal Reclaimer | 123 |
| 5.4.1 Nitrosamine Volatility Data Analysis and Results | 123 |
| 5.4.2 Total Nitrosamine Volatility in Degraded MEA | 125 |
| 5.4.3 MNPZ Volatility in Degraded PZ..... | 127 |
| 5.4.4 Nitrosamine Thermal Reclaiming Efficiency | 128 |
| 5.5 Conclusions..... | 130 |
| 5.5.1 High Temperature Nitrosamine Decomposition Kinetics..... | 130 |
| 5.5.2 MNPZ Decomposition Products and Mechanism..... | 130 |
| 5.5.3 Nitrosamine Volatility in the Thermal Reclaimer | 131 |
| Chapter 6: NO ₂ -Catalyzed Sulfite Oxidation..... | 132 |
| 6.1 Previous Research and Open Questions | 132 |
| 6.1.1 Sulfite Oxidation in Limestone Scrubbing | 132 |
| 6.1.2 Difference between SO ₂ Polisher with NaOH and Limestone Slurry Scrubber | 134 |
| 6.2 Sulfite Oxidation Experimental Method and Analysis | 134 |
| 6.2.1 Modified HGF Experimental Method for Sulfite Oxidation | 134 |
| 6.2.2 Data Analysis for Sulfite Oxidation..... | 135 |
| 6.3 Results and Discussion for Sulfite Oxidation | 137 |
| 6.3.1 Tabulated Kinetic Results | 137 |
| 6.3.2 Total Sulfur Balance | 139 |
| 6.3.3 Uninhibited Aerobic NO ₂ Absorption with Varying NO ₂ Flow | 140 |
| 6.3.4 Inhibited Aerobic NO ₂ Absorption with Varying Thiosulfate Concentrations | 141 |
| 6.3.5 Inhibited Aerobic NO ₂ Absorption with Varying Sulfite Concentrations | 142 |

| | |
|--|-----|
| 6.3.6 Inhibited Aerobic NO ₂ Absorption with Varying NO ₂ Flow.... | 144 |
| 6.3.7 Inhibited Aerobic NO ₂ Absorption with Added Iron..... | 145 |
| 6.3.8 Inhibited Aerobic NO ₂ Absorption with Varying Temperature | 146 |
| 6.3.9 Inhibited Aerobic NO ₂ Absorption with Varying Oxygen Flow | 147 |
| 6.4 Industrial Application for Sulfite Oxidation Results | 149 |
| 6.5 Conclusions..... | 152 |
| Chapter 7: Modeling Nitrosamine Accumulation in the Amine Scrubber | 154 |
| 7.1 Relevant Nitrosamine Limits in the Amine Scrubber..... | 154 |
| 7.1.1 Nitrosamine limits in Drinking Water and Air | 154 |
| 7.1.2 Connecting Point Source Emissions to Environmental Regulations | 155 |
| 7.1.3 Connecting Nitrosamine Concentration in the Scrubber to Point Source Emissions | 161 |
| 7.1.4 Nitrosamine Limits Based on Solvent Spills | 163 |
| 7.2 Modeling Nitrosamine Accumulation in the Amine Scrubber | 163 |
| 7.2.1 Description of the Nitrosamine Accumulation Process | 163 |
| 7.2.2 Mass Balances for Nitrosamine Accumulation..... | 166 |
| 7.2.3 Evaluating Generic Parameters for Nitrosamine Accumulation Model | 167 |
| 7.2.4 Evaluating Solvent-Specific Parameters for Nitrosamine Accumulation Model | 168 |
| 7.3 Prescrubbing with Triethanolamine and Sulfite | 170 |
| 7.3.1 Economic Benefit of Polishing Scrubbers for PZ..... | 170 |
| 7.3.2 Kinetics and Material Balances for NO ₂ Scrubbing with TEA | 171 |
| 7.3.3 Effect of Varying TEA..... | 174 |
| 7.3.4 Effect of Varying SO ₂ | 175 |
| 7.3.5 Effect of Varying Inlet NO ₂ | 177 |
| 7.3.6 Packing Height and TEA Optimization at Constant NO ₂ Penetration | 179 |
| 7.3.7 Prescrubbing with Sulfite Using Thiosulfate Inhibition | 181 |
| 7.4 Conclusions..... | 184 |

| | |
|--|-----|
| 7.4.1 Relevant Nitrosamine Limits in the Amine Scrubber | 184 |
| 7.4.2 Mass Balance for Nitrosamine Accumulation | 185 |
| 7.4.3 Prescrubbing with Triethanolamine and Sulfite | 186 |
| Chapter 8: Conclusions and Recommendations | 187 |
| 8.1 Conclusions..... | 187 |
| 8.1.1 Absorption of Nitrogen Oxides in Aqueous Amines | 187 |
| 8.1.2 High Temperature Nitrosation of Amines | 188 |
| 8.1.3 Nitrosamine Control in the Stripper and Thermal Reclaimer ... | 189 |
| 8.1.4 NO ₂ -Catalyzed Sulfite Oxidation | 189 |
| 8.1.5 Modeling Nitrosamine Accumulation in the Amine Scrubber . | 190 |
| 8.2 Recommendations for Screening Nitrosamines in Amine-Based Solvents | 192 |
| 8.3 Recommendations for Future Research | 195 |
| Appendix A: List of Abbreviations and Symbols | 196 |
| Appendix B: Nitrite Formation from Amine Oxidation | 200 |
| B.1 Nitrite Yield in PZ and MEA Solutions | 201 |
| B.2 Nitrite Yield Screening Using LGF and Peroxide Addition | 204 |
| Appendix C: Experimental Raw Data..... | 209 |
| Appendix D: Raw Input for AERSCREEN Results | 227 |
| D.1 AERSCREEN Inputs for Pilot Plant at the Technology Center in Mongstad | 227 |
| D.2 AERSCREEN Inputs for Full-Scale 500 MWe Plant..... | 229 |
| Appendix E: Procedure for Handling Toxic Gas Cylinders | 233 |
| Bibliography | 236 |
| Vita | 248 |

List of Tables

| | |
|--|----|
| Table 2.1: Operating conditions and reagents used in TONO | 18 |
| Table 2.2: Wetted wall column gas stream conditions | 31 |
| Table 2.3: HGF gas stream conditions..... | 33 |
| Table 2.1: H ₂ O ₂ addition conditions | 34 |
| Table 3.1: NO _x speciation in water under nitric acid manufacturing and flue gas conditions (T = 25 °C, P = 1 Bar). Equilibria and Henry's constants from Patwardhan et al. (2003). | 38 |
| Table 3.2: NO ₂ absorption kinetics in the WWC, P _{NO2} = 1–30 Pa | 43 |
| Table 3.3: NO ₂ absorbed in typical amine scrubbers; P [*] _{CO2} =0.5 kPa at α _{lean} , L/L _{min} = 1.2, 90 % CO ₂ removal, 40 °C inlet and intercooling T, intercooled halfway..... | 50 |
| Table 4.1: High temperature PZ nitrosation kinetics using thermal cylinders | 70 |
| Table 4.2. Reaction dependence on different carbamate species. Relative error represents the relative standard deviation for k _t for Exp. 4.5–4.12 found using Equation 4.9. | 77 |
| Table 4.3: High temperature nitrosation kinetics for MEA, DEA, MAE, and MDEA using the thermal cylinder experiment..... | 81 |
| Table 4.4: Rate constant and activation energy for modeled rate constants using Equation 4.12 | 83 |
| Table 4.5: Relative nitrosation reactivity of secondary amines compared to MEA (secondary amine varied 0–100 mM in 4–5 M MEA) | 86 |
| Table 4.6: MNPZ yield in PZ-promoted tertiary amine blends (7 m tertiary amine, 2 m PZ, α = 0.25, T = 150 °C) | 92 |

| | |
|---|-----|
| Table 4.7: High temperature nitrosation screening compounds | 96 |
| Table 4.8: Nitrosation rates in 0.1 m amines, amino acids, and imidazoles | 98 |
| Table 5.2: Nitrosamine decomposition using the thermal cylinder experiments; observed rate constants regressed from raw data and Equation 5.2. The calculated rate constants are regressed from observed rates and are given by Equation 5.4 and Table 5.2. | 109 |
| Table 5.2: High temperature nitrosamine decomposition parameters used in Equation 5.4..... | 111 |
| Table 5.3: Bottoms and Distillate results for thermal reclaiming of degraded MEA and degraded PZ; the Henry's coefficient is given by Equation 5.12 | 124 |
| Table 6.1: NO ₂ catalyzed sulfite oxidation in the HGF | 138 |
| Table 6.2: Raw data for experiment 6.14 with total S balance | 139 |
| Table 7.1: Relative MNPZ and PZ volatility from the absorber condensate (Voice 2013). | 162 |
| Table 7.2: Parameter values for steady-state nitrosamine concentration based on a flue gas from a coal-fired power plant | 167 |
| Table 7.3: Solvent specific parameters for determining steady-state nitrosamine concentration..... | 169 |
| Table 8.1: Range and base values for solvent-specific parameters in Equation 8.4 | 193 |
| Table 8.2: Method for estimating nitrosamine yield from nitrite in different amine blends based on available information..... | 194 |
| Table A.1: List of uncommon abbreviations and symbols | 196 |
| Table B.1: Nitrite yield form MEA oxidation at 55 °C in the LGF and HGF apparatuses (Sexton 2008) | 201 |
| Table B.2: Amine name abbreviations for Figure B.5 | 207 |

| | |
|---|-----|
| Table C.1: Raw data for Table 3.2 | 209 |
| Table C.2: Raw data for Table 4.1 | 211 |
| Table C.3: Raw data for Table 4.2 | 214 |
| Table C.4: Raw data for Table 4.5 | 216 |
| Table C.5: Raw data for Table 4.8 | 218 |
| Table C.6: Raw data for Table 5.1 | 220 |
| Table C.7: Raw data for Table 6.1 | 224 |

List of Figures

| | |
|--|----|
| Figure 1.1: Simplified amine scrubbing process (Bottoms 1930) modified for clarity and to include post-combustion flue gas conditions | 2 |
| Figure 1.2: Nitrosamine reactivity with DNA (Inami et al. 2009)..... | 3 |
| Figure 1.3: Nitrosamine accumulation in amine scrubbing | 7 |
| Figure 2.1: KOH ramp rate for sulfite, sulfate, and thiosulfate analysis | 10 |
| Figure 2.2: Retention times for MSA, sulfate, and thiosulfate using modified KOH ramp rate; MSA formed stoichiometrically from sulfite. | 11 |
| Figure 2.3: HPLC ramp rates for nitrosamine analysis..... | 12 |
| Figure 2.4: NHeGly and NDELA elution using the HPLC method | 13 |
| Figure 2.5: NHEEDA elution using the HPLC method..... | 14 |
| Figure 2.6: MNPZ elution using the HPLC method | 14 |
| Figure 2.7: DNPZ elution using the HPLC method..... | 15 |
| Figure 2.8: NHeGly calibration on the HPLC from TONO results | 16 |
| Figure 2.9: NHEEDA calibration from TONO results | 17 |
| Figure 2.10: Total nitrosamine apparatus (TONO)..... | 19 |
| Figure 2.11: Images of TONO reactor, condenser, and atmospheric bypass | 19 |
| Figure 2.12: Sample responses from the NO _x analyzer after nitrosamine injection in the TONO reactor; time to peak after injection is less than 10 seconds, time to baseline is less than 5 minutes | 20 |
| Figure 2.13: MeOH eluent ramp in (NH ₄) ₂ CO ₃ for total aldehyde analysis..... | 21 |
| Figure 2.14: Chromatograms of DNPH reaction with thermally degraded MNPZ | 22 |
| Figure 2.15: DNPH and DNPH derivatives peak areas along with Equation 2.2 regression | 23 |

| | |
|---|----|
| Figure 2.16: High Resolution Mass Spectroscopy of HeGly and NHeGly in MEA24 | |
| Figure 2.17: High Resolution Mass Spectrometry of 2PZOH in PZ | 25 |
| Figure 2.18: Stainless steel thermal cylinder for measuring high temperature nitrosamine formation and decomposition kinetics | 28 |
| Figure 2.19: Wetted wall column apparatus | 30 |
| Figure 2.20: High gas flow apparatus | 32 |
| Figure 2.21: Bench-scale thermal reclaimer | 35 |
| Figure 3.1: Series reaction to form nitrosamine (Challis and Kyrtopoulos 1976). | 39 |
| Figure 3.2: NO ₂ hydrolysis in the WWC at 20 °C (◆, Exp. 3.1) and 40 °C (●, Exp. 3.2) compared to NO ₂ hydrolysis in the stirred cell at 25 °C (Shen 1997) (■). | 45 |
| Figure 3.3: WWC raw data for NO ₂ Flux into unloaded 0.023 m MDEA at 40 °C (Exp. 3.17). | 47 |
| Figure 3.4: k _g ' in the WWC for MDEA (▲), MEA(◆), and PZ(■) at 40 °C; 1–15 Pa NO ₂ in hydrated N ₂ with CO ₂ ; free alkalinity in CO ₂ loaded MEA and PZ calculated using AspenPlus® Phoenix and Independence models respectively (Exp. 3.5, 7, 8, 10, 11, 13, 15 & 17). | 48 |
| Figure 3.5: NO ₂ absorption at 40 °C into 9 m MEA, $\alpha = 0.38$ (— Exp. 3.5) compared to water (- - - Exp 3.2). | 49 |
| Figure 3.6: Titration curve for determining pK _a of 0.01 m MDEA at room temperature. | 52 |
| Figure 3.7: NO ₂ absorption into 0.1 m MDEA using HGF. Data from Equation 3.15; Model from Equation 3.18 with C ₂ = 143.4; T= 20 °C, pH varied with 1 M H ₂ SO ₄ , 100 ppm NO, 30 ppm NO ₂ in hydrated N ₂ | 53 |

| | |
|---|----|
| Figure 3.8: NO ₂ absorption into 0.1 m tertiary amines using HGF; Model from Equation 3.18; T = 20 °C, pH varied with 1 M H ₂ SO ₄ , 100 ppm NO, 30 ppm NO ₂ in hydrated N ₂ | 55 |
| Figure 3.9: Nitrite (▲), nitrate (■), and sum (◆) from NO ₂ absorption into 0.1 m MDEA with 60 ppm NO ₂ in hydrated N ₂ at 20 °C. | 57 |
| Figure 3.10: MDEA loss and MAE formation from NO ₂ absorption into 0.1 m MDEA at 20 °C; ■ and - - - = 60 ppm NO ₂ in N ₂ , 0 ppm NO, no metals; ● and — = 50 ppm NO ₂ in air, 200 ppm NO, 0.4 mM Fe ²⁺ , 0.1 mM Ni ²⁺ , 0.05 mM Cr ³⁺ | 58 |
| Figure 3.11: Nitrate (■), Nitrite (◆) and Sum (▲) from NO ₂ absorption in 0.1 m MDEA at 20 °C; Closed points are NO ₂ in hydrated N ₂ ; Open points are NO ₂ with 200 ppm NO in hydrated air. | 59 |
| Figure 3.12: NO _x absorption products in 1 m PZ using HGF; 40 ppm NO ₂ , 100 ppm NO in hydrated N ₂ , 20 °C. | 61 |
| Figure 3.13: MNPZ yield in 1 m PZ with 100 ppm NO and varied NO ₂ in hydrated N ₂ (solid points) or air (open point); 20 °C. | 61 |
| Figure 3.14: MNPZ yield in PZ with 10 ppm NO ₂ and 100 ppm NO in hydrated N ₂ for 5 m PZ α = 0.3 (◆), 5 m PZ α = 0.15 (●) and 1 m PZ α = 0 (▲). | 63 |
| Figure 3.15: 2PZOH (■) accumulation from NO _x absorption in PZ; 10 ppm NO ₂ and 100 ppm NO in hydrated N ₂ ; 5 m PZ, α = 0.15 at 40 °C. | 63 |
| Figure 3.16: MNPZ yield in the HGF at 40 °C with addition of Inh A; 10 ppm NO ₂ and 100 ppm NO in hydrated N ₂ ; 5 m PZ with α = 0.3. | 64 |

| | |
|---|----|
| Figure 4.1: Dependence of initial rate of dimethylamine (DMA) nitrosation on pH at 310.0 K, [DMA] ₀ = 1.33 M and ionic strength = 2.0 M at different nitrite concentrations: [nitrite] ₀ (10 ² M) = (a) 3.00, (b) 4.00, (c) 5.00, (d) 6.00, (e) 7.00 (Cachaza et al. 1978) | 68 |
| Figure 4.2. A mechanism for the CO ₂ -catalyzed nitrosation of dimethylamine modeled by Lv and Sun.(Lv, Liu, and Zhong 2009; Sun, Liu, and Zhong 2011) | 69 |
| Figure 4.3: Raw data for PZ nitrosation kinetics using thermal cylinders; 5 M PZ, α = 0.30, 80 °C (Exp. 4.13)..... | 72 |
| Figure 4.4: Dependence of k _{obs} on pH; 0.5 M phosphate, 0.1 M PZ, α = 0.2, T = 135 °C, H ⁺ activity determined from pH (Exp 4.1–4.4) | 74 |
| Figure 4.5: Piperazine speciation with CO ₂ (Frailie 2014)..... | 75 |
| Figure 4.6: Reaction rate dependence after pH normalization on total dissolved CO ₂ ; α = 0.3 with 0.5, 1.7, and 5 M PZ and 5 M PZ with α = 0.05, 0.1, 0.15, and 0.4; 100 °C (Exp 4.5–4.12); Model using Equation 4.9 with k _t = 8.5 and C ₃ = 1. | 78 |
| Figure 4.7: Reaction rate dependence on temperature (Exp 4.1–4.14 excluding 4.12); Model using Equation 4.11 with k ₃ = 8.5*10 ³ M ⁻¹ s ⁻¹ and E _a = 84 kJ/mol. | 79 |
| Figure 4.8: Application of kinetic model to experimental data. The predicted k _{obs} from Equation 4.11. The line indicates perfect agreement between experimental and predicted data. | 80 |
| Figure 4.9: Pseudo-first order nitrite decomposition; Line using Equation 4.4 with k _{obs} = 227*10 ⁶ s ⁻¹ (Experiment 4.19, 2.6 M MEA, α = 0.36, T = 135 °C) | 84 |

| | |
|--|-----|
| Figure 4.10: Observed rate compared to third order nitrosation model (Equation 4.12) using rate constants from Table 4.4 for MEA (◆), DEA (■), and MAE (▲) (Experiments 4.15–4.39)..... | 84 |
| Figure 4.11: Relatively small change in observed nitrosation rate of MDEA (blue) compared to change in bicarbonate (red) (Exp. 4.40 & 4.41)..... | 85 |
| Figure 4.12: Linear dependence of NDELA yield on [DEA]/[MEA]; $\alpha = 0.38$, $T = 150\text{ }^{\circ}\text{C}$ (Exp. 4.49) | 90 |
| Figure 4.13: Relative rate of nitrosation of DEA to MEA at $120\text{ }^{\circ}\text{C}$. r_{exp} (■) regressed from data using Equation 4.23. r_{calc} (▲) calculated from Equation 4.15 using the speciation model and Table 4.4 (Experiments 4.42–4.47)..... | 91 |
| Figure 4.13: High temperature carbamate-catalyzed nitrosation mechanism..... | 94 |
| Figure 4.14: Nitrosation rate dependence on pH at $135\text{ }^{\circ}\text{C}$ (Experiments 4.74, 4.75, 4.77, 4.79, 4.81, 4.83, 4.85, 4.87) | 101 |
| Figure 5.1: Rate plot for thermal decomposition of N-nitrosopyrrolidine (NPyr); in citric acid/ K_2HPO_4 or NaOH/ K_2HPO_4 buffer; $T = 110\text{ }^{\circ}\text{C}$ (Fan and Tannenbaum 1972). | 105 |
| Figure 5.2: Raw data for MNPZ nitrosation kinetics using thermal cylinders at $120\text{ }^{\circ}\text{C}$ (■) $135\text{ }^{\circ}\text{C}$ (◆) and $150\text{ }^{\circ}\text{C}$ (●); 4.9 M PZ, $\alpha = 0.31$ (Exp. 5.2–5.4); lines are regressed pseudo-first order decomposition | 108 |
| Figure. 5.3: k_{obs} dependence on stainless steel ions and temperature; 4.9 M PZ, $\alpha = 0.31$, stainless steel ions = 0.4 mM Fe^{2+} , 0.1 mM Ni^{2+} , and 0.05 mM Cr^{3+} (Exp. 5.1–5.5) Line from Equation 5.4 with $k_{\text{obs } 135\text{ }^{\circ}\text{C}} = 10.2\text{ s}^{-1}$ and $E_a = 94\text{ kJ/mol}$ | 112 |
| Figure 5.4: MNPZ decomposition dependence on total PZ, $\alpha=0.3$ (■) and NaOH (◆) at $150\text{ }^{\circ}\text{C}$ (Exp. 5.4, 5.9–5.13, 5.18–5.20) | 113 |

| | |
|---|-----|
| Figure 5.5: MNPZ Decomposition in 5M PZ at 150 °C as a function of loading (Exp. 5.4 & 5.15–5.17) | 114 |
| Figure 5.6: MNPZ decomposition dependence on base strength at 150 °C (Exp. 5.15, 5.19, & 5.21) | 116 |
| Figure 5.7: NDELA decomposition in MEA, $\alpha = 0.4$ at 150 °C (■) and 120 °C (▲) and in unloaded MEA at 150 °C (●) (Exp. 5.22–5.28) | 117 |
| Figure 5.8: NDELA decomposition dependence on base strength at 150 °C (Exp. 5.28–5.32) | 118 |
| Figure 5.9: MNPZ (●) and total nitrosamine (■) decomposition in 4.7 M PZ, $\alpha = 0.39$ at 150 °C (Exp. 5.17) | 119 |
| Figure 5.10: MNPZ decomposition (◆) and 2-piperazinol formation (■) in unloaded 7.5 M PZ at 175 °C; 2-piperazinol formation modeled as first-order with a yield of 0.51. | 120 |
| Figure 5.11: N ¹⁵ NMR scan of decomposing MNPZ in 5M PZ, $\alpha = 0.4$, T = 150 °C | 121 |
| Figure 5.12: MNPZ base-catalyzed, high temperature, thermal decomposition mechanism | 122 |
| Figure 5.13: MEA (◆) and total nitrosamine (●) concentration in the reclaimer bottoms (filled points) and distillate (open points); initial solvent nominally 30 wt % MEA from NCCC pilot plant. Continuously reclaimed at 150 °C and 1 atm after the fourth hour. | 126 |
| Figure 5.14: MNPZ (■) and PZ (◆) volatilities in a degraded pilot plant solution at thermal reclaiming conditions; reclaimer operated at 1 atm, PZ solution from PP2, k_H defined by Equation 5.12, lines from Equations 5.14 & 5.15..... | 128 |

| | |
|---|-----|
| Figure 6.1: Uninhibited SO_3^{2-} oxidation with varying NO_2 flow to adjust concentration: 0.5 M NaHCO_3 ; pH = 9.2; 20 °C; 21 kPa O_2 (Experiments 6.2–6.4)..... | 140 |
| Figure 6.2: Sulfite oxidation with varying $\text{S}_2\text{O}_3^{2-}$ concentration: 0.5 M NaHCO_3 , pH = 9.2, 20 °C, 21 kPa O_2 , 5 ppm NO_2 (Experiments 6.1, 6.3, 6.5)..... | 142 |
| Figure 6.3: SO_3^{2-} oxidation with varying SO_3^{2-} concentration: 0.5 M NaHCO_3 , pH = 9.2, 20 °C, 21 kPa O_2 , 5 ppm NO_2 , 25 mM $\text{S}_2\text{O}_3^{2-}$ (Experiments 6.1, 6.6– 6.8) | 143 |
| Figure 6.4: SO_3^{2-} oxidation with varying SO_3^{2-} concentration, the secondary axis is normalized for variation in NO_2 absorption as SO_3^{2-} concentration varies: 0.5 M NaHCO_3 , pH = 9.2, 20 °C, 21 kPa O_2 , 5 ppm NO_2 , 25 mM $\text{S}_2\text{O}_3^{2-}$ (Experiments 6.1, 6.6–6.8)..... | 144 |
| Figure 6.5: Inhibited SO_3^{2-} oxidation with varying NO_2 concentration: 0.5 M NaHCO_3 , pH = 9.2, 20 °C, 21 kPa O_2 , 25 mM $\text{S}_2\text{O}_3^{2-}$ (Experiments 6.1, 6.9) | 145 |
| Figure 6.6: SO_3^{2-} oxidation with varying temperature: 0.5 M NaHCO_3 , pH = 9.2, 21 kPa O_2 , 5 ppm NO_2 , 25 mM $\text{S}_2\text{O}_3^{2-}$, 40 mM initial SO_3^{2-} (Experiments 6.1 & 6.11–6.13) | 147 |
| Figure 6.7: SO_3^{2-} oxidation with varying oxygen: 0.5 M NaHCO_3 , pH = 9.2, 5 ppm NO_2 , 25 mM $\text{S}_2\text{O}_3^{2-}$, 40 mM initial SO_3^{2-} (Experiments 6.1, 6.14–6.16) | 148 |
| Figure 6.8: Schematic for simultaneous NO_2 and SO_2 absorption in a NaOH scrubber using NaS_2O_3 inhibition..... | 150 |

| | |
|--|-----|
| Figure 7.1: Nitrosamine concentrations for worst case along the paths of minimum dispersion as function of time spent after emission along the south-east path (Koeijer and Talstad 2013) (CHP is the flue gas from natural gas combustion, RFCC is the flue gas from catalytic cracking). | 156 |
| Figure 7.2: Nitrosamine maximum concentration for TAPM (Koeijer and Talstad 2013) and AERSCREEN model; 100 m stack height, $3.6 \cdot 10^{-4}$ g/s nitrosamine emissions, dispersion time from Equation 7.1, emissions treated as inert, full AERSCREEN specifications in Appendix D. 157 | 157 |
| Figure 7.3: Nitrosamine maximum concentration assuming nitrosamine is: inert (solid), photolytically degrades with a half-life of 60 minutes (dashed), and photolytically degrades with a half-life of 10 minutes (dotted).158 | 158 |
| Figure 7.4: Nitrosamine maximum concentration from AERSCREEN model; dispersion time from Equation 7.1, 60 minute nitrosamine half-life, nitrosamine emissions are 0.018 g/s for 500 MW size and $3.6 \cdot 10^{-4}$ g/s for 10 MW size, full AERSCREEN specifications in Appendix D.159 | 159 |
| Figure 7.5: Coordinate system for the Gaussian Plume Equation (Allen and Durrenberger 2014)..... | 160 |
| Figure 7.6: Nitrosamine accumulation in amine scrubbing | 165 |
| Figure 7.7: Material balance for SO ₂ and NO ₂ absorption in a polishing scrubber with TEA..... | 173 |
| Figure 7.8: Polishing scrubber performance with varying TEA; pH = 8.0, T = 55 °C, $y_{\text{NO}_2 \text{ i}} = 5 \text{ ppm}$, $y_{\text{SO}_2 \text{ i}} = 50 \text{ ppm}$, $aeG = 1.52 \cdot 10^6 \text{ s Pa m}^2 \text{ mol}^{-1}$ (roughly 7 m Mellapak 250X, $u_{\text{gas}} = 1.5 \text{ m/s}$)..... | 175 |
| Figure 7.9: Savings and NO ₂ penetration for 7 m (Solid) and 3 m (dashed) of packing; pH = 8.0, T = 55 °C, $y_{\text{NO}_2 \text{ i}} = 5 \text{ ppm}$, $u_{\text{gas}} = 1.5 \text{ m/s}$, optimal TEA... | 177 |

| | |
|--|-----|
| Figure 7.10: Savings from NO ₂ scrubbing with varying inlet NO ₂ ; pH = 8.0, T = 55 °C, 7 m Mellapak 250X, u _{gas} = 1.5m/s, optimal TEA | 178 |
| Figure 7.11: MNPZ accumulation in PZ scrubber after economic optimal NO ₂ prescrubbing using Equation 7.13 with parameters from Tables 7.2 & 7.3..... | 178 |
| Figure 7.12: Savings for 90% NO ₂ removal; pH = 8.0, y _{NO₂i} = 5ppm, T = 55 °C, u _{gas} = 1.5m/s, optimal TEA, optimal packing height..... | 181 |
| Figure 7.13: Savings for 90% NO ₂ removal using either sulfite or TEA as the prescrubbing solvent; pH = 8.0, y _{NO₂i} = 5ppm, T = 55 °C, u _{gas} = 1.5m/s, optimal TEA (—) or sulfite (- - -), optimal additional packing height above 3 m..... | 183 |
| Figure B.1: Comparison of anion IC chromatograms for the final sample of OE25 before and after NaOH treatment; abbreviations: U, unidentified; UA, unidentified amide (8 m PZ, 70 °C, 1400 rpm, 100 mL/min, 94% O ₂ , 4 mM Cu ²⁺ , 14 days) (Freeman 2011) | 202 |
| Figure B.2: Nitrate and nitrite production during oxidation of 7 m MEA in the ISDA with 2% CO ₂ in oxygen cycling from 55 to 120 °C at 0.2 L/min. Initial metals added (mM): 0.4 Fe ²⁺ , 0.1 Mn ²⁺ , 0.1 Ni ²⁺ , 0.04 Cr ³⁺ (Voice, 2013) | 203 |
| Figure B.3: Formation of MNPZ from endogenous nitrite during oxidation of 8 m PZ in the ISDA cycling from 55 to 120 °C at 0.2 L/min (Voice 2013)..... | 204 |
| Figure B.4: Nitrite and formate formation from HMDA oxidation; LGF apparatus with 98 % O ₂ and 2 % CO ₂ ; Metals added (mM): 0.4 Fe ²⁺ , 0.1 Mn ²⁺ , 0.1 Ni ²⁺ , 0.04 Cr ³⁺ | 205 |

Figure B.5: The ratio of nitrite to formate (ζ) from amine oxidation with H_2O_2 addition; 10 m alkalinity amine, 0.2 CO_2 loading, 0.2 mM Mn^{2+} , 1 M 30 wt % H_2O_2 added. Full y-axis on bottom, close-up on top. Abbreviations in Table B.2.....207

Chapter 1: Introduction

Chapter 1 provides the context for nitrosamine management in amine scrubbing and the scope of this dissertation. The scientific community has reached a consensus that global warming is occurring due to the emission of greenhouse gases. Several technologies will be necessary to economically reduce greenhouse gas emissions; carbon capture and sequestration is one of these necessary technologies. Amine scrubbing is the only carbon capture technology proven on an industrial scale and available today for CO₂ capture from power plants. However, amine scrubbing can produce nitrosamines, a family of carcinogenic compounds, as byproducts. This dissertation aims to characterize the accumulation of nitrosamines in amine scrubbing and provide economically acceptable methods for reducing nitrosamines in the amine scrubber.

1.1 AMINE SCRUBBING FOR CARBON CAPTURE

Carbon dioxide (CO₂) emissions from coal-fired power plants represent the single largest source of greenhouse gas (GHG) emissions in the United States, accounting for approximately a fifth of all equivalent GHG emissions (Energy Information Agency 2012). The EPA has begun paying attention to GHG emissions from power plants, placing strict controls on CO₂ emissions for future electric utility generating units (EGU). The restriction favors the construction of cleaner natural gas EGUs, but it does not place any restrictions on existing EGUs (Environmental Protection Agency 2012). The move to natural gas has helped lower the total US CO₂ emissions for the first time in history, but the incremental decrease is too little to stem the tide of climate change. The International Energy Agency recognizes that GHG reductions due to increased efficiency and fuel-switching must be

supplemented by carbon capture and sequestration (CCS), which will account for approximately 20% of greenhouse gas reductions by 2050 (Price and Smith 2008).

Amine scrubbing remains the frontrunner for economic post-combustion carbon capture due to its high thermodynamic efficiency and its technological maturity. In amine scrubbing, a CO₂ lean amine solvent absorbs CO₂ from a flue gas at 40–70 °C in the absorber. The now CO₂ rich solvent exchanges heat with the CO₂ lean solvent in the heat exchanger and then enters a stripper where it desorbs the CO₂ at elevated temperatures of 100–160 °C. The CO₂ lean amine recycles back through the heat exchanger to the absorber, leaving the CO₂ for compression and sequestration (Figure 1.1).

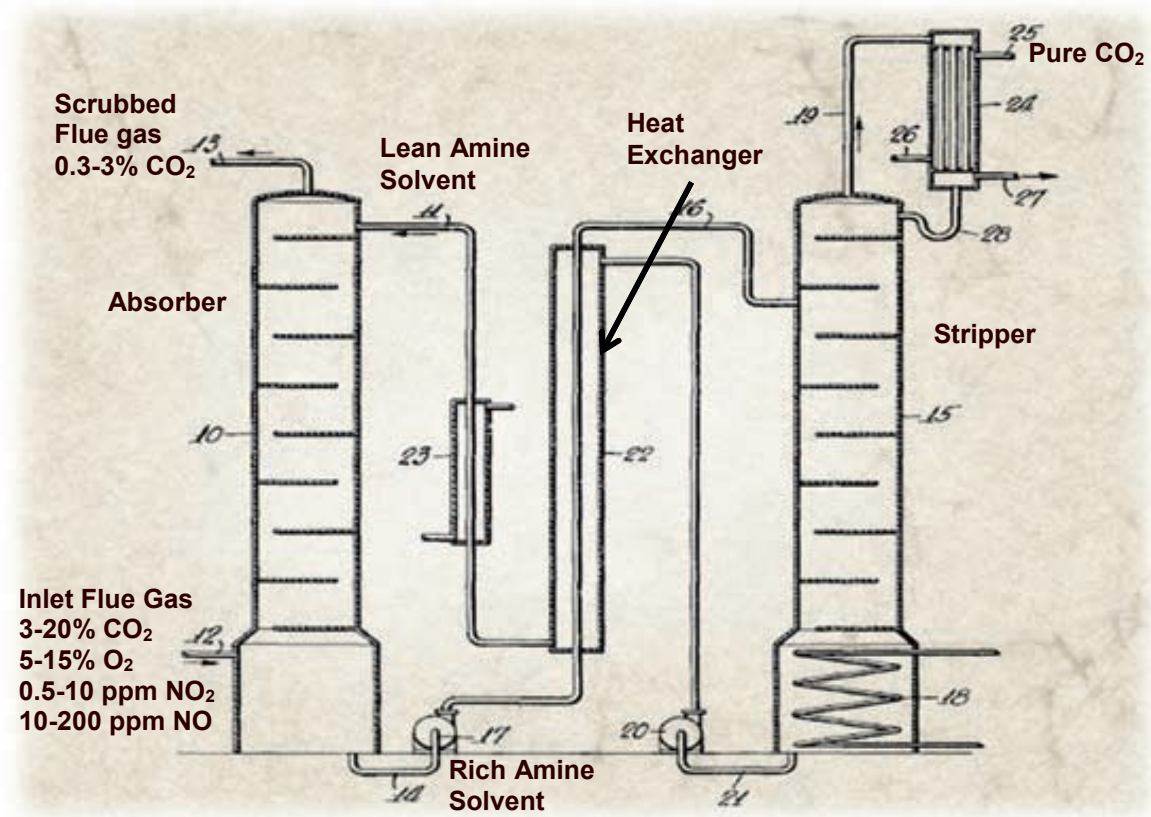


Figure 1.1: Simplified amine scrubbing process (Bottoms 1930) modified for clarity and to include post-combustion flue gas conditions

Direct contact with the contaminated flue gas, along with the high temperature in the stripper, can lead to amine degradation and formation of harmful byproducts. Nitrosamines, a family of organic compounds that contain an N-N=O functional group, are one of the largest environmental issues associated with amine scrubbing. Stable nitrosamines can form when a nitrosating agent, such as nitrogen dioxide or nitrite, reacts with a secondary amine. Over 80% of nitrosamines are carcinogenic to humans at low concentration due to their reactivity with DNA in target organs (Figure 1.2) (Garcia, Keefer, and Lijinsky 1970; Pai, Shirke, and Gothoskar 1981; Inami, Ishikawa, and Mochizuki 2009). Stable nitrosamines can only form from secondary amines, but all amine solvents will form secondary amines through oxidative and thermal degradation. Therefore nitrosamines are an inherent obstacle for the implementation of amine scrubbing.

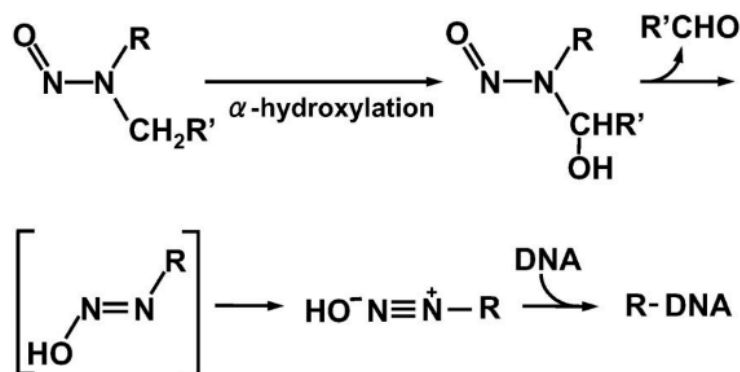


Figure 1.2: Nitrosamine reactivity with DNA (Inami et al. 2009)

1.2 NITROSAMINES IN AMINE SCRUBBING

This work was done in the context of ongoing nitrosamine work in amine scrubbing and other fields. Nitrosamines have been discovered in a variety of industries including tobacco, cosmetics, and meat products (Douglass and Kabacoff 1978) and have been speculated to form under amine scrubbing conditions (Rochelle et al. 2001). Nitrosamines were first reported in an amine scrubber in 2003 (Strazisar, Anderson, and White 2003).

The pilot plant study with monoethanolamine (MEA) found nitrosamines in the stripper and absorber, but no nitrosamines were detected in the thermal reclaimer. Other preliminary studies have detected very low nitrosamine levels in MEA solutions, presumably due to lack of MEA degradation (Dai et al. 2012; Mitch 2011). As research shifted towards piperazine as an advanced solvent (Freeman et al. 2010), interest in nitrosamine accumulation grew since PZ can directly form n-nitrosopiperazine (MNPZ) and dinitrosopiperazine (DNPZ). MNPZ directly forms when PZ is sparged with 0.8% nitrogen monoxide (NO) at absorber conditions, but DNPZ formation is negligible (Jackson and Attalla 2010). Other researchers have shown that morpholine, a secondary amine similar to PZ, will form nitrosomorpholine under absorber conditions when sparged with NO₂. Formation is heavily dependent on the pH of solution and carbamate loading (Chandan et al. 2013; Dai et al. 2012). In general, secondary amines have the highest rate of direct nitrosamine formation, followed by tertiary amines and then primary amines (Dai and Mitch 2013)

Research has also focused on nitrite instead of NO_x as a nitrosamine precursor. Nitrite is known to form nitrosamines at room temperature under acidic conditions and in basic conditions in the presence of formaldehyde (Cachaza et al. 1978; Casado et al. 1984). More current research has affirmed that nitrite is stable in basic CO₂-loaded amine solutions under absorber conditions (Dai and Mitch 2014a; Ashouripashaki 2012). Once exposed to high temperatures, nitrite reacts quickly to form nitrosamine (Voice 2013; Miguel, Voice, and Trap 2013). Previous computational models predict that CO₂ could be a powerful nitrosating catalyst with nitrite present but would inhibit nitrosation with stronger nitrosating agents such as dinitrogen trioxide (N₂O₃) (Lv et al. 2007; Sun, Liu, and Zhong 2011).

There are three main pathways to decompose nitrosamines: catalytic hydrogenation, photolytic decomposition, and thermal decomposition. Nitrosomorpholine hydrogenates to morpholine in the presence of iron and nickel catalysts at 120 °C, but the catalyst is expensive, necessitating regeneration (Chandan et al. 2014). Regeneration requires a source of H₂ and special equipment, adding to the complexity of the amine scrubbing process. Nitrosamines photolytically degrade in aqueous solutions and in the atmosphere (Miguel, Voice, and Trap 2013; Sørensen et al. 2013), but the solvent also degrades when exposed to UV radiation. Thus, photolytic degradation has focused on areas with low amine concentration such as the water wash and the thermal reclaimer vapor. Initial research proved that aqueous MNPZ is stable at 150 °C for 20 minutes (Jackson and Attalla 2011), but longer exposure consistent with amine lifetime in the scrubbing process showed MNPZ decomposition (Ashouripashaki 2012). Nitrosamine decomposition can be much faster than amine degradation at stripper temperature, making it an effective method for nitrosamine control with no additional cost. Previous and current studies qualitatively demonstrate that nitrosamines can form in the amine scrubber and that it is possible to control them via amine selection, additives, and process modifications. The scope of this work strives to explain nitrosamine accumulation, quantitatively model accumulation under industrial conditions, and provide tools to economically control nitrosamines to acceptably low levels.

1.3 RESEARCH SCOPE

Figure 1.3 gives a proposed sequence of processes that determine nitrosamine accumulation in amine scrubbing. Flue gas containing NO_x enters a polishing scrubber where a fraction (α_{pre}) of the NO₂ can be removed via reaction with sulfite or tertiary amine. The remaining NO_x then enters the absorber where a portion of the NO₂ (β_{abs}) can absorb

into the amine solution as nitrite. A fraction of the NO (γ_{abs}) can directly form nitrosamines by reacting with the amine radical formed during NO₂ absorption. The rest of the NO_x will vent from the absorber along with the scrubbed flue gas. A fraction of amine oxidation (ϵ) also yields nitrite in amine solvents that are not oxidatively stable. Nitrite from NO_x absorption and amine oxidation will then travel to the stripper where it can nitrosate a secondary amine with a yield of δ_{str} . The yield is determined by the concentration of secondary amines in the solvent and their relative nitrosation rates compared to the primary amine solvent. After nitrosation, the nitrosamine will thermally decompose in the stripper according to a pseudo-first order nitrosamine decomposition rate constant (k_{str}). In many amine scrubbing systems, a slipstream (x_{recl}) of the solvent is passed through a distillation reclaimer to remove any nonvolatile impurities. Efficiency of nitrosamine removal through thermal reclaiming will be determined by nitrosamine volatility ($k_{\text{H NNO}}$) and the thermal decomposition rate in the reclaimer (k_{Recl}). Finally, nitrosamines will exit the amine scrubber through gaseous emissions (y_{NNO}) or accidental spills (x_{spill}).

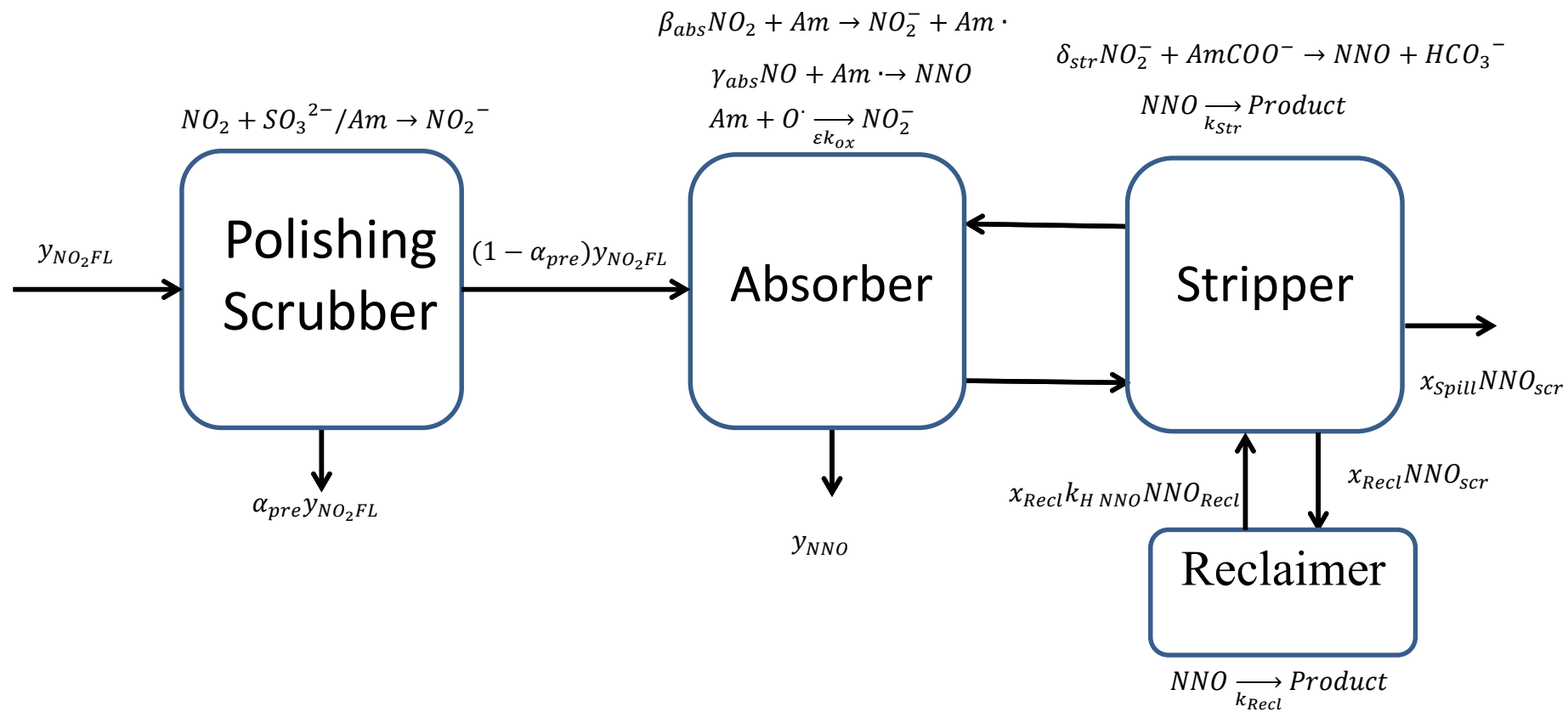


Figure 1.3: Nitrosamine accumulation in amine scrubbing

The scope of this dissertation includes the following:

- Quantify the fraction of NO_x absorption into amine solvents and determine the absorbing species under absorber conditions
- Quantify the yield and determine the mechanism for nitrosation under stripper conditions
- Quantify the rate and determine the mechanism for nitrosamine thermal decomposition under stripper conditions
- Determine the economic effectiveness of thermal reclaiming for nitrosamine control as a function of nitrosamine volatility and degradation under thermal reclaiming conditions
- Determine the economic effectiveness of NO_2 scrubbing using absorption into sulfite or tertiary amine solutions
- Establish conservative estimates for acceptable nitrosamine levels from an emissions perspective
- Quantify the fraction of amine oxidation into nitrite and determine its relative importance compared to NO_x absorption

The following are not contained within the scope of this dissertation:

- Nitrosamine formation in industries other than amine scrubbing
- Nitrosamine chemistry outside of the amine scrubber such as atmospheric and aquatic nitrosamine chemistry
- A detailed environmental and safety impact of nitrosamine emissions from the amine scrubber
- Other methods for nitrosamine management such as catalytic hydrogenation and UV photolysis

Chapter 2: Methods

Chapter 2 discusses all of the analytical and experimental methods used for this research. Many of these methods were created by previous researchers and only slightly modified in the context of this work. Newly developed methods are described with enough detail to understand and reproduce the research while descriptions of previous methods is brief and focused on any modifications.

2.1 ANALYTICAL METHODS

2.1.1 Anion Analysis

A Dionex ICS-3000 anion chromatograph with an IonPac AS15 column was used to quantify formate, and nitrite as previously described in detail (Freeman 2011; Sexton 2008). The chromatography unit separates anions in the adsorption column by anionic strength as a KOH eluent gradually displaces the anions from the adsorption sites. The analyte was quantified by measuring conductance across a fixed volume of solution. The resulting peaks were integrated and compared to calibration curves for quantitation. Concentrated amine samples were diluted gravimetrically in water 20–100x before analysis so that total ion concentration remained below 40 mM.

Experiments with sulfite, sulfate and thiosulfate were analyzed using anion chromatography with a modified method. Sulfite is oxidatively unstable at room temperatures, so it was indirectly analyzed by first injecting 1 mL of the sample into 0.1 g of 35 wt % formaldehyde to react all sulfite to methylsulfonic acid (MSA) (Equation 2.1) (Shen 1997).



The sample was then gravimetrically diluted and run through the chromatograph. The standard method for KOH ramp rate was elongated to better separate the MSA peak from the sulfate peak (Figure 2.1).

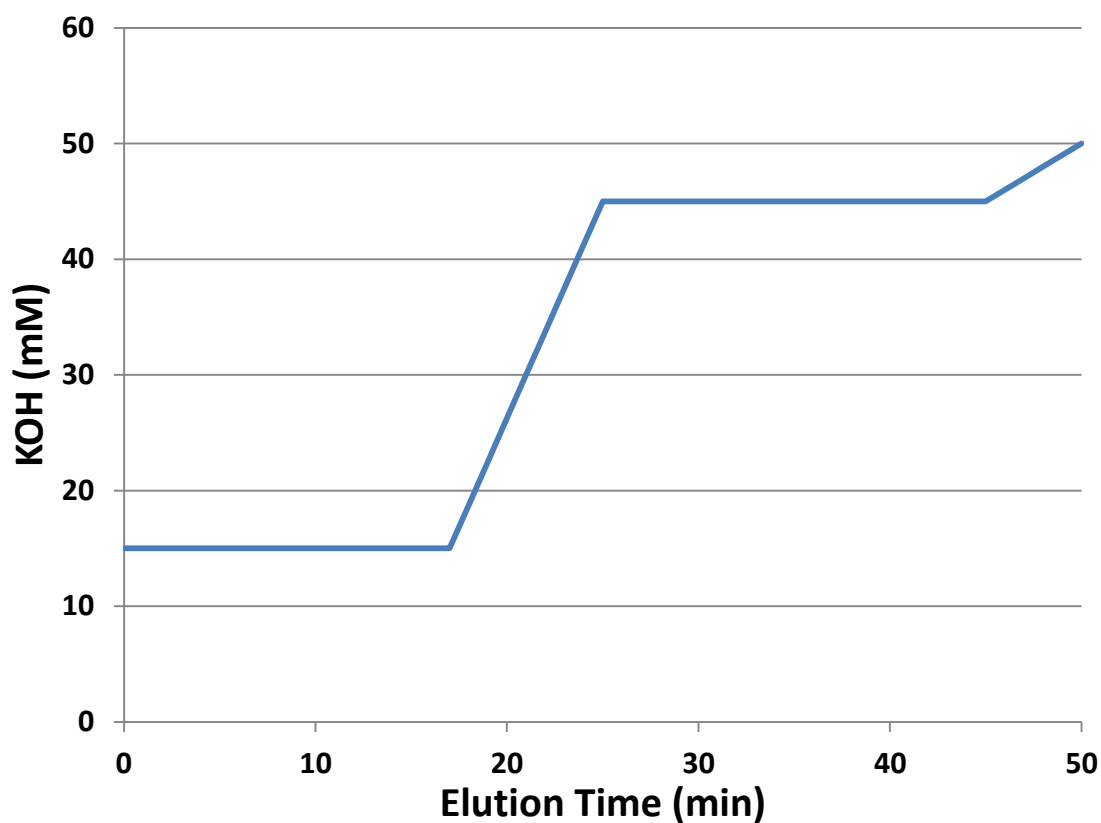


Figure 2.1: KOH ramp rate for sulfite, sulfate, and thiosulfate analysis

MSA from sulfite, sulfate, and thiosulfate eluted at approximately 21.3, 22.5, and 30.8 minutes respectively. A small formate peak from formaldehyde oxidation eluted at approximately 4 minutes (Figure 2.2).

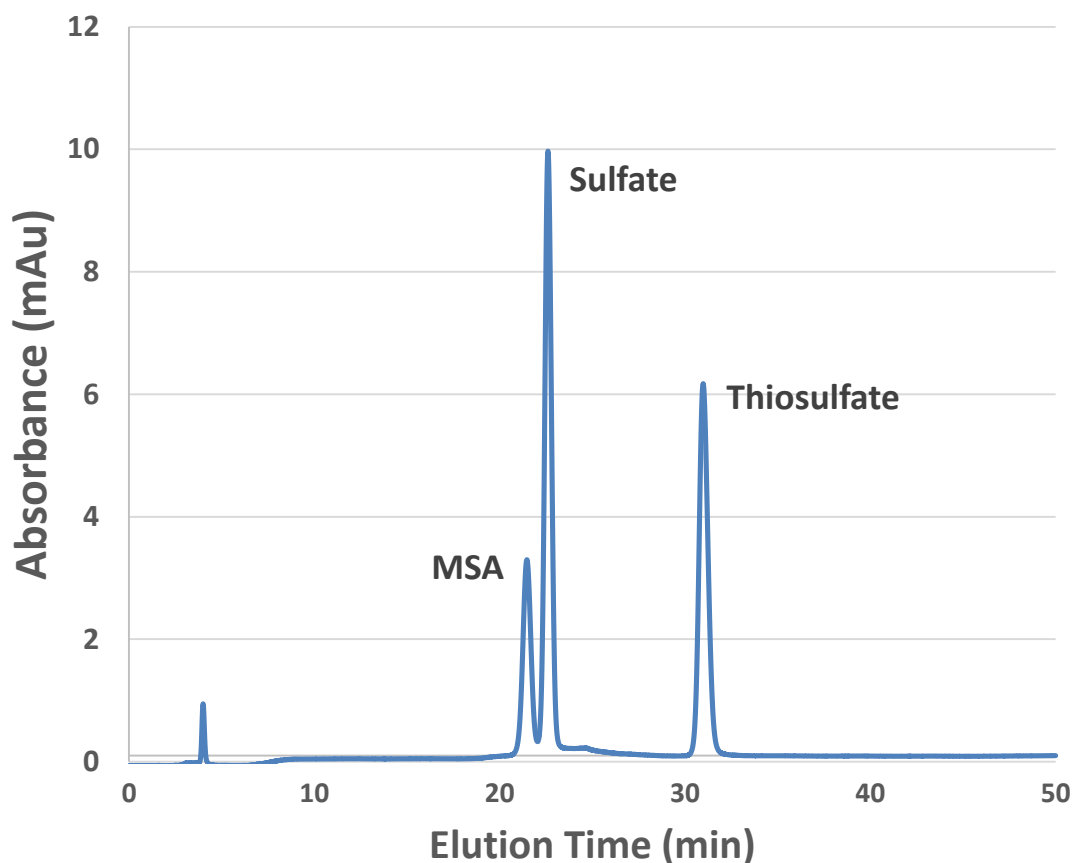


Figure 2.2: Retention times for MSA, sulfate, and thiosulfate using modified KOH ramp rate; MSA formed stoichiometrically from sulfite.

2.1.2 Cation Chromatography

Methyldiethanolamine (MDEA) and methylaminoethanol (MAE) were analyzed using a Dionex ICS-3000 cation chromatography unit as previously detailed (Davis 2009; Freeman 2011; Namjoshi 2015). The cations were separated using an MSA eluent passing through an IonPac CS17 analytical column. After elution, cations were quantified using a conductivity detector, and the resulting peaks were compared against calibration data. Concentrated amine samples were diluted gravimetrically in water by 10,000x before analysis so that amine concentration in the dilute sample was always less than 0.5 mM.

2.1.3 Individual Nitrosamine Analysis

The individual nitrosamines MNPZ, DNPZ, nitroso-(2-hydroxyethyl)glycine (NHeGly), nitroso-hydroxyethyl-ethylenediamine (NHEEDA), and nitroso-diethanolamine (NDELA) were analyzed using a Dionex Ultimate 3000 reverse-phase High Performance Liquid Chromatography unit with UV detection at 240 nm. The eluents used were 10 mM ammonium carbonate ($(\text{NH}_4)_2\text{CO}_3$) polar phase and an increasing acetonitrile (ACN) non-polar phase (Figure 2.3). The analytical chromatography column must be able to handle the basic buffer, so a Dionex Polar Advantage II 4 x 250 mm column was used (Voice 2013).

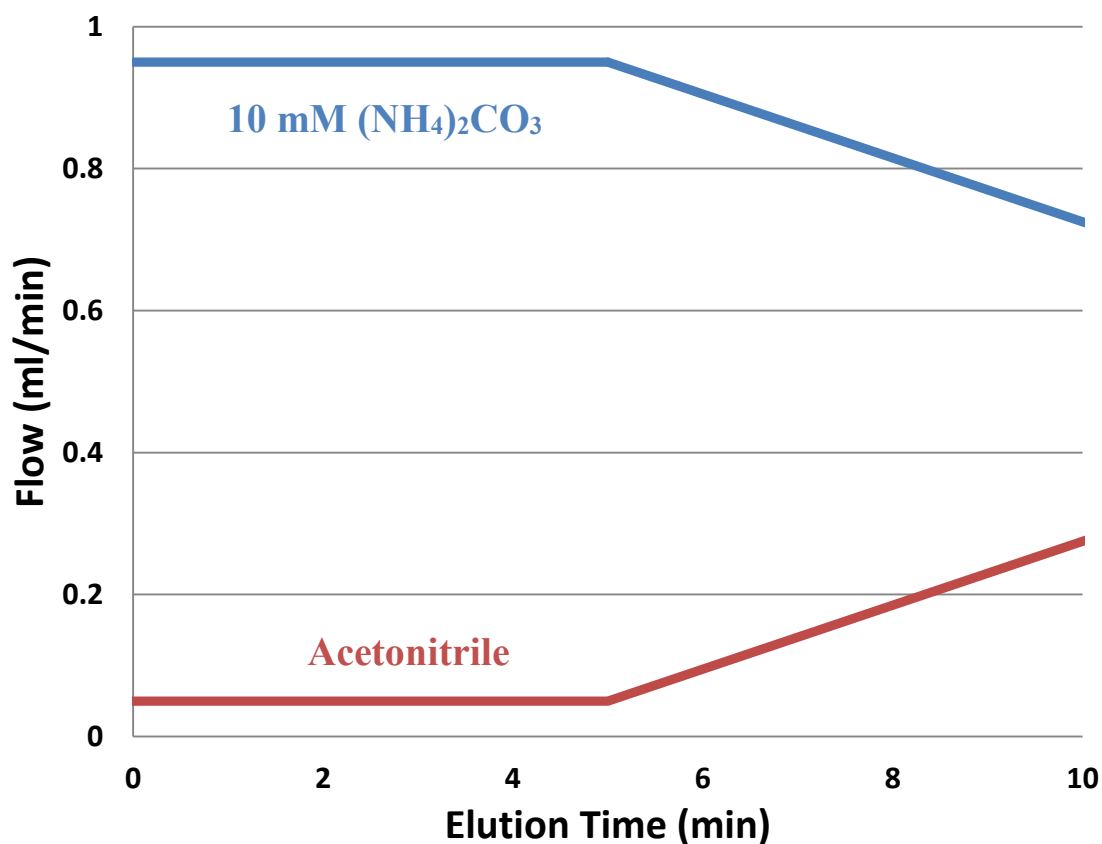


Figure 2.3: HPLC ramp rates for nitrosamine analysis

NHeGly, NDELA, NHEEDA, MNPZ, and DNPZ eluted at approximately and 2.5, 5.0, 5.4, 5.5, and, 7.9 minutes respectively (Figures 2.4–2.7). DNPZ had a distinctively bimodal shape possibly due to polarity differences between different molecule conformations (Figure 2.7). The carboxylic group on NHeGly makes it ionic in the basic ammonium carbonate buffer used as an eluent, leading to its elution in the void space of the column (2.5 minutes). In controlled experiments, the only other UV absorbing species eluting in the void space was nitrite. Thus nitrite concentration was kept to less than 5% of the total NHeGly for all experimental runs, and nitrite was manually accounted for by using results from the anion chromatography method. However, the current method for NHeGly analysis would be unsuitable for pilot plant samples that have a high concentration of UV absorbing ionic degradation products. Samples were diluted gravimetrically in water by 20–50x before analysis.

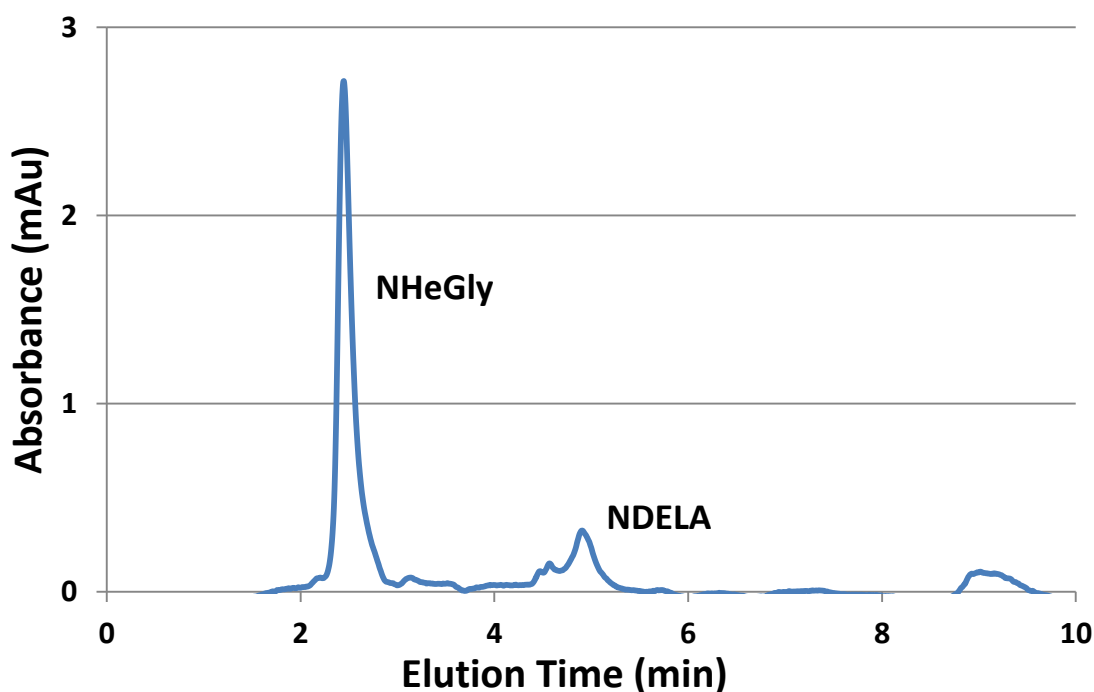


Figure 2.4: NHeGly and NDELA elution using the HPLC method

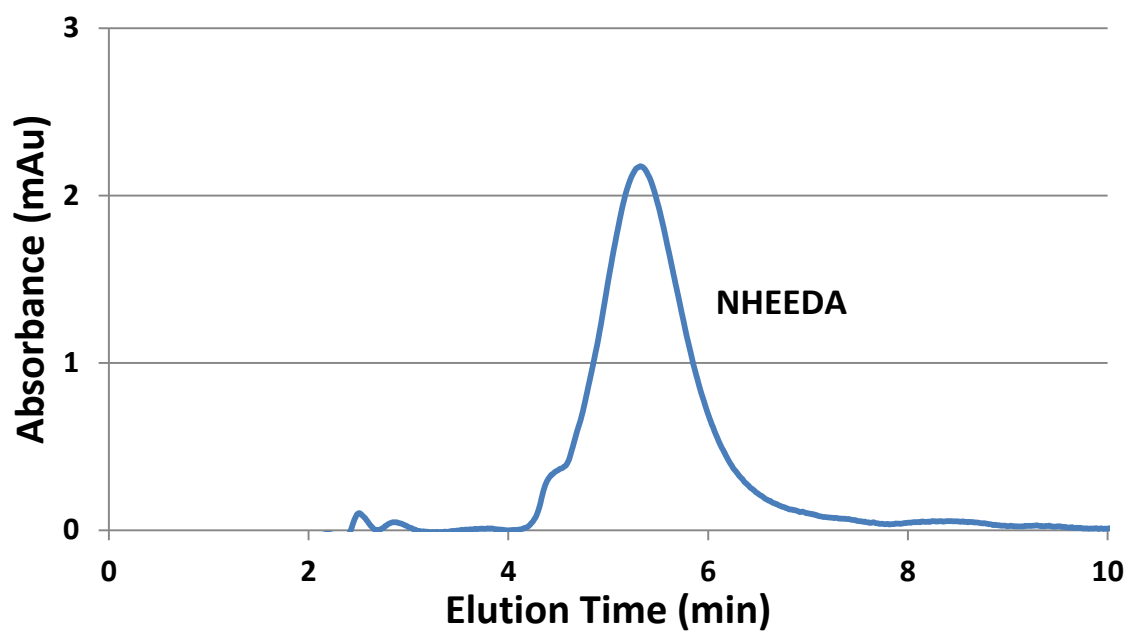


Figure 2.5: NHEEDA elution using the HPLC method

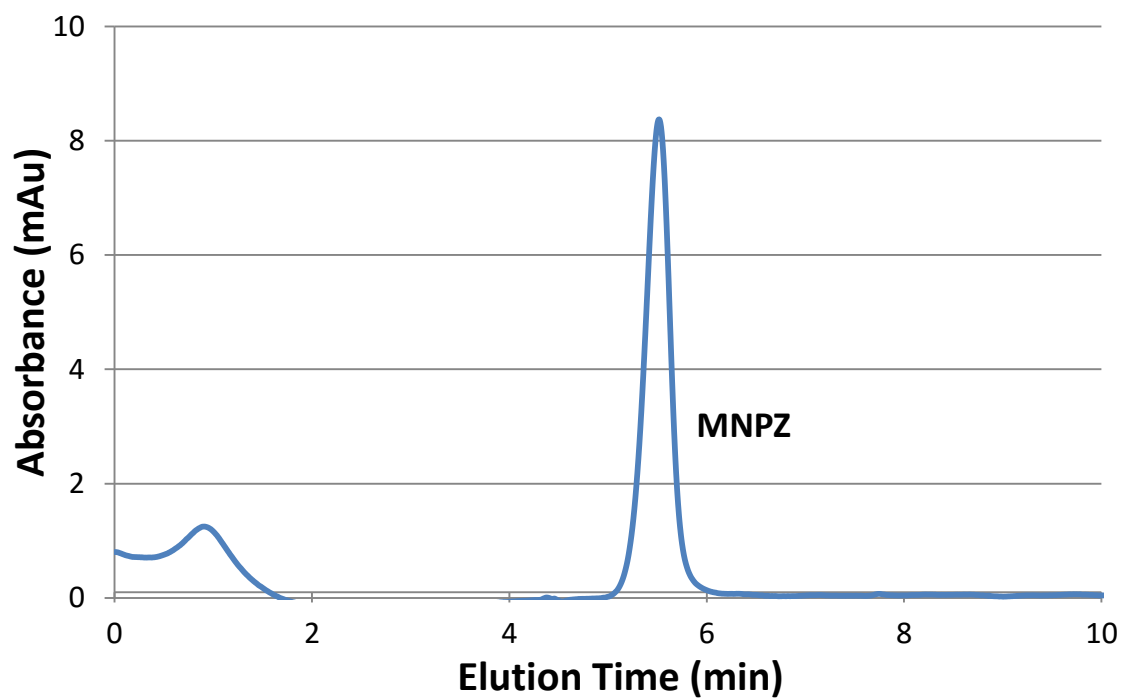


Figure 2.6: MNPZ elution using the HPLC method

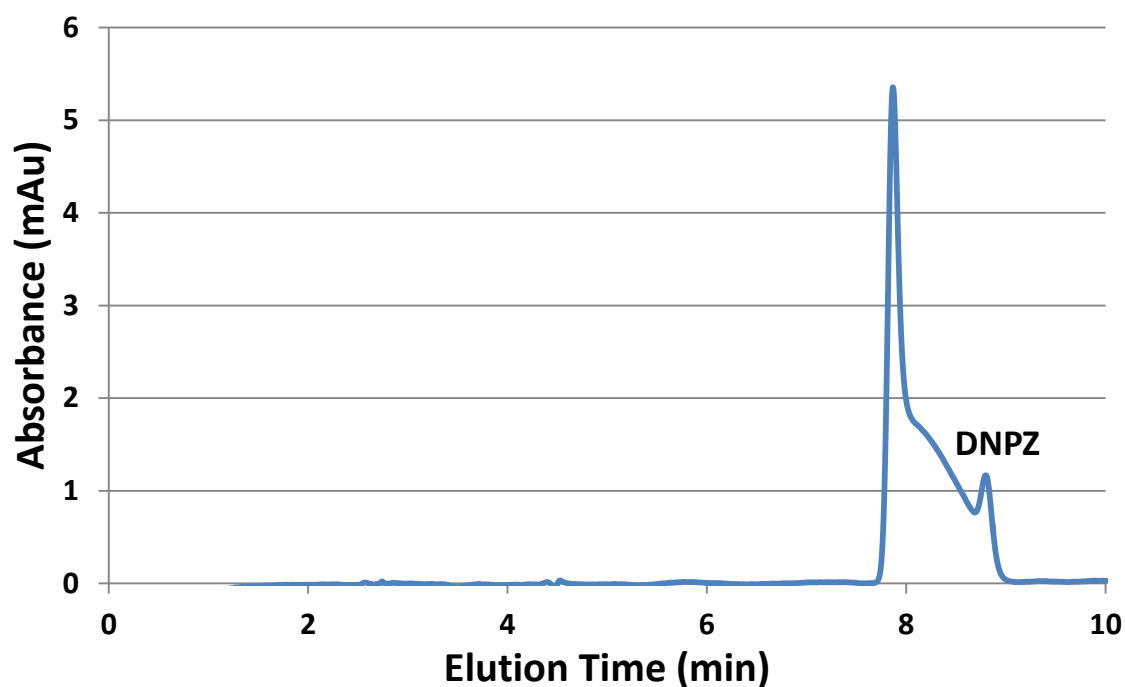


Figure 2.7: DNPZ elution using the HPLC method

2.1.4 NHeGly and NHEEDA Quantification

MNPZ, DNPZ, and NDELA standards were purchased for calibrating the HPLC method previously discussed, but NHeGly and NHEEDA standards were commercially unavailable. NHeGly was synthesized by nitrosating N-(2-hydroxyethyl)glycine (HeGly) in 5 M MEA with a CO₂ loading (α) of 0.4 mol CO₂/mol equivalent amine. MEA was spiked with 50 mM NaNO₂ at heated at 120 °C for 16 hours at varying concentrations of HeGly. MEA itself nitrosates when exposed to NaNO₂, forming an unstable nitrosamine that degrades into DEA (Mitch 2011); the resulting DEA reacts with nitrite to form NDELA. After nitrosation, the samples were analyzed using the HPLC method and the total nitrosamine method described in the next section. Under these conditions, the apparent nitrosamine concentration is the sum of nitrite, NDELA and NHeGly in the sample. NHeGly always comprised over 90% of the total nitrosamine peak with nitrite comprising less than 5% of the peak. NDELA was quantified using the same HPLC method

while nitrite was quantified separately using anion chromatography; both values were then subtracted from the apparent nitrosamine value to yield NHeGly concentration. NHeGly eluted at 2.5 minutes using the HPLC method, which was in interference with nitrite. Thus, a minor correction to the 2.5 minute peak area was made for any nitrite left in solution.

NHEEDA was synthesized by nitrosating 1 M HEEDA ($\alpha=0.3$) with 50 mM NaNO_2 at 120 °C for 16 hours. The sample was then diluted to three different concentrations and analyzed using the total nitrosamine and HPLC methods. No nitrite was detected in the final sample and there was negligible interference on the HPLC method. Thus, the peak on the HPLC was integrated and directly calibrated using the total nitrosamine results. Both NHeGly and NHEEDA calibration curves were linear within the calibration range (Figures 2.8 & 2.9).

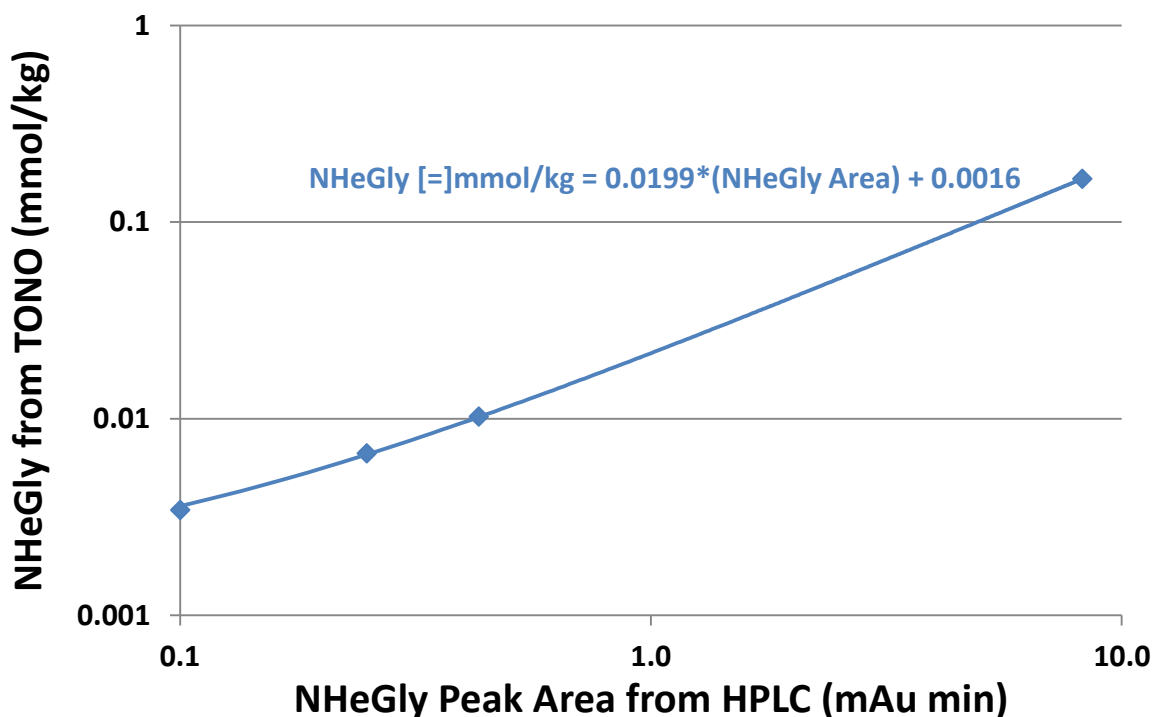


Figure 2.8: NHeGly calibration on the HPLC from TONO results

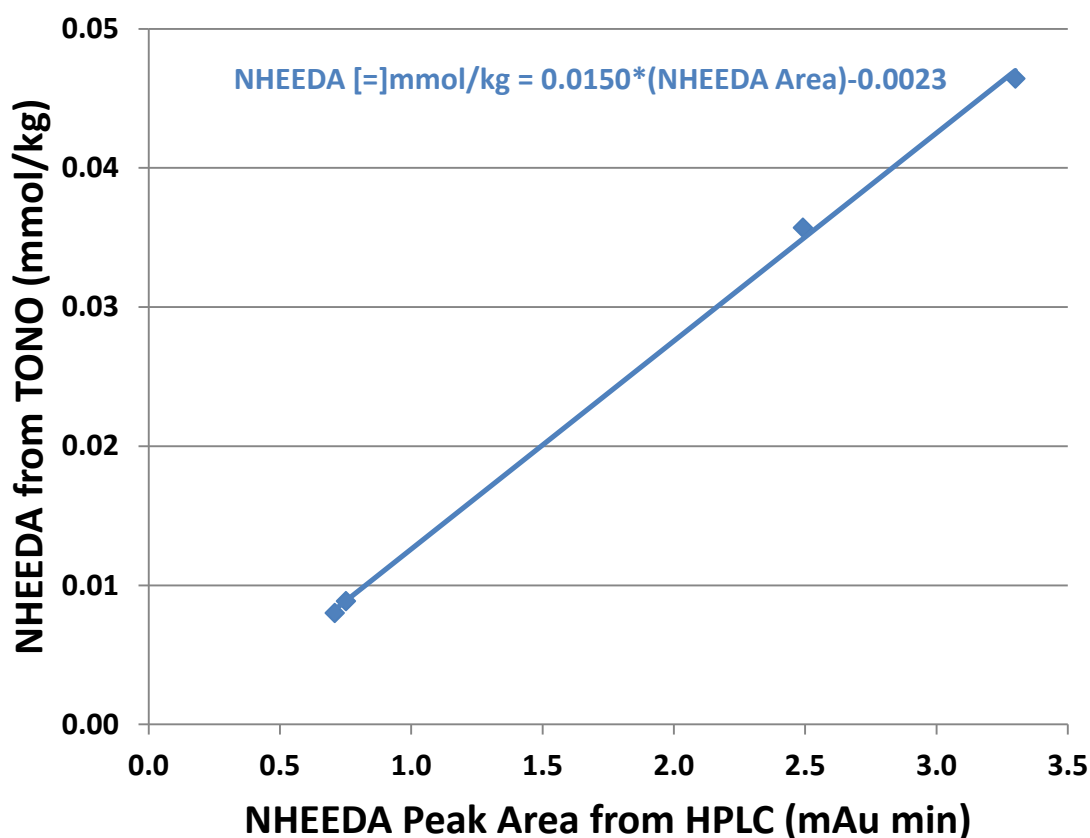


Figure 2.9: NHEEDA calibration from TONO results

2.1.5 Total Nitrosamine Analysis

Analysis for total nitrosamines was done by reacting a nitrosamine sample with hydrobromic acid (HBr) in a mixture of ethyl acetate, acetic acid, and acetic anhydride at ambient conditions (Drescher and Frank 1978; Williams 1994; Kulshrestha et al. 2010). The reaction selectively formed one mole of nitric oxide (NO) gas for every mole of nitrosamine. Approximately 10–1000 μL of sample was injected through a septum located at the bottom of the reactor depending on total nitrosamine concentration. The NO gas was sparged from the reactor with 1.5 SLPM of N_2 carrier gas passing through the fritted bottom of the reactor. The gas then passed through a condenser using circulating ice water to maintain the temperature at 0 °C. The dry exit gas passed an atmospheric bypass and was

pulled through a chemiluminescent NO_x analyzer using a vacuum pump under choked flow conditions. Sample injections were compared against an MNPZ calibration curve made daily. Nitrite, a signal interference for total nitrosamine analysis, was kept to less than 5% of the total nitrosamine. The conditions in the reactor, a schematic for the total nitrosamine apparatus, and an image of the entire apparatus are shown below (Table 2.1 and Figure 2.10 & 2.11).

Table 2.1: Operating conditions and reagents used in TONO

| Condition | Purity | Amount |
|------------------|--------------|-----------|
| Temperature | - | 21 °C |
| Pressure | - | 14.7 psig |
| Nitrogen | 99.99% | 1.5 SLPM |
| Ethyl Acetate | 98% | 12 mL |
| Acetic Acid | 99.85% | 2 mL |
| HBr | 48% in water | 0.4 mL |
| Acetic Anhydride | 99% | 0.6 mL |

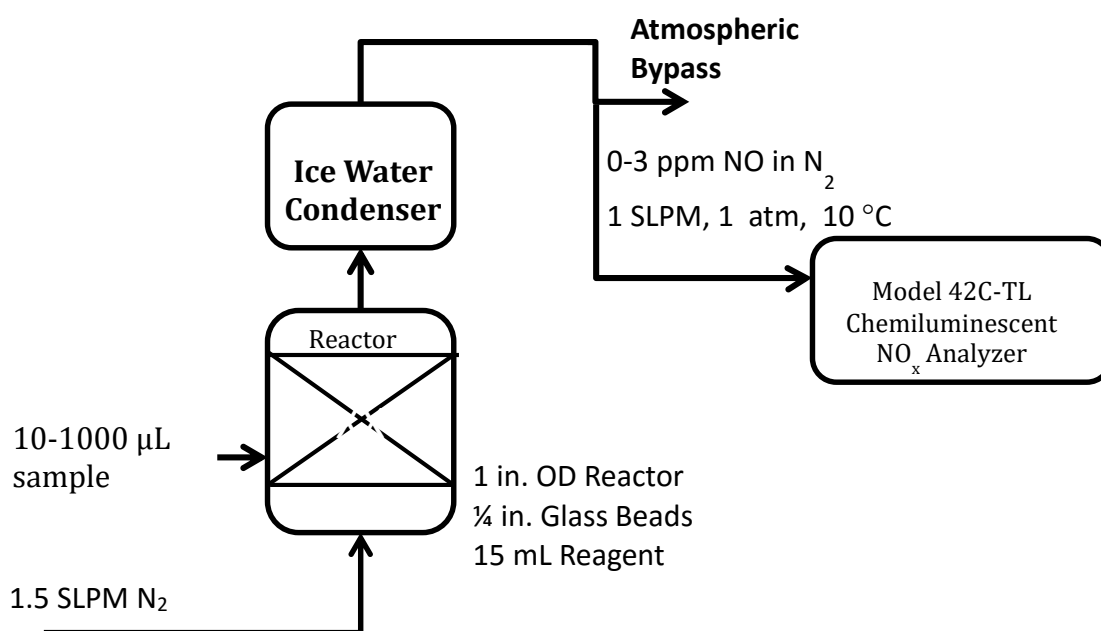


Figure 2.10: Total nitrosamine apparatus (TONO)

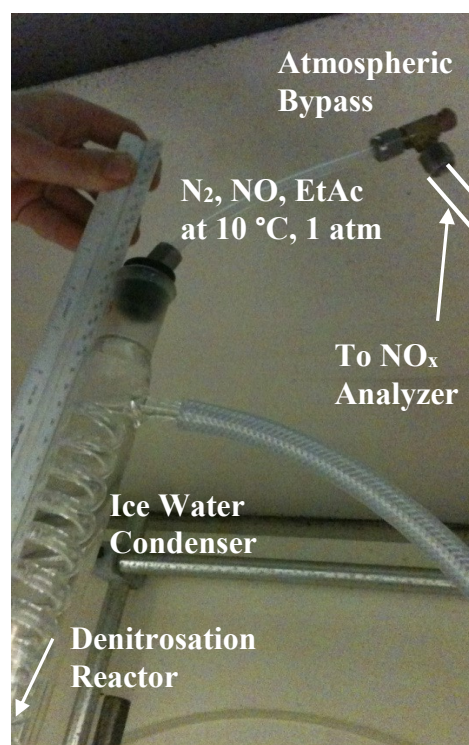
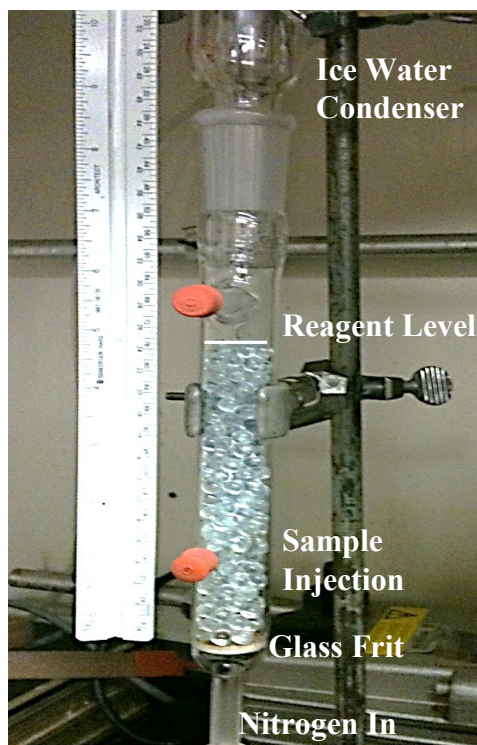


Figure 2.11: Images of TONO reactor, condenser, and atmospheric bypass

The peaks from the NO_x analyzer completed elution in approximately 2-5 minutes, showing fast and complete denitrosation of the nitrosamine using HBr (Figure 2.12). Peak area was proportional to nitrosamine concentration and the response was statistically equivalent across the three purchased nitrosamine standards (MNPZ, DNPZ, and NDELA). Reproducibility of this direct injection method was higher than previously described extraction methods since there was no extraction efficiency error confounding the results (Kulshrestha et al. 2010; Dai et al. 2012). In particular, MNPZ extraction efficiencies are approximately 50% in ethyl acetate, making reproducible quantification with an error of less than 20% extremely difficult.

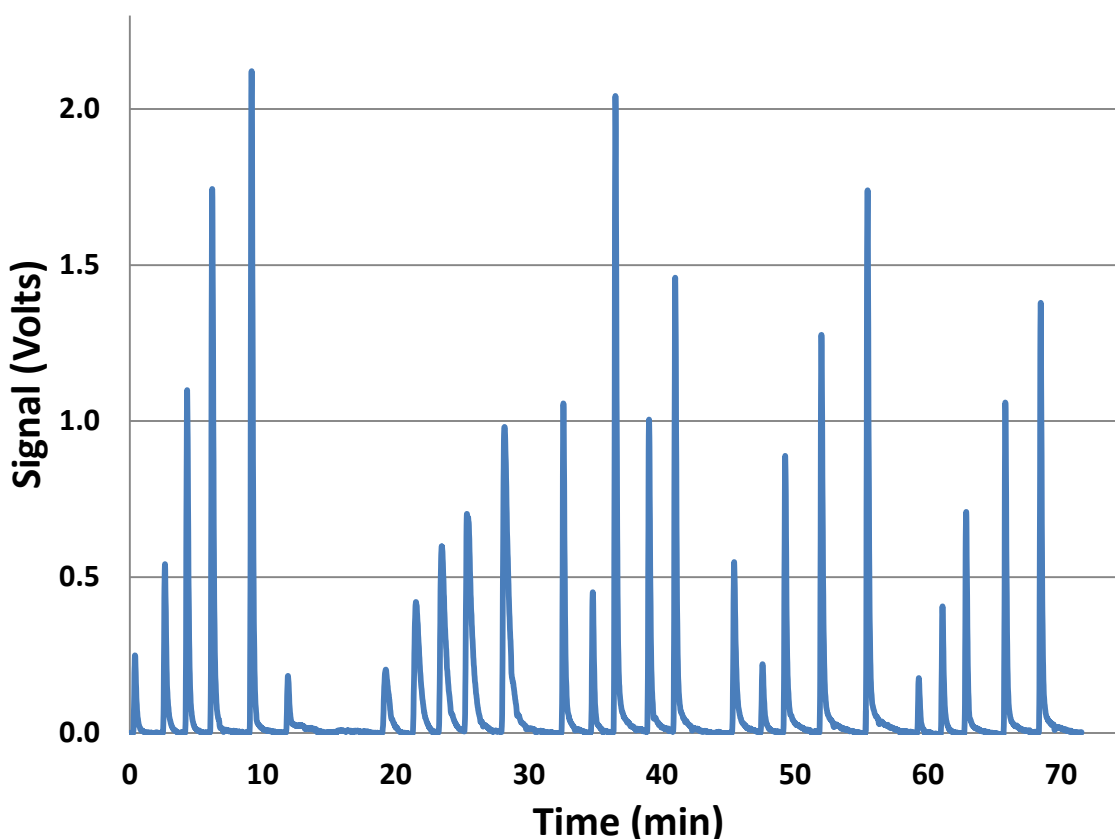


Figure 2.12: Sample responses from the NO_x analyzer after nitrosamine injection in the TONO reactor; time to peak after injection is less than 10 seconds, time to baseline is less than 5 minutes

2.1.6 Total Aldehyde and Hemiaminal Analysis

Aldehydes and hemiaminals from nitrosamine degradation were quantified by reacting the sample with 2,4-dinitrophenylhydrazine (DNPH) and analyzing the products on the HPLC. The concentrated sample was diluted gravimetrically by a factor of 50 into 1 mL of 2:1 vol:vol methanol and 10 mM ammonium carbonate buffer. A solution of 0.4 wt % DNPH diluted in acetonitrile was then added to react with the aldehydes. The solution was capped, stirred, and allowed to react at room temperature overnight. The reacted solution was then injected directly on HPLC using an Acclaim™ Polar Advantage II C18 5 µm 120 Å 4.6 x 150 mm reverse phase column with UV detection at 365 nm, using the eluent ramp shown below (Figure 2.13).

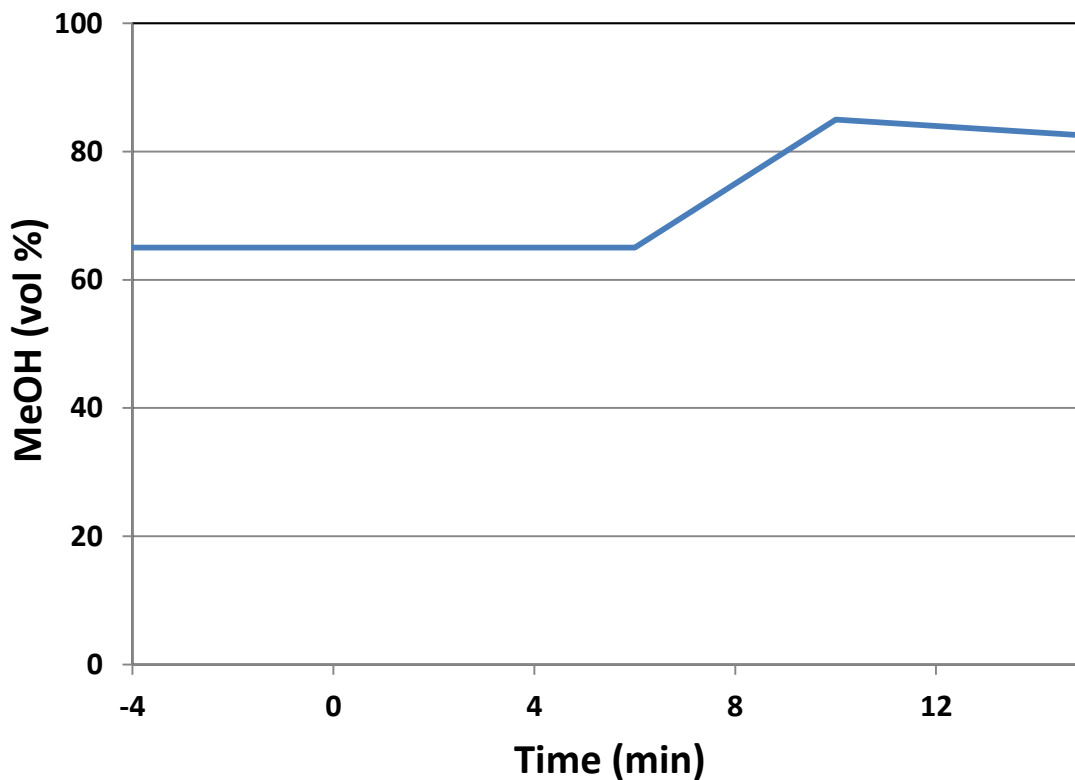


Figure 2.13: MeOH eluent ramp in $(\text{NH}_4)_2\text{CO}_3$ for total aldehyde analysis

A 50 mmol/kg sample of MNPZ was prepared in 7.5 M PZ and thermally degraded at 175 °C. The sample was then diluted, spiked with DNPH, and immediately run on the HPLC repeatedly for 20 hours. Figure 2.14 shows the initial chromatogram and the chromatogram 20 hours later. The first peak in the chromatogram at 2.2 minutes is postulated to be the DNPH-PZ derivative peak. It appeared in all DNPH-reacted PZ samples and accumulates steadily. The peak at 2.5 minutes appeared only in the degraded MNPZ samples. A direct injection mass spectroscopy analysis detailed in the next section was performed on the degraded MNPZ sample to confirm that the major product of MNPZ decomposition is 2-piperazinol (2PZOH). It is hypothesized that the peak at 2.5 minutes is the DNPH derivative of 2PZOH. The peak was over 95 % fully formed within 12 hours of mixing with DNPH (Figure 2.15).

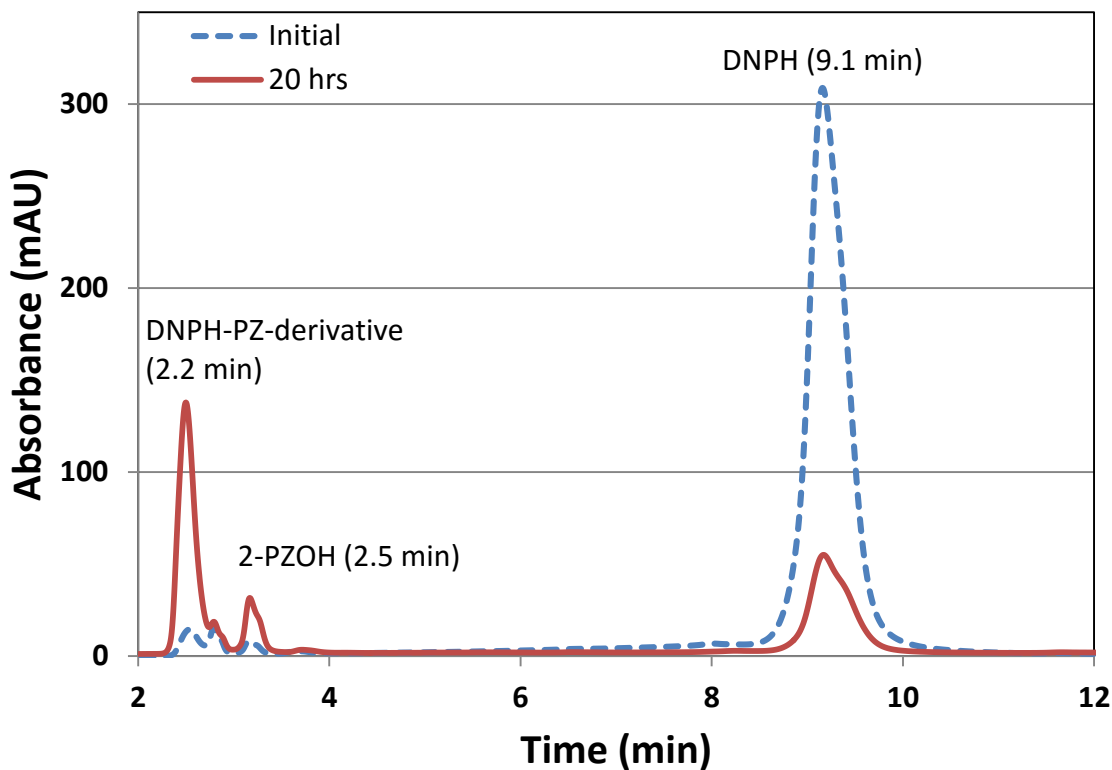


Figure 2.14: Chromatograms of DNPH reaction with thermally degraded MNPZ

Assuming that peak areas were proportional to analyte concentration, the DNPH peak disappearance was regressed over time using a least squares analysis with the absorption efficiencies of both DNPH derivatives as free parameters (Equation 2.2). The regression of the peak area showed that the absorption efficiency of 2PZOH is 0.0377 mmol/kg/(mAU*min) and that both DNPH derivatives could account for all of the DNPH disappearance (Figure 2.15).

$$Area_{DNPH} = Area_{DNPH\ i} - (C_1 * Area_{2.5\ min} + C_2 * Area_{2.2\ min}) \quad (2.2)$$

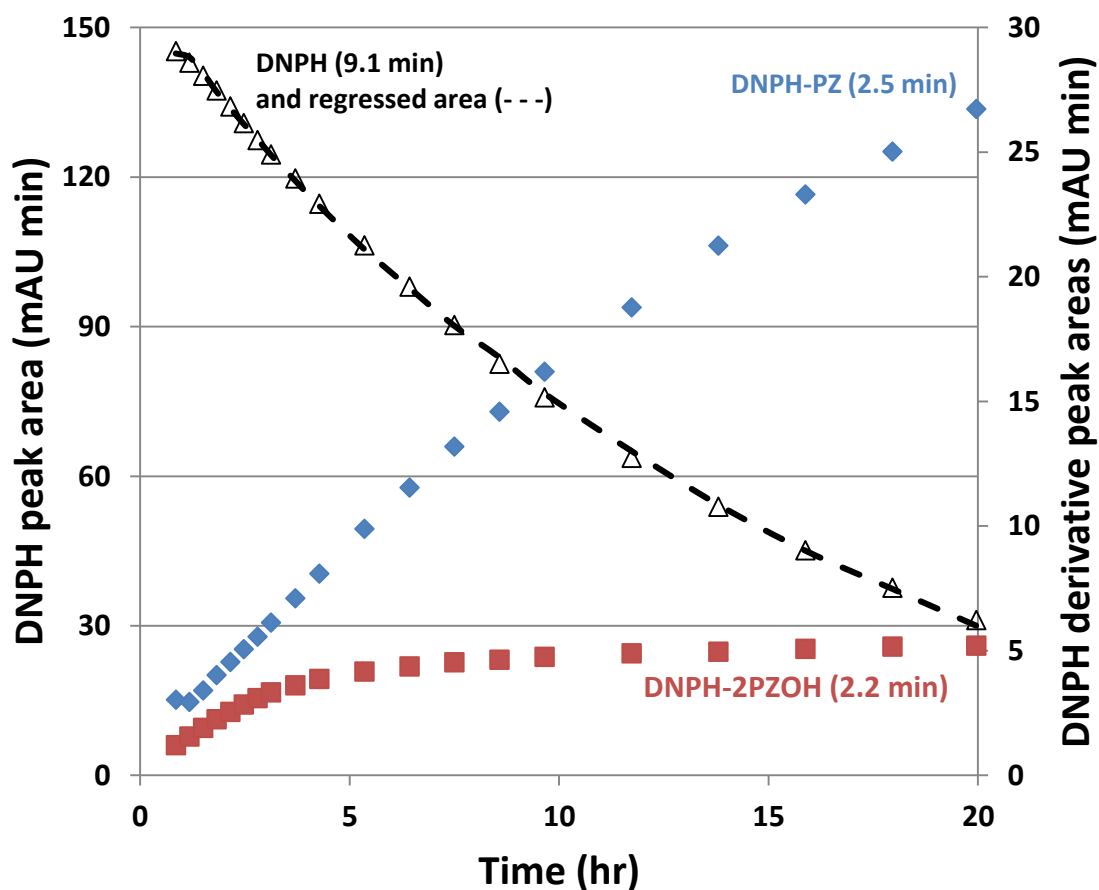


Figure 2.15: DNPH and DNPH derivatives peak areas along with Equation 2.2 regression

2.1.7 High Resolution Mass Spectrometry

Several samples were analyzed by the University of Texas Mass Spectrometry Facility (UTMSF) using high-resolution mass spectrometry by direct injection with chemical ionization to confirm a chemical species by observing its molecular weight. HeGly was the only amine not commercially available, so it was synthesized by adding 0.5 M sodium chloroacetate into 5 M monoethanolamine (MEA) and reacting at 65 °C for 6 hours to yield a stock solution of 0.5 M HeGly in 4.5 M MEA (Closmann 2011). The resulting solution was spiked with 50 mM NaNO₂ and nitrosated at high temperatures. Chemicals with the exact molecular weight of HeGly and NHeGly were confirmed via high resolution mass spectrometry (Figure 2.16).

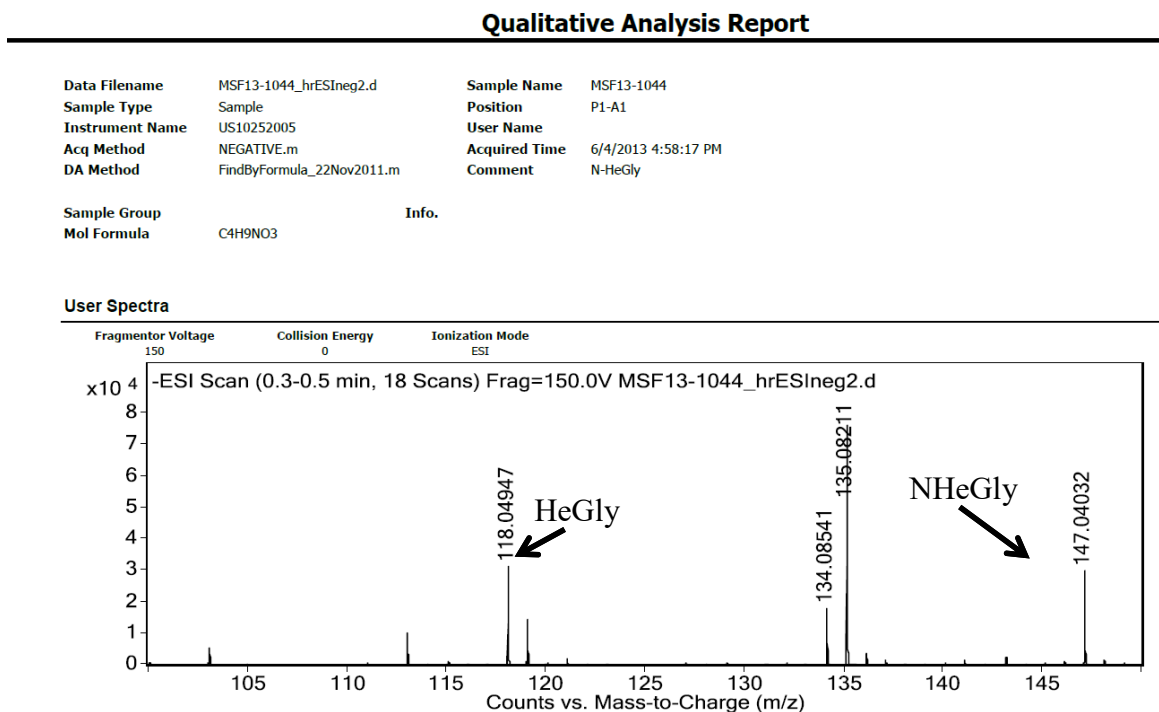


Figure 2.16: High Resolution Mass Spectroscopy of HeGly and NHeGly in MEA

Similarly a 50 mmol/kg sample of MNPZ was degraded in 12 m PZ at 175 °C and analyzed. The results confirmed a molecule with the same molecular weight as the 2PZOH, which is a hypothesized product of nitrosamine degradation (Figure 2.17).

Elemental Composition Report

Page 1

Multiple Mass Analysis: 9 mass(es) processed - displaying only valid results

Tolerance = 10.0 PPM / DBE: min = -1.5, max = 50.0

Selected filters: None

Monoisotopic Mass, Odd and Even Electron Ions

34 formula(e) evaluated with 3 results within limits (all results (up to 1000) for each mass)

Elements Used:

C: 0-100 H: 0-100 N: 2-2 O: 1-2

MJG12-4-12

MSF0113-0343_hrClpos1 68 (1.377) Cn (Cen,5, 50.00, Ar); Sm (Mn, 4x4.00); Cm (61.73)

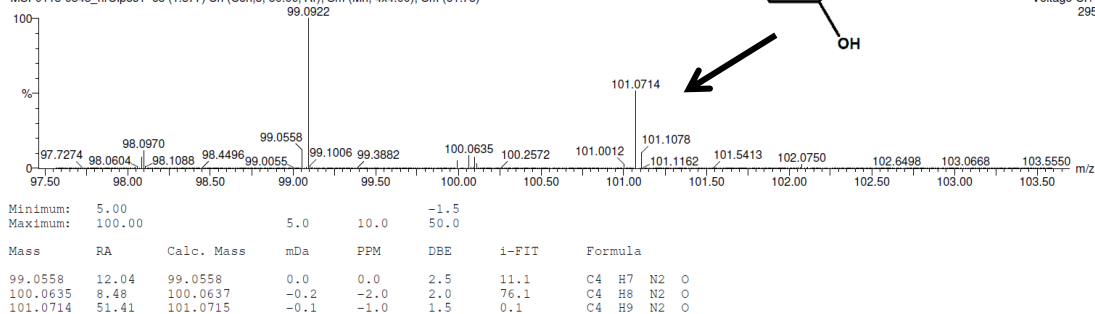


Figure 2.17: High Resolution Mass Spectrometry of 2PZOH in PZ

2.1.8 Total Inorganic Carbon Analysis

The CO₂ loading in an amine sample was quantified by reacting it with a strong acid and analyzing the product gas as previously detailed (Freeman 2011). Briefly, 2 mL of 30 wt % H₃PO₄ was loaded into a glass reactor and continuously sparged with N₂ gas through a fritted glass bottom. The amine sample was then injected into the reactor to desorb any CO₂ from solution. The N₂ gas swept the CO₂ out of the reactor, passed through a desiccant, and was analyzed by a Horiba PIR 200 infrared detector. The resulting peaks were then compared against a CO₂ calibration curve prepared hourly.

2.1.9 Total Alkalinity and pH Analysis

Total amine concentration in a sample was determined using a Metrohm automatic acid titrator previously described in detail (Freeman 2011). Sample was diluted in water by

a factor of 300 using 60 mL of water in a 100 mL beaker. A potentiometric pH probe was submerged into the sample, and the sample was mixed using a magnetic stir bar until the pH remained constant. The sample was then automatically dosed at 10 second intervals with 0.1 mL of 0.2 N sulfuric acid while the pH was recorded. The Titrando software automatically detected any equivalence points during the acid titration and recorded the sulfuric acid dosage needed to reach equivalence. The molality of total alkalinity in the sample was calculated from Equation 2.3.

$$molality_{sample} * mass_{sample} = N_{H_2SO_4} * V_{H_2SO_4} \quad (2.3)$$

The same pH probe was used to measure the pH of solution in diluted samples. To standardize for the effects of ionic strength, all samples were diluted to 10 mM total ions in solution regardless of ionic strength in the undiluted sample.

2.1.10 Nitrogen Monoxide and Nitrogen Dioxide Analysis

Both NO and NO₂ were analyzed using hot gas Fourier Transform Infrared spectroscopy (FTIR) as previously described in detail (Sexton 2008). Briefly, 5 SLPM at atmospheric pressure of the exit gas from an experiment was pulled through a heated line operating at 180 °C using a vacuum pump. The hot gas then passed through the Temet Gasmet™ DX-4000 FTIR for analysis. Inside the FTIR, the gas was irradiated using infrared radiation between 600-4200 cm⁻¹. Every molecule has a discrete absorption spectrum based on the energy needed for electron excitation which can be deconvoluted from the overall IR absorption of the gas mixture. Homo-nuclear molecules such as N₂ and O₂ are not detected by the FTIR, making them ideal as diluent gases. The analysis region for NO₂ was 2550-2933 cm⁻¹, and the analysis range for NO was 1760-1868 cm⁻¹ as suggested by Sexton (2008). Major interferences with water, amine, and CO₂ were automatically deconvoluted from the FTIR spectra using the Calcmeter software. The limit of quantification for both NO_x species was approximately 5 ppm under experimental

conditions with wet gas, necessitating the use of an alternative analyzer for low NO_x measurements.

Gas samples with less than 10 ppm of NO_x were analyzed using a Thermo Scientific Model 42C-TL (NO-NO₂-NO_x) Analyzer. The analyzer operates by reacting NO with ozone to form an excited NO₂ molecule. When the NO₂ molecule returns to its ground state, it gives off a photon that is magnified through a photomultiplier inside the NO_x analyzer. To analyze for NO₂, the sample gas must first pass through a molybdenum catalytic converter at 325 °C to convert any NO₂ to NO. The analyzer is designed for ambient conditions with an unsaturated gas, so water content was kept below 2% during all low-level NO_x analysis. The upper limit of detection was approximately 1 ppm; in some cases the sample gas was diluted with dry air to ensure that the whole span of NO_x concentration from 10 ppb to 1000 ppm could be well characterized with either the FTIR or the NO_x analyzer. All gas lines containing NO_x were either stainless steel or Teflon to insure that there was no adsorption onto the gas lines themselves.

2.2 EXPERIMENTAL METHODS

2.2.1 Thermal Cylinder

High temperature nitrosamine formation and decomposition experiments were performed using thermal cylinders to quantify nitrosamine kinetics at stripper conditions. Amine solvents were prepared gravimetrically at 0.1 m to 8 m. The solutions were then sparged with CO₂, which absorbs into the amine solution either as carbamate or bicarbonate; final CO₂ loadings were $\alpha = 0\text{--}0.4$ mol/equivalent amine. Amine concentration was varied by diluting the concentrated loaded amine solution with water to ensure a constant loading across a concentration range. Nitrosamine kinetics were also quantified in distilled deionized water, dilute NaOH, and a monobasic/dibasic phosphate

buffer ($\text{KH}_2\text{PO}_4/\text{K}_2\text{HPO}_4$) to examine the effect of base strength and pH. The prepared solutions were spiked with a small quantity of nitrosamine or NaNO_2 , up to 50 mM, and pipetted into 3/8 inch O.D. high pressure stainless steel cylinders (Figure 2.18). Each experimental batch consisted of at least five equivalent thermal cylinders. Special care was taken to exactly follow Swagelok instructions for capping the cylinders, which lowered the leak rate from 25 % (Freeman 2011; Closmann 2011) to less than 1 %.



Figure 2.18: Stainless steel thermal cylinder for measuring high temperature nitrosamine formation and decomposition kinetics

The closed cylinders were heated in convection ovens at 120–150 °C for nitrosamine decomposition experiments and 50–135 °C for nitrosamine formation experiments. The cylinders were kept at autogenous pressures from 1–15 bar similar to stripper pressure. Cylinders were removed periodically and immediately quenched in a water bath at room temperature. Typical experiment times ranged from three hours to three weeks, which usually allowed for greater than 90 % completion of the reaction. The samples were stored at room temperature in amber vials to prevent artifactual UV nitrosamine decomposition. Since all of the cylinders for a given experiment were prepared with the same stock solution, the periodic removal of cylinders allowed analysis for nitrosamine and nitrite concentrations as a function of time at elevated temperatures.

2.2.2 Wetted Wall Column Apparatus

The mass transfer of NO_2 into amine solutions was measured using the wetted wall column (WWC) previously described (Dugas 2009). An N_2 gas passed through a hydrator which was temperature controlled to approximately experimental conditions using a jacketed heater. The wet gas then mixed with 5000 ppm NO_2 in N_2 and pure CO_2 to give a final NO_2 partial pressure of 1–30 Pa (10–300 ppm NO_2 at ambient pressure). The gas was preheated to experimental conditions in an oil bath and then fed into the WWC chamber from the bottom. There, the gas countercurrently contacted an amine solution flowing down the WWC. Both water and CO_2 content of the gas were controlled so that they would be in equilibrium with the amine solution in the chamber. NO_2 concentration going through the wetted wall column chamber was measured using a hot-gas FTIR and compared to a bypass measurement (Figure 2.19). The temperature in the WWC chamber was measured by a thermocouple located in the liquid stream at the base of the WWC, the pressure in the chamber was controlled using a needle valve directly downstream of the chamber.

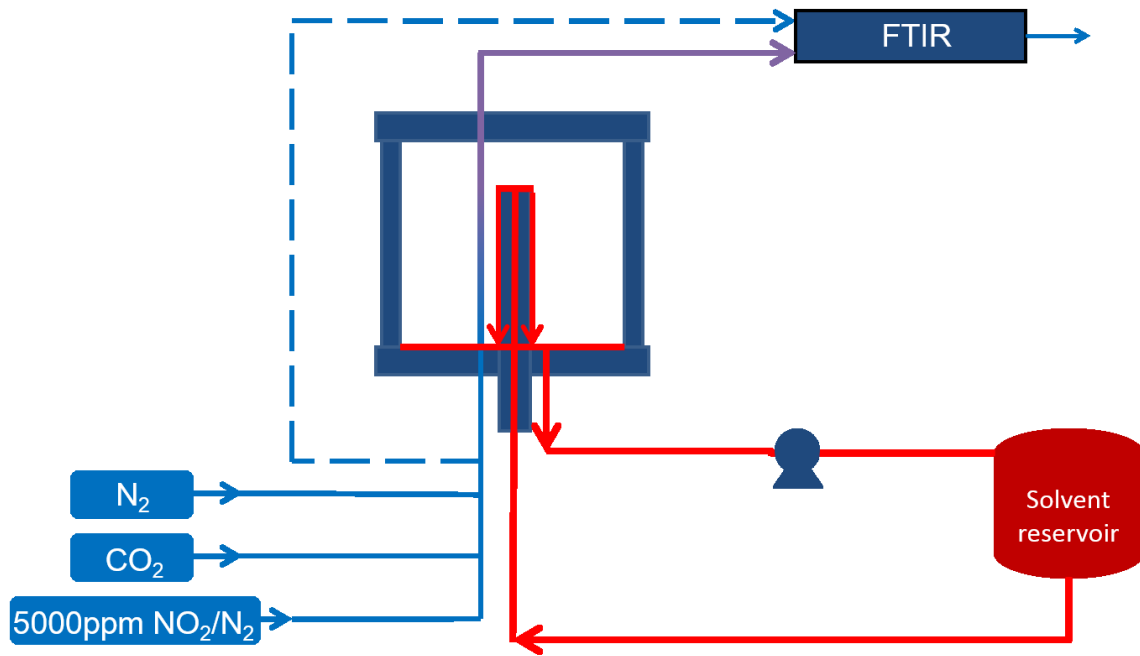


Figure 2.19: Wetted wall column apparatus

The gas-liquid interfacial area (38.5 cm^2) has been well-characterized at experimental conditions (Pacheco 1998; Bishnoi 2000). The gas-film mass transfer coefficient (k_g) in the WWC was measured by absorbing NO_2 into 5.9 m MDEA, which has negligible liquid-side mass transfer resistance. Due to the low experimental NO_2 partial pressures, total flux was much lower than typical fluxes measured using the WWC. Thus, diffusion of reactants and products from the gas-liquid interface was negligible, and all fluxes were assumed to be mass transfer with fast reaction in the pseudo-first-order regime. The reaction enhanced liquid mass transfer coefficient (k_g') could then be determined using the rate-based equation for NO_2 flux with a log mean partial pressure driving force (Equations 3–5).

$$N_{\text{NO}_2} = K_g * P_{\text{NO}_2 \text{ LM}} = \frac{G_{\text{WWC}} * (y_{\text{NO}_2 \text{ Bypass}} - y_{\text{NO}_2 \text{ WWC}})}{A_{\text{WWC}}} \quad (3)$$

$$P_{NO_2 LM} = \frac{P_{NO_2 wwc} - P_{NO_2 bypass}}{\ln \left(\frac{P_{NO_2 WWC}}{P_{NO_2 Bypass}} \right)} \quad (4)$$

$$\frac{1}{K_g} = \frac{1}{k_g} + \frac{1}{k_g'} \quad (5)$$

Conditions for the inlet gas stream are shown below (Table 2.2). The total solvent inventory for the WWC was approximately 2 L, which allowed for lengthy experiment times without appreciable accumulation of absorption products that might interfere with rate measurements.

Table 2.2: Wetted wall column gas stream conditions

| Condition | Range |
|-----------------------------|---------|
| Temperature (°C) | 20–40 |
| Pressure (psig) | 20–40 |
| Flow Rate (SLPM) | 2–7 |
| Inlet NO ₂ (ppm) | 50–300 |
| H ₂ O (%) | 2.3–7.4 |
| CO ₂ (%) | 0–4 |
| N ₂ (%) | 76–98 |

2.2.3 High Gas Flow Apparatus

The WWC is ill-suited to measure aqueous products from gas absorption because of its large inventory, so the high gas flow contactor (HGF) previously described (Sexton 2008) was modified to measure products of NO_x absorption into amines and rates of NO₂-catalyzed sulfite oxidation. Dry compressed air or N₂ passed through a temperature controlled hydrator to saturate the gas at HGF conditions. The gas was mixed with CO₂,

NO₂, and NO and then sparged at 7.5 SLPM through 350 mL of solvent (Figure 2.20); conditions for the sparging gas are given in Table 2.3. NO_x concentration at the inlet and outlet of the HGF were measured using the hot-gas FTIR or the Chemiluminescent NO_x analyzer. The gas was sparged through solution at 5–60 minute intervals to allow for the accumulation of absorption products in the liquid phase. The liquid was sampled by first setting the gas to bypass to allow the solvent to settle. The solvent was then manually mixed by drawing 20 mL of solvent into a syringe, re-injecting the solvent, and repeating three times through a septum located at the bottom of the HGF. Finally, 1 mL of sample was drawn through the septum for analysis. The sampling process was repeated at set time intervals to determine product accumulation as a function of time.

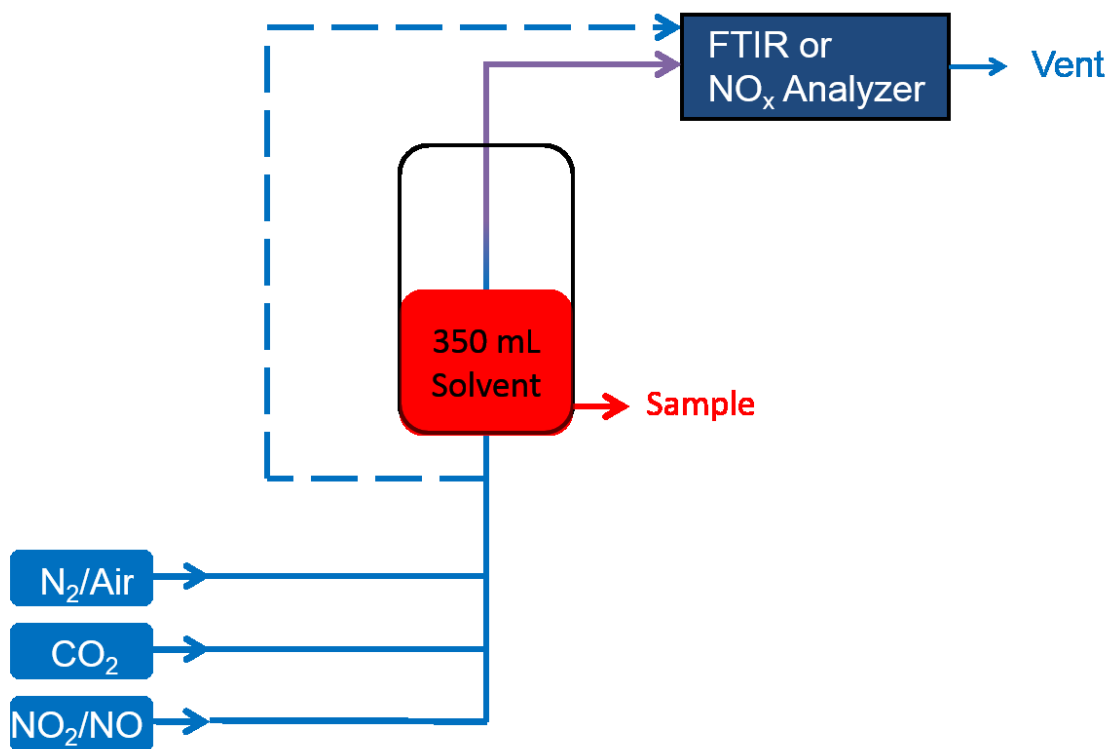


Figure 2.20: High gas flow apparatus

Table 2.3: HGF gas stream conditions

| Condition | Range |
|---------------------------|-------------|
| Temperature (°C) | 20–60 |
| Pressure | Atmospheric |
| Flow Rate (SLPM) | 7.5 |
| NO ₂ (ppm) | 2–150 |
| NO (ppm) | 0-100 |
| H ₂ O (%) | 2-20 |
| CO ₂ (%) | 0.5-6 |
| N ₂ or Air (%) | 74-98 |

The HGF was also used for relative kinetic measurements of NO_x absorption into tertiary amines at varying pH. Unlike the WWC, the area of the gas-liquid interface in the HGF is not well characterized. Therefore absorption kinetics in the HGF were only evaluated over a limited range of conditions in dilute amine solutions so that kinetics could be directly compared to each other and to WWC results. No attempt was made to quantify the gas-side mass transfer coefficient in the HGF, but the results in Chapter 3 show a strong and well-behaved absorption dependence on solvent pH. The dependence on liquid-side properties proves that gas-side mass transfer resistance was negligible at experimental conditions.

2.2.4 Hydrogen Peroxide Addition

Previous research has focused on amine oxidation with O₂ as the primary oxidizing agent (Closmann 2011; Sexton 2008; Voice 2013). These experiments took several weeks to complete due to the oxidative stability of amines. Furthermore since these experiments operated in semi-batch mode with O₂ sparging, experimental set up was intricate in order

to precisely maintain CO₂ and H₂O balance over the entire run. A quick screening experiment was conducted to replicate results obtained from the longer oxidation experiments and to screen further amines. Instead of O₂ sparging, 30 wt % hydrogen peroxide (H₂O₂) was added to loaded amine solutions spiked with dissolved manganese (Table 2.1).

Table 2.1: H₂O₂ addition conditions

| Condition | Value |
|---|-------------|
| Temperature | Room |
| Pressure | Atmospheric |
| Amine Alkalinity (m) | 10. |
| Total CO ₂ (m) | 2.0 |
| MnSO ₄ (mM) | 0.20 |
| 30 wt % H ₂ O ₂ (M) | 1.0 |
| Time (min) | > 5 |

Upon H₂O₂ addition, many amine solutions bubbled vigorously as the amine oxidized to volatile NH₃ and N₂O. A time series of degradation products from the sample showed that the reaction reached completion within the first five minutes of H₂O₂ addition. The reaction products nitrite and formate were quantified to determine the oxidation yield to nitrosating species. While this quick screening method could not be used to determine the kinetics of oxidation, it qualitatively predicted the role of amine oxidation in the accumulation of nitrosamines.

2.2.5 Thermal Reclaimer

A bench scale reclaimer was built to study the relative volatility of nitrosamines under thermal reclaiming conditions (Figure 2.21). The reclaimer consisted of a 500 mL round-bottom flask modified by the University of Texas, Department of Chemistry Glass Shop. Modifications included flattening the bottom of the flask for better heat transfer, adding three fittings to the top of the flask, and inserting a septum sample point at the bottom of the flask. The three additional fittings were used for a pressure relief valve, a liquid feed, and a temperature probe; a glass column with a fritted glass bottom was secured in the central fitting. The fittings were sealed using Teflon caps and FEP-encapsulated Viton® O-rings. The initial use of Buna O-rings in the high-temperature corrosive environment led to O-ring failure and gas leakage. The flask was wrapped with insulating cloth and placed on a combination hot-plate and stirrer.

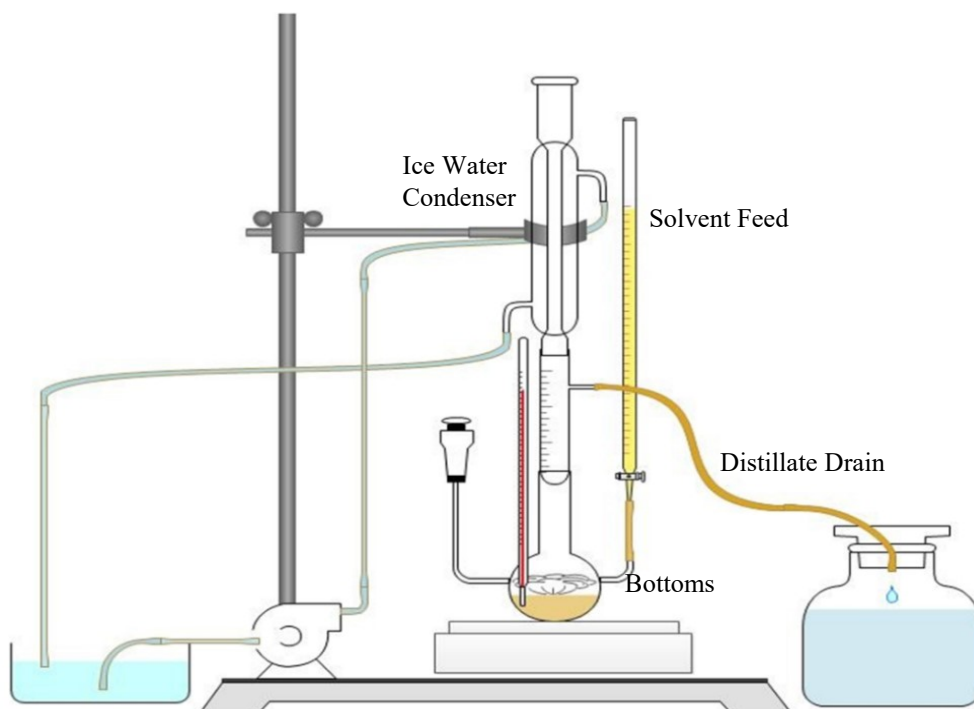


Figure 2.21: Bench-scale thermal reclaimer

Approximately 250 mL of degraded pilot plant solvent containing nitrosamines was loaded into the thermal reclaimer and heated to its bubble point at atmospheric pressure. During heating, the temperature would rise steadily until the bubble point was reached and then increase very gradually as volatile products evaporated. The gas traveled through the fritted glass into the glass column, condensing on the walls of the column. Any gas escaping the glass column would be refluxed back using an ice water condenser. Feed solvent from the original pilot plant sample was manually fed into the thermal reclaimer using a burette with a stop-cock to insure that the reclaimer inventory was maintained at 250 mL. Over time the distillate would accumulate in the glass column and drain into a collection vessel. The temperature could only be raised by evaporating enough volatile components that the bubble point of the bottoms changed, which took approximately 1 hour for every 10 °C at 120–160 °C. Samples of the distillate and the bottoms were collected during the process and analyzed to determine the relative volatility of nitrosamines and amine at reclaimer conditions. At high temperatures the bottoms became extremely viscous due to the build-up of viscous non-volatiles and the loss of water. The sample had a tendency to solidify upon cooling, so sample was immediately gravimetrically diluted in water by 10x before it could solidify.

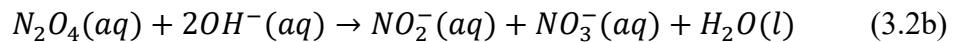
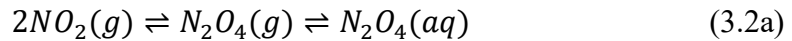
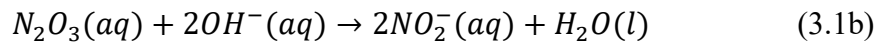
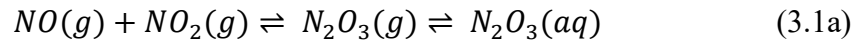
Chapter 3: Absorption of Nitrogen Oxides in Aqueous Amines

Chapter 3 gives results for NO_x absorption into amine solutions at the ppm-level NO_x concentrations typical of flue gas from fossil fuel power plants. The majority of this chapter has been previously published (Fine and Rochelle 2014). In Section 3.2, NO₂ absorption rates into amine solutions are quantified and used to model NO₂ uptake at typical absorber and pre-scrubber conditions. Yields for NO_x absorption product are quantified in Section 3.3 to understand the mechanism behind NO_x absorption and determine the relative importance of different nitrosating agents for total nitrosamine accumulation.

3.1 PREVIOUS RESEARCH ON NO_x ABSORPTION

3.1.1 NO_x Absorption into Aqueous Solutions

NO_x absorption at high NO_x partial pressures has been heavily studied for the manufacturing of nitric acid (Pradhan and Joshi 2000). With NO_x concentration at approximately 10 % by volume, NO_x absorption is dominated by the molecular absorption of dinitrogen trioxide (N₂O₃), and dinitrogen tetroxide (N₂O₄) via acid-base reactions (Equations 3.1 & 3.2).



Absorption of N_2O_4 is pH independent above a pH of 5 since the pK_a of HNO_3 is low enough that it is completely dissociated in solution. However, the absorption of N_2O_3 depends on basicity due to the speciation of HNO_2 in the boundary layer. The fastest absorption rates are above a pH of 7 where HNO_2 is also completely dissociated in the boundary layer (Patwardhan and Joshi 2003). Absorption is fast and only dependent on base strength, so relatively cheap sources of alkalinity such as NaOH and $\text{Ca}(\text{OH})_2$ are used.

The gas-phase equilibria for N_2O_3 and N_2O_4 are both second order in NO_x . Thus as NO_x partial pressures decrease, N_2O_3 and N_2O_4 comprise a decreasing proportion of total NO_x . Even after accounting for the greater solubility of N_2O_3 and N_2O_4 , only 0.2 % of total physically absorbed NO_x at the gas-liquid interface exists as N_2O_3 or N_2O_4 at typical flue gas conditions compared to 66 % during nitric acid manufacturing (Table 3.1).

Table 3.1: NO_x speciation in water under nitric acid manufacturing and flue gas conditions ($T = 25^\circ\text{C}$, $P = 1$ Bar). Equilibria and Henry's constants from Patwardhan et al. (2003).

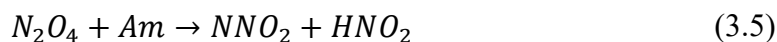
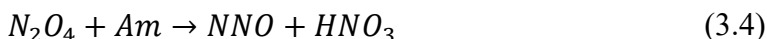
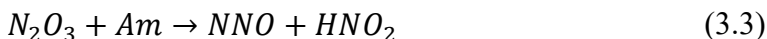
| Species | Henry's constant (M/Pa) | Conc. in equilibrium with 10 % NO_x , 0.5 % NO_2 (M) | Conc. in equilibrium with 100 ppm NO_x , 5 ppm NO_2 (M) |
|------------------------|----------------------------|---|--|
| NO | 1.84E-08 | 1.7E-04 | 1.7E-07 |
| NO_2 | 1.18E-07 | 2.9E-05 | 3.6E-08 |
| N_2O_3 | 5.92E-06 | 1.5E-04 | 1.5E-10 |
| N_2O_4 | 1.38E-05 | 2.3E-04 | 2.3E-10 |

Due to the low concentration of physically absorbed N_2O_3 and N_2O_4 , research for ppm-level NO_x absorption at flue gas conditions has focused on the direct free-radical absorption of NO_2 . Sulfite, bisulfite, and sulfide all absorb NO_2 directly, greatly enhancing absorption at low NO_x levels (Shen 1997; Takeuchi, Ando, and Kizawa 1977; Kameoka

and Pigford 1977). Amines also enhance NO_x absorption with tertiary amines offering the highest absorption rates (Mimura, Shimojo, and Mitsuoka 1997).

3.1.2 Nitrosamine Formation from NO_x Absorption

Nitrosamines and nitramines have been shown to form during NO_x absorption into amine solutions at alkaline conditions (Dai and Mitch 2013; Chandan et al. 2013; Challis and Kyrtopoulos 1976; Jackson and Attalla 2010). At high NO_x concentration, this can be attributed to the absorption of N₂O₃ and N₂O₄, two strong nitrosating and nitrating agents (Equations 3.3–3.5) (Douglass and Kabacoff 1978).



However, Challis et al. theorized that at low NO_x concentrations and low amine concentrations, nitrosation and nitration are more likely to occur through free-radical absorption of NO₂ followed by the amino radical reaction with NO or NO₂ (Figure 3.1). Unlike nitrosation with N₂O₃, the series reaction mechanism does not necessarily produce equivalent amounts of nitrosamine and nitrite since the intermediate amine radical may react with species other than NO.

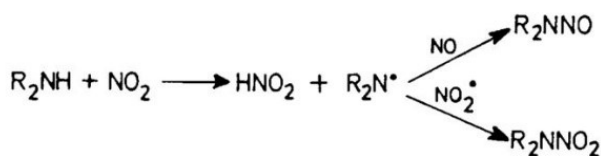


Figure 3.1: Series reaction to form nitrosamine (Challis and Kyrtopoulos 1976)

Various researchers have recently studied nitrosamine and nitramine yield from NO_x absorption in the context of amine scrubbing. In one experiment, an unloaded 5 M morpholine solution was sparged with dilute NO_x in air at varying ratios of NO and NO_2 . Rates of absorption with 25 ppm NO alone were exceedingly low. Nitrite dominated the absorption products, suggesting that NO must oxidize to NO_2 prior to absorption (Dai et al. 2012). Absorption of 25 ppm NO_2 yielded over 95% nitrite and less than 5 % nitramine/nitrosamine, proving that N_2O_4 could not be the absorbing species. Nitrosamine yield doubled when 25 ppm NO was added to the base case of 25 ppm NO_2 (Dai et al. 2012), corroborating the series reaction hypothesis (Figure 3.1). Dai et al. later discounted the possibility of the series reaction due to low nitramine yield at all reaction conditions (Dai and Mitch 2014b). They concluded that the amino radical is unstable and should be equally reactive towards NO_2 and NO. Since NO_2 , the nitramine precursor, is more soluble than NO, nitramine yield should be higher than nitrosamine yield when NO_2 and NO partial pressures are roughly equivalent. However, Dai et al. neglected the fast reaction of NO_2 with amine, which scavenges any physically dissolved NO_2 in the reaction boundary layer. In comparison, NO is unreactive towards the amine so physically dissolved NO has more opportunity to react with the amino radical.

Chandan et al. found that nitrosomorpholine production increased with increasing morpholine concentration and usually decreased with increasing CO_2 loading, demonstrating that free amine is most likely forming nitrosamines at absorber conditions (Chandan et al. 2013). At CO_2 loadings above 0.4, Chandan et al. reported that nitrosamine yield began to increase again, suggesting an alternative nitrosating pathway. Similarly, n-nitrosopiperazine was observed when 15 wt % PZ was sparged with 8,000 ppm NO in 5 % O_2 , but no effort was made to quantify other absorption products (Jackson and Attalla 2010).

3.1.3 Limiting Nitrosamine Formation in the Absorber

Two main approaches have been taken to limit nitrosamine formation under absorber conditions. Primary and tertiary amines have been chosen for CO₂ capture since they show very little direct formation of nitrosamines (Dai and Mitch 2013). However, caution must be taken with laboratory results since these experiments were run with laboratory-grade amines that contain almost no secondary amine impurity. Aker Solutions has formulated a proprietary solvent that contains no secondary amine (Gorset et al. 2013). Nitrosamine build-up has been relatively slow in the solvent, reaching 0.11 mmol/kg after 1400 hours of operation on a cement kiln flue gas containing 150 ppm NO_x (Knudsen et al. 2014). However, rate of nitrosamine formation has increased from an initial rate of 0.74 $\mu\text{mol/kg/day}$ to 2.01 $\mu\text{mol/kg/day}$, suggesting that build-up of secondary amine products is driving nitrosamine formation. Second, free-radical scavengers have been added to the solvent to react with the intermediate amino radical. This has proven to be successful under absorber conditions with a 95 % decrease in nitrosomorpholine yield upon addition of 5 mM ethoxyquin (Chandan, Remias, and Liu 2014). Unfortunately, free-radical scavenging can also enhance overall nitrosamine formation because the additives also aid in NO₂ uptake as nitrite. Since nitrite is a nitrosating agent under stripper conditions, free-radical scavengers could increase nitrosamine accumulation when the amine is regenerated (Chandan, Remias, and Liu 2014). Furthermore, traditional nitrite scavengers at gastric conditions such as ascorbic acid (Mirvish 1975) have not inhibited nitrosamine formation at high temperatures in loaded amine solutions due to fast amine nitrosation rates (Voice 2013).

3.1.4 Open Research Questions

Current research has conclusively shown that nitramines do not accumulate from ppm-level NO_x absorption in amines, nitrosamines quantifiably accumulate, and nitrite is

the dominant absorption product. However, rates for NO_x absorption have not been previously quantified in the literature. These rates determine NO_x uptake in the absorber, which in turn will help quantify the role of NO_x absorption in nitrosamine accumulation.

While some experiments operated close to flue gas conditions, the majority of experiments were run with high NO_x partial pressures. Since NO_x speciation is a strong function of partial pressure, it is important to run as close to real flue gas conditions as possible to minimize extrapolation errors. Other NO_x absorption products such as nitrite and nitrate are not quantified in most experiments, and a gas-phase mass balance around absorbed NO_x has never been performed, making it impossible to close the mass balance on NO_x absorption products. The lack of comprehensive mass balances at flue gas conditions has led to confusion in the absorption mechanism.

Finally, most work does not consider nitrite as a nitrosating agent, which leads to underprediction of overall nitrosamine formation in a real system. While some researchers have suggested NO_x scavenging using free-radical scavengers in the CO_2 scrubber, there is no published work on using tertiary amines for NO_x pre-scrubbing. Since the pre-scrubbing solvent is not heated, any nitrite formed in the pre-scrubber is stable and can be discounted from overall nitrosamine accumulation. Thus it is important to understand NO_x absorption kinetics and products under pre-scrubbing conditions in order to perform an economic evaluation of this nitrosamine mitigation technique.

3.2 NO_2 ABSORPTION KINETICS

3.2.1 Wetted Wall Column Results

Table 3.2 gives all the results for wetted wall column experiments measuring the overall liquid side mass transfer coefficient (k_g') for NO_2 absorption into aqueous amines. Fluxes were measured with 1–30 Pa NO_2 in hydrated N_2 and CO_2 such that water and CO_2

were always in equilibrium with the solvent. The overall mass-transfer coefficient was then linearly regressed from the flux; gas-side mass transfer resistance was subtracted from the total resistance, leaving only liquid-side resistance ($1/k_g'$). NO₂ absorption was modeled as a fast reaction in the liquid boundary layer with the pseudo-first-order assumption. NO₂ hydrolysis was assumed to be second order in NO₂ partial pressure while NO₂ absorption in amine was assumed to be first order.

Table 3.2: NO₂ absorption kinetics in the WWC, $P_{NO_2} = 1\text{--}30$ Pa

| Exp. # | Solution | CO ₂ Ldg | T (°C) | $k_g' \cdot 10^7$ |
|--------|--------------|---------------------|--------|---|
| | | Mol/equiv N | | (mol m ⁻² s ⁻¹ Pa ⁻¹) |
| 3.1 | 0.001 M NaOH | 0 | 20 | $0.13\sqrt{P_{NO_2}}$ |
| 3.2 | 0.001 M NaOH | 0 | 40 | $0.11\sqrt{P_{NO_2}}$ |
| 3.3 | 5 m MEA | 0.48 | 20 | 1.6 |
| 3.4 | 5 m MEA | 0.48 | 40 | 1.9 |
| 3.5 | 9 m MEA | 0.38 | 40 | 3.0 |
| 3.6 | 9 m MEA | 0.48 | 20 | 1.8 |
| 3.7 | 9 m MEA | 0.48 | 40 | 2.0 |
| 3.8 | 8 m PZ | 0.26 | 40 | 13.7 |
| 3.9 | 8 m PZ | 0.32 | 20 | 7.2 |
| 3.10 | 8 m PZ | 0.32 | 40 | 9.7 |
| 3.11 | 8 m PZ | 0.39 | 40 | 8.0 |
| 3.12 | 0.40 m MDEA | 0 | 20 | 36.9 |
| 3.13 | 0.40 m MDEA | 0 | 40 | 41.3 |
| 3.14 | 0.056 m MDEA | 0 | 20 | 11.8 |
| 3.15 | 0.056 m MDEA | 0 | 40 | 15.4 |

Table 3.2 Cont.

| | | | | |
|-------------|--------------|---|----|-----|
| 3.16 | 0.023 m MDEA | 0 | 20 | 7.5 |
| 3.17 | 0.023 m MDEA | 0 | 40 | 9.8 |

3.2.2 NO₂ Absorption Kinetics in Water

Under basic conditions NO₂ absorbs into water via N₂O₄ formation. Using film theory, the solution for NO₂ flux is given by Equation 3.6 (Kameoka and Pigford 1977). Gas side mass transfer resistance can be ignored due to the relatively slow reaction kinetics. The flux can also experimentally be determined using the gas molar flow rate, the NO₂ partial pressure difference going into and coming out of the WWC, and the gas-liquid contact area (Equation 3.7).

$$N_{NO_2} = P_{NO_2} \sqrt{\frac{2k_{H_2O} D_{N_2O_4} P_{NO_2}}{3H_{N_2O_4}^2}} = C_1 * P_{NO_2}^{3/2} = k'_g * P_{NO_2} \quad (3.6)$$

$$N_{NO_2} = \frac{1}{A} \frac{P\dot{V}}{RT} (P_{NO_2 \text{ Byp}} - P_{NO_2 \text{ WWC}}) \quad (3.7)$$

The flux of NO₂ into 0.001 M NaOH was measured from 2-30 Pa NO₂ at 20 °C and 40 °C. Flux as a function of NO₂ partial pressure was regressed using Equation 3.6 with C₁ as a free parameter. Values for C₁ were 0.13 and 0.11 $\frac{\text{mol}}{\text{m}^2 \text{ s Pa}^{3/2}}$ at 20 and 40 °C respectively. The data agree well with the literature even though the experiments were run at different partial pressures and on different apparatuses (Figure 3.2). The experiment was attempted at 60 °C, but the results drastically overpredicted k_g'. This was most likely due to water condensation in the lines directly after the WWC, which provided extra surface area for NO₂ absorption. Absorption rates for N₂O₄ hydrolysis show almost no dependence on temperature due to competing factors in Equation 3.6. The reaction kinetics and diffusivity increase with temperature, but N₂O₄ solubility decreases such that k_g' remains

approximately constant (Kameoka and Pigford 1977). A similar lack of temperature dependence on k_g has been observed for CO₂ absorption in PZ (Dugas 2009).

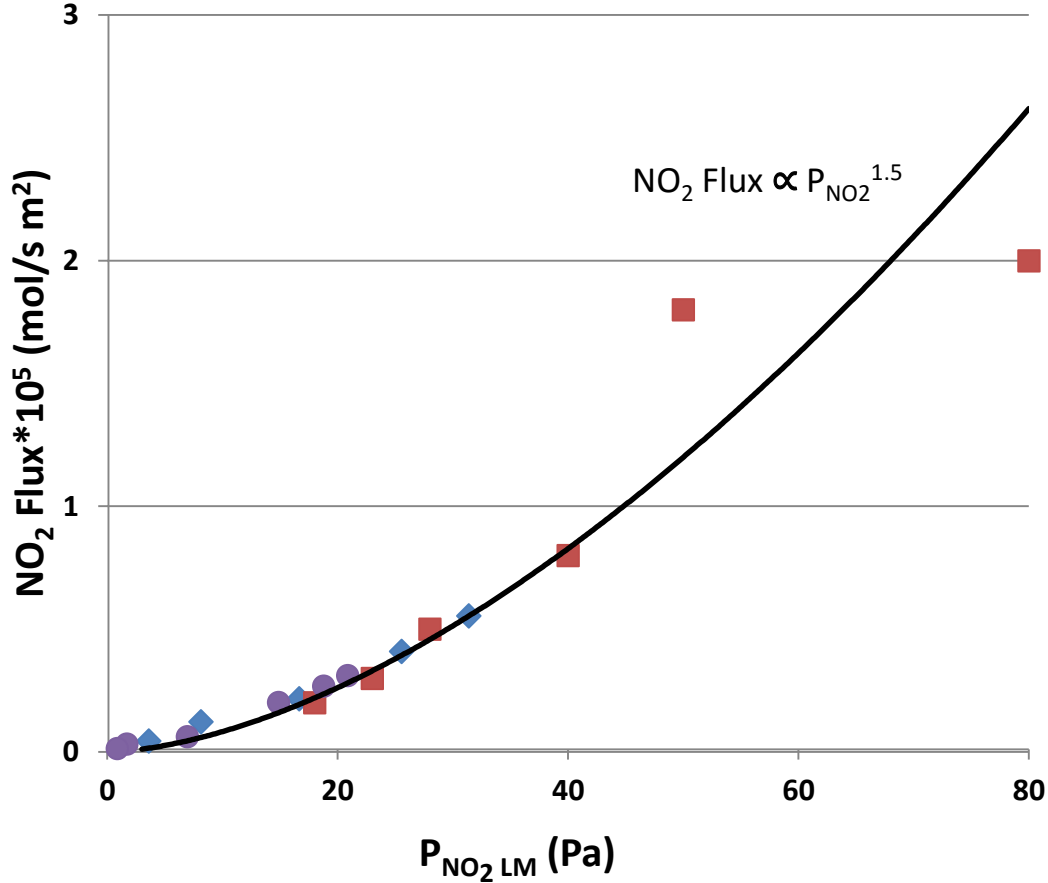


Figure 3.2: NO₂ hydrolysis in the WWC at 20 °C (◆, Exp. 3.1) and 40 °C (●, Exp. 3.2) compared to NO₂ hydrolysis in the stirred cell at 25 °C (Shen 1997) (■).

3.2.3 Data Analysis for NO₂ Absorption Kinetics in Amines

NO₂ flux was measured in the wetted wall column at partial pressures ranging from 1–15 Pa. The gas side mass transfer coefficient (k_g) was measured with NO₂ absorption into 5.9 m methyldiethanolamine (MDEA) at 2.9 SLPM and 20 °C, which has negligible liquid-side mass transfer resistance. The value for k_g was $25.2 \cdot 10^{-7} \frac{\text{mol}}{\text{m}^2 \text{ s Pa}}$, approximately

30% higher than the k_g predicted for the wetted wall column under these conditions (Pacheco 1998; Bishnoi 2000). In contrast to NO_2 hydrolysis, NO_2 flux into amine solutions was linear with respect to NO_2 partial pressure and passed through zero, suggesting that NO_2 absorption is dominated by first-order free-radical absorption under experimental conditions. Each experiment consisted of four or five absorption points that were linearly regressed with a y-intercept set to zero; the slope of the line represents the overall mass transfer coefficient (K_g). Sample raw data and calculations for Experiment 3.17 are shown in Equations 3.8–3.10 and Figure 3.3.

$$N_{\text{NO}_2} = K_g * P_{\text{NO}_2 \text{ LM}} = \frac{G_{\text{WWC}} * (P_{\text{NO}_2 \text{ Bypass}} - P_{\text{NO}_2 \text{ WWC}})}{A_{\text{WWC}}} \quad (3.8a)$$

$$K_g * P_{\text{NO}_2 \text{ LM}} = \frac{5.59 * 10^{-4} \frac{\text{mol}}{\text{s}}}{0.00385 \text{ m}^2} * (10.9 \text{ Pa} - 6.7 \text{ Pa}) \quad (3.8b)$$

$$P_{\text{NO}_2 \text{ LM}} = \frac{P_{\text{NO}_2 \text{ WWC}} - P_{\text{NO}_2 \text{ bypass}}}{\ln\left(\frac{P_{\text{NO}_2 \text{ WWC}}}{P_{\text{NO}_2 \text{ Bypass}}}\right)} \quad (3.9a)$$

$$P_{\text{NO}_2 \text{ LM}} = \frac{6.7 \text{ Pa} - 10.9 \text{ Pa}}{\ln\left(\frac{6.7 \text{ Pa}}{10.9 \text{ Pa}}\right)} = 8.6 \text{ Pa} \quad (3.9b)$$

$$\frac{1}{K_g} = \frac{1}{k_g} + \frac{1}{k_g'} \quad (3.10a)$$

$$k_g' = \left(\frac{1}{7.1 * 10^{-7}} - \frac{1}{25.2 * 10^{-7}} \right)^{-1} = 9.8 * 10^{-7} \frac{\text{mol}}{\text{s} \cdot \text{m}^2 \cdot \text{Pa}} \quad (3.10b)$$

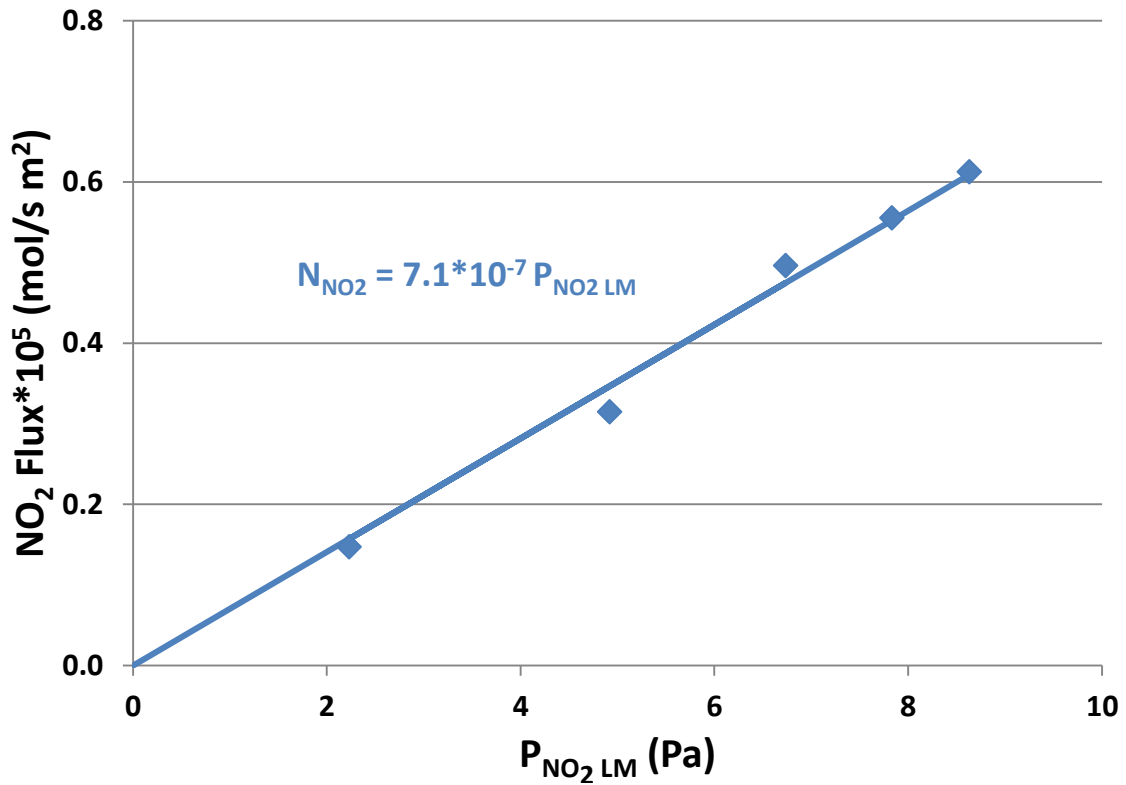


Figure 3.3: WWC raw data for NO₂ Flux into unloaded 0.023 m MDEA at 40 °C (Exp. 3.17).

3.2.4 Results for NO₂ Absorption Kinetics in Amines

The free-radical absorption of NO₂ as nitrite is hypothesized to be first order in free amine. Assuming that the diffusion of amine to the gas-liquid boundary layer is fast enough that the pseudo-first order approximation holds, the overall liquid-side mass transfer coefficient in partial pressure units (k'_g) will have a half-order amine dependence (Danckwerts 1950) (Equation 3.11).

$$k'_g = \sqrt{\frac{k_{Am}[Am]_{Free}D_{NO_2}}{H_{NO_2}^2}} \quad (3.11)$$

The k'_g for NO₂ absorption into dilute MDEA is approximately half-order in total MDEA as hypothesized. The k'_g also decreases with increased loading in PZ and MEA

solutions since the free amine alkalinity decreases (Figure 3.4). However, k_g' flattens out at higher PZ loadings, suggesting that other PZ species such as PZH^+ and $PZCOO^-$ could also absorb NO_2 . Finally, k_g' increases with increasing order of amines ($RNH_2 < R_2NH < R_3N$) similar to the free-radical absorption of ClO_2 in amines (Rochelle et al. 2001; Neta, Huie, and Ross 1988). Rates increase 10–30 % going from 20 to 40 °C across all three amines, for an apparent activation energy of 7 ± 3 kJ/mol. The small temperature dependence is expected due to the competing trends between reaction kinetics and NO_2 solubility.

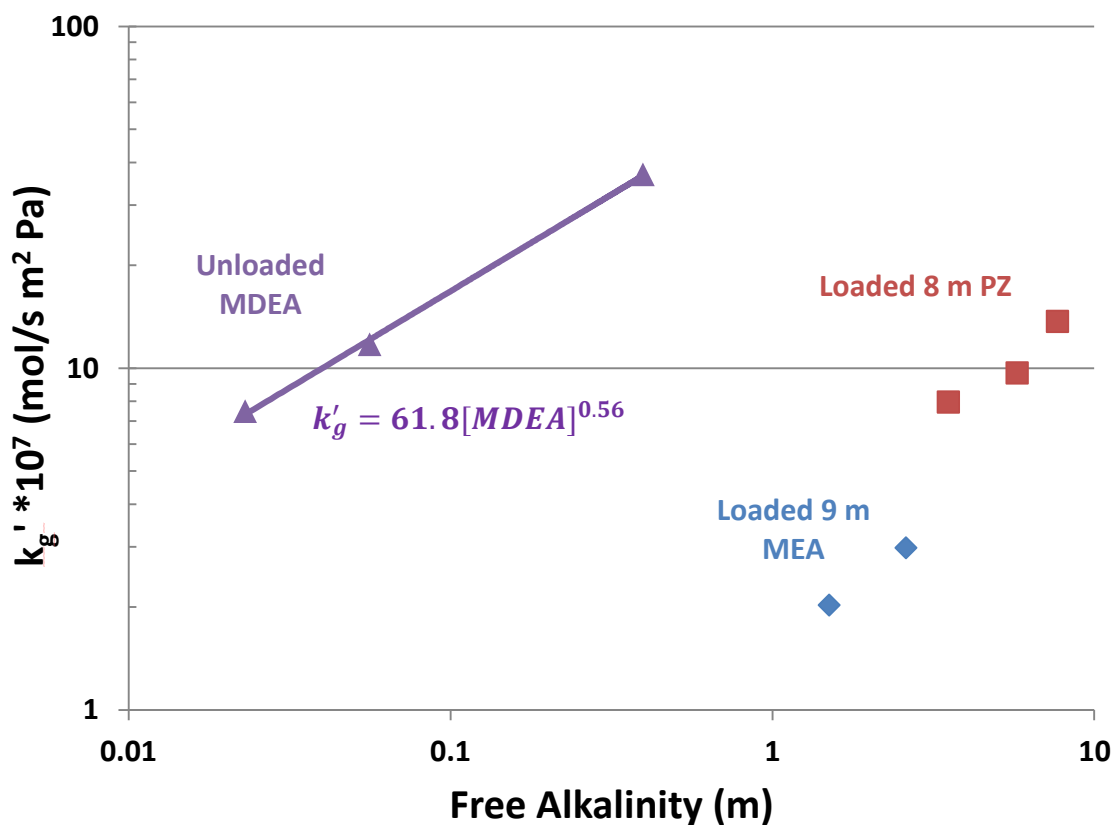


Figure 3.4: k_g' in the WWC for MDEA (\blacktriangle), MEA(\blacklozenge), and PZ(\blacksquare) at 40 °C; 1–15 Pa NO_2 in hydrated N_2 with CO_2 ; free alkalinity in CO_2 loaded MEA and PZ calculated using AspenPlus® Phoenix and Independence models respectively (Exp. 3.5, 7, 8, 10, 11, 13, 15 & 17).

3.2.5 Modeling Total NO₂ Uptake in the Absorber

NO₂ from a fossil-fuel fired power plant typically enters the absorber at 0.05 – 0.5 Pa depending on the burner technology, the fuel type, and the use of any NO_x mitigation technologies. Thus, while N₂O₄ hydrolysis plays a minor role at experimental conditions with NO₂ partial pressures greater than 1 Pascal, hydrolysis accounts for less than 3 % of NO₂ kinetics at flue gas conditions (Figure 3.5).

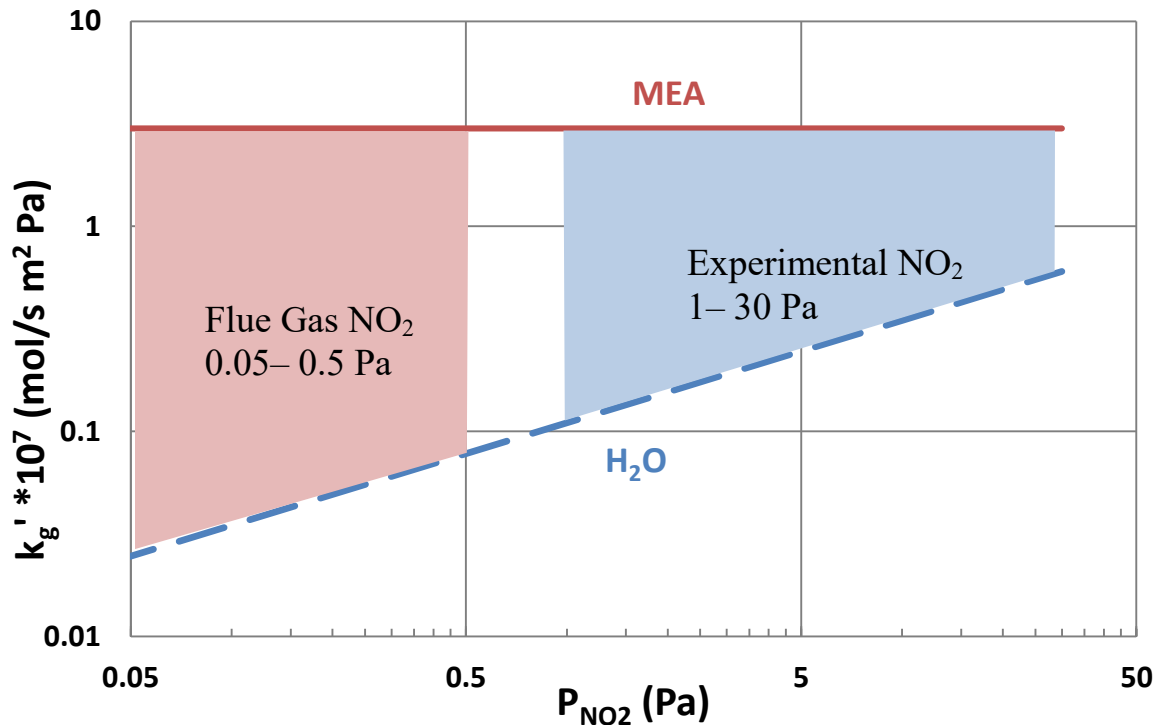


Figure 3.5: NO₂ absorption at 40 °C into 9 m MEA, $\alpha = 0.38$ (— Exp. 3.5) compared to water (- - - Exp 3.2).

The fraction of NO₂ absorbed during CO₂ scrubbing can be estimated from the mass transfer coefficients and total wetted area of an amine scrubber (Equations 3.12 & 3.13).

$$Uptake (\%) = 100 * \frac{NO_{2 \text{ absorbed}}}{NO_{2 \text{ Flue}}} = 100 * (1 - e^{-N_{OG}}) \quad (3.12)$$

$$N_{OG} = K_G * \frac{a_{e \text{ scrubber}}}{G} \quad (3.13)$$

The wetted area for a typical CO₂ scrubber can vary widely depending on the solvent, the packing type, and process specifications such as lean loading and solvent flow rate. Typical wetted areas for 9 m MEA and 8 m PZ were calculated using AspenPlus ® with the Phoenix model (Plaza 2011) and Independence model (Frailie 2014) respectively. The absorber columns were modeled for a pre-cooled flue gas from a 550 MW supercritical coal-fired power plant at 12 % inlet CO₂ and 40 °C (NETL 2010). The lean loading had a CO₂ equilibrium partial pressure of 0.5 kPa, the solvent flow rate was set to 1.2 times the minimum solvent flow rate needed for 90% CO₂ removal ($L/L_{min} = 1.2$), and the solvent was intercooled to 40 °C halfway through the column. Since CO₂ absorption rates are approximately twice as fast in PZ at process conditions, its a_e/G was much lower than that of MEA. The 7 m MDEA/ 2m PZ blend was conservatively given the same wetted area as PZ; NO₂ uptake solely from hydrolysis is shown to demonstrate the importance of determining free-radical NO₂ absorption to accurately model nitrosamine accumulation (Table 3.3). A typical MEA absorber designed for 90 % CO₂ capture will absorb roughly 70 % of inlet NO₂, PZ will absorb 90 %, and MDEA/PZ will absorb over 99 %. NO₂ hydrolysis can only account for 4 % of total NO₂ absorption.

Table 3.3: NO₂ absorbed in typical amine scrubbers; $P^*_{CO_2}=0.5$ kPa at α_{lean} , $L/L_{min} = 1.2$, 90 % CO₂ removal, 40 °C inlet and intercooling T, intercooled halfway.

| Solvent | A/G (m ² s Pa/mol) | K _g (mol/m ² s Pa) | NO ₂ Uptake (%) |
|------------------------|-------------------------------|--|----------------------------|
| 9 m MEA | 4.3*10 ⁶ | 3.0*10 ⁻⁷ | 73 |
| 8 m PZ | 2.6*10 ⁶ | 9.7*10 ⁻⁷ | 92 |
| 7 m MDEA/2 m PZ | 2.6*10 ⁶ | k _g limited | >99 |

Table 3.3 Cont.

| | | | |
|--|---------------------|-----------------------|---|
| Water at 2 ppm NO₂ | 2.6*10 ⁶ | 0.16*10 ⁻⁷ | 4 |
|--|---------------------|-----------------------|---|

3.2.6 Data Analysis for NO₂ Absorption into Dilute Tertiary Amines

NO₂ absorption rates were also measured in dilute tertiary amines using the High Gas Flow Apparatus (HGF). The HGF was inherently less accurate than the WWC since the gas-liquid interfacial area was created through turbulence from gas sparging. This limited the range of experimental conditions that were directly comparable since physical properties such as viscosity, surface tension, and density must be held constant across all experiments. Additionally, since the contact area was unknown, rates could only be compared relative to each other.

Relative NO₂ absorption rates for 0.1 m MDEA, triethanolamine (TEA), and 4-(2-hydroxyethyl)morpholine (2HeMorph) were measured at varying pH. The sparging gas was hydrated N₂ with 100 ppm NO and 30 ppm NO₂; NO absorption was below quantification for all runs (less than 3 ppm NO difference between inlet and outlet conditions). Since flux was only measured at one partial pressure for each condition, Equation 3.9 can be directly solved for the K_gA of the HGF (Equations 3.14 & 3.15).

$$N_{NO_2} = K_g * P_{NO_2 LM} = \frac{G_{HGF} * (P_{NO_2 Bypass} - P_{NO_2 HGF})}{A_{HGF}} \quad (3.14)$$

$$K_g A_{HGF} = -G_{HGF} * \ln \left(\frac{y_{NO_2 Bypass}}{y_{NO_2 HGF}} \right) \quad (3.15)$$

A 6 mL sample of the stock solution was taken prior to the experiment, diluted a factor of 10, and directly titrated to empirically determine the pK_a of the amine at experimental concentration (Figure 3.6). After each data point, a 1 mL sample was removed from the HGF, diluted a factor of 10, and analyzed for pH. Approximately 1 mL

of 1 M H₂SO₄ was then added to solution and the experiment was repeated. Free amine in solution was calculated using the pH after H₂SO₄ addition and the amine pK_a (Equations 3.16 & 3.17). NO₂ absorption was assumed to be half-order in the free amine concentration and first order in NO₂. Assuming mass transfer was reaction-limited in the HGF, K_gA could then be modeled using Equation 3.18 with C₂ as a free parameter.

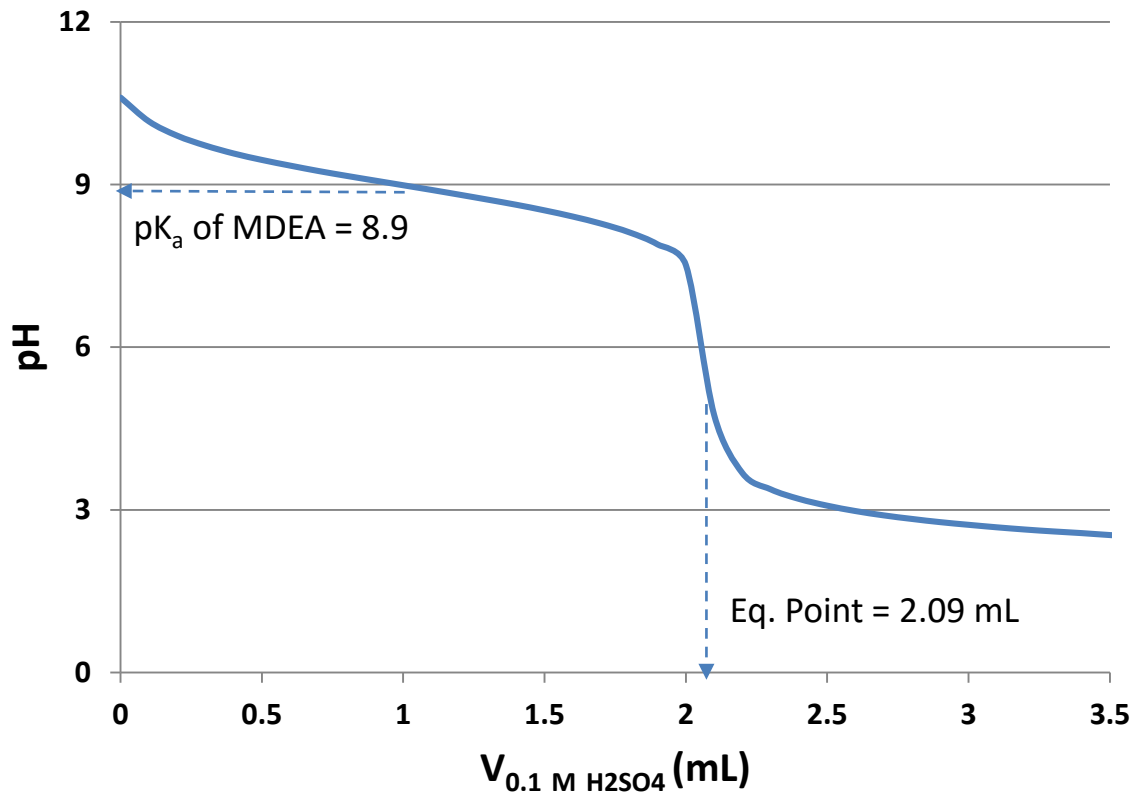


Figure 3.6: Titration curve for determining pK_a of 0.01 m MDEA at room temperature.

$$[Am]_T = [Am]_{free} + [AmH^+] \quad (3.16)$$

$$\frac{[Am]_{free}}{[AmH^+]} = 10^{pH - pK_{a, Am}} \quad (3.17)$$

$$K_g A \approx k'_g A = C_2 \sqrt{[Am]_{free}} \quad (3.18)$$

3.2.7 Results for NO₂ Absorption into Dilute Tertiary Amines

Figure 3.7 shows $K_g A$ varying with the square root of MDEA concentration, proving that mass transfer in the HGF is reaction-limited. A small amount of NO₂ continued to absorb as free MDEA concentration approached zero, most likely from N₂O₄ or N₂O₃ absorption. A k_g' value for 0.08 m MDEA was interpolated from the MDEA WWC experimental results and used as a comparison point for all of the HGF values. The area of the gas-liquid interface in the HGF under these sparging conditions is approximately 0.027 m² (Equation 3.19).

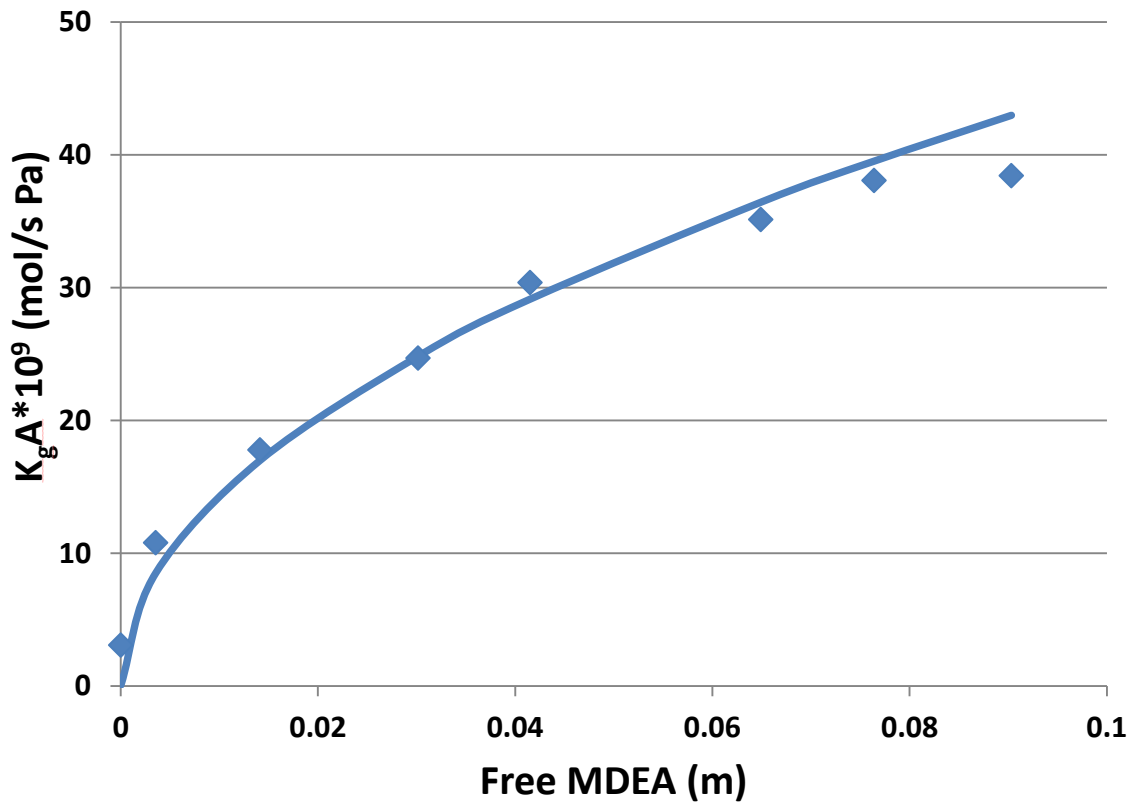


Figure 3.7: NO₂ absorption into 0.1 m MDEA using HGF. Data from Equation 3.15; Model from Equation 3.18 with $C_2 = 143.4$; $T = 20$ °C, pH varied with 1 M H₂SO₄, 100 ppm NO, 30 ppm NO₂ in hydrated N₂.

$$K_g A_{HGF} = 4.1 * 10^{-8} \frac{\text{mol}}{\text{s} \cdot \text{Pa}} = k_g'_{0.08 \text{ m MDEA}} * A_{HGF} \quad (3.19a)$$

$$A_{HGF} = \frac{4.1 * 10^{-8} \frac{\text{mol}}{\text{s} \cdot \text{Pa}}}{1.5 * 10^{-6} \frac{\text{mol}}{\text{s} \cdot \text{Pa} \cdot \text{m}^2}} = 0.027 \text{m}^2 \quad (3.19b)$$

In an SO₂ pre-scrubber, NaOH primarily acts as the alkalinity source for SO₂ removal to sulfite or sulfate. A small excess of NaOH is usually added for pH control; the NaOH absorbs CO₂ to create a CO₂/HCO₃⁻ buffer at pH = 7–8. Rates for NO₂ absorption in TEA and 2HeMorph, two tertiary amines with a lower pK_a than MDEA, were quantified as a function of pH. At a pH greater than 9, MDEA absorbs NO₂ the fastest with rates 50 % higher than TEA and 100 % higher than 2HeMorph. However, in the pH range of a NaOH pre-scrubber, TEA absorption rates are 35–100 % faster than MDEA since there is more free TEA available in this pH range. None of the tertiary amines absorb NO₂ below pH = 6 where the free tertiary amine concentration approaches zero (Figure 3.8). Since TEA is an inexpensive tertiary amine with high NO₂ absorption rates at pre-scrubbing conditions, it was chosen for a techno-economic analysis on NO₂ pre-scrubbing (Chapter 7).

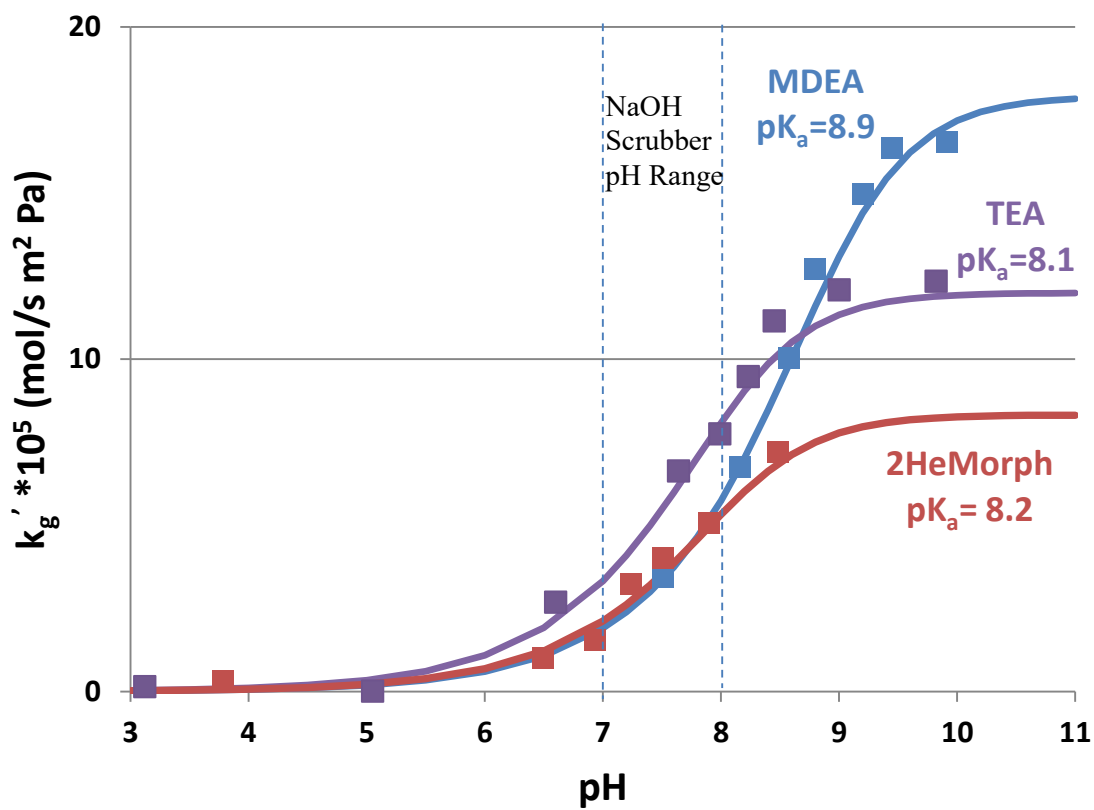


Figure 3.8: NO_2 absorption into 0.1 m tertiary amines using HGF; Model from Equation 3.18; $T = 20^\circ\text{C}$, pH varied with 1 M H_2SO_4 , 100 ppm NO, 30 ppm NO_2 in hydrated N_2 .

3.3 NO_x ABSORPTION PRODUCTS

3.3.1 NO_2 Pre-scrubbing using Tertiary Amines

Tertiary amines are promising candidates for scrubbing NO_2 in a polishing scrubber before it reaches the absorber. Since NO does not absorb into solution by itself, only NO_2 needs to be removed from the flue gas prior to the CO_2 scrubber to reduce the available nitrite, and ultimately reduce nitrosamine accumulation. As discussed further in Chapter 7, a NaOH polishing scrubber designed for SO_2 removal could remove 90 % of inlet NO_2 with approximately 0.2 m tertiary amine additive.

Previously, sodium sulfite has been studied for scrubbing NO₂ from flue gas. However, in aerobic environments sulfite catalytically oxidizes, drastically decreasing free sulfite in the boundary layer. The oxidation can decrease the rate of NO₂ absorption by 40 % compared to an oxygen-free environment, necessitating the use of oxidation inhibitors (Kameoka and Pigford 1977; Shen and Rochelle 1999). In comparison, tertiary amines are oxidatively stable at low temperatures, so there is no expected penalty for NO_x absorption in aerobic environments. NO_x was sparged into 0.1 m MDEA solution using the HGF apparatus under both aerobic and anaerobic conditions to show that NO₂ can effectively be removed from the flue gas without directly forming nitrosamines or catalytically oxidizing the amine.

3.3.2 NO₂ Absorption into 0.1 m MDEA

Hydrated N₂ gas with 60 ppm NO₂ was absorbed into a solution of 0.1 m MDEA at 20 °C for 2 hours using the HGF. The samples were extracted periodically and analyzed for nitrite and nitrate using anion chromatography. NO₂ concentration at the inlet and outlet of the HGF was measured using a hot-gas FTIR to determine an overall yield for NO₂ absorption species (Equation 3.20).

$$[NO_{2Abs}] = \frac{PG_{HGF}}{RT} * m_{Sol} * (y_{NO_2 in} - y_{NO_2 out})t \quad (3.20)$$

Nitrite and nitrate increased linearly with absorbed NO₂ (Figure 3.9); individual product yield was defined as the slope of the regressed line (Equation 3.21).

$$[Nitrite] = Yield * [NO_{2Abs}] + b \quad (3.21)$$

Nitrite was the dominant product from NO₂ absorption, disproving the hypothesis that NO₂ mainly absorbs as N₂O₄ even at a relatively high partial pressure of 6 Pa NO₂. Nitrite and nitrate together accounted for 95 % of the absorbed NO₂, practically closing the

mass balance for absorbed NO_2 . The same samples were analyzed for MDEA and MAE using cation chromatography. MDEA decomposition was not catalyzed by NO_2 absorption in the anaerobic environment with only 1.1 moles of MDEA decomposing for every mole of NO_2 absorbed. MAE is the only quantified amine product from NO_2 absorption, accounting for 67 % of the decomposed MDEA (Figure 3.10). The experiment was repeated with air as the diluent and metal catalysts added to the amine solution. Metals predictably did not catalyze the oxidation of MDEA due to its oxidative stability at low temperatures (Closmann 2011).

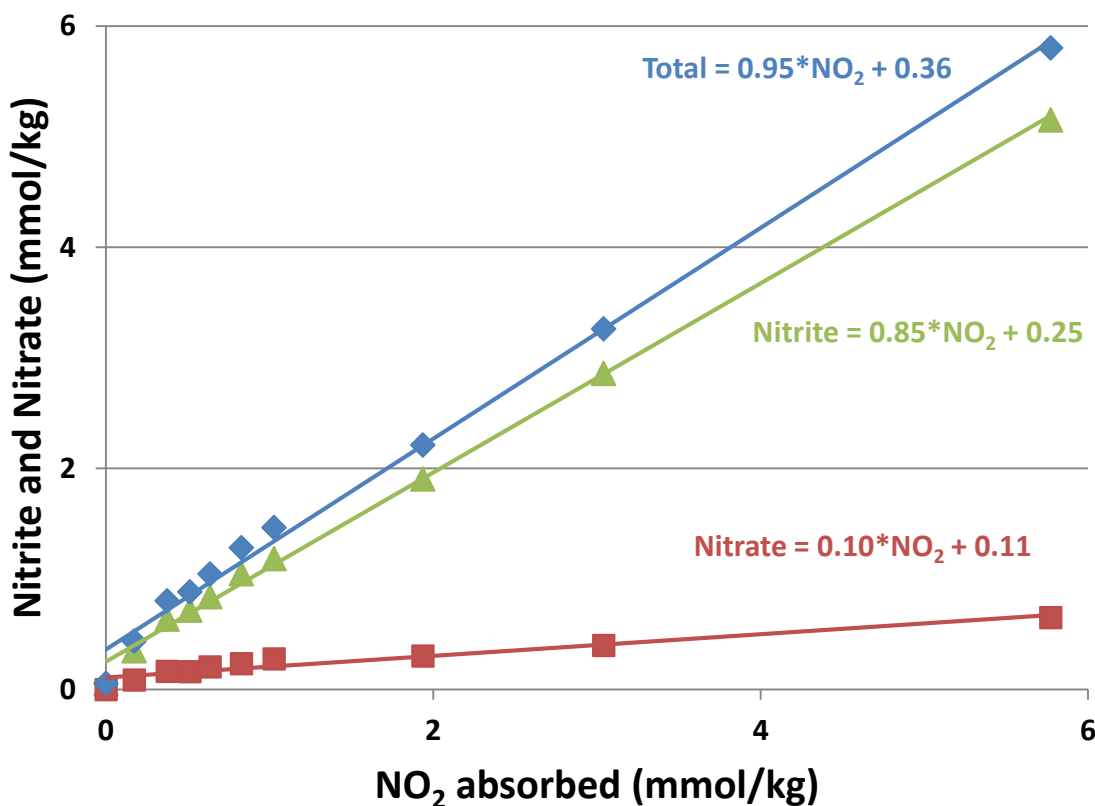


Figure 3.9: Nitrite (\blacktriangle), nitrate (\blacksquare), and sum (\blacklozenge) from NO_2 absorption into 0.1 m MDEA with 60 ppm NO_2 in hydrated N_2 at 20 °C.

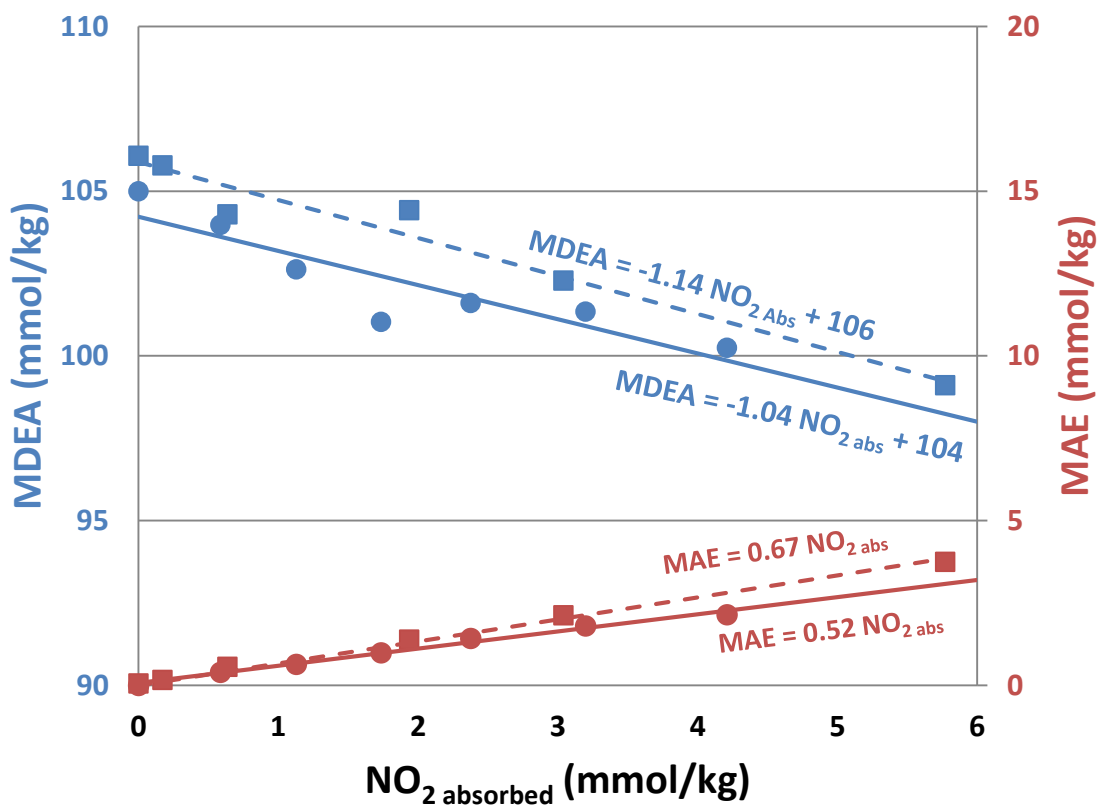


Figure 3.10: MDEA loss and MAE formation from NO₂ absorption into 0.1 m MDEA at 20 °C; ■ and - - - = 60 ppm NO₂ in N₂, 0 ppm NO, no metals; ● and — = 50 ppm NO₂ in air, 200 ppm NO, 0.4 mM Fe²⁺, 0.1 mM Ni²⁺, 0.05 mM Cr³⁺.

NO₂ partial pressure in the sparging gas was varied from 0.4 Pa to 14.4 Pa (4–144 ppm at 1 bar). The mole balance closed with an average of 97 % of the total absorbed NO_x accounted for in the aqueous phase. Thus nitrosamine formed in MDEA could account for a maximum of approximately 3 % of total absorbed product. Under similar conditions, Dai et al. reported that less than 1 % of NO_x absorbed in MDEA formed nitrosamine (Dai and Mitch 2013). At very low concentrations of NO₂ almost all of the NO₂ absorbed as nitrite, which is consistent with free-radical absorption of NO₂. As the concentration of NO₂ increased, the yield to nitrate increased, which shows the growing importance of N₂O₄ hydrolysis at higher NO₂ partial pressures (Figure 3.11). Both NO and oxygen had very

little effect on the overall absorption products, proving that N_2O_3 is not an important absorption species under experimental conditions. A similar result with nitrite yield unaffected by NO concentration was obtained by Dai et al. in morpholine solution (Dai and Mitch 2014b).

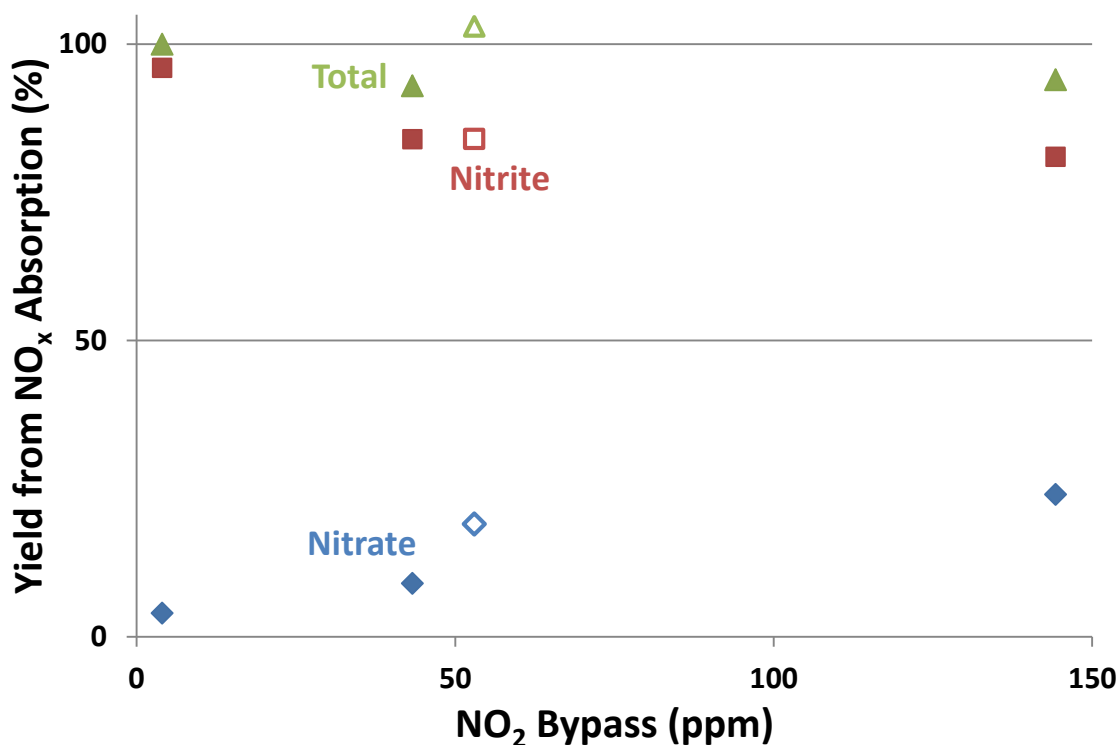
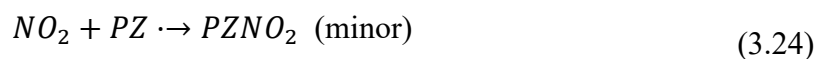
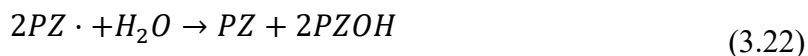


Figure 3.11: Nitrate (■), Nitrite (◆) and Sum (▲) from NO₂ absorption in 0.1 m MDEA at 20 °C; Closed points are NO₂ in hydrated N₂; Open points are NO₂ with 200 ppm NO in hydrated air.

3.3.3 NO_x Absorption into Unloaded 1 m PZ

Unlike the amino radical formed during NO₂ absorption in MDEA, the PZ radical can directly react with NO to form a stable nitrosamine. Previous research has shown that secondary amines will yield the highest nitrosamine concentrations during NO_x absorption (Dai and Mitch 2013) with nitrosamine yields of 6 ± 2 % of total absorbed NO_x in PZ at absorber conditions. The HGF was again used to study NO_x absorption products in 1 m PZ

at 20 °C. All experiments were performed with 100 ppm NO and 10–100 ppm NO₂ in either hydrated N₂ or air. MNPZ, nitrite, and nitrate were all proportional to total absorbed NO_x and together closed the mole balance within 4 % (Figure 3.12). Nitrosamine yield varied from 20 % to 35 % of the total absorbed NO_x with no dependence on oxygen in the gas (Figure 3.13). Nitrosamine yield decreased with increasing NO₂ partial pressure, most likely due to the free-radical termination step. At high concentrations of NO₂, there are more amino radicals formed in the boundary layer. These can react with each other to form 2PZOH with a second-order dependence on amino radical concentration (Equation 3.22). As the NO₂ partial pressure decreased, the radical concentration decreased and was more likely to terminate by reacting with NO to yield MNPZ (Equation 3.23). The free-radicals may also react with NO₂ to form the nitramine (Equation 3.24). However, nitramine concentration has been shown to be much lower than nitrosamine concentration (Dai et al. 2012) because NO₂ reacts quickly with the amine and is thus at a much lower concentration throughout the reaction boundary layer.



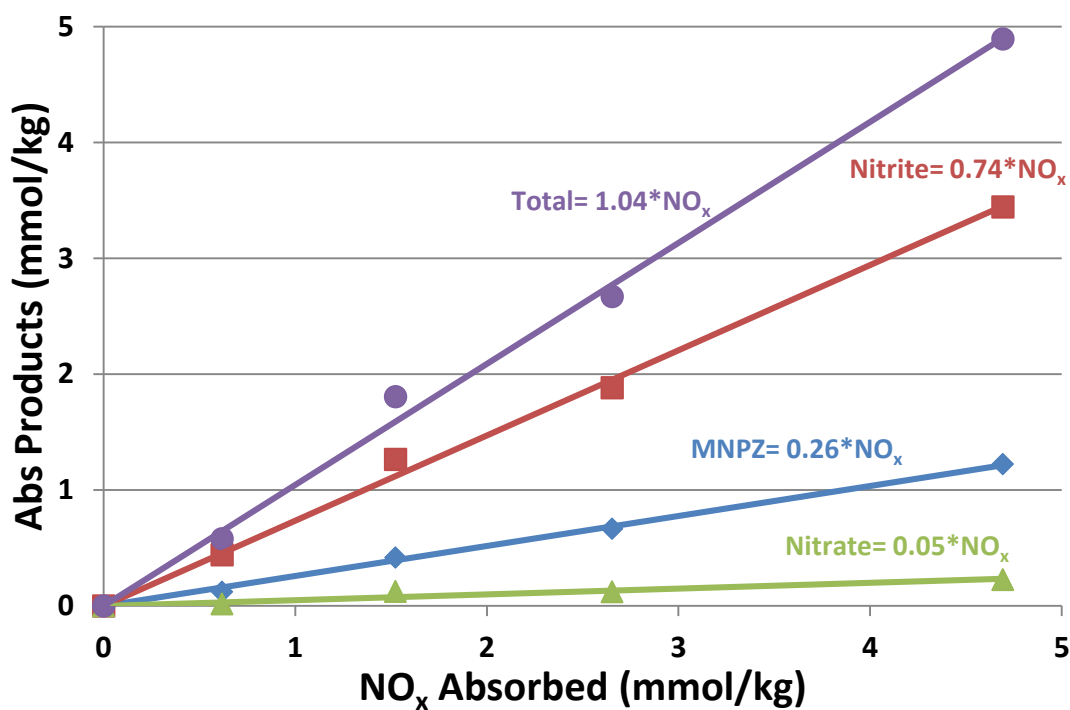


Figure 3.12: NO_x absorption products in 1 m PZ using HGF; 40 ppm NO₂, 100 ppm NO in hydrated N₂, 20 °C.

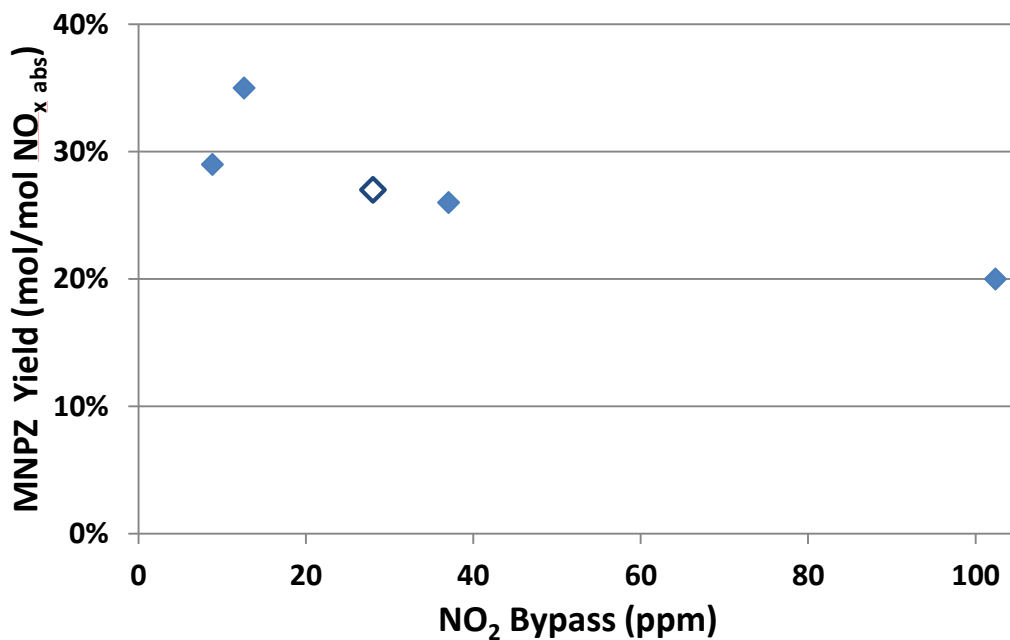


Figure 3.13: MNPZ yield in 1 m PZ with 100 ppm NO and varied NO₂ in hydrated N₂ (solid points) or air (open point); 20 °C.

3.3.4 NO_x Absorption into Loaded 5 m PZ

A standard gas composition of 10 ppm NO₂ and 100 ppm NO in hydrated N₂ was sparged through loaded 5 m PZ to more closely simulate absorber conditions. MNPZ yield was independent of CO₂ loading and amine concentration as expected from the hypothesized termination mechanisms (Equations 3.20–3.22). Nitrosamine yield also decreased drastically from 27 % to 7 % as temperature increases from 20 °C to 60 °C, possibly due to the decreased solubility of NO at higher temperatures (Figure 3.14). At 40 °C, MNPZ yield was 17 % which is roughly triple the MNPZ yield found by Dai et al. at the same temperature. However, Dai et al. sparged with an NO₂:NO_x ratio of 1:2 (Dai and Mitch 2013), which favors termination as 2PZOH instead of MNPZ.

One experiment was analyzed for 2PZOH using the DNPH derivitization method discussed in Section 2.1.6. Although 2PZOH concentrations were close to the quantification limit, it is clear that 2PZOH increases with increasing absorbed NO_x (Figure 3.15). Since the stoichiometry of Equation 3.20 predicts 1 mol of 2PZOH for every two moles of self-terminating amine radicals, the obtained yield of 65 % is higher than expected. The high yield could possibly be explained by poor quantification of 2PZOH at such low concentrations. No 2PZOH would form during N₂O₃/N₂O₄ hydrolysis since these mechanisms do not go through amine radicals. Thus, the accumulation of 2PZOH further corroborates the theory that free-radical absorption of NO₂ is dominant at these conditions.

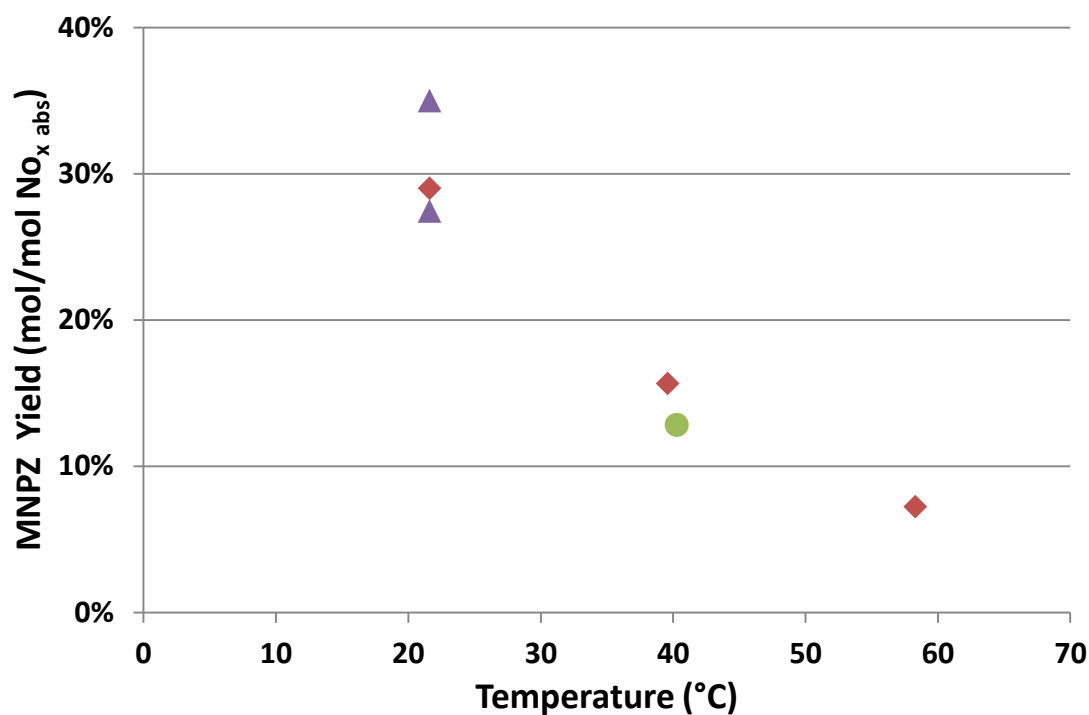


Figure 3.14: MNPZ yield in PZ with 10 ppm NO₂ and 100 ppm NO in hydrated N₂ for 5 m PZ $\alpha = 0.3$ (◆), 5 m PZ $\alpha = 0.15$ (●) and 1 m PZ $\alpha = 0$ (▲).

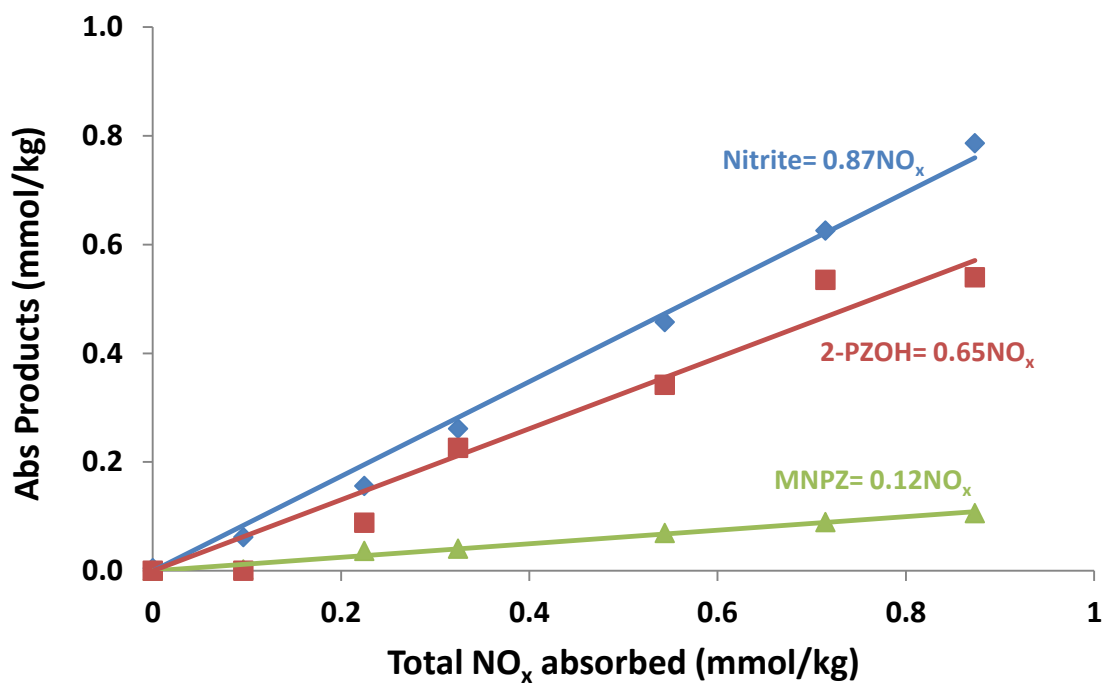


Figure 3.15: 2PZOH (■) accumulation from NO_x absorption in PZ; 10 ppm NO₂ and 100 ppm NO in hydrated N₂; 5 m PZ, $\alpha = 0.15$ at 40 °C.

Two experiments were also performed with Inhibitor A (Inh A), a proprietary oxidative inhibitor that works as a free-radical scavenger. As the concentration of Inh A increases, more of the PZ radical terminates by reacting with the scavenger instead of the NO. This decreased the MNPZ yield from 17 % to 8 % as Inh A increased from 0 to 200 mmol/kg (Figure 3.16). However, even though the MNPZ yield in the absorber decreases by 50%, this only has a minimum effect on total nitrosamine accumulation since the absorbed nitrite will go on to nitrosate PZ under stripper conditions.

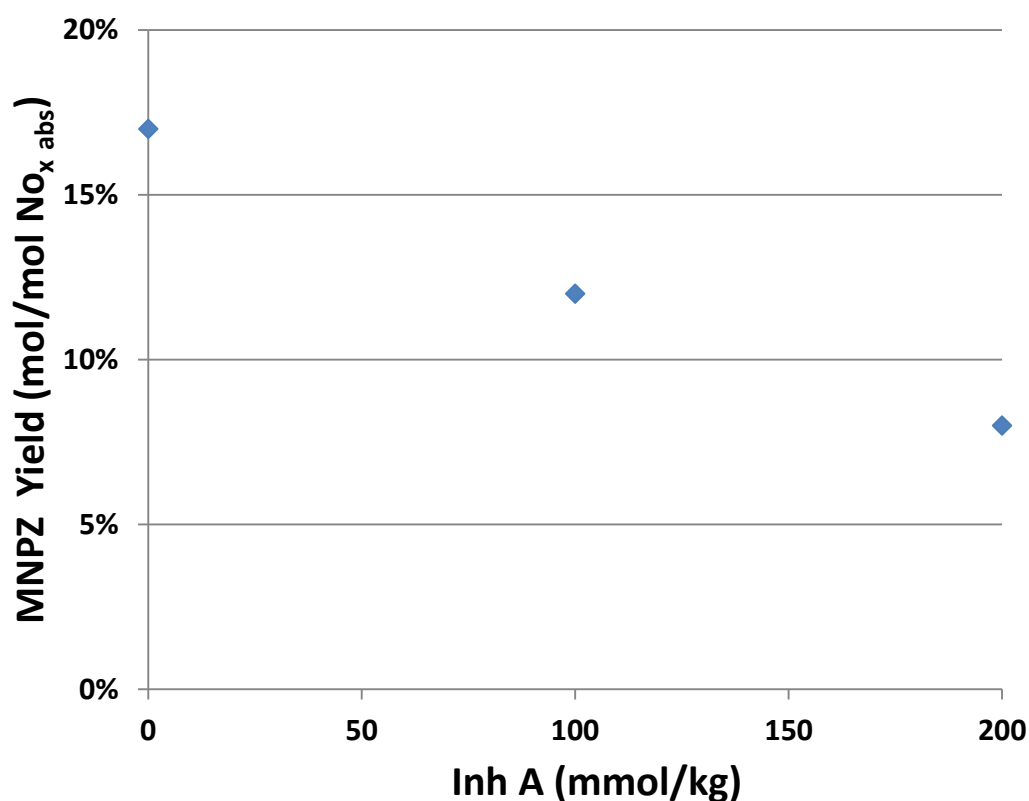


Figure 3.16: MNPZ yield in the HGF at 40 °C with addition of Inh A; 10 ppm NO₂ and 100 ppm NO in hydrated N₂; 5 m PZ with $\alpha = 0.3$.

3.4 CONCLUSIONS

3.4.1 NO_x Absorption Kinetics

- NO_x absorption at ppm levels of NO_x is dominated by the free-radical absorption of NO₂.
- Free-radical absorption of NO₂ is first order in NO₂ partial pressure and half order in free amine concentration.
- Absorption can be modeled as mass transfer with fast reaction in the pseudo-first-order regime.
- NO₂ absorption kinetics are fastest with tertiary amines and slowest with primary amines similar to ClO₂ free-radical absorption into amines.
- 70–99 % of NO₂ will absorb in amine scrubbers designed to capture 90 % of CO₂; only 4 % of NO₂ absorption can be attributed to hydrolysis.
- Tertiary amines are effective enough NO₂ absorbers to be useful for NO₂ prescrubbing.
- Only free tertiary amine species absorb NO₂; the pK_a of the tertiary amine and the pH of the scrubbing solution are deciding factors in scrubbing effectiveness.
- MDEA has faster NO₂ absorption rates than TEA above pH = 9, but NO₂ absorption into TEA is 35–100 % faster than MDEA at pH = 7–8.

3.4.2 NO_x Absorption Products

- MDEA oxidation is not catalyzed by NO₂ absorption in the presence of air and stainless steel ions.
- 10 ppm of NO₂ absorbs into 0.1 m MDEA with a 95 % nitrite yield and a 5 % nitrate yield.
- Nitrite yield is independent of NO and oxygen, proving that the absorption species is NO₂ directly instead of N₂O₃.

- NO_2 hydrolysis through N_2O_4 becomes the dominating absorption mechanism when NO_2 partial pressure is above 10 Pa (100 ppm at atmospheric pressure).
- Nitrosamine is less than 3 % of total absorption product in 0.1 m MDEA.
- NO can directly absorb into amine solution by reacting with the amino radical formed by NO_2 absorption.
- In PZ solution, NO absorption forms MNPZ with yields of 20–35 % of total absorbed NO_x at 20 °C as $\text{NO}_2:\text{NO}_x$ varies 1:2–1:12.
- PZ free radicals can also react with themselves or free-radical scavengers to lower the yield to MNPZ.
- MNPZ yield is independent of amine concentration and loading, but yield increases as the ratio of $\text{NO}_2:\text{NO}_x$ decreases.
- Increasing absorption temperature from 20 °C to 60 °C decreases MNPZ yield by 60 % due to the decreased solubility of NO.
- MNPZ yield at 40 °C in 5 m PZ with an $\text{NO}_2:\text{NO}_x$ ratio of 1:10 is 17 % with nitrite closing the mole balance.
- 200 mM of Inhibitor A, a free-radical scavenger, can reduce MNPZ formation in the absorber by 50 %.
- High temperature nitrosation from nitrite is the dominating mechanism for nitrosamine formation in amine scrubbing.

Chapter 4: High Temperature Nitrosation of Amines

Chapter 3 demonstrated that nitrite is the dominant product from NO_2 absorption, accounting for over 80 % of all absorption products at absorber conditions. Any nitrite formed in the absorber will cycle through the high temperature stripper where it can react with a secondary amine to form a stable nitrosamine. Chapter 4 gives results for the kinetics of high temperature nitrosation with nitrite. In Section 4.2, nitrosation kinetics for nitrite in PZ solutions are given over a range of temperature (50–150 °C), amine concentration (0.1 M–5 M), and loading ($\alpha = 0$ –0.4). PZ was chosen as the initial amine since MNPZ and DNPZ standards were readily available, the method for MNPZ quantification was well-developed, and PZ speciation was well-characterized. The majority of Section 4.2 has previously been published (Goldman, Fine, and Rochelle 2013).

Once the rate law was developed for PZ nitrosation, several other amines were nitrosated to determine if they followed the same kinetics (Section 4.3). When more than one amine is present in solution, nitrosamine yield is a function of the relative nitrosation rates of each amine. In Section 4.4, nitrosamine yields were determined in amine blends with a focus on yields in degraded MEA solvents as well as PZ-promoted tertiary amine solvents. The majority of Sections 4.3 & 4.4 have previously been published (Fine, Goldman, and Rochelle 2014). Finally, the proposed nitrosation mechanism and screening results for nitrosation kinetics in a variety of amines, amino acids, and imidazoles are given in Section 4.5 to predict nitrosamine formation in other amine-based solvents.

4.1 PREVIOUS RESEARCH ON NITROSATION WITH NITRITE

4.1.1 Nitrosation Mechanisms under Acidic and Basic Conditions

Nitrosation from nitrite has been extensively studied in the food industry since sodium nitrite has historically been used as a meat preservative (Honikel 2008). Nitrite can be ingested and react with amines present in gastric juices. In this low temperature acidic environment, nitrosation is second order in nitrite and first order in free amine. The nitrosation mechanism goes through nitrous acid (Equation 4.1), so there is a strong dependence on pH with maximum rates around pH = 3–4 (Figure 4.1) (Douglass and Kabacoff 1978; Challis and Kyrtopoulos 1979; Cachaza et al. 1978).

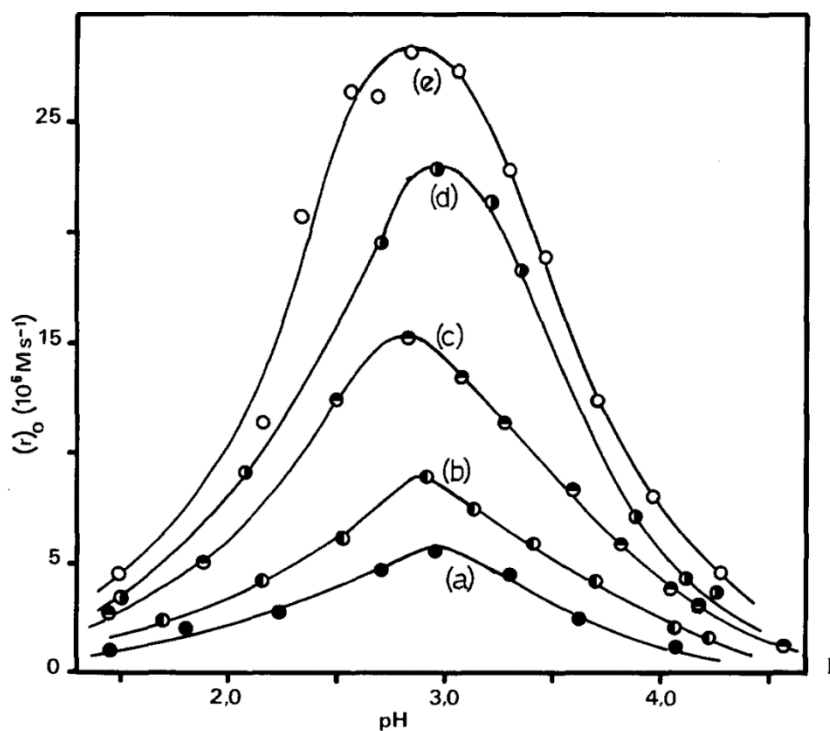
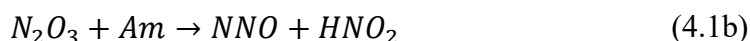
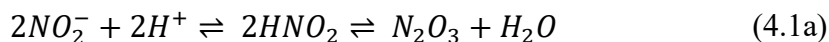


Figure 4.1: Dependence of initial rate of dimethylamine (DMA) nitrosation on pH at 310.0 K, $[DMA]_0 = 1.33$ M and ionic strength = 2.0 M at different nitrite concentrations: $[nitrite]_0$ (10^2 M) = (a) 3.00, (b) 4.00, (c) 5.00, (d) 6.00, (e) 7.00 (Cachaza et al. 1978)



There is no nitrous acid present under the basic conditions in an amine scrubber, but nitrite can still rapidly nitrosate amines in the presence of a formaldehyde catalyst (Challis and Outram 1979; Challis and Kyrtopoulos 1976). Computational modeling has shown that carbamate groups might also catalyze nitrosation at high pH (Figure 4.2), but would inhibit nitrosation at low pH (Lv, Liu, and Zhong 2009; Sun, Liu, and Zhong 2011). Sun et al. modeled the energetic landscape for the mechanism in basic solutions and determined that the mechanism required a solvated activation energy of 45 kcal/mol.

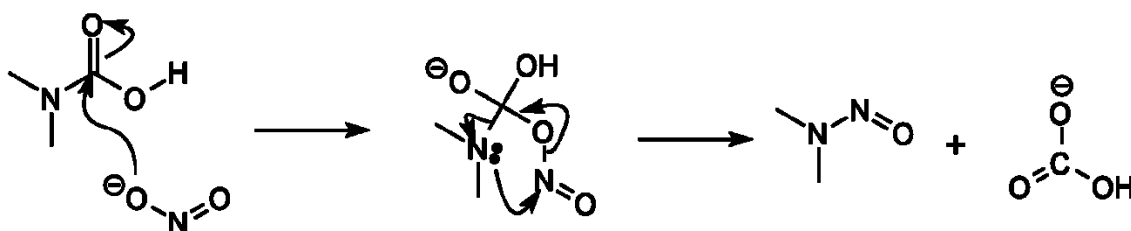


Figure 4.2. A mechanism for the CO_2 -catalyzed nitrosation of dimethylamine modeled by Lv and Sun. (Lv, Liu, and Zhong 2009; Sun, Liu, and Zhong 2011)

4.1.2 Open Research Questions for High Temperature Nitrosation

Although theoretical studies have been performed, there are no systematic experimental studies of nitrosation by nitrite in the presence of CO_2 . Previous work has shown that nitrite will nitrosate amines at high temperatures, but rates for nitrosation have not been determined. Furthermore the mechanism for nitrosation has not been developed. Since nitrite is the dominant nitrosating agent, a fundamental understanding of its

nitrosation mechanism is important to predict nitrosamine yield in amine blends and degraded amine solutions where more than one nitrosatable amine is present.

4.2 HIGH TEMPERATURE NITROSATION OF PIPERAZINE

4.2.1 Thermal Cylinder Results

Table 4.1 summarizes kinetics for PZ nitrosation from 50–135 °C. The total absorbed CO₂ was determined using TIC and the PZ concentration was found using total alkalinity. The pH at experimental conditions was estimated using the Independence Model in AspenPlus® (Frailie 2014). The experimental rate (k_{obs}) was regressed as the pseudo-first-order decomposition of nitrite. The model k_{obs} values were regressed using the rate law from Section 4.2.6 and the experimental k_{obs} values. The stoichiometric yield describes how much nitrite formed MNPZ.

Table 4.1: High temperature PZ nitrosation kinetics using thermal cylinders

| Exp # | T (°C) | PZ (M) | Total CO ₂ (M) | pH** (at T) | $k_{\text{obs}} * 10^{-6} \text{ (s}^{-1}\text{)}$ | | Yield (%) |
|-------|--------|--------|---------------------------|-------------|--|-------|-----------|
| | | | | | Exp. | Model | |
| 4.1* | 135 | 0.099 | 0.040 | 7.37 | 120 ± 10 | 148 | 114 |
| 4.2* | 135 | 0.099 | 0.040 | 7.58 | 72 ± 4 | 90 | 106 |
| 4.3* | 135 | 0.099 | 0.040 | 7.85 | 52 ± 6 | 49 | 82 |
| 4.4* | 135 | 0.099 | 0.040 | 8.04 | 30 ± 2 | 31 | 112 |
| 4.5 | 100 | 5.0 | 1.00 | 9.09 | 6.3 ± 0.2 | 6.9 | 94 |
| 4.6 | 100 | 5.0 | 2.13 | 8.72 | 32 ± 1 | 35 | 80 |
| 4.7 | 100 | 5.0 | 2.94 | 8.36 | 112 ± 4 | 110 | 90 |
| 4.8 | 100 | 5.0 | 4.14 | 7.69 | 675 ± 26 | 726 | 94 |
| 4.9 | 100 | 4.9 | 3.05 | 8.30 | 149 ± 3 | 131 | 101 |
| 4.10 | 100 | 1.7 | 1.07 | 8.22 | 70 ± 3 | 55 | 97 |

Table 4.1 Cont.

| | | | | | | | |
|-------------------------|-----|------|-------|------|-----------------|-----|----|
| 4.11 | 100 | 0.48 | 0.30 | 8.18 | 13.7 ± 0.2 | 17 | 93 |
| 4.12⁺ | 100 | 4.29 | 0.011 | 8.24 | 3.1 ± 0.1 | 0.5 | 82 |
| 4.13 | 80 | 5.0 | 2.96 | 8.61 | 13.3 ± 0.3 | 13 | 79 |
| 4.14 | 50 | 5.0 | 2.96 | 9.08 | 0.43 ± 0.01 | 0.3 | 99 |

*Buffered by 0.5 M phosphate adjusted by KOH

⁺Included 2.5 M H₂SO₄, not regressed in the rate law model

4.2.2 Data Analysis for High Temperature Nitrosation

Aqueous solutions were prepared with 0.5–5 M PZ and a CO₂ loading of $\alpha = 0$ –0.4. Before heating, sodium nitrite was added to solution at less than 50 mmol/kg. In one set of experiments, a phosphate buffer was used to vary pH at low PZ. These experiments used a solution of 0.1 M PZ with 0.01 M KHCO₃ and 0.5 M K₂HPO₄ (Kirsch et al. 2000). The pH was measured at room temperature and adjusted to the desired value using KOH. The solutions for each experiment were placed in at least five stainless steel cylinders and heated in convection ovens at 100–135 °C or in water baths at 50–80 °C. Cylinders were removed at selected time intervals and quenched in room temperature water. MNPZ and nitrite were quantified using the HPLC method. Total absorbed CO₂ and PZ were prepared gravimetrically and confirmed using the TIC method and the total alkalinity method respectively.

The formation of MNPZ and decomposition of nitrite followed a first order dependence on nitrite (Figure 4.3); nitrite loss was linearized, and a regression was performed on nitrite as a function of reaction time with the first order rate constant (k_{obs}) as a free parameter (Equations 4.3 & 4.4). The standard error from the regression for almost all experiments was less than 5 % of the observed rate constant.

$$\frac{dMNPZ}{dt} = \frac{-d[NO_2^-]}{dt} = k_{obs}[NO_2^-] \quad (4.3)$$

$$\ln([NO_2^-]) = \ln([NO_2^-]_{initial}) - k_{obs}t \quad (4.4)$$

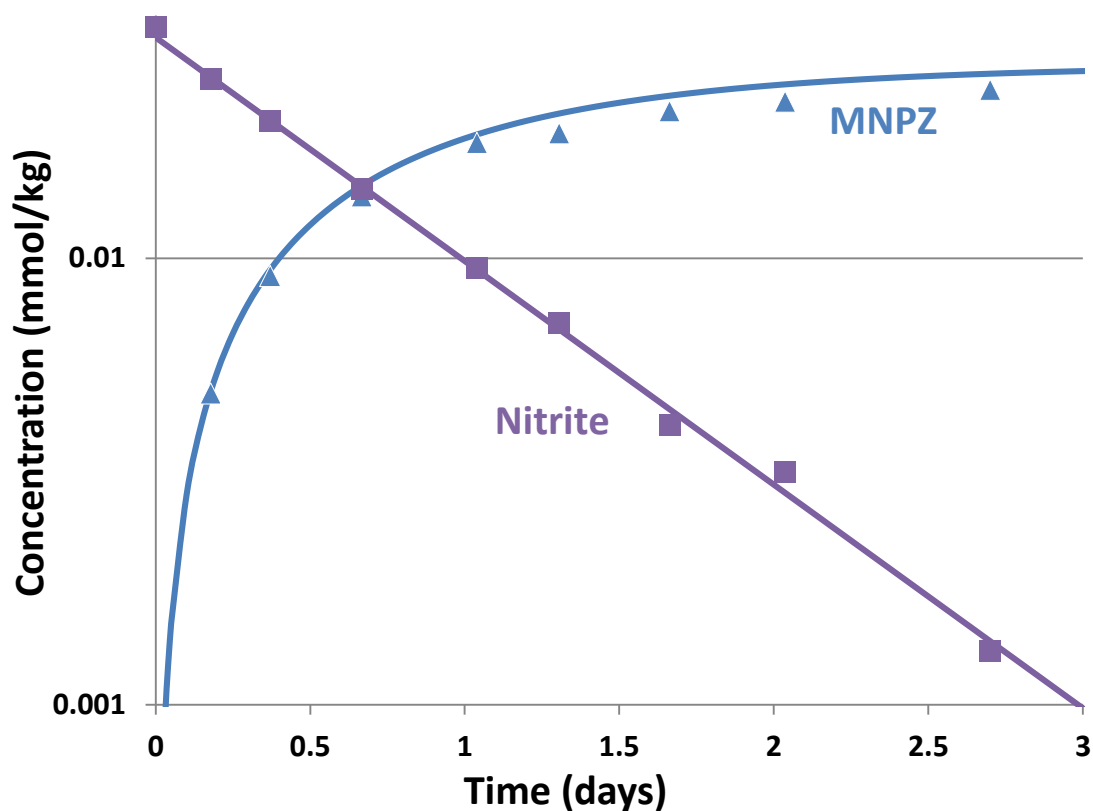


Figure 4.3: Raw data for PZ nitrosation kinetics using thermal cylinders; 5 M PZ, $\alpha = 0.30$, 80 °C (Exp. 4.13)

4.2.3 MNPZ and DNPZ Yield

MNPZ yield was defined as the final MNPZ over the difference in the final and initial nitrite (Equation 4.5). An average yield of 95 % was obtained for the 14 experiments. The high yield indicated that no major competing reactions consuming nitrite occur in the PZ solution. The yield was slightly below unity because MNPZ decomposed slowly at most reaction conditions as discussed further in Chapter 5. Quantifiable amounts of

dinitrosopiperazine (DNPZ) were found in several samples. However, the nitrite yield to DNPZ was less than 1% under these conditions. This is expected since MNPZ is the precursor for DNPZ. Initial nitrite was kept very low, so the nitrosatable MNPZ was low throughout the experiments.

$$Yield_{MNPZ} = \frac{[MNPZ]_f}{[NO_2^-]_i - [NO_2^-]_f} \quad (4.5)$$

4.2.4 PZ Nitrosation Dependence on pH

Four experiments at constant CO₂ loading and PZ were buffered with varying proportions of monobasic and dibasic phosphate at pH = 7.1–7.8. The van't Hoff equation and thermodynamic data were used to estimate the pH at experimental conditions from the pH at room temperature (Equations 4.6 and 4.7) (Goldberg, Kishore, and Lennen 2002; Atkins and de Paula 2006). This difference corresponds to a similar change in pH for the four solutions because the solutions were in the range of the phosphate buffer. The pH measurements at room temperature were adjusted to account for the increase in K_a of the buffer at 135 °C.

$$pH_{exp} = pH_{Room\ T} - (pK_{a\ Room\ T} - pK_{a\ exp\ T}) \quad (4.6)$$

$$pK_{a\ exp} = pK_{a\ Room\ T} - \log \left(e^{\frac{-\Delta H_{Diss}}{R} \left(\frac{1}{T_{exp}} - \frac{1}{T_{Room}} \right)} \right) \quad (4.7)$$

As the H⁺ activity increased, nitrosation kinetics increased proportionally, demonstrating a first-order dependence (Figure 4.4). PZ solutions without the phosphate buffer also have a relatively stable pH as the amine nitrosates because they contain two buffers: PZH⁺/PZ and H⁺PZCOO⁻/PZCOO⁻. This natural buffering effect, along with the minimal concentration of nitrite added, reduced the potential change in pH during nitrosation of the more concentrated PZ solutions. Thus, the Independence model in

AspenPlus[®], a thermodynamic model for the PZ/H₂O/CO₂ system, could be used to predict pH at experimental conditions.

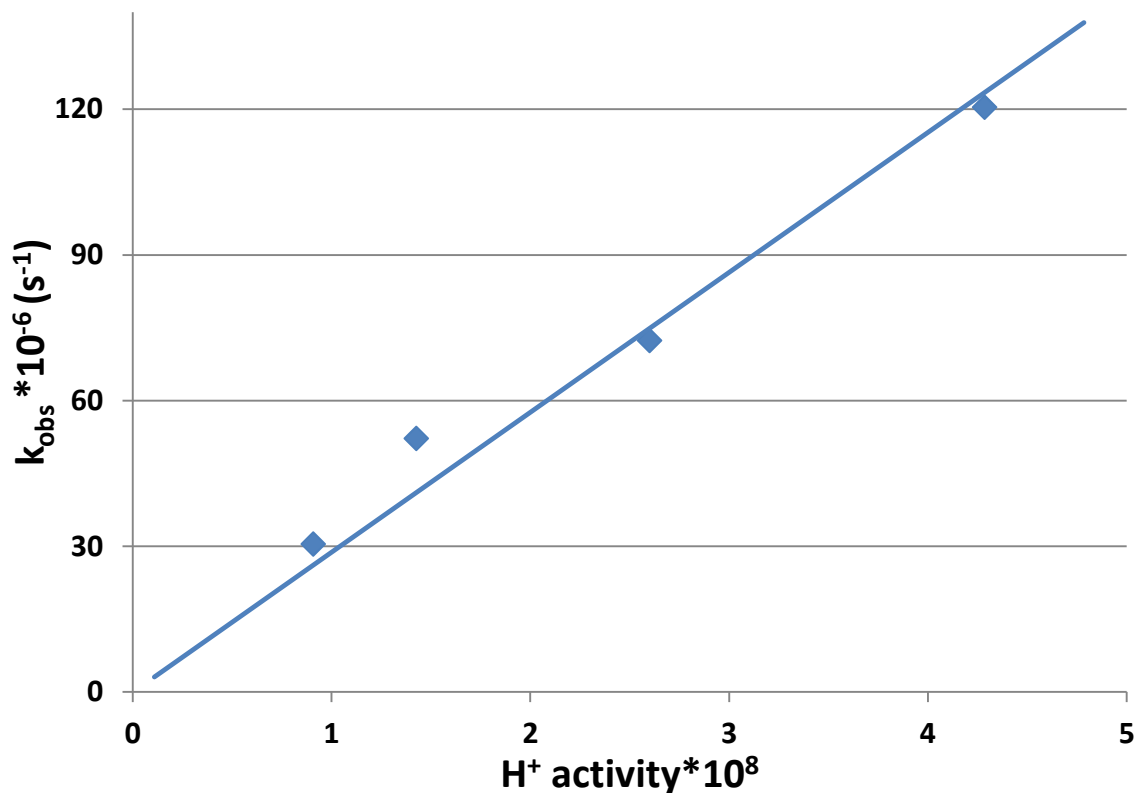


Figure 4.4: Dependence of k_{obs} on pH; 0.5 M phosphate, 0.1 M PZ, $\alpha = 0.2$, $T = 135\text{ }^{\circ}\text{C}$, H^+ activity determined from pH (Exp 4.1–4.4)

4.2.5 PZ Nitrosation Dependence on Carbamate

Previous computational work has suggested that CO₂ might play a role in nitrosation of CO₂ capture solvents. To test the effect of CO₂, sulfuric acid was added to a PZ solution to match the pH of solutions with and without significant quantities of CO₂. A 4.3 M PZ solution with 0.25 mol H₂SO₄/ mol PZ was heated to 100 °C to determine how nitrosation occurs with low total CO₂. The solution absorbed a small amount of atmospheric CO₂ to a loading of $\alpha = 0.002$ during preparation. The k_{obs} for the low CO₂

condition was $3.1 \times 10^6 \text{ s}^{-1}$, which is over 30 times slower than the rate in 5 M PZ with a loading of $\alpha = 0.3$ (Experiments 4.9 & 4.12). Despite the large rate difference, the pH difference between the two experiments was only 0.06. Since the two solutions with different amounts of carbamate resulted in large reaction rate differences, total dissolved CO_2 significantly impacted the nitrosation rate.

To understand how absorbed CO_2 affects nitrosation, the speciation of CO_2 inside piperazine solution must be understood. All of the CO_2 added to the system can exist as physically absorbed CO_2 , bicarbonate, or as a carbamate with PZ. Since PZ contains two secondary amines, a PZ carbamate can either contain an unprotonated amine, a protonated amine, or a carbamate group (Figure 4.5). At high pH and low total dissolved CO_2 , PZ carbamate dominates. As more CO_2 is added, the PZ carbamate starts to decrease while protonated PZ carbamate and PZ dicarbamate increase. When the total dissolved CO_2 approaches the amount of PZ, significant bicarbonate concentrations rise. The high temperature stripper regenerates the amine to its lean loading where almost all of the absorbed CO_2 is present as a carbamate species. Thus all experiments were performed at loadings where bicarbonate was negligible.

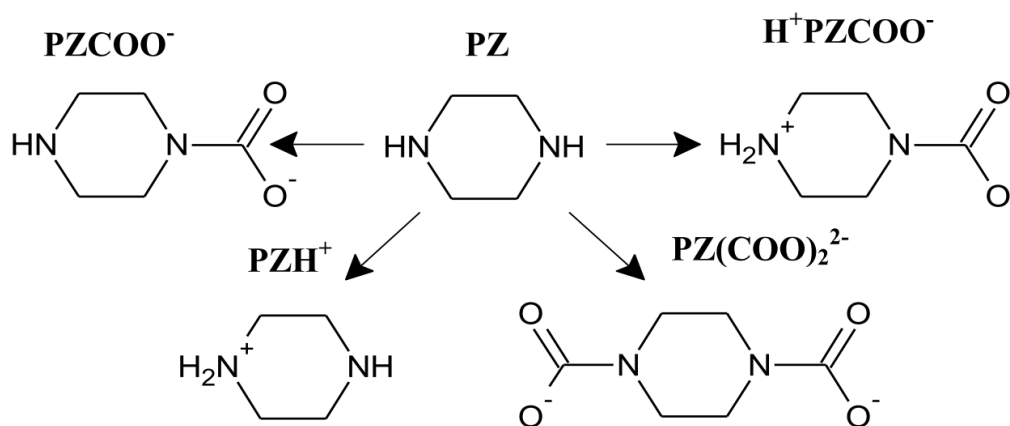


Figure 4.5: Piperazine speciation with CO_2 (Frailie 2014)

To discover which CO₂-containing species were reactive, the Independence thermodynamic model in Aspen Plus[®] was used to calculate the pH and speciation at experimental conditions for Experiments 4.5–4.11 (Frailie 2014). The observed rate constant was normalized for pH dependence (Equation 4.8). To see which species might be susceptible to nitrosation, k_3 was defined to account for the rate dependence for a CO₂ species at a given order of reaction (Equation 4.9).

$$k_2 = \frac{k_{obs}}{10^{-pH_{exp}}} \quad (4.8)$$

$$k_3 = \frac{k_2}{[CO_2 \text{ species}]^{C_3}} \quad (4.9)$$

The C_3 value is the regressed order of reaction, and k_3 is the potential rate constant that should not vary for the seven experiments. For each species in Table 4.2, an order of reaction was found that resulted in the smallest relative standard deviation in k_3 between the 7 experiments while the rest of the species were assumed to have no effect on the rate. A low relative standard deviation represents a good correlation between the reaction rate and the species concentration.

The smallest deviation in k_t corresponded to the total dissolved CO₂, which yielded approximately first order dependence. C_3 was then set at unity to determine the corresponding relative errors for a first-order dependence (Table 4.2). The large errors corresponding to physically dissolved CO₂ and bicarbonate indicate that they are not likely active species. The variation in the carbamate species errors is likely due to multiple carbamate species participating in nitrosation. Multiple PZ carbamate species can participate in nitrosation as long as the two amine groups on PZ function semi-independently. Previous research indicates that protonation of the inactive nitrogen on PZ does not make the other nitrogen-containing group unreactive (Castro, Hormazabal, and

Santos 1997). The ability for multiple carbamate groups to participate in reaction would explain why none of the individual carbamate species had both an order of reaction similar to stoichiometric orders of reaction (e.g. 0.5, 1, 2) and a low relative error. The total carbamate species correlated better than any particular carbamate species because of this additive affect. Since the different carbamate species are likely to have slightly different rate constants, there is some error associated with using the sum of all carbamate species.

Table 4.2. Reaction dependence on different carbamate species. Relative error represents the relative standard deviation for k_t for Exp. 4.5–4.12 found using Equation 4.9.

| Species | Relative Error of k_t | Corresponding C_3 value | Relative Standard Deviation of k_t with $C_3 = 1$ |
|--|-------------------------|---------------------------|---|
| Physically Dissolved CO_2 | 0.50 | 0.30 | 1.46 |
| Bicarbonate | 0.51 | 0.50 | 0.94 |
| PZ carbamate | 0.74 | 0.00 | 0.91 |
| Protonated PZ carbamate | 0.19 | 0.77 | 0.30 |
| PZ dicarbamate | 0.37 | 0.39 | 1.32 |
| Total CO_2 as carbamate | 0.22 | 0.87 | 0.28 |
| Total Dissolved CO_2 | 0.17 | 1.09 | 0.18 |

Figure 4.6 demonstrates the first-order fit using total dissolved CO_2 , the best fitting correlation. Since most of the CO_2 forms carbamate in the stripper, the absorbed CO_2 closely corresponds to the sum of carbamate species present. Using the effect of carbamate, Equation 4.10 represents a simplified rate equation which corresponds to the experimental data.

$$\frac{dMNPZ}{dt} = k_3[NO_2^-]10^{-pH}[R_2NCOO^-] \quad (4.10)$$

At loadings where bicarbonate is not a major species, R_2NCOO^- can be calculated using the total amount of CO_2 absorbed. As total absorbed CO_2 approaches the PZ concentration, significant levels of bicarbonate form, and the full speciation needs to be performed to determine the concentration of total carbamate species.

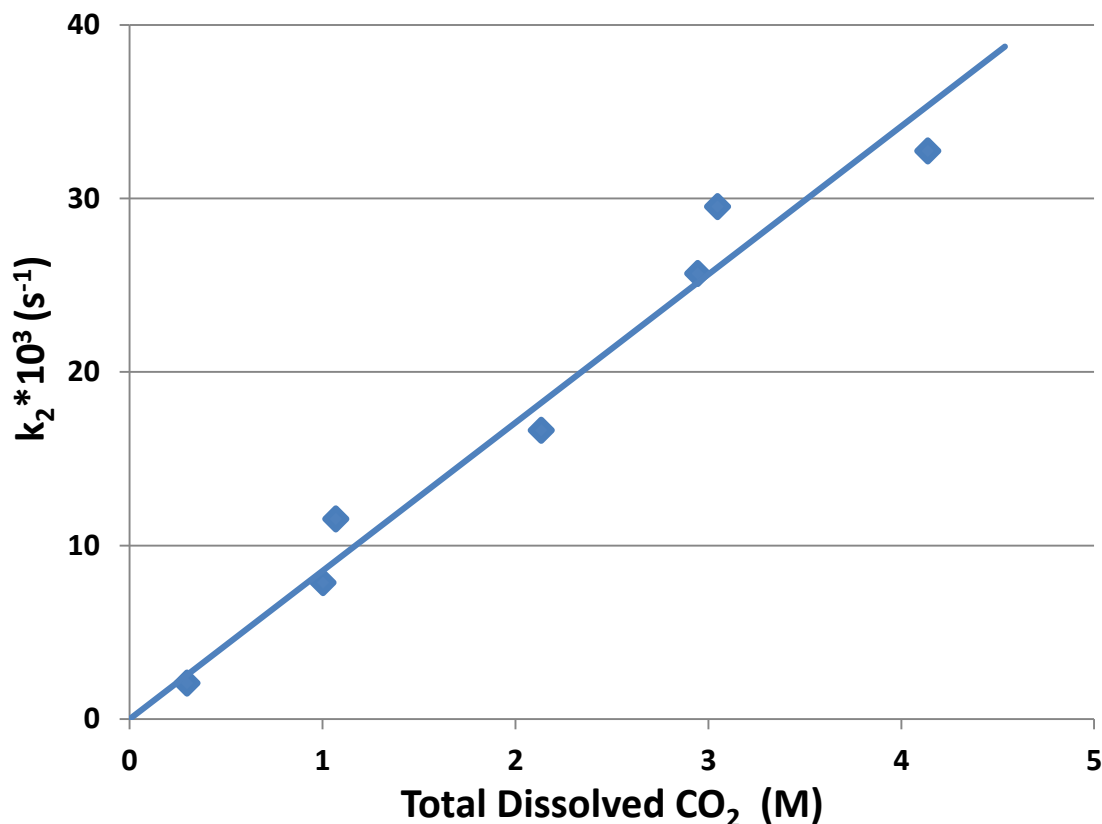


Figure 4.6: Reaction rate dependence after pH normalization on total dissolved CO_2 ; $\alpha = 0.3$ with 0.5, 1.7, and 5 M PZ and 5 M PZ with $\alpha = 0.05, 0.1, 0.15$, and 0.4; 100 °C (Exp 4.5–4.12); Model using Equation 4.9 with $k_t = 8.5$ and $C_3 = 1$.

4.2.6 PZ Nitrosation Dependence on Temperature

Experiments 4.1–4.14 excluding 4.12 were regressed to determine nitrosation temperature dependence. PZ nitrosation kinetics increased with temperature following Arrhenius behavior due to two effects: there is more thermal energy to overcome the

activation energy, and the pH decreases with temperature due to the temperature dependence of the pK_a of PZ. After normalizing the rate constant for the pH and total carbamate, the activation energy was determined to be 84 ± 2 kJ/mol with a k_3 value at 100 °C of $8.5 \cdot 10^3 \pm 1.4 \cdot 10^3$ M⁻¹ s⁻¹ (Equation 4.11) (Figure 4.7).

$$\frac{dMNPZ}{dt} = k_3 * e^{\frac{E_a}{R} \left(\frac{1}{373.15 K} - \frac{1}{T_{exp}} \right)} [NO_2^-] 10^{-pH} [R_2NCOO^-] \quad (4.11)$$

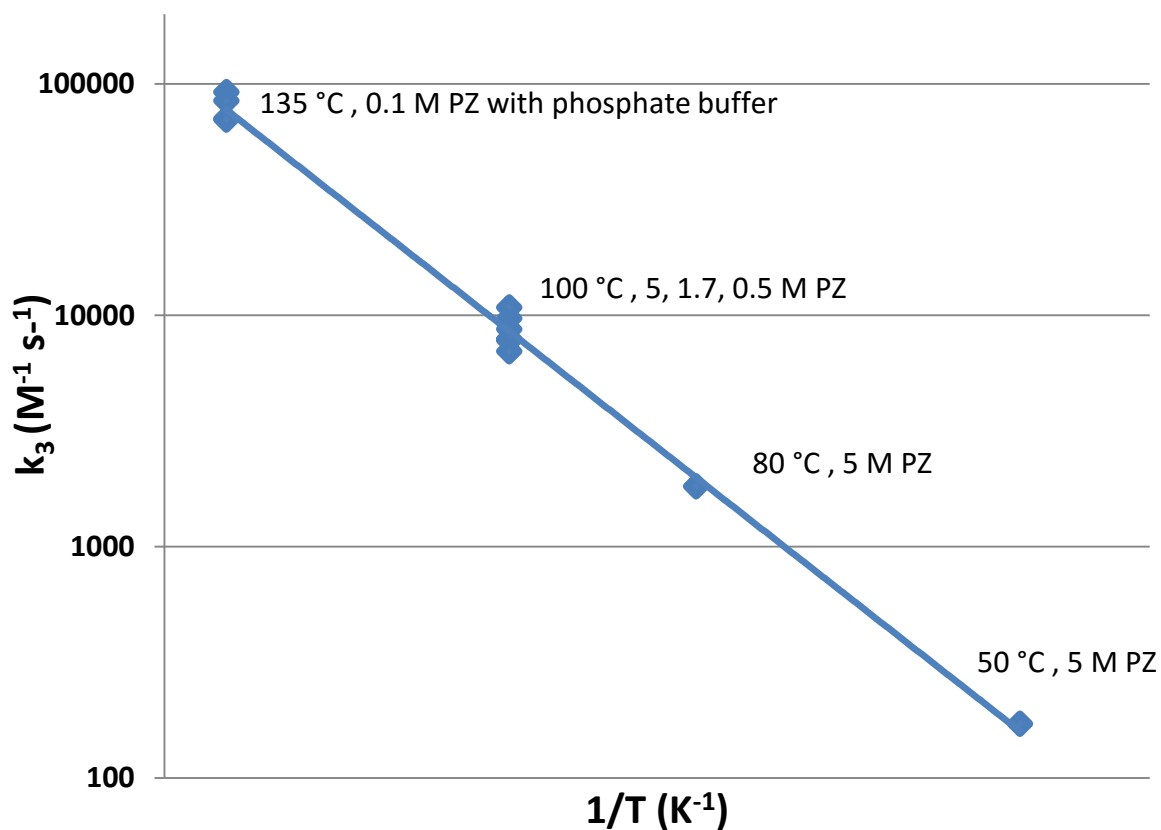


Figure 4.7: Reaction rate dependence on temperature (Exp 4.1–4.14 excluding 4.12); Model using Equation 4.11 with $k_3 = 8.5 \cdot 10^3$ M⁻¹ s⁻¹ and $E_a = 84$ kJ/mol.

Figure 4.8 shows how the observed first order rate constants, k_{obs} , compared to values predicted from Equation 4.11. Only the acid addition experiment (Experiment 4.12)

deviated significantly from the model, indicating that at very low carbamate, a different nitrosation mechanism may dominate.

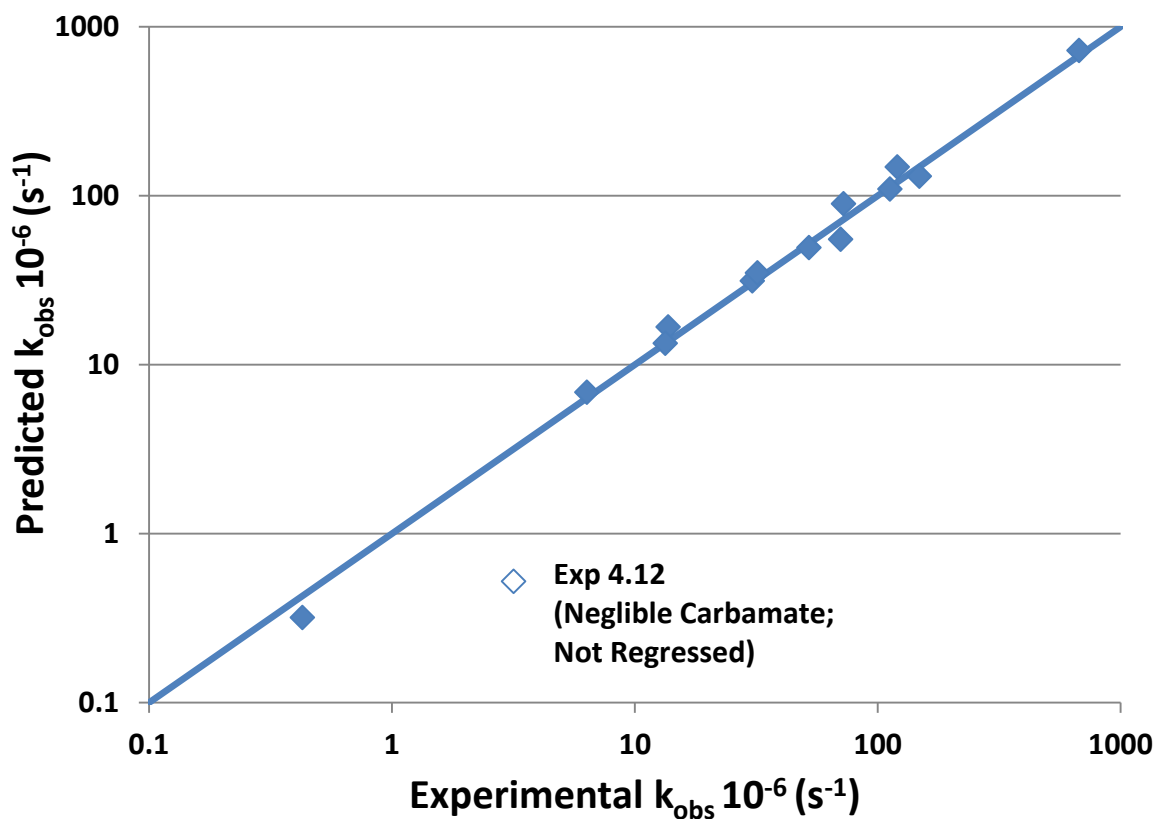


Figure 4.8: Application of kinetic model to experimental data. The predicted k_{obs} from Equation 4.11. The line indicates perfect agreement between experimental and predicted data.

4.3 HIGH TEMPERATURE AMINE NITROSATION

4.3.1 Thermal Cylinder Results

The nitrosation kinetics for MEA, DEA, MAE, and MDEA were measured over a range of temperature (80–135 °C), concentration (1–5 M), and loading ($\alpha = 0$ –0.04) using the same methods for measuring PZ nitrosation. Table 4.3 gives the observed kinetics using Equation 4.4 and the modeled rate constant using Equation 4.11. The experimental pH was

determined by measuring the pH at room temperature and extrapolating to reaction conditions using Equations 4.6 & 4.7 with the enthalpies of dissociation taken from literature (Kim et al. 2011; Hamborg and Versteeg 2009). The activation energy and k_3 value for MEA, DEA, MAE, and PZ using Equation 4.12 are given in Table 4.4

Table 4.3: High temperature nitrosation kinetics for MEA, DEA, MAE, and MDEA using the thermal cylinder experiment.

| Exp. # | T (°C) | Amine (M) | α ($\frac{mol CO_2}{mol N}$) | pH _{exp} | $k_{obs} * 10^{-6} (s^{-1})$ | $k_{model} * 10^{-6} (s^{-1})$ |
|------------|--------|-----------|--|-------------------|------------------------------|--------------------------------|
| MEA | | | | | | |
| 4.15 | 120 | 5.0 | 0.35 | 7.67 | 79±4 | 87 |
| 4.16 | 100 | 4.9 | 0.35 | 8.06 | 9.7±0.2 | 10.2 |
| 4.17 | 135 | 5.1 | 0.18 | 7.89 | 55±3 | 61 |
| 4.18 | 120 | 5.1 | 0.18 | 8.17 | 11.3±0.3 | 13.9 |
| 4.19 | 135 | 2.6 | 0.36 | 7.39 | 227±5 | 196 |
| 4.20 | 120 | 2.6 | 0.36 | 7.67 | 44.0±0.3 | 44.6 |
| 4.21 | 135 | 2.5 | 0.17 | 7.89 | 35.0±0.7 | 29.4 |
| 4.22 | 120 | 2.5 | 0.17 | 8.17 | 8.4±0.3 | 6.7 |
| 4.23 | 150 | 2.5 | 0.17 | 7.39 | 97±4 | 119.0 |
| DEA | | | | | | |
| 4.24 | 100 | 4.1 | 0.42 | 7.66 | 545±15 | 464 |
| 4.25 | 80 | 4.1 | 0.42 | 8.21 | 81±4 | 62 |

Table 4.3 Cont.

| | | | | | | |
|-------------|-----|-----|--------|------|----------|------|
| 4.26 | 100 | 4.1 | 0.18 | 7.99 | 77.6±0.2 | 90.9 |
| 4.27 | 80 | 4.1 | 0.18 | 8.54 | 10.7±0.3 | 12.2 |
| 4.28 | 100 | 2.3 | 0.42 | 7.73 | 217±5 | 219 |
| 4.29 | 80 | 2.3 | 0.42 | 8.27 | 35.2±0.4 | 29.3 |
| 4.30 | 100 | 2.3 | 0.18 | 7.98 | 46.8±0.4 | 53.7 |
| 4.31 | 80 | 2.3 | 0.18 | 8.52 | 6.8±0.4 | 7.2 |
| 4.32 | 120 | 2.3 | 0.18 | 7.58 | 264±11 | 263 |
| 4.33 | 60 | 4.1 | 0.42 | 8.60 | 9.4±1.1 | 10.7 |
| MAE | | | | | | |
| 4.34 | 80 | 3.7 | 0.19 | 9.27 | 2.5±0.1 | 2.1 |
| 4.35 | 100 | 3.7 | 0.19 | 8.92 | 15.0±0.5 | 14.3 |
| 4.36 | 80 | 0.9 | 0.38 | 8.85 | 2.8±0.1 | 2.7 |
| 4.37 | 100 | 0.9 | 0.38 | 8.50 | 15.5±0.6 | 18.5 |
| 4.38 | 100 | 0.9 | 0.19 | 8.81 | 4.5±0.3 | 4.5 |
| 4.39 | 120 | 0.9 | 0.19 | 8.49 | 25.0±0.9 | 25.8 |
| MDEA | | | | | | |
| 4.40 | 120 | 1.4 | 0.0003 | 7.23 | 69±4.1 | N/A |
| 4.41 | 120 | 1.4 | 0.16 | 7.23 | 190±7.4 | N/A |

Table 4.4: Rate constant and activation energy for modeled rate constants using Equation 4.12

| Amine | k_3 ($M^{-1} s^{-1}$) | E_a (kJ/mol) |
|-------|---------------------------|----------------|
| MEA | 680 | 73 |
| DEA | 12000 | 42 |
| MAE | 17000 | 62 |
| PZ | 8500 | 84 |

4.3.2 Nitrite, Total CO₂, and pH Dependence for Primary and Secondary Amines.

As with PZ nitrosation, several experiments were allowed to go to completion with nitrite decomposition following first order decay up to the nitrite detection limit (Figure 4.9). The standard error from fitting the linearized data to Equation 4.4 was always less than 5%, suggesting a very good fit for first order nitrite decay. The modeled rate constant generalized from Equation 4.11 (Equation 4.12) was almost always within 10% of the observed rate constant with no clear biases even though the rates varied by over 2 orders of magnitude (Figure 4.10). All nitrosation kinetics for the primary and secondary amines tested were therefore first order in carbamate species and H^+ activity.

$$\frac{dNNO}{dt} = k_3 * e^{\frac{E_a}{R} \left(\frac{1}{373.15 K} - \frac{1}{T_{exp}} \right)} [NO_2^-] 10^{-pH} [R_2NCOO^-] \quad (4.12)$$

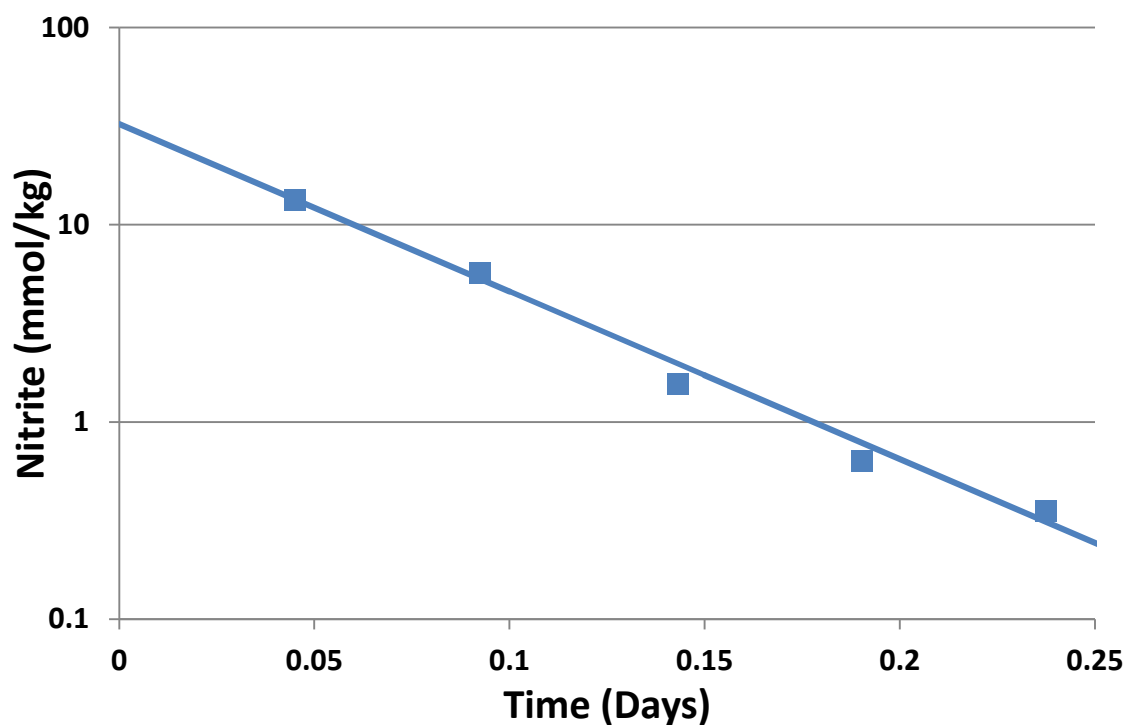


Figure 4.9: Pseudo-first order nitrite decomposition; Line using Equation 4.4 with $k_{\text{obs}} = 227 \cdot 10^6 \text{ s}^{-1}$ (Experiment 4.19, 2.6 M MEA, $\alpha = 0.36$, $T = 135 \text{ }^\circ\text{C}$)

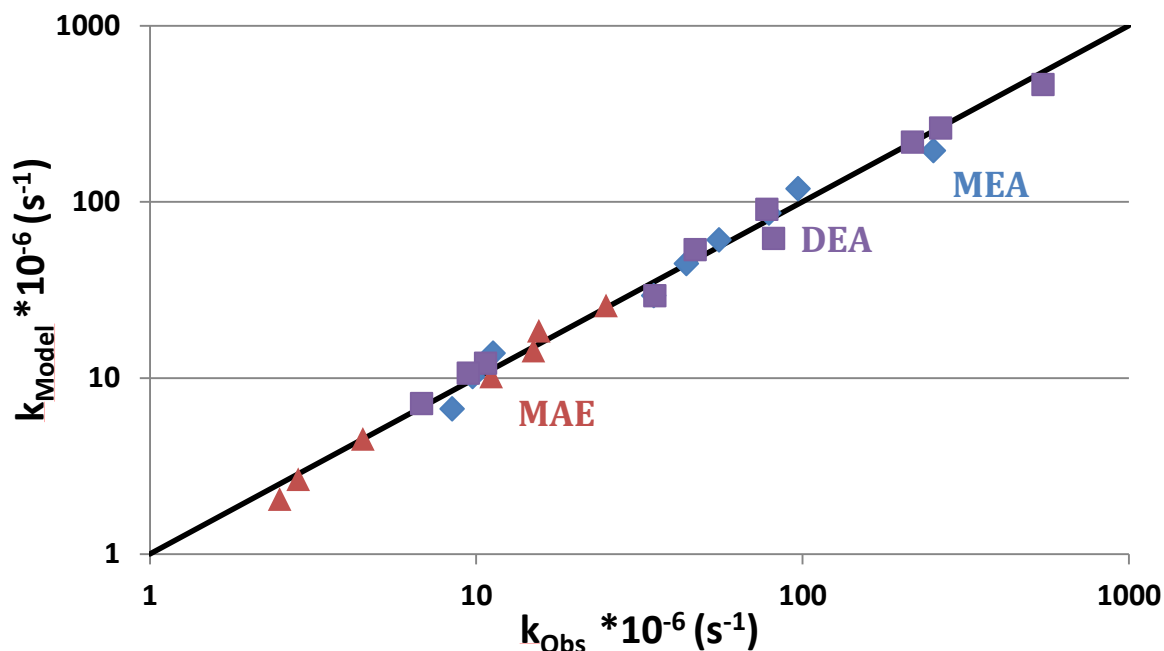


Figure 4.10: Observed rate compared to third order nitrosation model (Equation 4.12) using rate constants from Table 4.4 for MEA (\blacklozenge), DEA (\blacksquare), and MAE (\blacktriangle) (Experiments 4.15–4.39)

4.3.3 High Temperature Nitrosation of MDEA

MDEA is a tertiary amine, so it does not form the carbamate necessary for nitrosation catalysis. A stock MDEA solution was split into two parts; half the solution was loaded using KHCO_3 as a bicarbonate source without varying pH. The loaded MDEA nitrosated only 3 times faster than unloaded MDEA, even though bicarbonate increased by a factor of 500 (Figure 4.11). The pH of the solutions at room temperature were exactly the same ($\text{pH} = 8.88$), and MDEA was equivalent (1.43 mol MDEA/kg). Since the rate increase was not proportional to the increase in CO_2 loading, MDEA nitrosation does not follow the same mechanism as primary and secondary amine nitrosation. Instead, the rate increase could be caused by the higher ionic strength in the loaded MDEA.

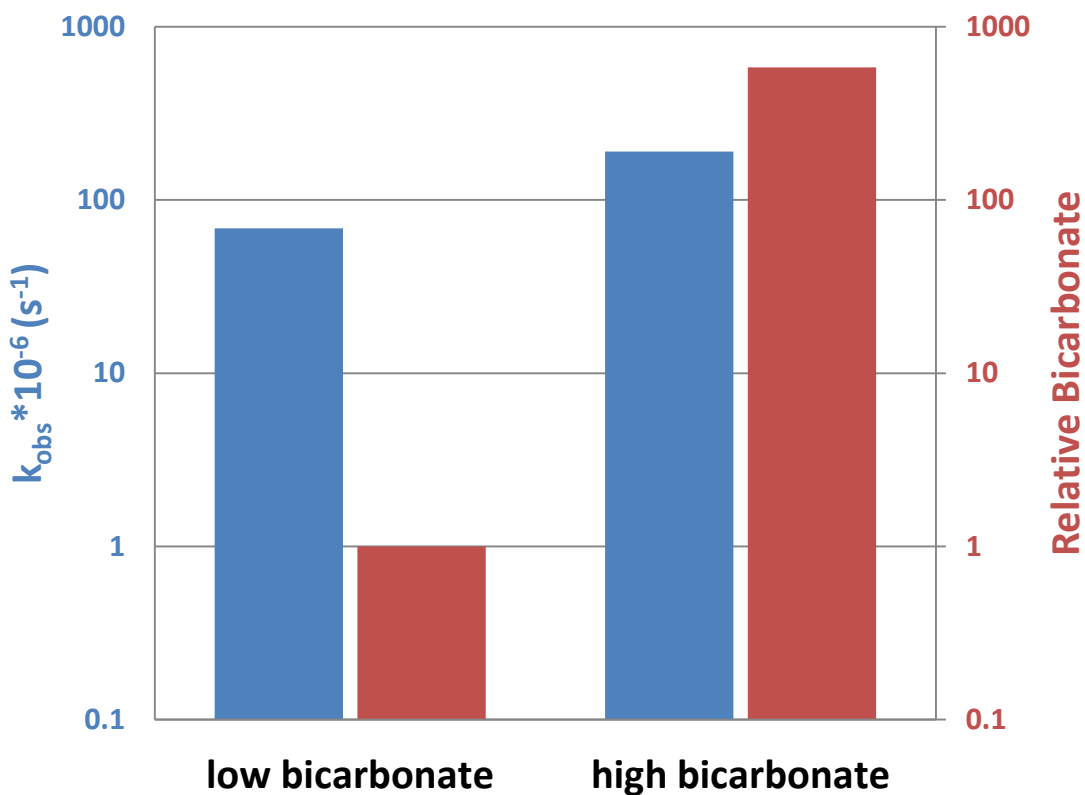


Figure 4.11: Relatively small change in observed nitrosation rate of MDEA (blue) compared to change in bicarbonate (red) (Exp. 4.40 & 4.41)

4.4 NITROSAMINE YIELD IN DEGRADED MEA AND PZ-PROMOTED TERTIARY AMINE BLENDS

4.4.1 Results for Nitrosamine Yield in Degraded MEA

Table 4.5 summarizes the results for nitrosamine formation in MEA spiked with low concentrations of secondary amines to represent degraded MEA. The experimental reactivity (r_{exp}) represents the selectivity of secondary amine nitrosation over MEA as shown in Section 4.4.2 while r_{calc} represents the calculated reactivity with the speciation model detailed in Section 4.4.2 and assuming competitive reactions with the kinetics tabulated in Table 4.4.

Table 4.5: Relative nitrosation reactivity of secondary amines compared to MEA (secondary amine varied 0-100 mM in 4–5 M MEA)

| Exp. # | T (°C) | $\alpha \left(\frac{\text{mol CO}_2}{\text{mol MEA}} \right)$ | r_{exp} | r_{calc} |
|--------------|--------|--|------------------|-------------------|
| DEA | | | | |
| 4.42 | 120 | 0.10 | 9.1±2.0 | 10.7 |
| 4.43 | 120 | 0.16 | 7.7±0.5 | 8.3 |
| 4.44 | 120 | 0.20 | 5.0±0.2 | 7.2 |
| 4.45 | 120 | 0.30 | 3.6±0.6 | 5.4 |
| 4.46 | 120 | 0.38 | 3.2±0.1 | 4.5 |
| 4.47 | 120 | 0.40 | 3.4±0.4 | 4.4 |
| 4.48 | 150 | 0.16 | 4.9±0.1 | - |
| 4.49 | 150 | 0.38 | 2.4±0.1 | - |
| HEEDA | | | | |
| 4.50 | 120 | 0.17 | 2.6±0.02 | - |
| 4.51 | 120 | 0.38 | 2.8±0.1 | - |
| 4.52 | 150 | 0.17 | 2.0±0.1 | - |

Table 4.5 Cont.

| | | | | |
|--------------|-----|------|----------|---|
| 4.53 | 150 | 0.38 | 2.2±0.03 | - |
| HeGly | | | | |
| 4.54 | 120 | 0.17 | 6.2±0.2 | - |
| 4.55 | 120 | 0.38 | 4.6±0.1 | - |
| 4.56 | 150 | 0.17 | 5.4±0.1 | - |
| 4.57 | 150 | 0.38 | 4.2±0.2 | - |

4.4.2 Data Analysis for High Temperature Nitrosation Yield in Degraded MEA

MEA is the industry standard and most researched solvent for amine scrubbing. As a primary amine, MEA nitrosates into an unstable nitrosamine that immediately deaminates into a carbocation and nitrogen gas (Mitch 2011). Any nitrosamine accumulation in an MEA solvent will therefore not come from the MEA, but from secondary amines formed during MEA degradation. DEA, HeGly, and HEEDA are all secondary amine products stemming from MEA degradation (da Silva et al. 2012; Voice 2013). Furthermore, NDELA and NHeGly have been quantified in degraded MEA pilot plant samples (Einbu et al. 2013). To study the formation of these nitrosamines in a synthetic degraded MEA sample, low concentrations (0–0.1 M) of DEA, HeGly, and HEEDA were added to concentrated (5–6 M) MEA and heated to stripper conditions.

Assuming the nitrosation of secondary amines happens in parallel with the nitrosation of MEA, the nitrosamine yield can be calculated by Equation 4.13. At low concentrations of secondary amine almost all of the nitrite reacts with MEA so that $k_{obs\ 2^o\ Am} \ll k_{obs\ MEA}$. Equation 4.13 then simplifies to Equation 4.14, which can be expanded by substituting the calculated rate for the observed rate constants (Equation 4.15). The final form has no explicit pH dependence since both the primary and secondary amine will nitrosate at the pH of solution.

$$Yield = \frac{k_{obs\ 2^\circ Am}}{k_{obs\ 2^\circ Am} + k_{obs\ MEA}} \quad (4.13)$$

$$Yield \approx \frac{k_{obs\ 2^\circ Am}}{k_{obs\ MEA}} \quad (4.14)$$

$$Yield \approx \frac{k_{3\ 2^\circ Am} e^{\frac{E_{a\ 2^\circ Am}}{R} \left(\frac{1}{373K} - \frac{1}{T_{exp}} \right)} [2^\circ Am\ COO^-]}{k_{3\ MEA} e^{\frac{E_{a\ MEA}}{R} \left(\frac{1}{373K} - \frac{1}{T_{exp}} \right)} [MEACOO^-]} \quad (4.15)$$

The amine carbamate concentrations can be found by solving the mass (Equations 4.16 & 4.17), charge (Equation 4.18), and equilibria (Equations 4.19 & 4.20) balances for the CO₂ speciation in solution.

$$[MEA] + [MEACOO^-] + [MEA H^+] = [MEA_T] \quad (4.16)$$

$$[2^\circ Am] + [2^\circ AmCOO^-] + [2^\circ AmH^+] = [2^\circ Am_T] \quad (4.17)$$

$$[MEACOO^-] + [2^\circ AmCOO^-] = [MEA H^+] + [2^\circ AmH^+] \quad (4.18)$$

$$[MEA] + [2^\circ Am\ COO^-] \xrightleftharpoons[\frac{K_{C\ 2^\circ Am}}{\frac{K_{C\ MEA}}{K_{C\ 2^\circ Am}}}]{} [MEACOO^-] + [2^\circ Am] \quad (4.19a)$$

$$\frac{K_{C\ MEA}}{K_{C\ 2^\circ Am}} = \frac{[MEACOO^-][2^\circ Am]}{[MEA][2^\circ Am\ COO^-]} \quad (4.19b)$$

$$[MEA] + [2^\circ Am] H^+ \xrightleftharpoons[\frac{K_{a2^\circ Am}}{\frac{K_{a\ MEA}}{K_{a2^\circ Am}}}]{} [MEA H^+] + [2^\circ Am] \quad (4.20a)$$

$$\frac{K_{a\ MEA}}{K_{a\ 2^\circ Am}} = \frac{[MEA H^+][2^\circ Am]}{[MEA][2^\circ Am\ H^+]} \quad (4.20b)$$

Assuming that the secondary amine is much less than MEA and there is minimal bicarbonate formation, MEA speciation is given by Equations 4.21 & 4.22. Secondary

amine speciation can then be solved with Equations 4.17, 4.19b, & 4.20b using Excel solver. To minimize speciation error, all experiments were done with a low loading ($\alpha < 0.4$) so that bicarbonate accounted for less than 5% of total absorbed CO₂ (Plaza 2011).

$$[MEACOO^-] = [MEA H^+] \approx \alpha * [MEA_T] \quad (4.21)$$

$$[MEA] \approx (1 - 2\alpha) * [MEA_T] \quad (4.22)$$

By substituting Equation 4.19b into Equation 4.15, it is apparent that nitrosamine yield is proportional to the relative concentrations of amines in solution (Equation 4.23) where the reactivity (r) takes into account the speciation of the amines as well as relative nitrosation rates.

$$Yield = r * \frac{[2^\circ Am]}{[MEA]} \quad (4.23)$$

Each experiment consisted of four thermal cylinders filled with varying amounts of secondary amine in an MEA stock solution. Nitrosamine yields were quantified using the HPLC method and regressed using Equation 4.23. Experimentally, nitrosamine yield was proportional to the relative concentrations of amines with the linear regression of the reactivity parameter consistently giving standard errors less than 10% (Figure 4.12). There was consistently a small yield of NDELA in MEA solution without any added DEA. The NDELA most likely comes from small DEA impurities in the laboratory grade MEA as well as the formation of DEA *in situ* from MEA nitrosation (Mitch 2011; Ridd 1961).

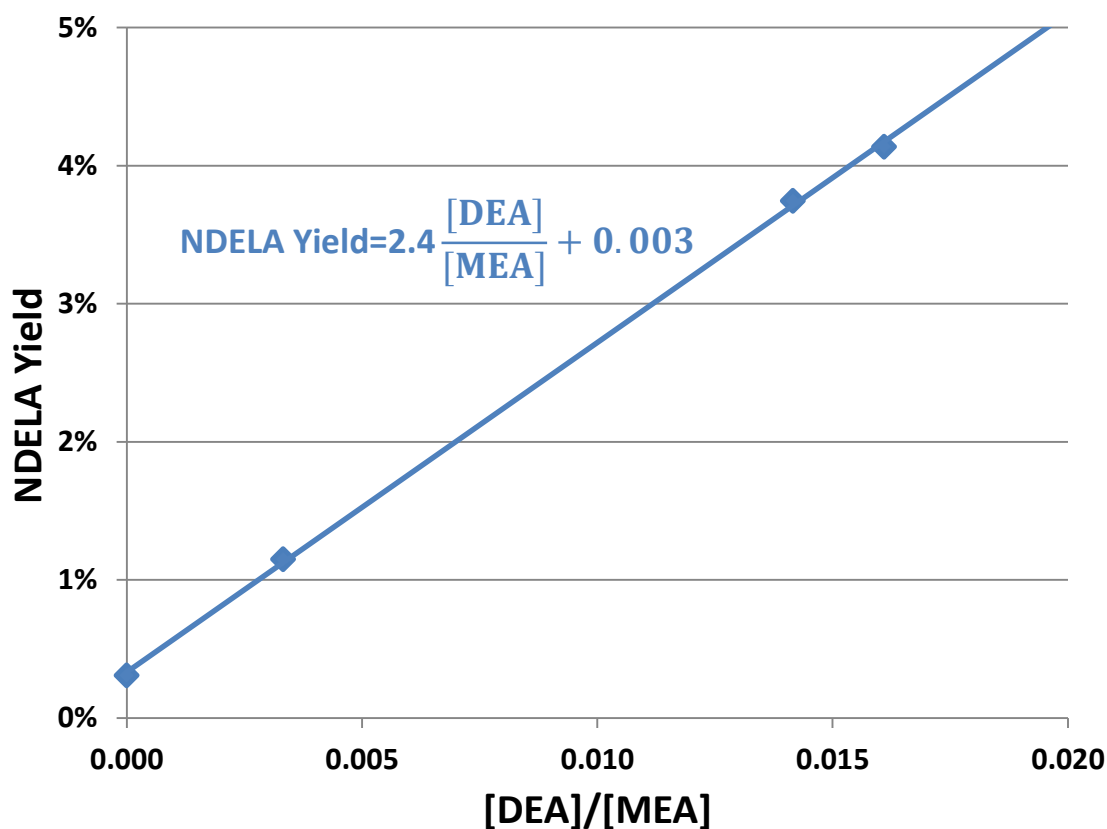


Figure 4.12: Linear dependence of NDELA yield on $[DEA]/[MEA]$; $\alpha = 0.38$, $T = 150\text{ }^{\circ}\text{C}$ (Exp. 4.49)

4.4.3 NDELA Yield Dependence on Loading in a DEA/MEA Blend

The reactivity (r) is a function of loading since the speciation of CO_2 between the amines changes with loading. A speciation model for DEA in MEA was built using carbamate stability constants and pK_a data measured at lower temperatures and then extrapolating to reaction conditions (Kim et al. 2011; Fernandes et al. 2012). Calculated reactivity of DEA at $120\text{ }^{\circ}\text{C}$ using Equation 4.15 and kinetics from Table 4.4 overpredicted the experimental reactivity by approximately 30% for MEA loadings from $\alpha = 0.1$ to $\alpha = 0.4$ (Figure 4.13). This error is to be expected given the uncertainties in estimating high temperature carbamate and protonate stability.

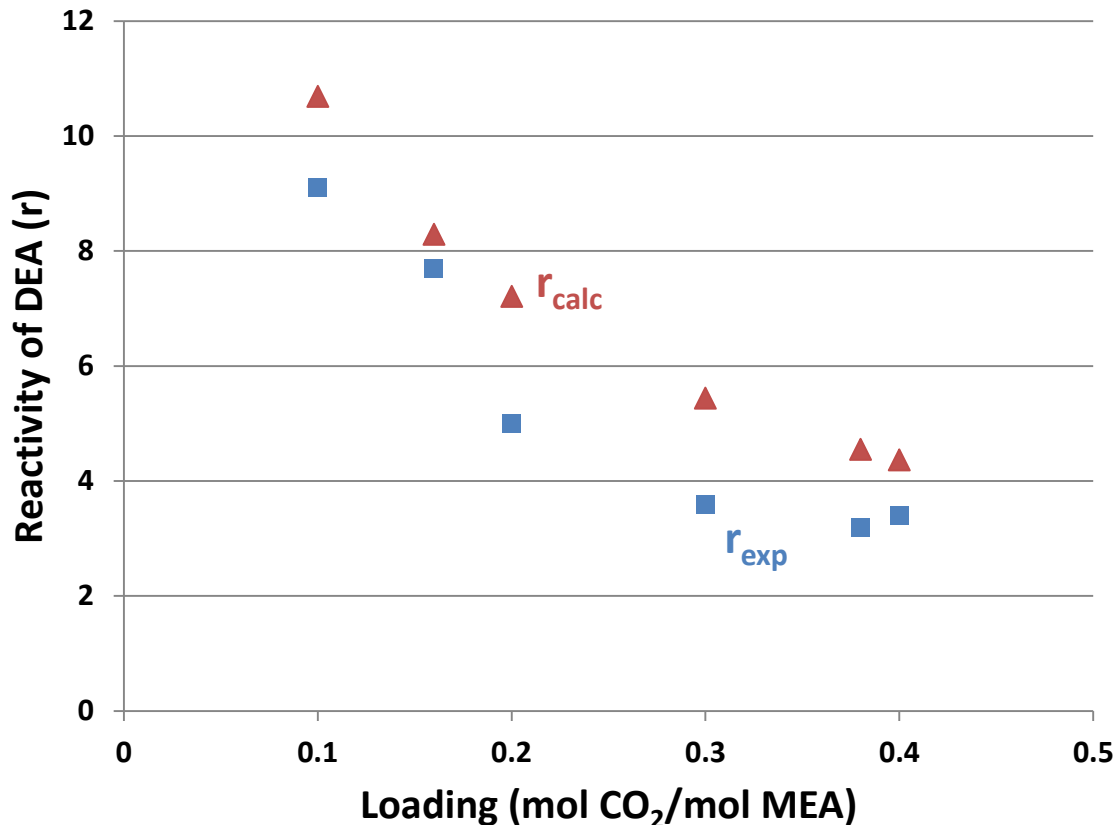


Figure 4.13: Relative rate of nitrosation of DEA to MEA at 120 °C. r_{exp} (■) regressed from data using Equation 4.23. r_{calc} (▲) calculated from Equation 4.15 using the speciation model and Table 4.4 (Experiments 4.42–4.47)

4.4.4 Nitrosamine Yield in HeGly/MEA and HEEDA/MEA Blends

DEA, HEEDA, and HeGly all had reactivities greater than one, which demonstrates that they nitrosate faster than MEA on a per mole basis. If only 1% of the total amine in a degraded MEA solvent is present as these secondary amines, then 2–8% of nitrite can be expected to yield a secondary nitrosamine. HeGly is the dominant secondary amine product found in degraded MEA samples. It has been quantified at concentrations as high as 8000 $\mu\text{g/ml}$ (≈ 70 mM) in pilot plant samples that were run for 20 weeks without reclaiming (da Silva et al. 2012; Einbu et al. 2013). At standard stripper conditions, HeGly nitrosates 5 times faster than MEA. Assuming MEA is approximately 5 M, NHeGly yield would be

approximately 7 % of total inlet nitrite under standard operating conditions. NHeGly yield could be decreased by preventing MEA from degrading into HeGly or by removing the HeGly using a reclaiming technique.

4.4.5 Nitrosamine yield in PZ-promoted tertiary and hindered amines

Tertiary and moderately hindered amines do not form carbamates; instead CO₂ absorbs into solution as bicarbonate (Sartori and Savage 1983). Since an amine group is not taken up by the formation of carbamate, tertiary amines normally have higher capacities than primary or secondary amines. Unfortunately, tertiary amines also do not absorb CO₂ quickly, so PZ is often added as an absorption rate promoter. Table 4.6 gives nitrosamine yield results for PZ-promoted tertiary amines. While these amines can nitrosate, they are not catalyzed by absorbed CO₂ and thus do not compete well with PZ nitrosation. Even though PZ only makes up 22% of the total amine, it accounts for nearly all of the nitrosation. Therefore, in tertiary/hindered amine blends with secondary amines, almost all nitrite will react with the secondary amine, giving nitrosamine yields close to unity.

Table 4.6: MNPZ yield in PZ-promoted tertiary amine blends (7 m tertiary amine, 2 m PZ, $\alpha = 0.25$, T = 150 °C)

| Exp. # | Amine Blend | MNPZ Yield (%) |
|----------|---------------------------------|----------------|
| 4.1–4.14 | 0.1-5M PZ | 95±11 |
| 4.58 | PZ/Methyldiethanolamine (MDEA) | 85 |
| 4.59 | PZ/Triethanolamine (TEA) | 102 |
| 4.60 | PZ/Dimethylaminopropanol (DMAP) | 93 |
| 4.61 | PZ/Diethylaminoethanol (DEAE) | 96 |
| 4.62 | PZ/Aminomethylpropanol (AMP) | 79 |

4.5 HIGH TEMPERATURE NITROSATION MECHANISM AND SCREENING

4.5.1 High Temperature Nitrosation Mechanism

Carbamate-catalyzed nitrosation is theorized to follow the mechanism in Figure 4.13 with step 4 as the rate-limiting step. The pK_a of the amino group in step 3 is much greater than the pH of solution due to the neighboring negative charge; thus step 3 equilibrates far to the right. Using the pseudo-steady-state approximation, the rate law can be written as Equation 4.24. The concentration of amine carbamic acid can be determined from the pH and pK_a (Equations 4.25 & 4.26). Generally, the presence of the amine carbamic acid ($AmCOOH$) is neglected because the amine buffer is much more basic than the carbamate group. However, as temperatures approach stripper conditions, the pK_a of the amine drops substantially, lowering the pH and possibly allowing a small quantity of $AmCOOH$ to form.

$$\frac{d[NO_2^-]}{dt} = -k_2[AmCOOH][NO_2^-] \quad (4.24)$$

$$[AmCOOH] = K_{a\ AmCOO^-}[AmCOO^-]_{Free} 10^{-pH} \approx K_{a\ AmCOO^-}[AmCOO^-]_{Tot} a_{H^+} \quad (4.25)$$

$$\frac{d[NO_2^-]}{dt} = -k^\circ K_{a\ AmCOO^-}[AmCOO^-] a_{H^+} [NO_2^-] \quad (4.26)$$

The mechanism fits the empirical rate laws in Equation 4.12 and corroborates theoretical results (Lv, Liu, and Zhong 2009). There is exceedingly limited data on carbamic acid stability since it is unimportant at absorber conditions. The pK_a of MEA carbamate at 30 °C has been measured as 7.5 (McCann et al. 2009), but there is no data for temperature dependence so it is not possible to calculate $K_{a\ AmCOO^-}$ at stripper conditions.

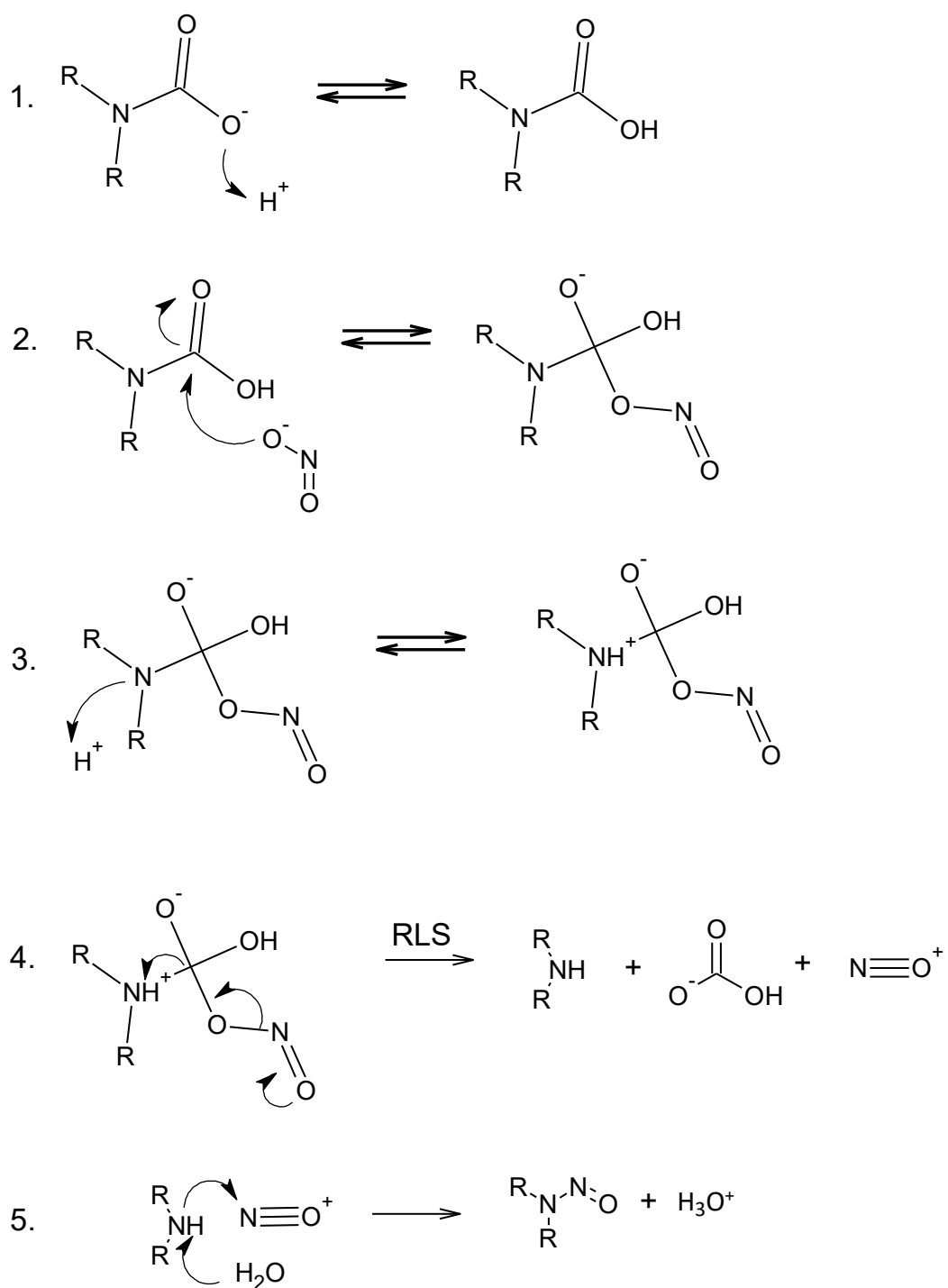


Figure 4.13: High temperature carbamate-catalyzed nitrosation mechanism

4.5.2 Screening Methods and Data Analysis

High temperature nitrosation screening was performed for a range of primary amines, secondary amines, amino acids, and imidazoles to further elucidate the nitrosation mechanism and help predict nitrosation kinetics for other amine-based solvents. To limit exposure to the wide range of nitrosamines, all screening was performed with 0.1 M amine and 1 mM NaNO₂. All screening solutions were loaded with CO₂; to minimize bicarbonate formation in solution, CO₂ loading was limited to $\alpha = 0.3$. Since all amines and amino acids screened are carbamate formers, the CO₂ was assumed to speciate to the carbamate. The concentration of CO₂ in the 50 mL of solution prepared for each experiment was approximately 0.03 M, which equates to only 0.066 g CO₂. The small mass was too difficult to determine gravimetrically, so first CO₂ was sparged directly into a 2 liter stock solution of distilled de-ionized water. The amine and nitrite were then added to the CO₂-loaded water and pipetted into the thermal cylinders. Amine loading was measured with undiluted samples using the TIC method, and the pH of solution was measured at room temperature using a potentiometric pH probe.

Each experiment consisted of five thermal cylinders that were heated to 120–165 °C for experiment times ranging from 6 hours to 7 days. Cylinders were removed periodically and the solutions were analyzed directly for nitrite using anion chromatography. For secondary amines and some primary amines, nitrite disappearance was first order in nitrite. The nitrite concentration was linearized and regressed to yield a pseudo-first-order rate constant (Equations 4.3 & 4.4 reproduced below). The third-order rate constant was determined using the solution pH at experimental conditions and carbamate concentration (Equation 4.27). Solutions are buffered by the amine, so the pH at experimental conditions was calculated by correcting for the change in amine pK_a from room temperature to the reaction temperature (Equations 4.6 & 4.7 reproduced below).

$$\frac{d[NO_2^-]}{dt} = -k_{obs}[NO_2^-] \quad (4.3)$$

$$\ln[NO_2^-] = \ln[NO_2^-]_i - k_{obs}t \quad (4.4)$$

$$k_3 = \frac{k_{obs}}{10^{-pH_{exp}}[CO_2 \text{ absorbed}]} \quad (4.37)$$

$$pH_{exp} = pH_{RT} - (pK_{a \text{ RT}} - pK_{a \text{ exp}}) \quad (4.6)$$

$$pK_{a \text{ exp}} = pK_{a \text{ RT}} - \log \left(e^{\frac{-\Delta H_{Diss}}{R} \left(\frac{1}{T_{exp}} - \frac{1}{T_{RT}} \right)} \right) \quad (4.7)$$

Each amine was nitrosated at two temperatures; the two k_3 values were then used to find the activation energy with the Arrhenius equation (Equation 4.38).

$$\ln \left(\frac{k_3 T_1}{k_3 T_2} \right) = \frac{-E_a}{R} * \left(\frac{1}{T_1} - \frac{1}{T_2} \right) \quad (4.38)$$

4.5.3 Screening Results

Table 4.7 gives the compounds used for nitrosation screening along with their structures and enthalpies of proton dissociation; Table 4.8 summarizes all of the observed pseudo-first-order nitrosation screening rates along with the third-order rate constants and activation energies.

Table 4.7: High temperature nitrosation screening compounds

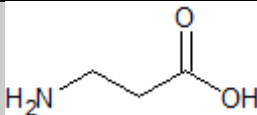
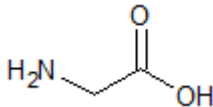
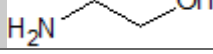
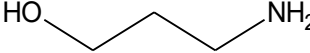
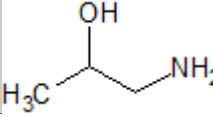
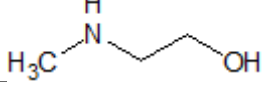
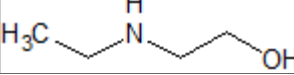
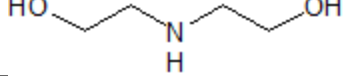
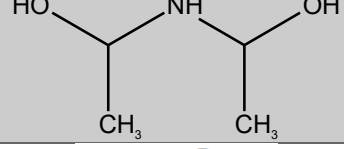
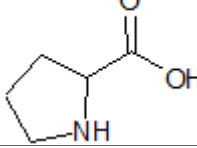
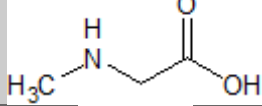
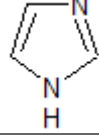
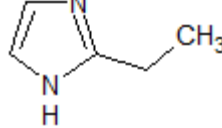
| Amine | CAS # | Structure | ΔH_{Diss} (kJ/mol) |
|----------------------------------|----------|--|-------------------------------|
| β -Alanine (β -Ala) | 107-95-9 |  | 44.5* |

Table 4.7 Cont.

| | | | |
|----------------------------------|-----------|--|--------------------|
| Glycine (Gly) | 54-40-6 |  | 44.2 ⁺ |
| Ethanolamine (MEA) | 141-43-5 |  | 50.2 ⁺ |
| Propanolamine (PA) | 156-87-6 |  | 45 ^{oo} |
| Isopropanolamine (IPA) | 78-96-6 |  | 45 ^{oo} |
| Methylaminoethanol (MAE) | 109-83-1 |  | 44.4 ⁺ |
| Ethylaminoethanol (EAE) | 110-73-6 |  | 45 ^{oo} |
| Diethanolamine (DEA) | 111-42-2 |  | 42.1 ⁺ |
| Diisopropanolamine (DIPA) | 110-97-4 |  | 34.8 ^{**} |
| L-Proline (Pro) | 147-85-3 |  | 43.2 ^o |
| Sarcosine (Sar) | 107-97-1 |  | 40.5 ⁺⁺ |
| Imidazole (Im) | 288-32-4 |  | 36.6 ⁺ |
| 2-Ethylimidazole (2-EIm) | 1072-62-4 |  | 36.6 ^{oo} |

^{**}(Blauwhoff and Bos 1981; ⁺Goldberg, Kishore, and Lennen 2002; ⁺⁺Grzybowski and Datta 1958; ^oSorenson et al. 2003; ^{*}Tsurko and Kuchtenko 2014) ^{oo} Default Values

Table 4.8: Nitrosation rates in 0.1 m amines, amino acids, and imidazoles

| Exp. # | Amine | α | pH _{exp} | T (°C) | k _{obs} (s ⁻¹ *10 ⁶) | k _{3 135 C} (M ⁻¹ s ⁻¹) | E _a (kJ/mol) |
|------------------|-------|----------|-------------------|--------|--|---|-------------------------|
| Primary | | | | | | | |
| 4.63 | β-Ala | 0.36 | 8.1 | 135 | <2 | N/A | N/A |
| 4.64 | | 0.36 | 7.9 | 150 | <2 | | |
| 4.65 | Gly | 0.29 | 8.0 | 135 | 5.2±0.7 | 18000 | 40 |
| 4.66 | | 0.29 | 7.8 | 150 | 12±2 | | |
| 4.67 | MEA | 0.28 | 7.6 | 135 | 4.4±0.1 | 6600 | 50 |
| 4.68 | | 0.28 | 7.2 | 165 | 34±5 | | |
| 4.69 | PA | 0.23 | 8.7 | 135 | <2 | N/A | N/A |
| 4.70 | | 0.23 | 8.3 | 165 | <2 | | |
| 4.71 | IPA | 0.23 | 8.1 | 135 | <2 | N/A | N/A |
| 4.72 | | 0.23 | 7.7 | 165 | <2 | | |
| Secondary | | | | | | | |
| 4.73 | MAE | 0.25 | 8.7 | 120 | 4±0.2 | 180000 | 70 |
| 4.74 | | 0.25 | 8.5 | 135 | 14±0.2 | | |
| 4.75 | EAE | 0.27 | 8.4 | 135 | 4.5±0.3 | 39700 | 50 |
| 4.76 | | 0.27 | 8.0 | 165 | 19±2.2 | | |
| 4.77 | DEA | 0.28 | 7.5 | 135 | 14±0.7 | 16000 | 50 |
| 4.78 | | 0.28 | 7.3 | 150 | 30±3 | | |

Table 4.8 Cont.

| | | | | | | | |
|-------------------|-------|------|-----|-----|----------|--------|----|
| 4.79 | DIPA | 0.21 | 8.1 | 135 | 16±2 | 94000 | 50 |
| 4.80 | | 0.21 | 7.9 | 150 | 42±6 | | |
| 4.81 | Pro | 0.30 | 8.6 | 135 | 7.6±1.4 | 102000 | 40 |
| 4.82 | | 0.30 | 8.4 | 150 | 18.5±1.6 | | |
| 4.83 | Sar | 0.35 | 7.8 | 135 | 7.9±0.4 | 21000 | 90 |
| 4.84 | | 0.35 | 7.6 | 150 | 33±2 | | |
| Imidazoles | | | | | | | |
| 4.85 | Im | 0.25 | 6.7 | 135 | 4.5±0.1 | 940 | 50 |
| 4.86 | | 0.25 | 6.5 | 150 | 11.5±0.7 | | |
| 4.87 | 2-Elm | 0.25 | 6.1 | 135 | 5.1±0.4 | 240 | 60 |
| 4.88 | | 0.25 | 5.9 | 150 | 13.2±3.4 | | |

4.5.4 Effect of Amine Order

The yield of stable secondary nitrosamines in amine solutions depends on the nitrosation rates of secondary amines compared to other nitrosating species. In Section 4.4, tertiary amines and heavily hindered amines that do not form carbamates were shown not to nitrosate competitively with piperazine. MEA nitrosated competitively with DEA, HeGly, and HEEDA, but reacted 3–9 times slower than the secondary amines. Of all the primary amines and amino acids screened, only MEA and glycine had measurable nitrosation rates (Experiments 4.63–4.72), and these rates were much slower than those of the secondary amines, most likely due to the reaction occurring in step 4 of the nitrosation mechanism (Figure 4.13). The rate-limiting step depends on the elimination of the bicarbonate and nitrosonium cation from the intermediate species. In effect, the carbamate catalyzes the reaction by adding steric hindrance around the amino group, creating a better

leaving group for the nitrosonium cation. The strength of the leaving group depends on the instability of the intermediate. With primary amines, the amino group is bonded to two hydrogens, releasing some of the steric hindrance and strengthening the bond between the amine and the nitroso-carbamic leaving group. In contrast, secondary amines are under severe steric stress in step 4, and the breakup of the intermediate species is much more rapid. The effect is that secondary amines will likely react much faster than primary amines in all solvents.

4.5.4 Effect of pK_a on Nitrosation of Secondary Nitrogens

For secondary nitrogens the third-order rate constant varies over three orders of magnitude even though it is hypothesized that all compounds go through the same mechanism. The large variance is not due to differences in steric hindrance, but rather differences in the pK_a $AmCOO^-$. Figure 4.14 shows how k_3 varies with the pH of solution for all experiments containing secondary nitrogens (Experiments 4.73–4.88). Since the amines buffer the solution at approximately the same loading, the pH is indicative of the pK_a of the amine. Counterintuitively, the more basic amines have larger k_3 values so that all observed rate constants are within an order of magnitude. It is likely that the pK_a of the carbamate tracks with the pK_a of the amine, which causes the $AmCOOH$ to remain relatively constant for all experiments. However, in blends where the nitrosating amine does not buffer the solution, the pK_a of the reactive $AmCOOH$ will be decoupled from the pH. Since the $AmCOOH$ increases with the pK_a of the carbamate, which should increase with the pK_a of the amine, secondary amines with higher basicity should nitrosate faster. DIPA is an outlier on Figure 2 with a nitrosation rate constant approximately 5 times greater than amines and amino acids with similar pK_a values. This is most likely due to additional steric hindrance on the amino group from the isopropanol arms, which weakens the bond between DIPA and the nitroso-carbamic leaving group.

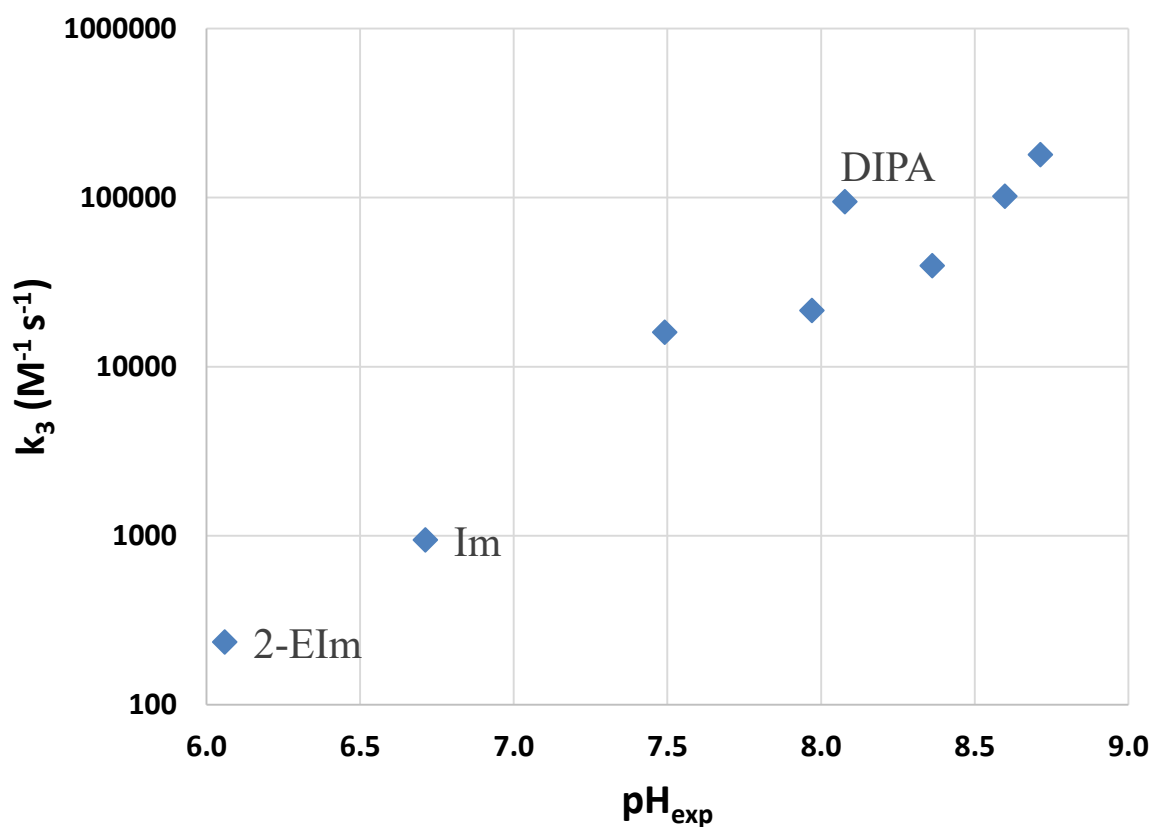


Figure 4.14: Nitrosation rate dependence on pH at 135 °C (Experiments 4.74, 4.75, 4.77, 4.79, 4.81, 4.83, 4.85, 4.87)

4.6 CONCLUSIONS

4.6.1 High Temperature PZ Nitrosation

- High temperature PZ nitrosation is first order in nitrite, H^+ activity, and carbamate concentration.
- PZ nitrosation kinetics fit an Arrhenius temperature dependence; the third-order rate constant is $8500 \text{ L mol}^{-1} \text{ s}^{-1}$ at 100°C with an activation energy of 84 kJ/mol .
- At loadings where bicarbonate is low, total carbamate can be well-approximated by total absorbed CO_2 .

4.6.2 High Temperature Amine Nitrosation

- The nitrosation mechanism is hypothesized to go through the amine carbamic acid, which fits the empirically determined third-order rate law.
- Carbamic acid catalyzes nitrosation by reacting with nitrite to form an unstable intermediate that breaks into a nitrosyl cation and bicarbonate.
- Secondary amines nitrosate the fastest by providing more steric hindrance to aid the nitroso-carbamic leaving group.
- Nitrosation kinetics increase with secondary amine pK_a since more carbamate will be present as carbamic acid at a given pH for higher pK_a amines.
- Primary amines nitrosate slower than secondary amines since they provide less steric hindrance for the nitroso-carbamic leaving group.
- Tertiary and moderately hindered amines nitrosate slowest since they do not form carbamates for nitrosation catalysis.

4.6.3 Nitrosamine Yield in Degraded MEA, PZ, and PZ-Promoted Tertiary Amines

- MNPZ yield in PZ solutions is unity for all reaction conditions.
- Nitrosamine yield in MEA is proportional to the concentration of secondary amine in solution and the relative kinetics of nitrosation.
- DEA nitrosates 3–9 times faster than MEA depending on the loading and temperature.
- NDELA yields in a DEA/MEA blend were predicted within 30% of experimental yields despite the limited speciation data at high temperatures.
- HeGly nitrosates 4–6 times faster than MEA at stripper conditions.
- With 70 mM HeGly in solution, approximately 7 % of absorbed NO_2 as nitrite can be expected to nitrosate to NHeGly.

- PZ-promoted tertiary amines will have MNPZ yields close to unity due to the low nitrosation rate of tertiary amines.

Chapter 5: Nitrosamine Control in the Stripper and Thermal Reclaimer

Once nitrosamines form either from nitric oxide (Chapter 3) or nitrite (Chapter 4), they will accumulate in the amine scrubber until they are emitted, decomposed, or reclaimed out of the system. The emission rate has a negligible effect on nitrosamine loss since nitrosamines formed during amine scrubbing are relatively non-volatile and will have emissions less than one part-per-billion (Chapter 7). Therefore, high temperature decomposition and thermal reclaiming are the two primary methods for nitrosamine control without significantly modifying the amine scrubber. Section 5.2 gives results for nitrosamine thermal decomposition in the stripper and the reclaimer with an initial focus on MNPZ. Decomposition kinetics at stripper conditions were also measured for NDELA and NHeGly, two nitrosamines found in MEA pilot plant samples. The products and mechanism for MNPZ decomposition are discussed in Section 5.3; the majority of Sections 5.2 & 5.3 has been previously published (Fine and Rochelle 2013; Fine, Nielsen, and Rochelle 2014). Section 5.4 covers nitrosamine volatility under thermal reclaiming conditions for MEA and PZ pilot plant samples. The volatility and decomposition rate of nitrosamines in the thermal reclaimer bottoms will determine the efficiency of reclaiming nitrosamines out of the solvent as well as the possible carcinogenicity of the reclaimer waste.

5.1 PREVIOUS RESEARCH AND OPEN QUESTIONS

Previous research has shown that nitrosamines can decompose in basic solutions at high temperatures common to the stripper (Chandan et al. 2013; Fan and Tannenbaum 1972). Fan et al. found that n-nitrospyrrolodine (NPyr) decomposition was first order in nitrosamine and a strong function of basicity with a half-life decreasing from 55 days at

pH = 4.0 to 1 day at pH = 12.5 (Figure 5.1). While nitrite was the expected major product from NPyr decomposition, it only contributed to 15 % of the products when NPyr was decomposed at pH = 8.5.

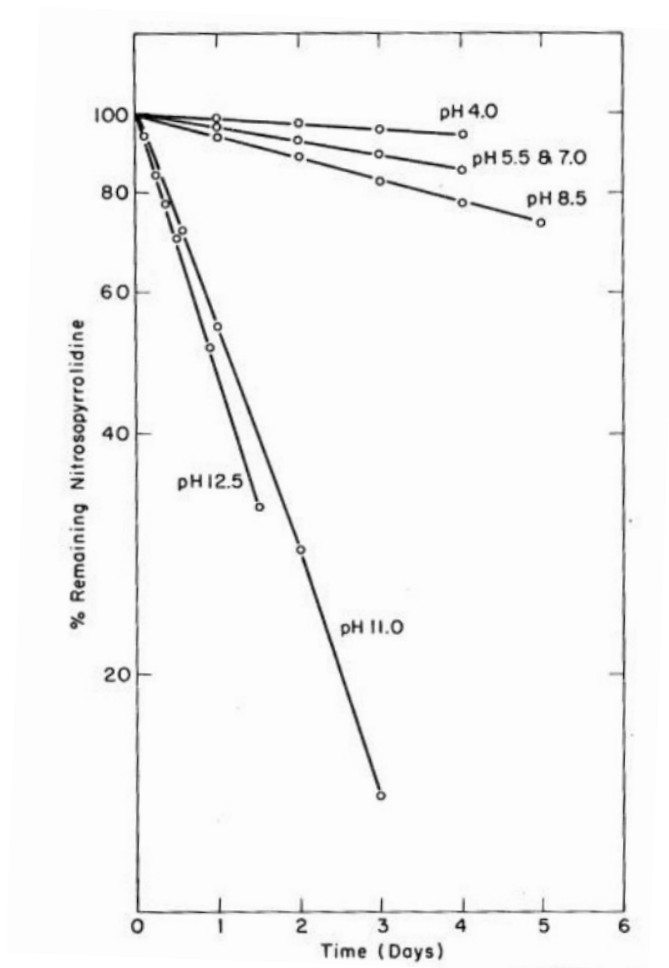


Figure 5.1: Rate plot for thermal decomposition of N-nitrosopyrrolidine (NPyr); in citric acid/ K_2HPO_4 or NaOH/ K_2HPO_4 buffer; $T = 110\text{ }^{\circ}\text{C}$ (Fan and Tannenbaum 1972).

Voice (2013) also found that MNPZ decomposed in loaded PZ solutions at temperatures between $160\text{ }^{\circ}\text{C}$ and $200\text{ }^{\circ}\text{C}$ with an activation energy of $104 \pm 12\text{ kJ/mol}$. However, his experiments had relatively poor temperature control, leading to large

propagated errors to the rate constants themselves (Voice 2013). Several pilot plant studies have noted that nitrosamines decrease when stripper temperature is increased (P. T. Nielsen, Li, and Rochelle 2013; Einbu et al. 2013), but do not provide a mechanism for the nitrosamine loss.

While there has been no published work for nitrosamine decomposition at thermal reclaiming conditions, two pilot plant studies have shown that nitrosamine concentration in the thermal reclaimer is either low or unquantifiable (Gorset et al. 2013; Strazisar, Anderson, and White 2003). Strazisar et al. found no nitrosamine in the reclaimer bottoms despite finding 2.9 mM total nitrosamine in the circulating solvent. They theorized that nitrosamine volatility must be greater than that of MEA at reclaimer conditions, allowing almost all of the nitrosamine to distill out of the reclaimer bottoms. Gorset et al. also showed that the reclaimed bottoms from the Aker proprietary amine (ACCTM S26) only contained a few ppm nitrosamine despite having heavily concentrated the metals to 2.5 wt %. However, Gorset et al. disproved that their nitrosamines were volatilizing since no nitrosamine was present in the return from the thermal reclaimer (Gorset et al. 2013). Thus, the nitrosamine must be decomposing in the thermal reclaimer to account for the nitrosamine loss.

While there is some evidence that nitrosamines decompose at stripper and thermal reclaimer conditions, there is no previous literature on nitrosamine decomposition kinetics in concentrated amines. Furthermore, nitrosamine decomposition products have not been determined in any previous work with amines. Since the scrubber has a high concentration of amines, the nitrosamine can transnitrosate (react with a secondary amine to form a separate nitrosamine), which could lead to overprediction of overall nitrosamine loss. Finally, there has been no work on nitrosamine volatility at thermal reclaimer conditions,

which is necessary to determine the effectiveness of thermal reclaiming in limiting nitrosamine accumulation.

5.2 HIGH TEMPERATURE NITROSAMINE DECOMPOSITION KINETICS

5.2.1 Data Analysis for Nitrosamine Decomposition Kinetics

Nitrosamine decomposition kinetics were quantified using four amine solvents common to amine scrubbing (MEA, PZ, MDEA, and AMP). The solutions were prepared gravimetrically at 0.1–6 M and sparged with CO₂; final CO₂ loadings were $\alpha = 0\text{--}0.4$. Different amine concentrations were made by diluting the concentrated loaded amine solution with distilled deionized water to ensure a consistent loading across a concentration range. Nitrosamine decomposition was also studied in distilled deionized water and dilute NaOH to examine the effect of base strength on decomposition kinetics. The prepared solution was spiked with a small quantity of nitrosamine or NaNO₂, up to 50 mM, and pipetted into 3/8 inch O.D. high pressure stainless steel cylinders for thermal decomposition.

The closed cylinders were heated to 100–165 °C in convection ovens and kept at autogenous pressures similar to those in the stripper. The cylinders were removed periodically and immediately quenched in a water bath at room temperature. Typical experiment times ranged from three hours to three weeks, which usually allowed for greater than 90% decomposition. The samples were stored at room temperature in amber vials to prevent artifactual UV nitrosamine decomposition. Since all of the cylinders for a given experiment were prepared with the same stock solution, the periodic removal of cylinders allowed analysis for nitrosamine as a function of time at elevated temperature. Nitrosamine decomposition was first order in the nitrosamine (Figure 5.2) under all conditions as previously reported (Fan and Tannenbaum 1972). Experimental results were therefore

linearly regressed as a pseudo-first order decomposition (Equations 5.1 & 5.2) with NNO_i and k_{obs} as regressed parameters. The observed pseudo-first order rate constants (k_{obs}) were then transformed and linearly regressed as a function of experiment parameters such as temperature, base concentration, and base strength (Equation 5.3). In some experiments, especially at low CO_2 loading or low temperature, nitrite was still present in solution after the first sample. Only samples where nitrite was below 1 % of the initial nitrite were regressed into the observed rate constant so as to deconvolute nitrosamine formation kinetics from nitrosamine decomposition kinetics.

$$\frac{dNNO}{dt} = -k_{obs}NNO \quad (5.1)$$

$$\ln(NNO) = \ln(NNO_i) - k_{obs}t \quad (5.2)$$

$$\log(k_{obs}) = a * \log(Par) + b \quad (5.3)$$

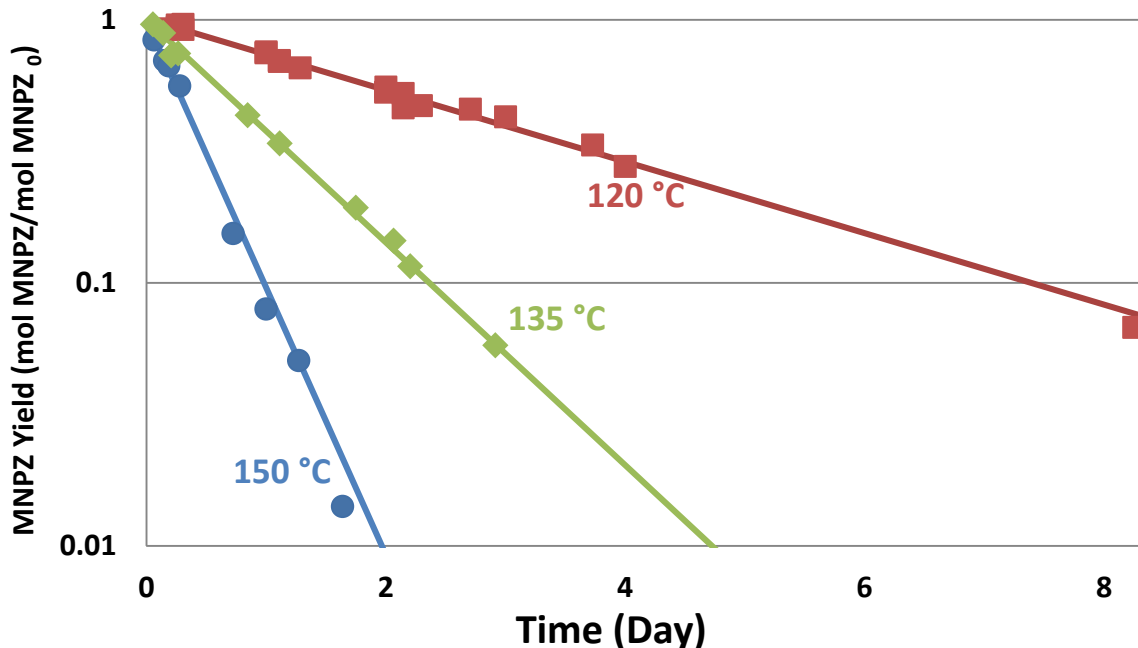


Figure 5.2: Raw data for MNPZ nitrosation kinetics using thermal cylinders at 120 °C (■) 135 °C (◆) and 150 °C (●); 4.9 M PZ, $\alpha = 0.31$ (Exp. 5.2–5.4); lines are regressed pseudo-first order decomposition

5.2.2 Thermal Cylinder Kinetic Results for Nitrosamine Decomposition

Table 5.1 summarizes all of the observed pseudo-first order decomposition rates for MNPZ, NDELA, and NHeGly. The error represents the standard error given by the linear regression from Equation 5.2 and is almost always less than 5% of the observed rate. Across all experiments, the average error in estimating the observed pseudo-first order rate constant was approximately 3%. The calculated pseudo-first order rate constant as a function of solvent basicity, temperature, and amine concentration is given by Equation 5.4 with parameters from Table 5.2.

Table 5.1: Nitrosamine decomposition using the thermal cylinder experiments; observed rate constants regressed from raw data and Equation 5.2. The calculated rate constants are regressed from observed rates and are given by Equation 5.4 and Table 5.2.

| Exp. # | T (°C) | Base (M) | $\alpha \left(\frac{\text{mol CO}_2}{\text{mol N}} \right)$ | $k_{\text{obs}} (\text{s}^{-1} \cdot 10^{-6})$ | $k_{\text{calc}} (\text{s}^{-1} \cdot 10^{-6})$ |
|-------------|--------|----------|--|--|---|
| MNPZ | | | | | |
| 5.1 | 100 | 4.9 PZ | 0.31 | 0.72±0.03 | 0.76 |
| 5.2 | 120 | 4.9 PZ | 0.31 | 3.7±0.1° | 3.6 |
| 5.3 | 135 | 4.9 PZ | 0.31 | 11.1±0.5 | 10.2 |
| 5.4 | 150 | 4.9 PZ | 0.31 | 26.9±1.6° | 27.4 |
| 5.5 | 165 | 4.9 PZ | 0.31 | 65.3±0.7 | 68.3 |
| 5.6 | 150 | 4.9 PZ | 0.30 | 28.0±1.8 ^x | 27.4 |
| 5.7 | 150 | 4.9 PZ | 0.30 | 31.4±1.5 ^{+x} | 27.4 |
| 5.8 | 150 | 4.9 PZ | 0.30 | 32.4±1.3 ^{+x} | 27.4 |
| 5.9 | 150 | 3.0 PZ | 0.30 | 22.6±0.6 | 21.2 |
| 5.10 | 150 | 1.7 PZ | 0.30 | 15.4±0.3 | 15.8 |
| 5.11 | 150 | 0.9 PZ | 0.30 | 10.7±0.2 | 11.4 |
| 5.12 | 150 | 0.4 PZ | 0.30 | 6.8±0.3 | 7.4 |

Table 5.1 Cont.

| | | | | | |
|---------------|-----|-----------|--------------------------------------|-----------------------|------|
| 5.13 | 150 | 0.2 PZ | 0.30 | 5.0±0.2 | 5.2 |
| 5.14 | 150 | 1.7 PZ | 0.6 M H ₂ SO ₄ | 19.0 ±0.8 | 15.8 |
| 5.15 | 150 | 4.9 PZ | 0.01 | 31.3±1.0 ^x | 27.4 |
| 5.16 | 150 | 4.9 PZ | 0.1 | 28.6±0.4 ^x | 27.4 |
| 5.17 | 150 | 4.7 PZ | 0.39 | 17.9±0.8 ^x | 26.8 |
| 5.18 | 150 | 0.05 NaOH | ≈0 | 223±8 | 260 |
| 5.19 | 150 | 0.1 NaOH | ≈0 | 350±20 | 380 |
| 5.20 | 150 | 0.5 NaOH | ≈0 | 810±60 | 850 |
| 5.21 | 150 | DDI Water | ≈0 | 0.58±0.03 | 0.66 |
| NDELA | | | | | |
| 5.22 | 150 | 6.6 MEA | 0.40 | 5.2±0.1 | 5.0 |
| 5.23 | 150 | 2.9 MEA | 0.40 | 3.1±0.02 | 3.3 |
| 5.24 | 150 | 1.0 MEA | 0.40 | 1.7±0.07 | 1.7 |
| 5.25 | 120 | 6.6 MEA | 0.40 | 0.49±0.01 | 0.49 |
| 5.26 | 120 | 2.9 MEA | 0.40 | 0.31±0.05 | 0.32 |
| 5.27 | 120 | 1.0 MEA | 0.40 | 0.18±0.01 | 0.18 |
| 5.28 | 150 | 6.6 MEA | ≈0 | 3.8±0.2 ^x | 5.0 |
| 5.29 | 150 | 0.1 NaOH | ≈0 | 110±6 | 110 |
| 5.30 | 150 | 3 MDEA | ≈0 | 1.1±0.04 | 1.0 |
| 5.31 | 150 | 4.9 PZ | 0.38 | 6.0±0.1 | 6.3 |
| 5.32 | 150 | 3.5 AMP | ≈0 | 2.8±0.03 | 2.6 |
| NHeGly | | | | | |
| 5.33 | 120 | 6.7 M MEA | 0.41 | 1.1±.04 | 1.1 |
| 5.34 | 150 | 6.7 M MEA | 0.41 | 17±1.8 | 17 |

° 0.4 mM Fe²⁺, 0.1 mM Ni²⁺, and 0.05 mM Cr³⁺ added to solution

⁺ Additional metal surface area for reaction

^x Loading and surface area effects not regressed into Equation 5.4

$$k_{calc} = k_o K_{a\ Base}^{\beta} [Base]^{\gamma} * e^{\frac{E_a}{R}(\frac{1}{423K} - \frac{1}{T})} \quad (5.4)$$

Table 5.2: High temperature nitrosamine decomposition parameters used in Equation 5.4

| Nitrosamine | k_o (s ⁻¹ M ^{-γ}) | β | γ | E_a (kJ/mol) |
|---------------|--|-------------------|-------------------|----------------|
| MNPZ | 4.6±0.2*10 ⁻¹⁰ | 0.52±.02 | 0.53±.02 | 94±3 |
| NDELA | 2.2±0.2*10 ⁻¹⁰ | 0.51±.02 | 0.54±.03 | 105±4 |
| NHeGly | 8.2±NA*10 ⁻¹⁰ | 0.50 ⁺ | 0.53 ⁺ | 112±NA |

⁺ Assumed parameters from MNPZ and NDELA results

5.2.3 MNPZ Decomposition Dependence on Temperature and Stainless Steel

Solutions of 4.9 M PZ loaded to 0.31 mol CO₂/mol N were heated at 100–165 °C. The rate constant was assumed to follow an empirical Arrhenius model centered at 135 °C (Equation 5.5). The Arrhenius model fit the data well with an activation energy of 94±3 kJ/mol and a rate constant at 135 °C of 10.2 ± 0.5*10⁻⁶ s⁻¹.

$$\ln k_{Decomp}(T) = \ln k_{Decomp}(408\ K) + \frac{E_a}{R} \left(\frac{1}{408} - \frac{1}{T} \right) \quad (5.5)$$

The dependence of MNPZ kinetics on stainless steel ions was tested by spiking the solutions for the 120 °C and 150 °C temperature experiments with 0.4 mM Fe²⁺, 0.1 mM Ni²⁺, and 0.05 mM Cr³⁺. At this temperature and reaction time, there will be minimal corrosion in the cylinders (Freeman 2011), therefore the only source of stainless steel ions in the experiments is expected to come from spiking the solutions. The Arrhenius model

fit the regressed rate constants regardless of whether stainless steel ions were added (Figure 5.3). Thus, MNPZ decomposition is not catalyzed by stainless steel ions.

To test for dependence on stainless steel surface area, solutions of 4.9 M PZ and a CO₂ loading of 0.30 were heated at 150 °C in ½-inch OD thermal cylinders, ⅜-inch OD cylinders, and ½-inch OD cylinders with stainless steel packing (Experiments 5.6–5.8). The stainless steel packing has a surface area of approximately 1200 m²/m³, which roughly quadrupled the surface area available for reaction in the ½-inch cylinders. The decomposition rate constant was not statistically different for the three experiments, so MNPZ decomposition is not catalyzed by the stainless steel surface.

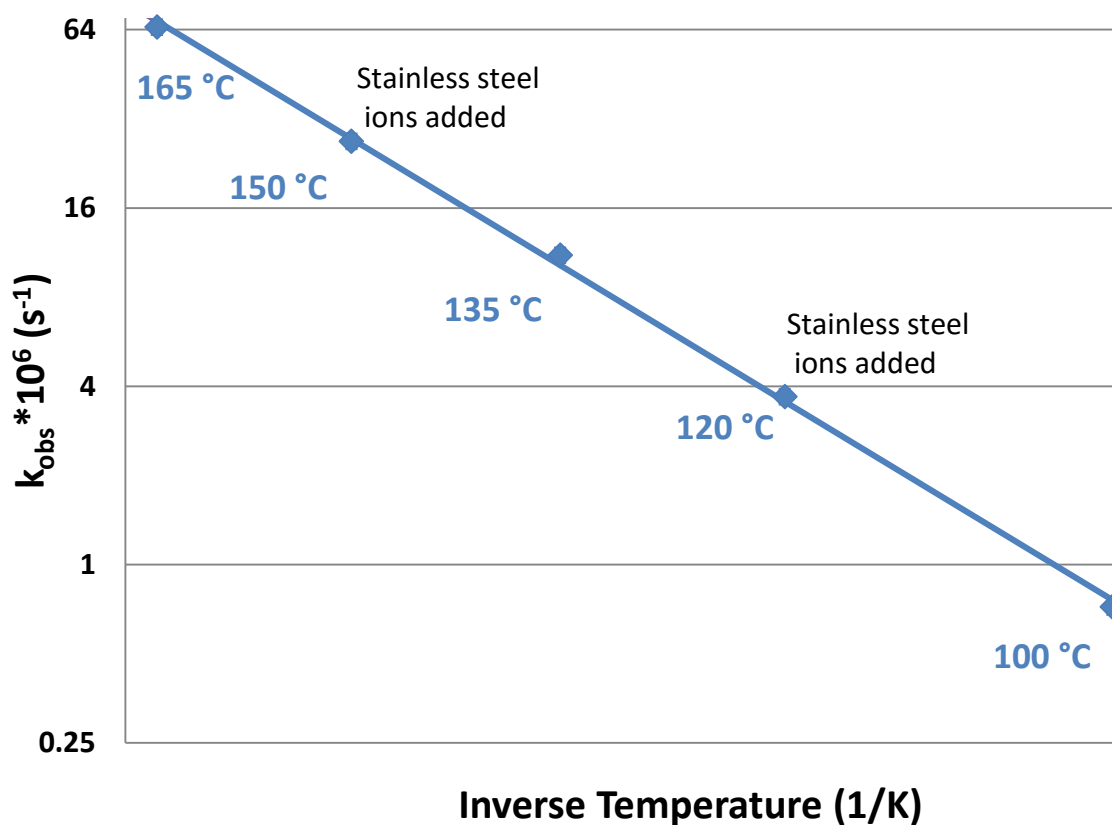


Figure. 5.3: k_{obs} dependence on stainless steel ions and temperature; 4.9 M PZ, $\alpha = 0.31$, stainless steel ions = 0.4 mM Fe²⁺, 0.1 mM Ni²⁺, and 0.05 mM Cr³⁺ (Exp. 5.1–5.5) Line from Equation 5.4 with $k_{obs \text{ } 135 \text{ } ^\circ\text{C}} = 10.2 \text{ s}^{-1}$ and $E_a = 94 \text{ kJ/mol}$

5.2.4 MNPZ Decomposition Dependence on Base Concentration

To study the dependence of MNPZ decomposition on base concentration, MNPZ was decomposed at 150 °C in loaded aqueous PZ with PZ ranging 1–5 M. The observed rate constant had a roughly half-order dependence on total PZ concentration. Approximately 1–5 mM of MNPZ standard was then added to 0.05–0.5 M NaOH and decomposed at 150 °C. MNPZ decomposition was half-order in NaOH concentration and two orders of magnitude faster than decomposition in the PZ solutions (Figure 5.4).

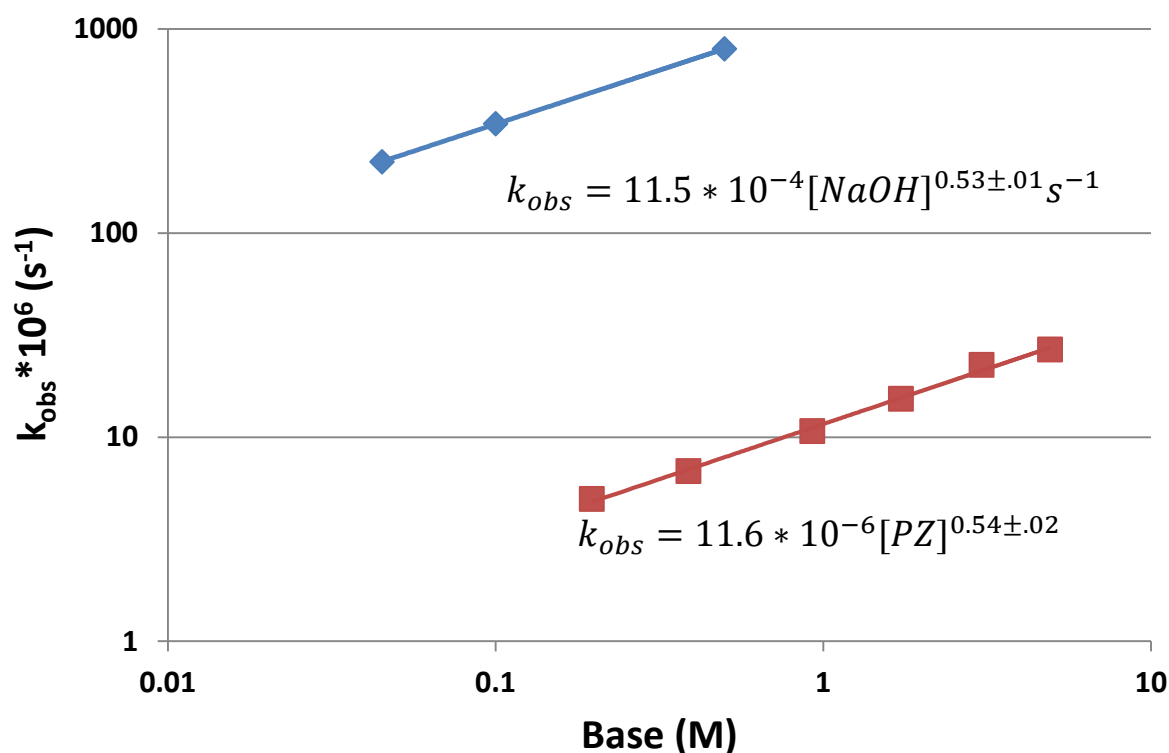


Figure 5.4: MNPZ decomposition dependence on total PZ, $\alpha=0.3$ (■) and NaOH (♦) at 150 °C (Exp. 5.4, 5.9–5.13, 5.18–5.20)

5.2.5 MNPZ Decomposition Dependence on Loading and pH

Nitrosamine decomposition has been reported to have a strong dependence on pH (Fan and Tannenbaum 1972). To study this dependence, MNPZ was decomposed in 5 M PZ with 0–0.4 mol CO₂/mol N. Since CO₂ is an acid gas, it acidifies the PZ solution as it

chemically absorbs. The pH change due to CO₂ loading did not have a dramatic impact on decomposition rates. Even though pH varied by more than a decade as PZ loading increased to 0.4, the rates only decreased by 50 % (Figure 5.5). Loading might also affect decomposition by reducing the free amine in solution. The rate decreased as PZ was loaded with CO₂, but decomposition was not half-order in free nitrogen as estimated using Equation 5.6. Difference in ionic strength at different loadings is the most probable explanation for the low dependence on loading. The higher ionic strength in loaded solutions could stabilize any charged intermediates in nitrosamine decomposition and counteract the loss of free amine. Since CO₂ loading only had a significant impact at very high loadings where the concentration of free amine plummets, it was not regressed into the final model.

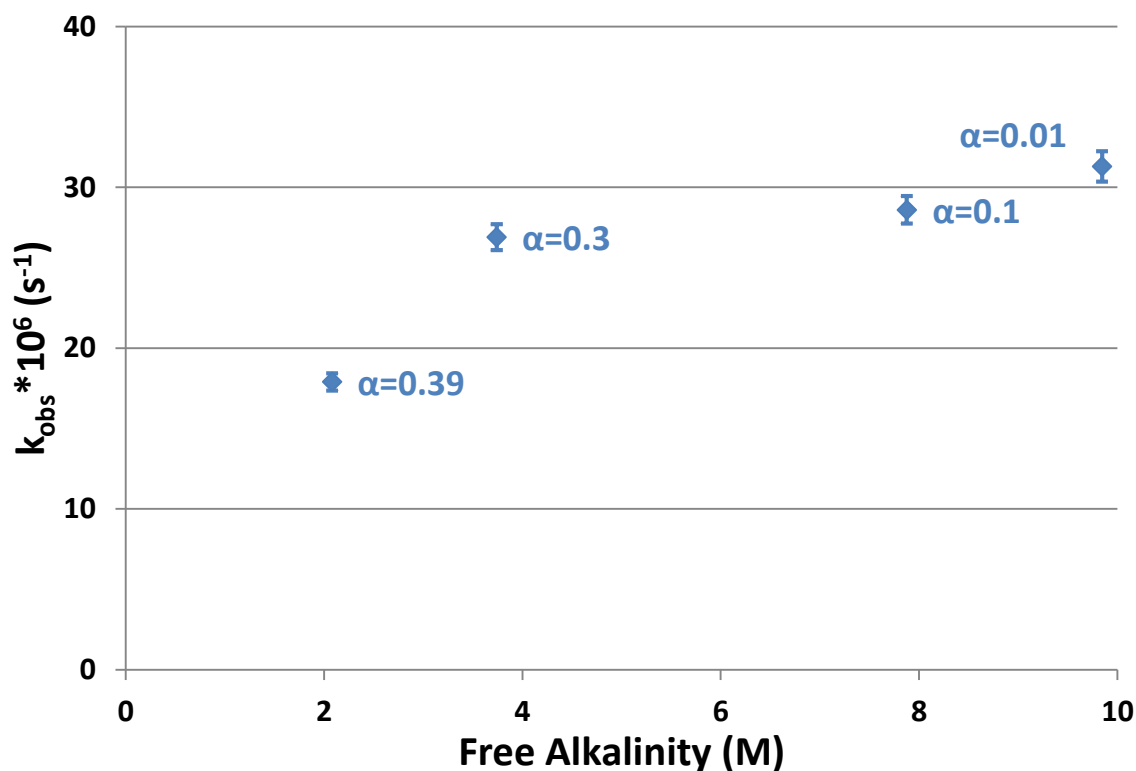


Figure 5.5: MNPZ decomposition in 5 M PZ at 150 °C as a function of loading (Exp. 5.4 & 5.15–5.17)

$$Free\ Nitrogen = [PZ] * \frac{2\ N}{PZ} * \frac{1}{1 - 2\alpha} \quad (5.6)$$

5.2.6 MNPZ Decomposition Dependence on Base Strength

The observed MNPZ decomposition constant at 150 °C was normalized for base concentration (Equation 5.7) and compared across three different bases of varying pK_a (H₂O, PZ, and NaOH). Since each base exhibits different temperature behavior, the pK_a values for the bases were extrapolated to 150 °C using available literature and the van't Hoff equation (Equation 5.8) (Goldberg, Kishore, and Lennen 2002; Hummer, Pratt, and Garcia 1995; Kim et al. 2011). Since there is very little pK_a data at these high temperatures and pressures, base strength estimation represented the largest source of error for these experiments. MNPZ decomposition was found to be base catalyzed with a Brønsted slope of $\beta = 0.52$ across the entire range (Equation 5.9) (Figure 5.6). This suggests that MNPZ decomposition is a concerted mechanism with the abstraction of a hydrogen in the rate limiting step (Jenks 1972; Schwetlick, Noack, and Stebner 1994).

$$k_2 = \frac{k_{obs}}{[Base]^{0.53}} \quad (5.7)$$

$$pK_{a\ exp} = pK_{a\ Room\ T} - \log \left(e^{\frac{-\Delta H_{Diss}}{R} * \left(\frac{1}{T_{exp}} - \frac{1}{T_{Room}} \right)} \right) \quad (5.8)$$

$$Log(k_2) = 0.52 * pK_{a\ Base} - 9.3 \quad (5.9)$$

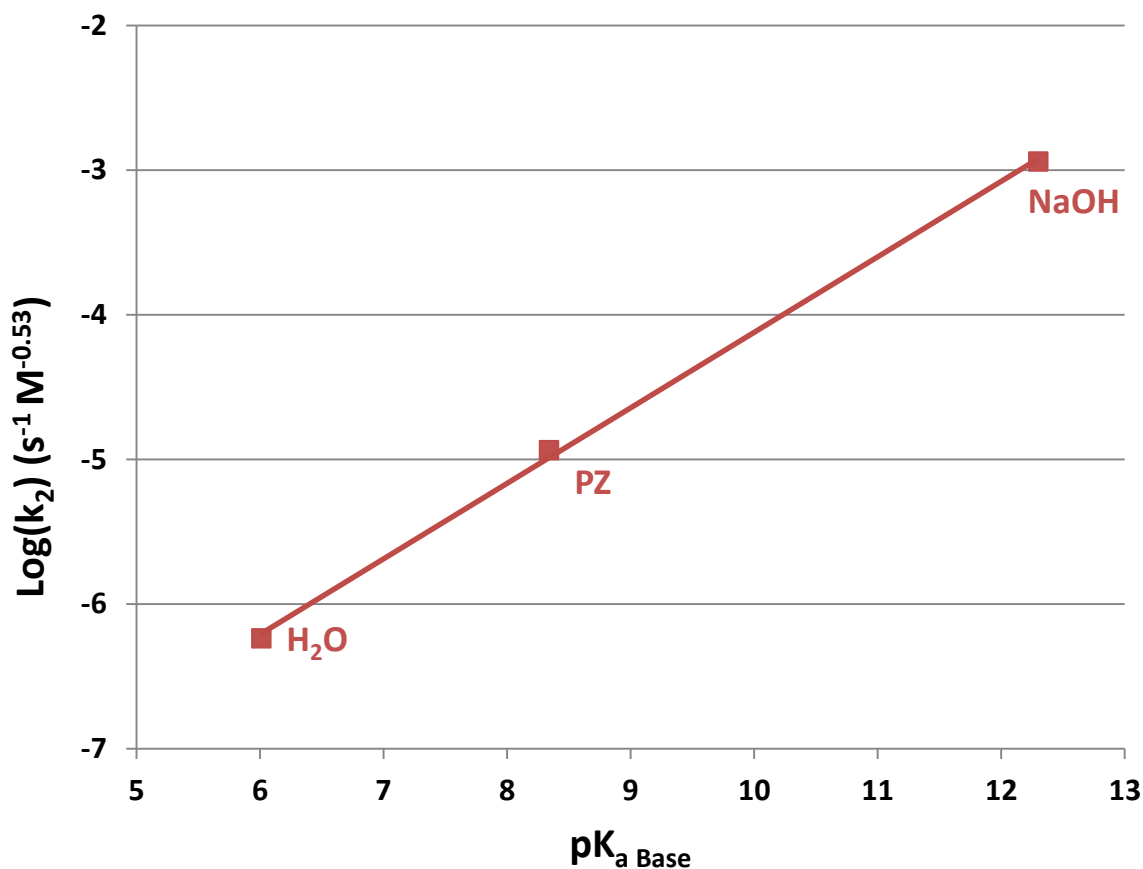


Figure 5.6: MNPZ decomposition dependence on base strength at 150 °C (Exp. 5.15, 5.19, & 5.21)

5.2.7 NDELA and NHeGly Decomposition Kinetics

Similar to the nitrosation experiments with NDELA and NHeGly formation in MEA (Section 4.4), nitrosamine decomposition of NDELA and NHeGly was characterized in MEA to simulate nitrosamine behavior under stripper conditions in an MEA-based scrubber. Laboratory-grade NDELA was spiked at 50 mmol/kg into CO_2 loaded, 1–7 M MEA and decomposed at 120–150 °C. Like MNPZ, NDELA decomposition was first order in NDELA and roughly half-order in amine concentration. Decomposition had an activation energy of 105 ± 2 kJ/mol with a rate of $1.7 \cdot 10^{-6} \text{ s}^{-1}$ in 1 M MEA at 150 °C. NDELA actually decomposed more slowly in unloaded MEA than in loaded MEA even

though unloaded MEA has more free base for reaction, possibly due to ionic strength effects (Figure 5.7). NDELA decomposition kinetics were also measured in MDEA, PZ, AMP, and NaOH; decomposition was base catalyzed with a Brønsted slope of 0.51 (Equations 5.10 & 5.11) (Figure 5.8).

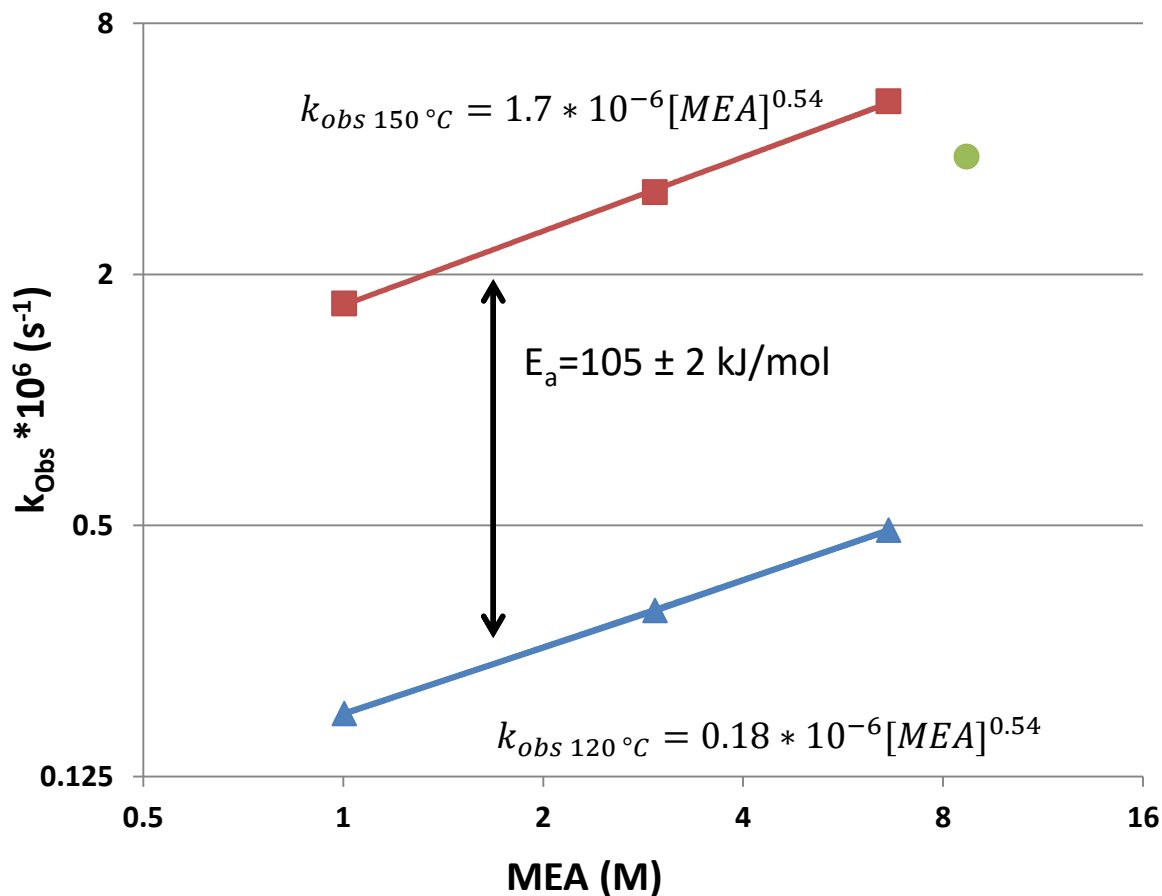


Figure 5.7: NDELA decomposition in MEA, $\alpha = 0.4$ at 150 °C (■) and 120 °C (▲) and in unloaded MEA at 150 °C (●) (Exp. 5.22–5.28)

$$k_2 = \frac{k_{obs}}{[Base]^{0.54}} \quad (5.10)$$

$$\text{Log}(k_2) = 0.51 * pK_{a\text{Base}} - 9.77 \quad (5.11)$$

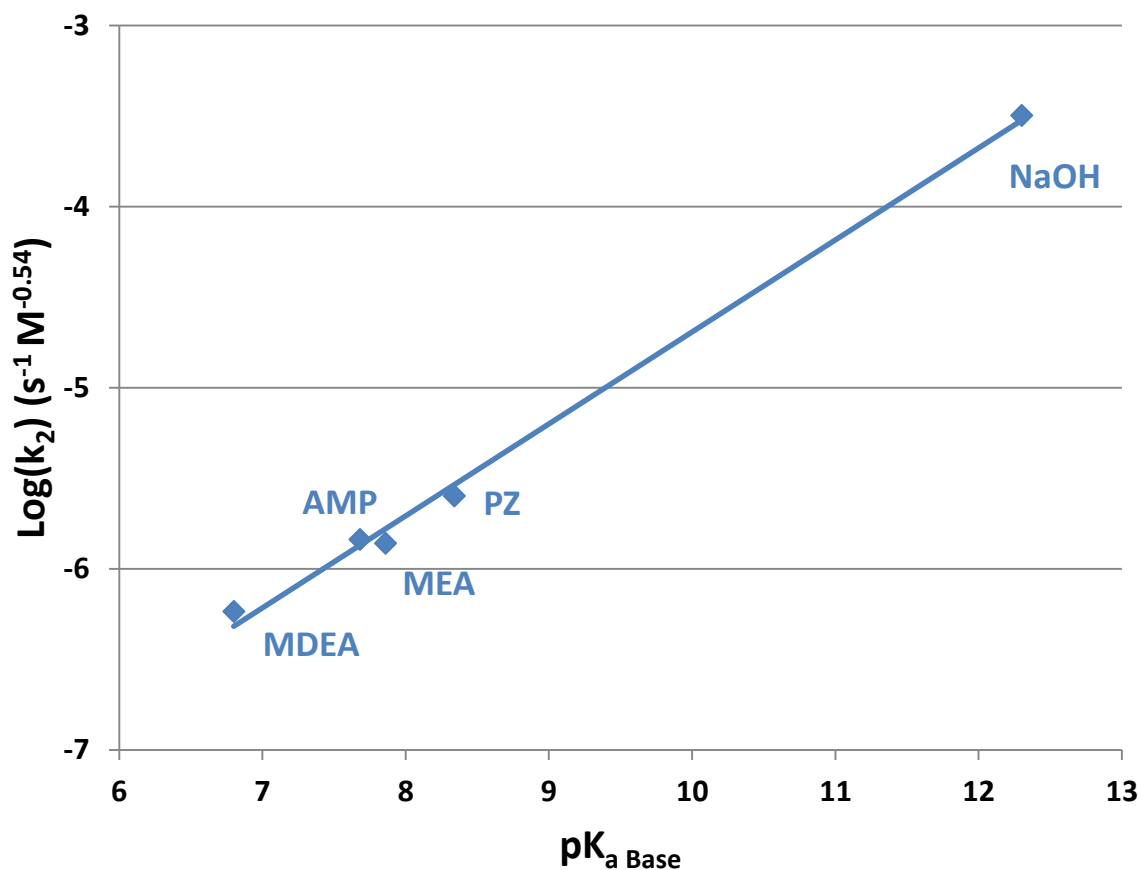


Figure 5.8: NDELA decomposition dependence on base strength at 150 °C (Exp. 5.28–5.32)

It was difficult to synthesize NHeGly safely at high concentrations, so its decomposition was measured in MEA where it was made *in situ*. NHeGly decomposition was $1.1 \cdot 10^{-6} \text{ s}^{-1}$ in 7 M MEA at 120 °C with an apparent activation energy of 112 kJ/mol (Experiments 5.33 & 5.34). Assuming that NHeGly has similar base and concentration dependencies to the other nitrosamines, NHeGly decomposition is fastest ($k_o = 8.2 \cdot 10^{-10} \text{ s}^{-1} \text{ M}^{-0.5}$), followed by MNPZ decomposition ($k_o = 4.6 \cdot 10^{-10} \text{ s}^{-1} \text{ M}^{-0.53}$) and NDELA ($k_o = 2.2 \cdot 10^{-10} \text{ s}^{-1} \text{ M}^{-0.54}$). In 6.7 M MEA at a loading of 0.4 moles CO₂/mol N and 150 °C, the pseudo-first order decomposition rate constants for NHeGly, MNPZ, and NDELA are predicted to be $17.0 \cdot 10^{-6} \text{ s}^{-1}$, $10.1 \cdot 10^{-6} \text{ s}^{-1}$, and $5.0 \cdot 10^{-6} \text{ s}^{-1}$ respectively.

5.3 MNPZ DECOMPOSITION PRODUCTS AND MECHANISM

5.3.1 Aqueous MNPZ Decomposition Products

Nitrosamines are good nitrosating agents themselves, so it is possible that nitrosamines transnitrosate into other nitrosamines at high temperatures (Douglass and Kabacoff 1978). Since nitrosamines as a family are carcinogenic, transnitrosation would appear to decompose the specific nitrosamine, but would not necessarily reduce the carcinogenicity of the solvent. To test for the possibility of transnitrosation, samples of decomposed MNPZ were analyzed for both MNPZ and total nitrosamine. Total nitrosamine decomposed at the same rate as MNPZ, disproving transnitrosation (Figure 5.9).

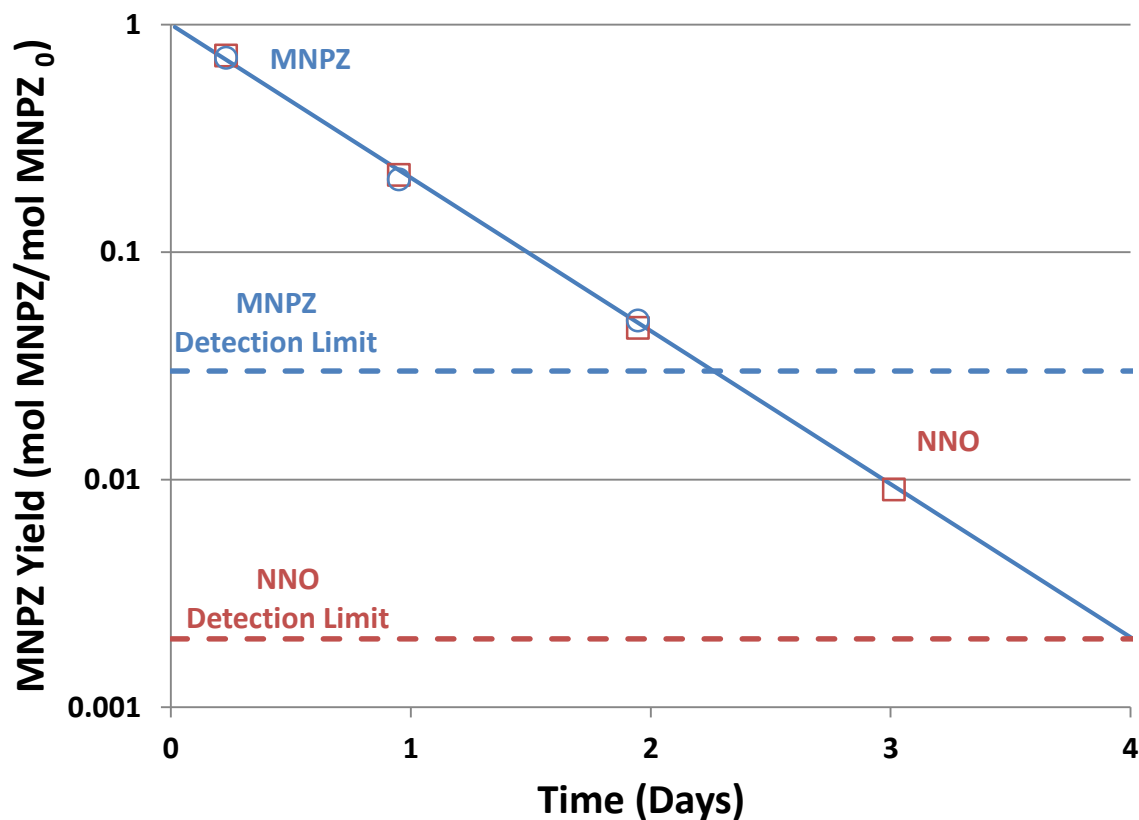


Figure 5.9: MNPZ (●) and total nitrosamine (■) decomposition in 4.7 M PZ, $\alpha = 0.39$ at 150 °C (Exp. 5.17)

In a separate experiment, decomposed MNPZ was analyzed using the total aldehyde method. The total aldehyde accumulated as MNPZ decomposed with a yield of 0.51 ± 0.09 (Figure 5.10). The final sample was analyzed using high resolution mass spectrometry, and 2-piperazinol was positively identified in the solution matrix. PZ is also hypothesized to form during MNPZ decomposition, but the high concentration of PZ in the original solution prohibited analysis of formed PZ.

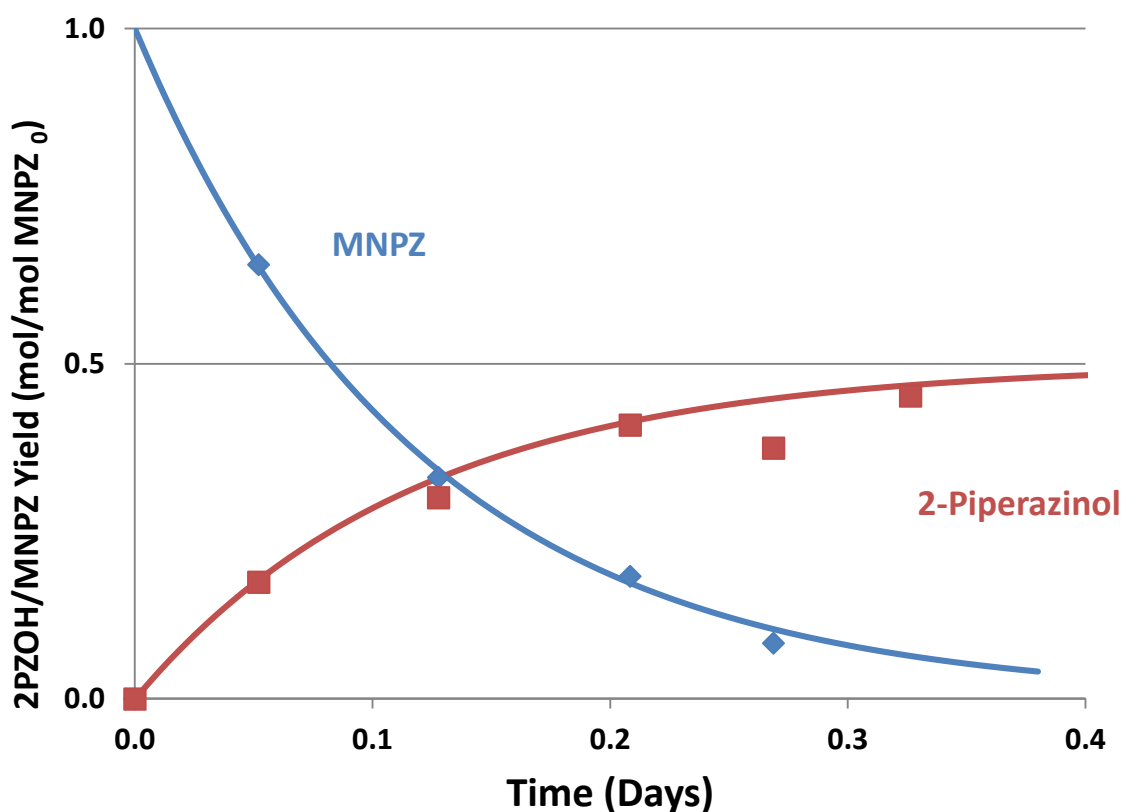


Figure 5.10: MNPZ decomposition (◆) and 2-piperazinol formation (■) in unloaded 7.5 M PZ at 175 °C; 2-piperazinol formation modeled as first-order with a yield of 0.51.

5.3.2 Gaseous MNPZ Decomposition Products

A solution of 5 M PZ at $\alpha = 0.4$ was spiked with 600 mM $\text{NaN}^{15}\text{O}_2$, and heated to 150 °C in the thermal cylinders. The cylinders were removed periodically and cooled at

room temperature. Once cooled, the solution was removed from the cylinders, allowing nitrogenous gases to escape, and then analyzed using N^{15} NMR. The unheated sample showed a spike at a 610 ppm shift from ammonia, agreeing well with literature values for nitrite shift (Lambert, Binsch, and Roberts 1964). After heating for 1 hour at 150 °C all the nitrite had reacted to form nitrosamine, which had a 540 ppm shift from ammonia. The sample after one day of heating showed much less nitrosamine without any other major peaks, while the sample after two days showed no signs of N^{15} above the naturally occurring N^{15} in the PZ solution (Figure 5.11). The disappearance of spiked N^{15} from the aqueous phase proves the formation of nitrogenous gaseous products from nitrosamine decomposition; the most likely gas product is N_2O .

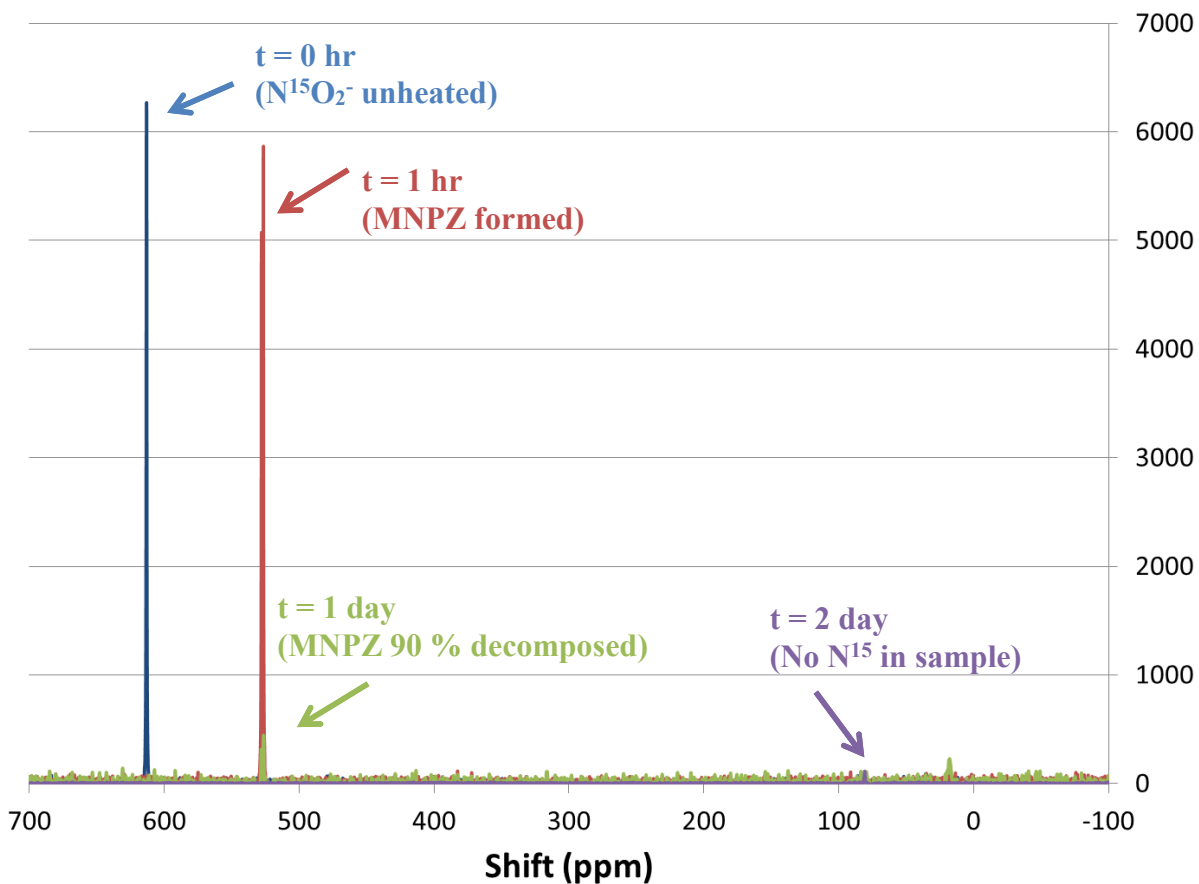


Figure 5.11: N^{15} NMR scan of decomposing MNPZ in 5M PZ, $\alpha = 0.4$, $T = 150$ °C

5.3.3 MNPZ Thermal Decomposition Mechanism

The mechanism for MNPZ decomposition can now be hypothesized based on the empirical rate law and decomposition products. The mechanism starts with the abstraction of the hydrogen on the carbon alpha to the nitroso group and the breaking of the N-N bond to form a nitrosyl anion via an E2 elimination. The nitrosyl anion goes on to form hyponitrous acid and then nitrous oxide (Buchholz and Powell 1963) while the PZ imine equilibrates with 2PZOH (Figure 5.12). First order dependence on nitrosamine follows directly from the mechanism. However, dependence on amine concentration should also be first order; variance in ionic strength of the solution and the activity of the amine are the most likely reasons for the discrepancy.

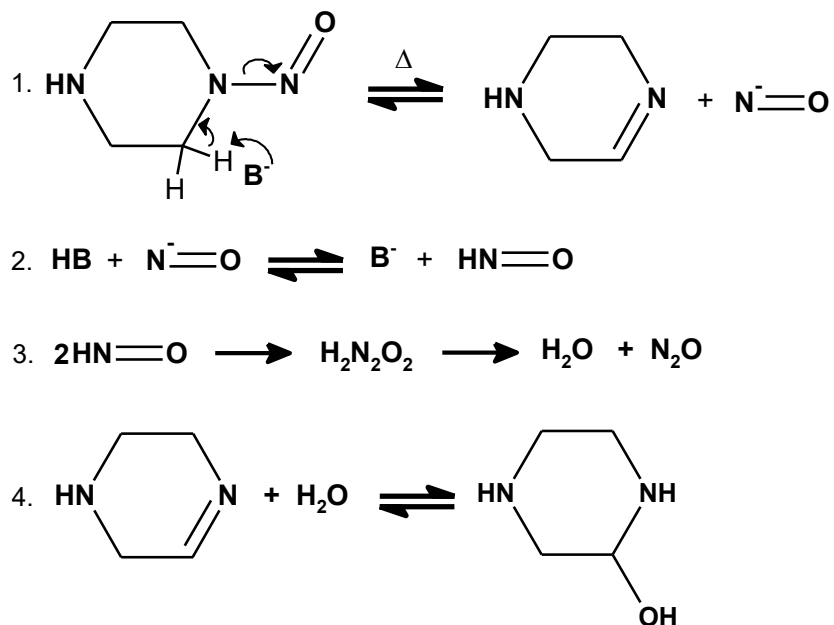


Figure 5.12: MNPZ base-catalyzed, high temperature, thermal decomposition mechanism

5.3.4 Environmental Impact of Nitrosamine Decomposition Products

The main aqueous product for nitrosamine decomposition is hypothesized to be a hemiaminal which is generally non-toxic. The main gaseous product is hypothesized to be

N₂O, an extremely potent GHG with 180 times the global warming potential of CO₂ (Lashof and Ahuja 1990). Most likely the trace levels of N₂O will exit the desorber with the CO₂ for compression and sequestration, but N₂O might be emitted from the absorber along with the scrubbed flue gas. The maximum N₂O emission is half of the 1–5 ppm of NO₂ in the inlet flue gas, approximately 100–300 ppm equivalent CO₂. A scrubbed flue gas usually emits over 1% CO₂, so the maximum N₂O is too dilute to add significantly to overall GHG emissions.

5.4 NITROSAMINE VOLATILITY IN THE THERMAL RECLAIMER

5.4.1 Nitrosamine Volatility Data Analysis and Results

The bench scale thermal reclaimer described in Section 2.2.6 was used to measure the relative volatility of amines and nitrosamines at reclaimer conditions. Briefly, a pilot plant solution containing nitrosamines was introduced into a constantly heated round-bottom flask and distilled at 130–170 °C and atmospheric pressure. The temperature was controlled by periodically introducing more solvent into the bottoms as it evaporated. At set time intervals, the distillate chamber was completely drained, and allowed to refill by approximately 5 mL. Samples were then taken from both the fresh distillate and the reclaimer bottoms. The fresh distillate results thus gave the instantaneous amine and nitrosamine volatility at a given temperature and composition of the reclaimer bottoms. The samples were analyzed for the reclaimed amine using cation chromatography and for nitrosamines using either the HPLC method or the TONO method. A unit-less Henry's coefficient on a wt % basis represents the ratio of concentrations in the distillate and the bottoms (Equation 5.12) (Table 5.3).

$$[A]_{Distillate} = k_H * [A]_{Bottoms} \quad (5.12)$$

Table 5.3: Bottoms and Distillate results for thermal reclaiming of degraded MEA and degraded PZ; the Henry's coefficient is given by Equation 5.12

| Exp. # | Time (hrs) | T (°C) | Bottoms MEA (wt%) | Distillate MEA (wt%) | k _H MEA | Bottoms NNO (mmol/kg) | Distillate NNO (mmol/kg) | k _H NNO |
|--------------------------------|------------|--------|-------------------|----------------------|--------------------|------------------------|---------------------------|---------------------|
| Degraded MEA from NCCC | | | | | | | | |
| 5.35 | 0.0 | 20 | 28% | | | 0.25 | | |
| 5.36 | 4.0 | 150 | 75% | 61% | 0.82 | | | |
| 5.37 | 4.7 | 150 | 71% | 57% | 0.80 | | | |
| 5.38 | 5.4 | 150 | 22% | 43% | 1.97 | | | |
| 5.39 | 6.3 | 150 | 20% | 27% | 1.35 | 1.06 | 0.043 | 0.041 |
| 5.40 | 6.8 | 150 | 20% | 28% | 1.42 | 1.1 | 0.045 | 0.041 |
| 5.41 | 7.3 | 150 | 18% | 28% | 1.59 | 1.12 | 0.040 | 0.036 |
| Exp. # | T (°C) | | Bottoms PZ (wt%) | Distillate PZ (wt%) | k _H PZ | Bottoms MNPZ (mmol/kg) | Distillate MNPZ (mmol/kg) | k _H MNPZ |
| Degraded PZ from Pilot Plant 2 | | | | | | | | |
| 5.42 | 20 | | 34% | | | 1.0 | | |
| 5.43 | 130 | | 35% | 33% | 0.93 | 25.7 | 0.5 | 0.018 |
| 5.44 | 140 | | 31% | 49% | 1.58 | 30.0 | 0.8 | 0.028 |
| 5.45 | 150 | | 31% | 59% | 1.92 | 36.4 | 1.6 | 0.045 |
| 5.46 | 160 | | 27% | 49% | 1.85 | 38.2 | 2.0 | 0.052 |
| 5.47 | 170 | | 22% | 47% | 2.20 | 37.1 | 1.9 | 0.051 |

5.4.2 Total Nitrosamine Volatility in Degraded MEA

Partially degraded MEA solvent from a pilot plant campaign running at the National Carbon Capture Center (NCCC) was heated from 20 to 150 °C in semi-batch operation for four hours as the bottoms concentrated. Temperature was then maintained at 150 °C during continuous distillation for another three hours to approximate steady state operation of the thermal reclaimer. MEA in the reclaimer bottoms initially increased over the first three hours while the temperature increased to 150 °C. This was due to water and CO₂ evaporating out of solution at lower temperatures while MEA remained relatively non-volatile. At the four hour mark, the temperature reached 150 °C and was maintained by constantly feeding solvent into the bottoms. For the next hour, the MEA in the bottoms decreased as MEA volatilized and the reclaimer bottoms became concentrated in non-volatile degradation products. After five hours, MEA stabilized as the rate of MEA feed roughly equaled the rate of MEA distillation. Once steady state was reached for MEA, samples were also analyzed for total nitrosamine. The nitrosamine in the reclaimer bottoms had concentrated by a factor of four while the distillate contained almost no nitrosamine (Figure 5.13). Total nitrosamine in the reclaimer bottoms was still concentrating after seven hours, indicating that it had not yet reached steady state.

The Henry's coefficient for MEA was $k_H = 1.45 \pm 0.15$ at steady-state, implying that MEA in the reclaimer purge will be 63–75 % the concentration of MEA in the distillate. Along with thermal decomposition of MEA in the reclaimer, this represents the major loss of MEA from thermal reclaiming. Total nitrosamines were 30–40 times less volatile than MEA at thermal reclaimer conditions, demonstrating that they can be effectively reclaimed out of the circulating solvent. However, it is important to note that total nitrosamine is a sum of all nitrosamines in the degraded MEA solvent, each of which will have different volatility. For instance, NHeGly is ionic due to its carboxylate group and will therefore be completely non-volatile. NDELA has been shown to be volatile at water wash conditions (Khakharia et al. 2014) and may be the volatilizing nitrosamine species in this pilot plant solvent. However, NDELA was not quantifiable in either the

reclaimer bottoms or distillate due to interferences from other degradation products on the HPLC chromatograph. Total nitrosamine volatility for an MEA solvent will thus be dependent on the scrubber operating conditions, which can affect the relative concentrations of volatile and non-volatile nitrosamines.

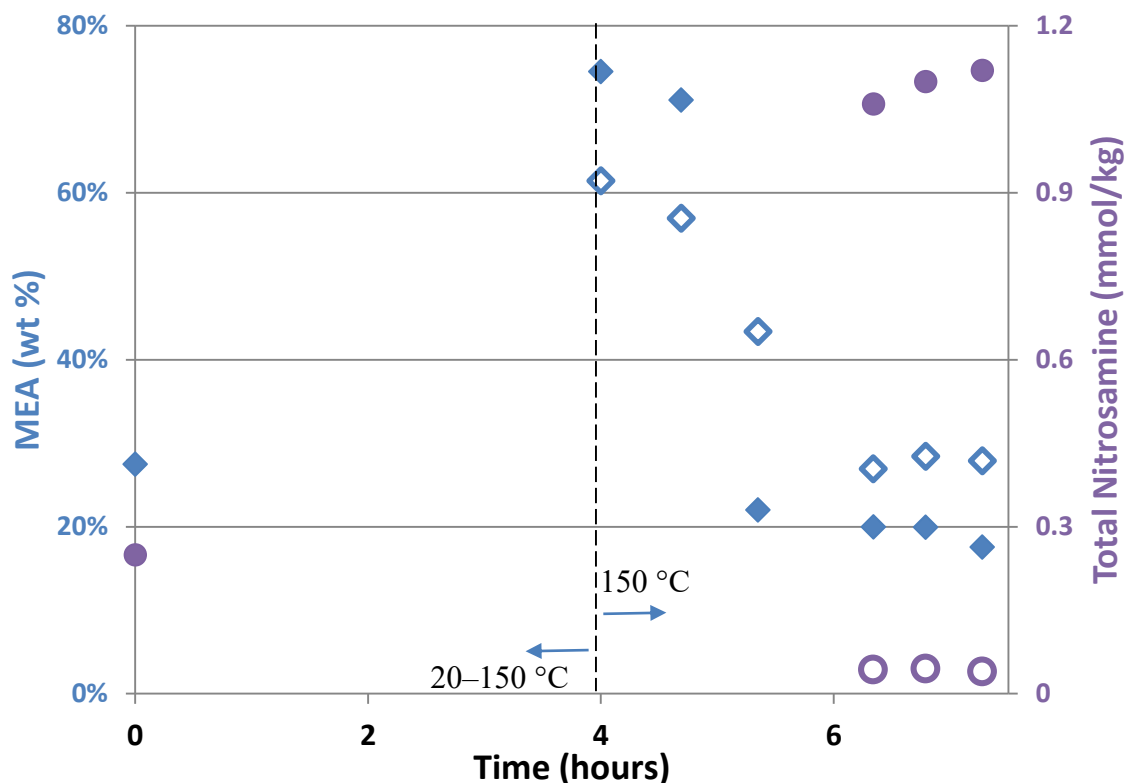
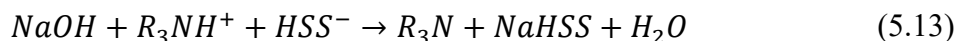


Figure 5.13: MEA (◆) and total nitrosamine (●) concentration in the reclaimer bottoms (filled points) and distillate (open points); initial solvent nominally 30 wt % MEA from NCCC pilot plant. Continuously reclaimed at 150 °C and 1 atm after the fourth hour.

The total nitrosamine accumulation in the reclaimer bottoms seems to be in direct conflict with earlier reports (Strazisar, Anderson, and White 2003). However, excess NaOH has been traditionally added to thermal reclaimers to liberate the amine from the heat stable salt (HSS) and increase amine recovery (Equation 5.13) (Sexton et al. 2014).



NaOH will also catalyze nitrosamine decomposition, which could explain the lack of nitrosamine found in pilot plant reclaimer bottoms. Other unspecified factors such as the reclaimer residence time and temperature could also affect nitrosamine accumulation in the thermal reclaimer.

5.4.3 MNPZ Volatility in Degraded PZ

A previously characterized, partially degraded PZ solvent from Pilot Plant 2 (P. T. Nielsen, Li, and Rochelle 2013) was thermally reclaimed at $T = 130\text{--}170\text{ }^{\circ}\text{C}$. Like the MEA solvent, PZ was initially heated to the reclaiming temperature and maintained at that temperature for one hour to simulate continuous thermal reclaiming. The temperature was then maintained for ten more minutes and a sample was taken of the distillate and bottoms. The thermal reclaimer temperature was allowed to increase by $10\text{ }^{\circ}\text{C}$ and then maintained at the new set point for at least ten minutes before sampling again.

PZ volatility increased from $k_H = 0.93$ to $k_H = 2.20$ as temperature increased from $130\text{--}170\text{ }^{\circ}\text{C}$. PZ volatility was $30\pm 10\%$ higher than MEA volatility at $150\text{ }^{\circ}\text{C}$, suggesting that PZ losses in the reclaiming purge will be lower than MEA losses as previously predicted (Rochelle et al. 2011). Like total nitrosamine volatility in MEA, MNPZ volatility was much lower than PZ volatility with k_H values of $0.018\text{--}0.051$, approximately 40–60 times lower than PZ. The k_H temperature dependence was linearly regressed for both PZ and MNPZ (Equations 5.14 & 5.15), which matched the data within 20 % (Figure 5.14).

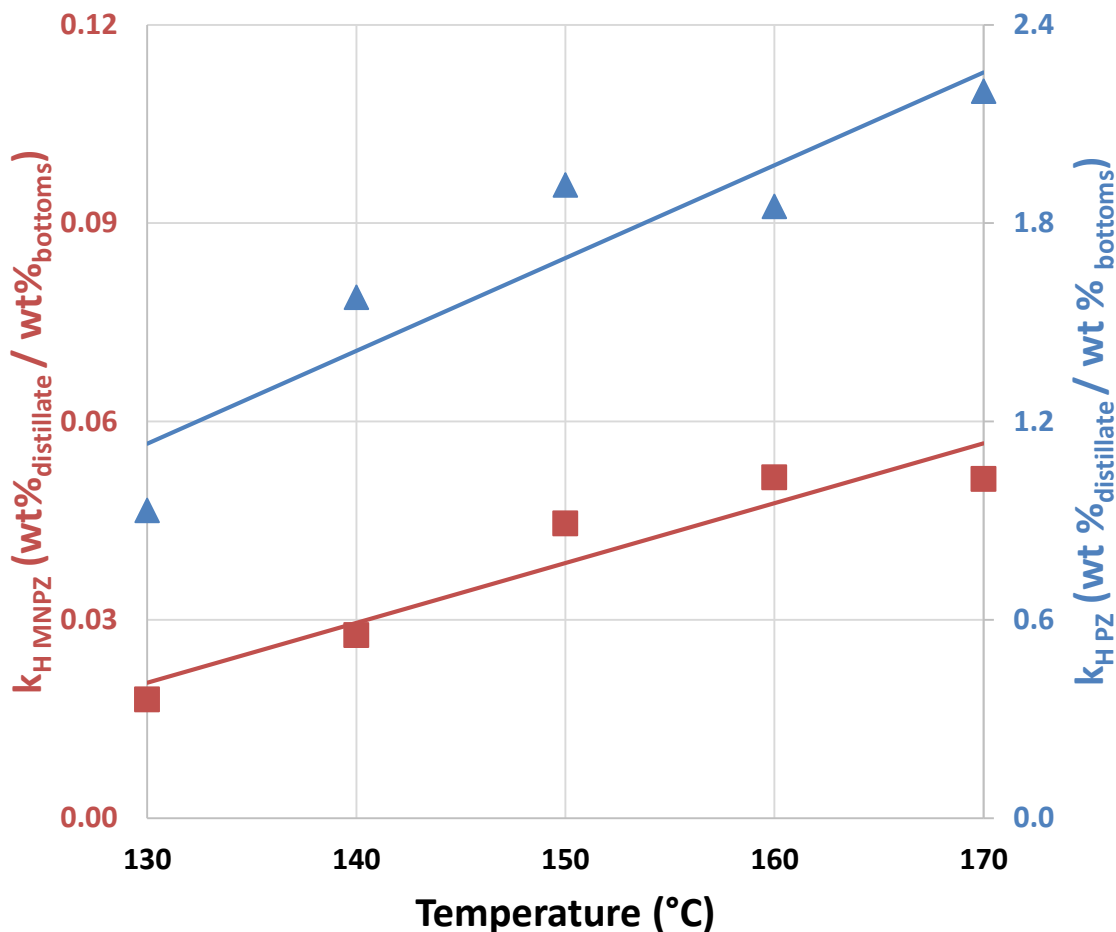


Figure 5.14: MNPZ (■) and PZ (◆) volatilities in a degraded pilot plant solution at thermal reclaiming conditions; reclaimer operated at 1 atm, PZ solution from PP2, k_H defined by Equation 5.12, lines from Equations 5.14 & 5.15.

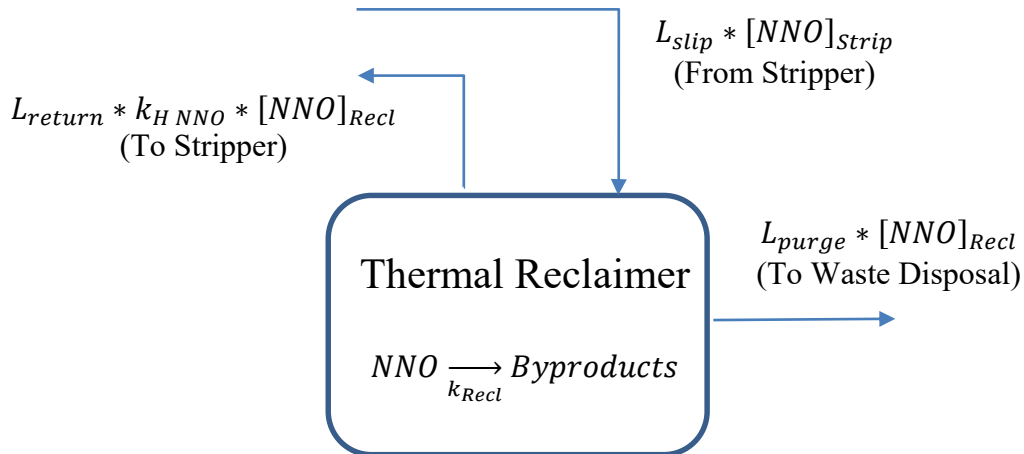
$$k_{H \text{ PZ}}(T) = 1.7 + 0.028 * (T - 150 \text{ } ^\circ\text{C}) \quad (5.14)$$

$$k_{H \text{ MNPZ}}(T) = 0.039 + 0.00091 * (T - 150 \text{ } ^\circ\text{C}) \quad (5.15)$$

5.4.4 Nitrosamine Thermal Reclaiming Efficiency

Unlike HSS and metal ions, nitrosamines have a small but non-zero volatility at reclaimer conditions. Nitrosamines will therefore concentrate in the reclaimer bottoms, but some nitrosamine will always be returned to the circulating solvent through the reclaimer distillate. A steady-state mass balance around the thermal reclaimer must be performed to determine the efficiency for removing nitrosamines through thermal reclaiming. Nitrosamines are fed to the thermal reclaimer

through a slipstream from the stripper; they are removed from the reclaimer either through evaporation, decomposition, or purge (Figure 5.15).



Performing a mole balance around nitrosamine accumulation in the thermal reclaimer yields Equation 5.16.

$$\frac{d n_{NNO \text{ Reclaimer}}}{dt} = L_{slip} * [NNO]_{Strip} - L_{return} * k_{H \text{ NNO}} * [NNO]_{Recl} - k_{recl} * [NNO]_{Recl} V_{recl} - L_{purge} * [NNO]_{Recl} \quad (5.16)$$

Assuming steady-state and the purge rate is much lower than the slip/return rate, Equation 5.16 can be solved for the nitrosamine concentration in the reclaimer (Equation 5.17).

$$[NNO]_{Recl} = \frac{[NNO]_{Strip}}{k_{H \text{ NNO}} + k_{Recl} * \tau_{Recl}} \quad \text{Where: } \tau_{Recl} = \frac{V_{recl}}{L_{slip}} = \frac{V_{recl}}{L_{Return}} \quad (5.17)$$

The removal efficiency for thermal reclaiming can be defined as the percentage of nitrosamine in the slipstream from the stripper that is removed in the thermal reclaimer instead of returned in the distillate (Equation 5.18). The MNPZ removal efficiency can then be calculated for reclaiming PZ assuming operation at 150 °C, a residence time of 600 seconds in the thermal reclaimer, and 1 M excess NaOH in the reclaimer bottoms (Equation 5.19).

$$Removal \text{ Efficiency} = 1 - \frac{L_{return} k_{H \text{ NNO}} [NNO]_{Recl}}{L_{slip} [NNO]_{Strip}} = 1 - \frac{k_{H \text{ NNO}}}{k_{H \text{ NNO}} + k_{Recl} * \tau_{Recl}} \quad (5.18)$$

$$\text{Removal Efficiency of MNPZ} = 1 - \frac{0.039}{0.039 + 11.5 * 10^{-4} \text{ s}^{-1} * 600 \text{ s}} = 95 \% \quad (5.19)$$

Almost all of the MNPZ fed to the thermal reclaimer will be removed from the solvent due to the low volatility and low thermal stability of MNPZ at reclaimer conditions. Nitrosamine removal from the purge stream before disposal could also be easily accomplished by further heat treatment. Therefore, nitrosamines pose no potential risk for reclaimer waste disposal. Removal efficiencies for total nitrosamines in MEA could not be determined due to the expected large variance in nitrosamine volatilities and thermal stabilities in the pilot plant solvent. However, the residence time in the thermal reclaimer could be increased so that relatively non-volatile nitrosamines could be efficiently removed from the MEA solvent.

5.5 CONCLUSIONS

5.5.1 High Temperature Nitrosamine Decomposition Kinetics

- Nitrosamines thermally decompose at stripper conditions in amine solutions.
- Nitrosamine decomposition is first order in nitrosamine; the pseudo-first order decomposition rate of MNPZ in 4.9 M PZ at $\alpha = 0.31$ and 150 °C is $2.7 * 10^{-5} \text{ s}^{-1}$.
- Nitrosamine decomposition is not catalyzed by stainless steel ions or stainless steel surface area.
- Decomposition follows an Arrhenius temperature dependence with an activation energy around 100 kJ/mol.
- Decomposition is half-order in total base concentration and a weak function of loading at lean amine conditions.
- Decomposition is base-catalyzed with a Brønsted slope of approximately 0.5.

5.5.2 MNPZ Decomposition Products and Mechanism

- MNPZ does not form other nitrosamines when decomposing in loaded PZ solutions.
- MNPZ decomposition forms 2PZOH with an approximate yield of 0.5 moles 2PZOH per mole of MNPZ decomposed.

- The nitrogen on the nitroso-group decomposes into a gaseous product predicted to be N_2O .
- The hypothesized, base-catalyzed MNPZ decomposition mechanism goes through an E2 elimination, forming an imine and N_2O ; the imine equilibrates in aqueous solution with 2PZOH.
- N_2O emissions from nitrosamine decomposition will be around 1-3 ppm depending on inlet NO_2 ; even after accounting for its GHG potency, N_2O emissions will be dwarfed by CO_2 emissions.

5.5.3 Nitrosamine Volatility in the Thermal Reclaimer

- In the steady state bench-scale MEA thermal reclaimer operating at 150 °C, MEA in the reclaimer bottoms/purge was approximately 60-75 % MEA in the distillate/feed.
- Total nitrosamine volatility in the thermal reclaimer was 30–40 times less volatile than MEA, showing that it can be effectively removed.
- Total nitrosamines accumulated in the MEA thermal reclaimer since NaOH was not added to catalyze nitrosamine decomposition.
- PZ was 30 % more volatile than MEA in the thermal reclaimer at 150 °C; PZ volatility doubled from 130 °C to 170 °C.
- MNPZ was 40–60 times more volatile than PZ at $T = 130\text{--}170$ °C.
- MNPZ removal efficiency using thermal reclaiming will be 95 % with a reclaimer temperature of 150 °C, a reclaimer residence time of 10 minutes, and 1 M excess NaOH added to liberate PZ from HSS and catalyze nitrosamine decomposition.

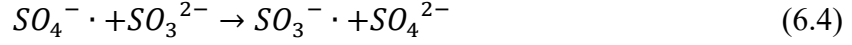
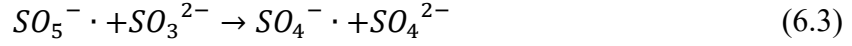
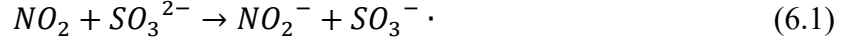
Chapter 6: NO₂-Catalyzed Sulfite Oxidation

Chapter 5 presented nitrosamine control through high temperature decomposition and reclaiming. However, many amines are thermally unstable, limiting stripper temperatures to less than 120 °C. At these lower regeneration temperatures nitrosamine decomposition is slower, allowing nitrosamines to accumulate to possibly unacceptable levels. Thermal reclaiming may also not be viable if the amines are non-volatile, which is likely if they are tertiary amines or amino acids. While nitrosamines can also be decomposed via hydrogenation or UV photolysis, these processes require additional equipment and complexity that will most likely not be economically viable. Using the SO₂ polisher to remove the nitrosating agents out of the flue gas before they can react with the amine solvent is an economic and simple approach to nitrosamine reduction. Sulfite is one possible prescrubbing solvent that readily absorbs NO₂. However, sulfite is also oxidatively unstable, necessitating the use of oxidation inhibitors to maintain sulfite concentration in the prescrubber. Section 6.3 builds a framework for sulfite oxidation in the presence of NO₂ at SO₂ polisher conditions. A mass balance over the NaOH prescrubber can then be performed to determine the steady-state sulfite concentration at operating conditions. These results are then synthesized with NO₂ absorption kinetics in sulfite to perform a techno-economic analysis of NO₂ prescrubbing in Chapter 7. The majority of Chapter 6 has been previously published (Sapkota, Fine, and Rochelle 2015).

6.1 PREVIOUS RESEARCH AND OPEN QUESTIONS

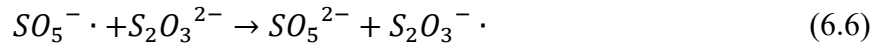
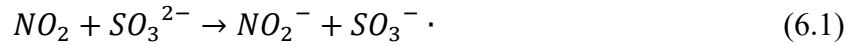
6.1.1 Sulfite Oxidation in Limestone Scrubbing

Limestone slurry scrubbing is a common method for flue gas desulfurization. The process also removes some NO₂, although it does not remove NO because of the limited solubility and reactivity of NO in aqueous SO₃²⁻. In the presence of gas phase O₂, the absorption of NO₂ is accepted as follows:



Equation 6.1 was first outlined by Nash (1979) and Equations 3–5 were proposed by Huie and Neta (1984). These occur in the liquid mass transfer boundary layer. They imply that for every mole of NO_2 absorbed, several moles of SO_3^{2-} can be consumed due to free-radical propagation. Because NO_2 absorption is first order in SO_3^{2-} , NO_2 absorption is strongly affected by sulfite oxidation (Shen 1997). In a limestone slurry scrubber, SO_2 gas is absorbed into solution as SO_3^{2-} , which balances the SO_3^{2-} loss from oxidation and leads to a steady state SO_3^{2-} concentration.

Several factors affect the oxidation rate. Free-radical scavengers, such as thiosulfate, can provide an alternative termination step to the free-radical process, drastically reducing the amount of sulfite oxidized (Shen 1997).



Takeuchi studied the effects of other antioxidants, such as hydroquinone, phenol, ethanalamines, ethylene glycol monoethyl ether, glycine, ethylenediaminetetraacetic acid (EDTA), and acetic acid. All of these antioxidants slowed sulfite oxidation (Takeuchi, Ando, and Kizawa 1977). Changes in other process variables such as NO_2 flow, O_2 flow, initial sulfite concentration, metals, and temperature could affect the sulfite oxidation rate. Shen studied the

absorption of NO₂ into sulfite and thiosulfate inhibited solutions, investigated the effects of adding Fe²⁺, chloride, and EDTA, and quantified the effects of sulfite, oxygen, and gas-phase SO₂ (Shen and Rochelle 1998).

6.1.2 Difference between SO₂ Polisher with NaOH and Limestone Slurry Scrubber

While much research effort has gone into characterizing sulfite oxidation in limestone slurry solutions, there is no previous research on sulfite oxidation in NaOH solutions pertinent to the SO₂ polishing scrubber. The polishing scrubber runs at a higher pH and lower inlet SO₂ partial pressure than common limestone slurry scrubbers, changing the equilibrium of sulfite and bisulfite in solution. Furthermore, previous research focused on removing total NO_x instead of selectively removing NO₂. Since NO is relatively insoluble, NO_x scrubbing was accomplished by first oxidizing NO to NO₂ and then absorbing the NO₂ in the scrubber. Thus, research centered on NO₂ partial pressures greater than 5 Pa (50 ppm atmospheric). NO_x speciation is a strong function of partial pressure, so previous research may not capture the chemistry at the low NO₂ partial pressures relevant to selective NO₂ removal in the SO₂ polishing scrubber. Finally, limestone slurry scrubbers contain high dissolved metals due to metal impurities in the limestone feed and fly ash impurities in the flue gas. However, the NaOH feed for the SO₂ polisher contains little or no dissolved metals, and most of the fly ash will be removed before SO₂ polishing. Therefore, a NaOH scrubber may be economically controlled to low dissolved metals with the addition of chelating agents. The results in Chapter 6 build upon the previous work on sulfite oxidation in limestone slurry scrubbers to include conditions relevant to NaOH scrubbers.

6.2 SULFITE OXIDATION EXPERIMENTAL METHOD AND ANALYSIS

6.2.1 Modified HGF Experimental Method for Sulfite Oxidation

The HGF previously used for measuring NO₂ absorption products into amine solutions (Section 3.3) was repurposed for measuring NO₂-catalyzed sulfite oxidation. Briefly, dry air exited the mass flow controller and was passed through a temperature controlled water saturator to maintain water balance in the HGF. CO₂ and dilute NO₂ were then directly mixed with the hydrated

air stream. The resulting gas stream was either sparged directly into the bottom of the HGF or put through a bypass using the same method as NO₂ absorption into amines.

The absorbing solution (approximately 360 g) included aqueous sulfite and thiosulfate in a 0.5 M NaHCO₃ buffer with EDTA added to chelate any trace metals. The initial solution was adjusted to pH 9.2 with NaOH. During startup, the gas stream was set to HGF bypass mode while pouring the solution into the HGF. The gas stream was then sparged into the HGF for a short period in order to coat the walls of the HGF and ensure the solution was well mixed. The gas was set back to bypass mode and 1 ml of initial sample was taken from a sample port at the bottom of the HGF. The sample was immediately injected into 0.1 g of 35 wt % formaldehyde and analyzed using anion chromatography (Section 2.1.1).

Once the sample was taken, NO₂ concentration values from the trace level NO_x analyzer were recorded while in bypass mode. The gas was set back to sparge into the HGF, and NO₂ values were recorded as soon as they stabilized at a new value. At predetermined intervals, the liquid sampling procedure was repeated to get sulfite oxidation kinetics in the semi-batch process.

6.2.2 Data Analysis for Sulfite Oxidation

NO₂ flux was initially determined by using a chemiluminescent trace level NO_x analyzer to measure the difference between the concentration of NO₂ when the gas passed through the HGF and when it bypassed the HGF. Assuming no leaks, this difference in NO₂ concentration was the amount of NO₂ absorbed into solution. However, this method was not reliable at higher temperature, when the sparging gas was over-saturated at room temperature. Having significant amounts of water vapor present in the exit stream presented a risk to the analyzer used in the experiment, which typically operates under ambient, unsaturated conditions. Instead, an empirical model regressed from NO₂ flux measurements at 20 °C was used to estimate NO₂ absorbed:

$$NO_2 \text{ absorbed} [=] \frac{\text{mol}}{\text{kg}_{\text{solution}} \cdot \text{min}} = \frac{(1 - e^{-N_{og}})[NO_2]_{\text{Bypass}} \dot{V}}{m_{\text{solution}}} * \left[\frac{1 \text{ mol}}{22.4 \text{ L}} \right] \quad (6.9)$$

$$\dot{V} = 7.5 \frac{L}{min}, m_{solution} = 0.36 kg, N_{og} = k_g' * \frac{a_e}{G_{HGF}} = 7.37 \sqrt{\frac{[SO_3^{2-}]}{1 M}}$$

This model assumes that the HGF operates in a semi-batch mode and that NO₂ flux is first order in NO₂ partial pressure. The mass-transfer kinetics for determining the number of theoretical transfer units (N_{og}) is assumed to be controlled by mass transfer with fast reaction in the liquid boundary layer with minimal impact from the diffusion of reactants and products (Kameoka and Pigford 1977). The model fit all the NO₂ flux data measured at 20 °C for inhibited solutions. However, NO₂ flux into uninhibited solutions was noticeably slower due to significant sulfite depletion at the gas-liquid interface, so NO₂ flux measured by the NO_x analyzer was used in place of the model. Similar slow rates of aerobic NO₂ absorption into uninhibited sulfite solutions have been reported in the literature (Shen 1997; Takeuchi, Ando, and Kizawa 1977).

For all experiments with thiosulfate added, sulfite was assumed to follow pseudo-first order oxidation (Equation 6.10) and was regressed in its linear form. Uninhibited sulfite oxidation was regressed using a previously determined semi-empirical model (Shen 1997) with both zeroth order and first order sulfite terms (Equation 6.11). The data was analyzed using a simple least-squares regression on the numerical solution of the ODE.

$$\frac{d[SO_3^{2-}]}{dt} = k_{1,obs}[SO_3^{2-}] \quad (6.10a)$$

$$\ln[SO_3^{2-}] = \ln[SO_3^{2-}]_i - k_{1,obs}t \quad (6.10b)$$

$$\frac{d[SO_3^{2-}]}{dt} = k_{1,obs}[SO_3^{2-}] + k_{0,obs} \quad (6.11)$$

The amount of sulfite oxidized per mole of NO₂ absorbed (f) was calculated from the k_{obs} and the NO₂ absorbed at a normalized sulfite concentration of 0.040 mol/kg. High values imply that a single NO₂ molecule catalyzes large amounts of sulfite oxidation. In Experiments 6.6–6.8 when the effect of SO₃²⁻ was examined, the f value is shown for the initial concentration of SO₃²⁻ instead of the normalized 0.040 mol SO₃²⁻/kg. The calculated f was determined using Equation

6.12 and a simple least-squares regression with the prefactor and activation energy as free parameters; the effect of iron and O₂ partial pressure were not regressed.

$$f = f_o \sqrt{\frac{5 * 10^{-6}}{(1 - e^{-N_{og}})y_{NO_2}}} * \frac{[SO_3^{2-}]}{\sqrt{[S_2O_3^{2-}] * \sqrt{1.0 \text{ M}}}} * \exp \left[\frac{-E_a}{R} \left(\frac{1}{293 \text{ K}} - \frac{1}{T} \right) \right] \quad (6.12)$$

Where: $f_o = 233 \frac{\text{mol } SO_3^{2-}}{\text{mol } NO_{2Abs}}$ $E_a = 24.1 \text{ kJ/mol}$

Many of the various species were changed independently during separate experiments, but in all of the following: the total gas flow rate was kept at 7.5 SLPM; the volume of solution introduced to the HGF was constant; 0.5 M NaHCO₃ was added to maintain a buffered solution; NaOH was added to buffer to pH = 9.2; and 0.02 mM EDTA was added to chelate any metal impurities. Additionally, a base case was picked to compare all of the variations in the different independent conditions. The base case solution started with 0.040 mol Na₂SO₃/kg and 0.025 mol/kg Na₂S₂O₃. The temperature of the HGF was held at 20 °C, and the gas contained 5 ppm NO₂ in hydrated air diluent.

6.3 RESULTS AND DISCUSSION FOR SULFITE OXIDATION

6.3.1 Tabulated Kinetic Results

Table 6.1 gives overall results for the entire experimental set. A gas mixture of hydrated N₂, Air, CO₂, and NO₂ gases was sparged through aqueous solutions containing compositions of sodium sulfite (NaSO₃), sodium thiosulfate (NaS₂O₃), sodium bicarbonate (NaHCO₃), and EDTA in the High Gas Flow apparatus (HGF). The sulfite and sulfate concentrations were measured at various times in the semi-batch process using anion chromatography. The decrease in the sulfite concentration over time was attributed to sulfite oxidation, and the time series was used to regress sulfite oxidation rate constants. The standard error for each rate constant was on average 4% of the regressed constant.

Table 6.1: NO₂ catalyzed sulfite oxidation in the HGF

| Exp. # | Sulfite (mM) | Thiosulfate (mM) | T (°C) | Oxygen (kPa) | NO ₂ (ppm) | k _{1 obs} *10 ³ (1/min) | k _{0 obs} *10 ³ (mol/kg/min) | NO ₂ Flux*10 ⁶ (mol/kg/min) | f _{obs} $\left(\frac{SO_3^{2-}{}_{ox}}{NO_2 Flux}\right)$ | f _{calc} |
|--------------------|--------------|------------------|--------|--------------|-----------------------|---|--|---|--|-------------------|
| 6.1 | 40.2 | 25 | 20 | 21 | 5 | 6.5±0.3 | - | 3.6 | 73.4 | 67.2 |
| 6.2* | 44.3 | 0 | 20 | 21 | 2 | 70.1 | 97.5 | 1.2 | 1750 | - |
| 6.3* | 39.2 | 0 | 20 | 21 | 5 | 110.8 | 154.1 | 3.0 | 1110 | - |
| 6.4* | 33.8 | 0 | 20 | 21 | 10 | 156.7 | 218.0 | 6.0 | 783 | - |
| 6.5 | 40.0 | 100 | 20 | 21 | 5 | 3.4±0.4 | - | 3.6 | 37.9 | 33.6 |
| 6.6 | 7.2 | 25 | 20 | 21 | 5 | 4.0±0.1 | - | 2.1 | 13.1 | 15.6 |
| 6.7 | 67.0 | 25 | 20 | 21 | 5 | 7.0±0.2 | - | 3.9 | 119.4 | 107.0 |
| 6.8 | 135.6 | 25 | 20 | 21 | 5 | 6.4±0.3 | - | 4.3 | 201.7 | 210.9 |
| 6.9 | 45.0 | 25 | 20 | 21 | 2 | 3.7±0.1 | - | 1.4 | 102.9 | 106.2 |
| 6.10* ⁺ | 37.2 | 25 | 20 | 21 | 5 | 18.4±0.2 | - | 3.6 | 207.0 | 67.2 |
| 6.11 | 45.2 | 25 | 35 | 21 | 5 | 10.3±0.6 | - | 3.6 | 115.9 | 108.9 |
| 6.12 | 7.4 | 25 | 53 | 21 | 5 | 15.0±0.7 | - | 2.2 | 175.5 | 183.3 |
| 6.13 | 33.9 | 25 | 64 | 21 | 5 | 22.1±0.7 | - | 3.6 | 248.6 | 245.3 |
| 6.14* | 41.6 | 25 | 20 | 10 | 5 | 5.9±0.1 | - | 3.6 | 66.8 | 67.2 |
| 6.15* | 48.2 | 25 | 20 | 5 | 5 | 5.6±0.1 | - | 3.6 | 63.0 | 67.2 |
| 6.16* | 49.1 | 25 | 20 | 2 | 5 | 3.9±0.2 | - | 3.6 | 44.3 | 67.2 |

*Experiments 6.2–6.4, 6.10, and 6.14–6.16 were not used to regress f_{Calc}

+In Experiment 6.10, 0.1 mM Fe was added instead of 0.02 mM EDTA.

For Experiments 6.1 and 6.5–6.16, the rate law was assumed $\frac{d[\text{SO}_3^{2-}]}{dx} = k_{1,\text{obs}}[\text{SO}_3^{2-}]$ and linearly regressed using $\ln[\text{SO}_3^{2-}] = \ln[\text{SO}_3^{2-}]_i - k_{1,\text{obs}}t$

For Experiments 6.2–6.4, the rate law was assumed $\frac{d[\text{SO}_3^{2-}]}{dx} = k_{1,\text{obs}}[\text{SO}_3^{2-}] + k_{0,\text{obs}}$ and regressed using a least squares regression on the numerical solution of the ODE.

6.3.2 Total Sulfur Balance

Sulfite and sulfate concentrations were used to check for mass balance closure. Since almost all sulfite should oxidize to sulfate (Equation 6.3), total S (sulfite + sulfate) should remain constant throughout the run. In Experiment 6.14, the sum of sulfite and sulfate held at an average 43.3 mmol/kg with a standard deviation of 0.6 mmol/kg (Table 6.2). With the exception of the first sample, there was a small but clear loss of total S over the run, possibly due to dithionate formation (Equation 6.4). All experiments showed near constant total S as sulfite oxidized, proving that sulfate is the dominant product of sulfite oxidation.

Table 6.2: Raw data for experiment 6.14 with total S balance

| Time (min:sec) | Sulfite (mM) | Sulfate (mM) | Total S (mM) |
|----------------|--------------|--------------------|--------------|
| 0 | 41.56 | 1.10 | 42.66 |
| 5:00 | 40.67 | 3.94 | 44.61 |
| 13:00 | 37.82 | 5.74 | 43.57 |
| 20:50 | 35.68 | 7.72 | 43.40 |
| 28:00 | 33.60 | 9.63 | 43.22 |
| 37:40 | 31.91 | 10.99 | 42.90 |
| 45:35 | 30.07 | 12.73 | 42.80 |
| | | Average | 43.31 |
| | | Standard Deviation | 0.61 |

6.3.3 Uninhibited Aerobic NO₂ Absorption with Varying NO₂ Flow

The rates for uninhibited sulfite oxidation were quantified in solutions with no added thiosulfate. The dilute NO₂ flow rate was varied, but sulfite, temperature, and pH were kept constant at base case conditions (Figure 6.1).

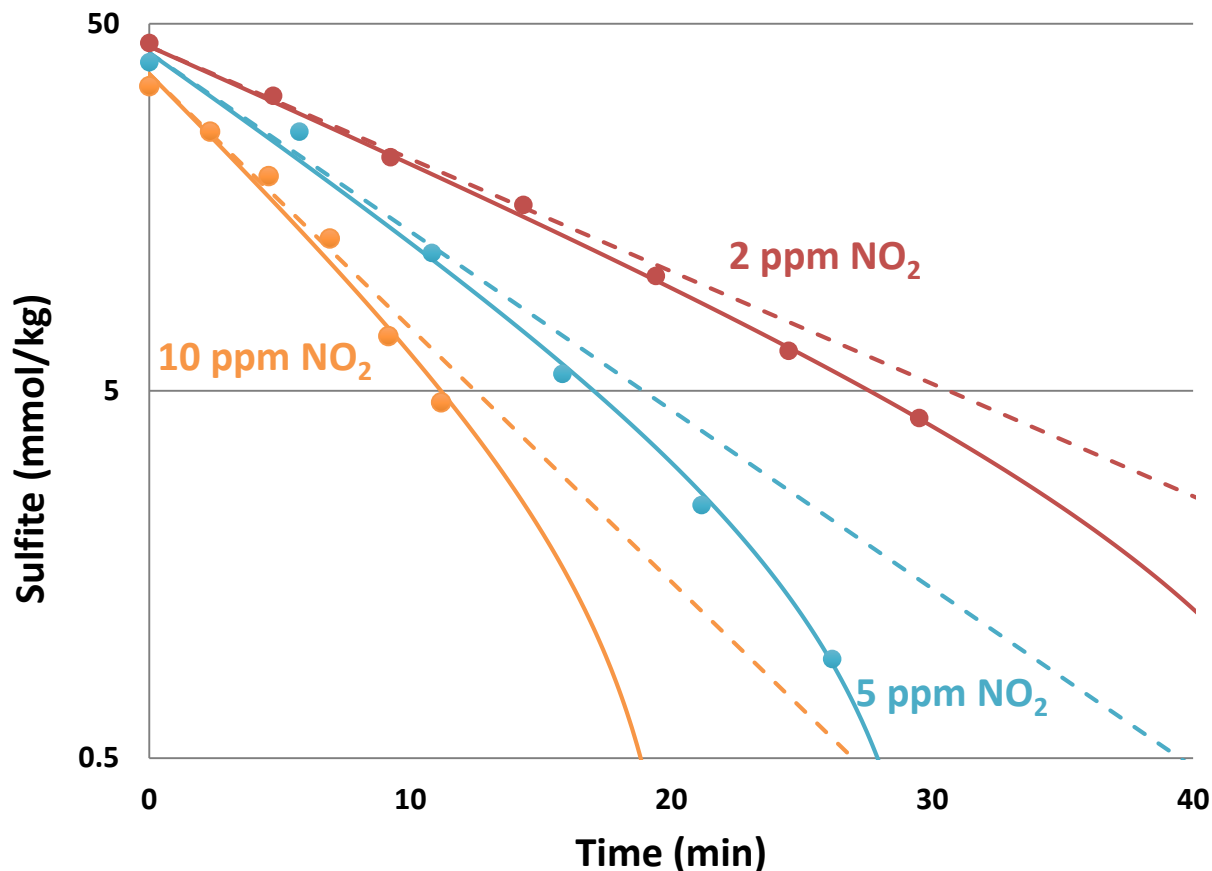


Figure 6.1: Uninhibited SO₃²⁻ oxidation with varying NO₂ flow to adjust concentration: 0.5 M NaHCO₃; pH = 9.2; 20 °C; 21 kPa O₂ (Experiments 6.2–6.4)

The sulfite concentrations were fit with the following rate law equation, graphed with solid lines above:

$$\frac{d[SO_3^{2-}]}{dt} = k_{1\text{ obs}}[SO_3^{2-}] + k_{0\text{ obs}} \quad (6.13)$$

The first order term dominates at high sulfite; the dashed line models pseudo-first-order oxidation:

$$\frac{d[SO_3^{2-}]}{dt} = k_{1\text{ obs}}[SO_3^{2-}] \quad (6.14)$$

The observed oxidation only deviates significantly from the pseudo-first-order rate when the sulfite is below 5 mmol/kg.

The oxidation kinetics at the three NO_2 partial pressures also verify the half-order relationship of NO_2 on sulfite oxidation. In all runs, increases in NO_2 result in half that proportional increase in $k_{1 \text{ obs}}$ and $k_{0 \text{ obs}}$. Additionally, increases in NO_2 have a half-order effect on reducing the ratio of SO_3^{2-} oxidized to NO_2 absorbed (f). From the 2 to the 5 ppm cases, f dropped by a factor of 1.56, and from the 2 to 10 ppm cases, f dropped by a factor of 2.22. However, the large f values imply very low sulfite when oxidation is uninhibited, making these systems poor absorbers of NO_2 .

6.3.4 Inhibited Aerobic NO_2 Absorption with Varying Thiosulfate Concentrations

The rates for inhibited sulfite oxidation were quantified in solutions with thiosulfate added at 0 mM, 25 mM, and 100 mM. Sulfite, temperature, pH, gas composition and gas flow were kept constant at base case conditions. Data for the 0 mM run came from the 5 ppm uninhibited experiment and data for the 25 mM run were treated as the base case for all experiments (Figure 6.2). SO_3^{2-} for the 25 mM $\text{S}_2\text{O}_3^{2-}$ and 100 mM $\text{S}_2\text{O}_3^{2-}$ runs was fit with Equation 6.14 because the sulfite remained much higher than 5 mmol/kg. The results without $\text{S}_2\text{O}_3^{2-}$ were modeled with Equation 6.12. Thiosulfate inhibited sulfite oxidation by an order of magnitude. Increasing thiosulfate from 25 mM to 100 mM decreased both sulfite oxidation and f by approximately a factor of 2. This half-order correlation in oxidation rate is corroborated in previous work (Shen 1997). Because sulfite oxidation inhibited by thiosulfate is an order of magnitude slower than uninhibited oxidation, sulfite will accumulate to a higher concentration in the SO_2 scrubber. A higher sulfite concentration will lead to high levels of simultaneous absorption of SO_2 and NO_2 in the scrubber.

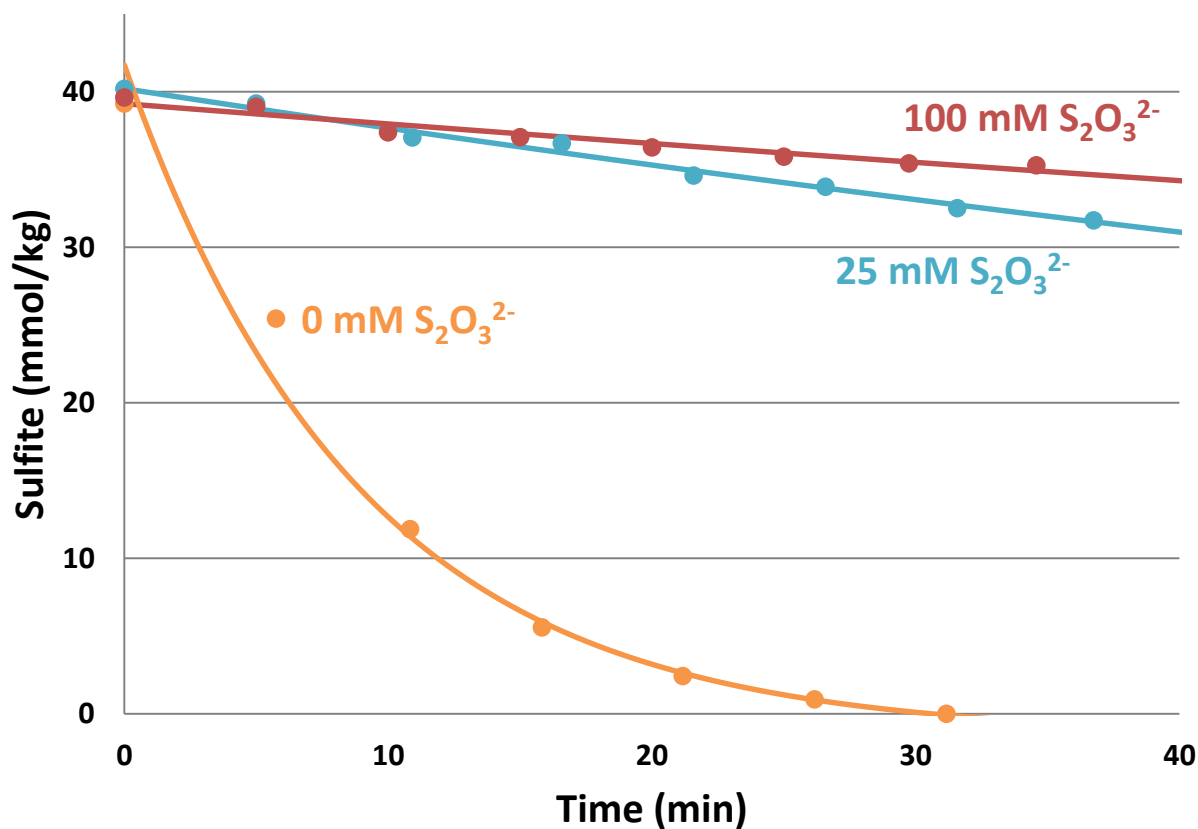


Figure 6.2: Sulfite oxidation with varying $S_2O_3^{2-}$ concentration: 0.5 M $NaHCO_3$, pH = 9.2, 20 °C, 21 kPa O_2 , 5 ppm NO_2 (Experiments 6.1, 6.3, 6.5)

6.3.5 Inhibited Aerobic NO_2 Absorption with Varying Sulfite Concentrations

The kinetics for sulfite oxidation were measured with sulfite varying 7–135 mM. Thiosulfate, temperature, pH, gas composition, and gas flow were kept constant at base case conditions (Figure 6.3).

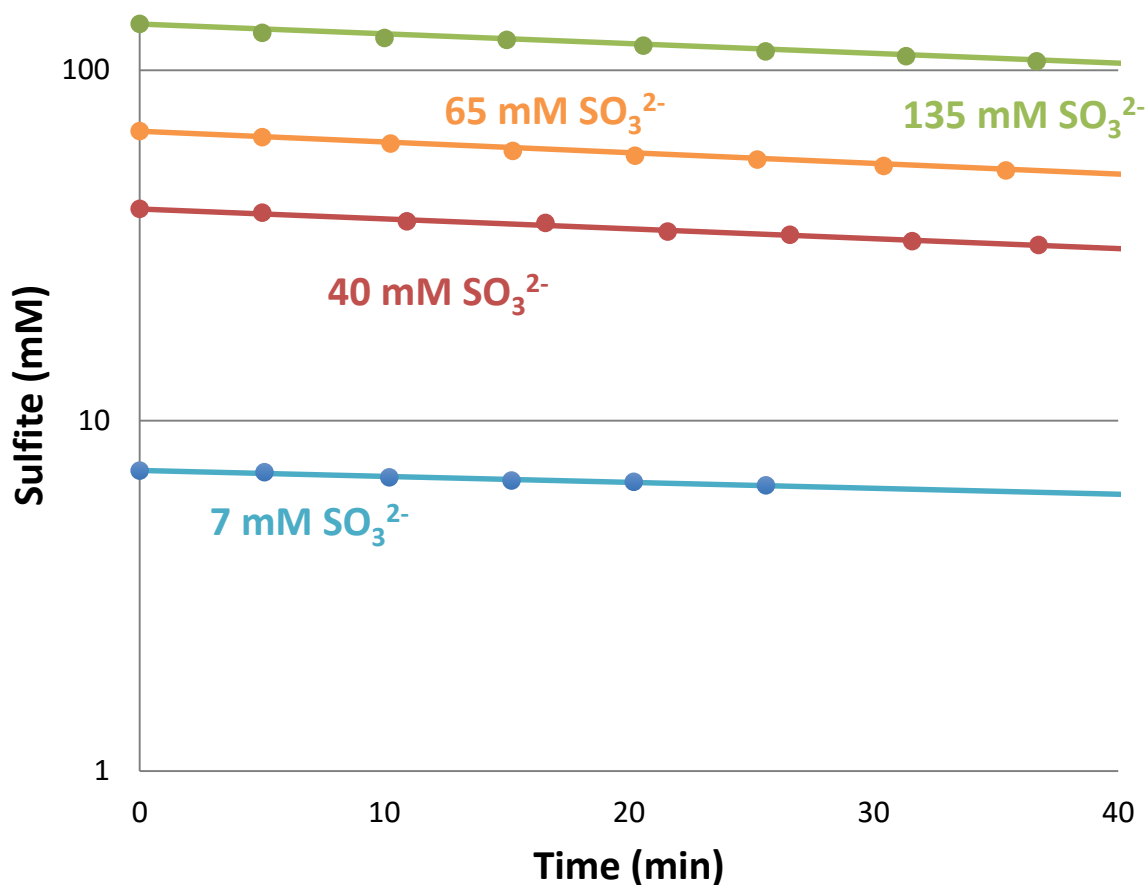


Figure 6.3: SO_3^{2-} oxidation with varying SO_3^{2-} concentration: 0.5 M NaHCO_3 , pH = 9.2, 20 °C, 21 kPa O_2 , 5 ppm NO_2 , 25 mM $\text{S}_2\text{O}_3^{2-}$ (Experiments 6.1, 6.6–6.8)

The sulfite concentrations were fitted with Equation 6.14 since sulfite remained above 5 mM for each experiment. Because Equation 6.14 assumes sulfite oxidation is pseudo-first order in sulfite, $k_{1 \text{ obs}}$ should be the same for all runs. However, the $k_{1 \text{ obs}}$ for the 7 mM SO_3^{2-} case is significantly lower than the rest. This is due to low NO_2 absorption in the low initial SO_3^{2-} concentration. Once normalized for NO_2 absorption, the ratio of the amount of SO_3^{2-} oxidized to NO_2 absorbed is first order in sulfite (Figure 6.4).

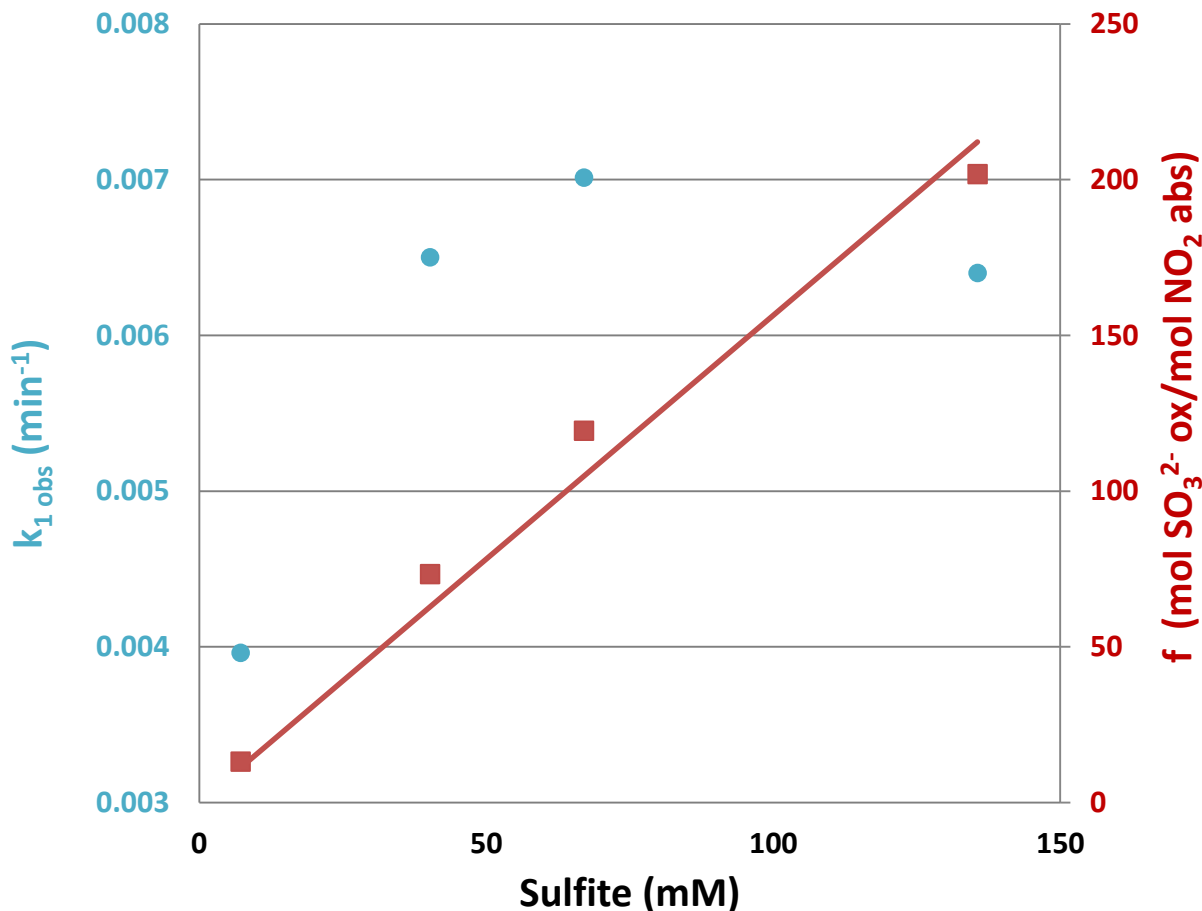


Figure 6.4: SO_3^{2-} oxidation with varying SO_3^{2-} concentration, the secondary axis is normalized for variation in NO_2 absorption as SO_3^{2-} concentration varies: 0.5 M NaHCO_3 , pH = 9.2, 20 °C, 21 kPa O_2 , 5 ppm NO_2 , 25 mM $\text{S}_2\text{O}_3^{2-}$ (Experiments 6.1, 6.6–6.8)

6.3.6 Inhibited Aerobic NO_2 Absorption with Varying NO_2 Flow

Sulfite oxidation rates were quantified with NO_2 concentrations of 2 ppm and 5 ppm while thiosulfate, sulfite, temperature, pH, and total gas flow were kept constant at base case conditions (Figure 6.5). Between the 2 ppm and 5 ppm cases, the $k_{1\text{ obs}}$ increased by a factor of 1.78 while NO_2 increased by a factor of 2.5, indicating half-order behavior. This half-order correlation is corroborated in previous work (Shen 1997). However, f decreased by a factor of 1.63 when NO_2 increased by a factor of 2.5, suggesting an inverse half-order relationship between NO_2 absorbed and f . Shen showed that NO_2 absorption is first order in NO_2 , but that SO_3^{2-} oxidation is half-order in NO_2 . Thus, increases in NO_2 partial pressure increase NO_2 absorption faster than it increases SO_3^{2-} oxidation. This has important implications for NO_2 absorbing applications; higher partial

pressures of NO_2 are more efficiently removed with less sulfite loss per unit NO_2 absorbed even though the absolute rate of sulfite oxidation increases.

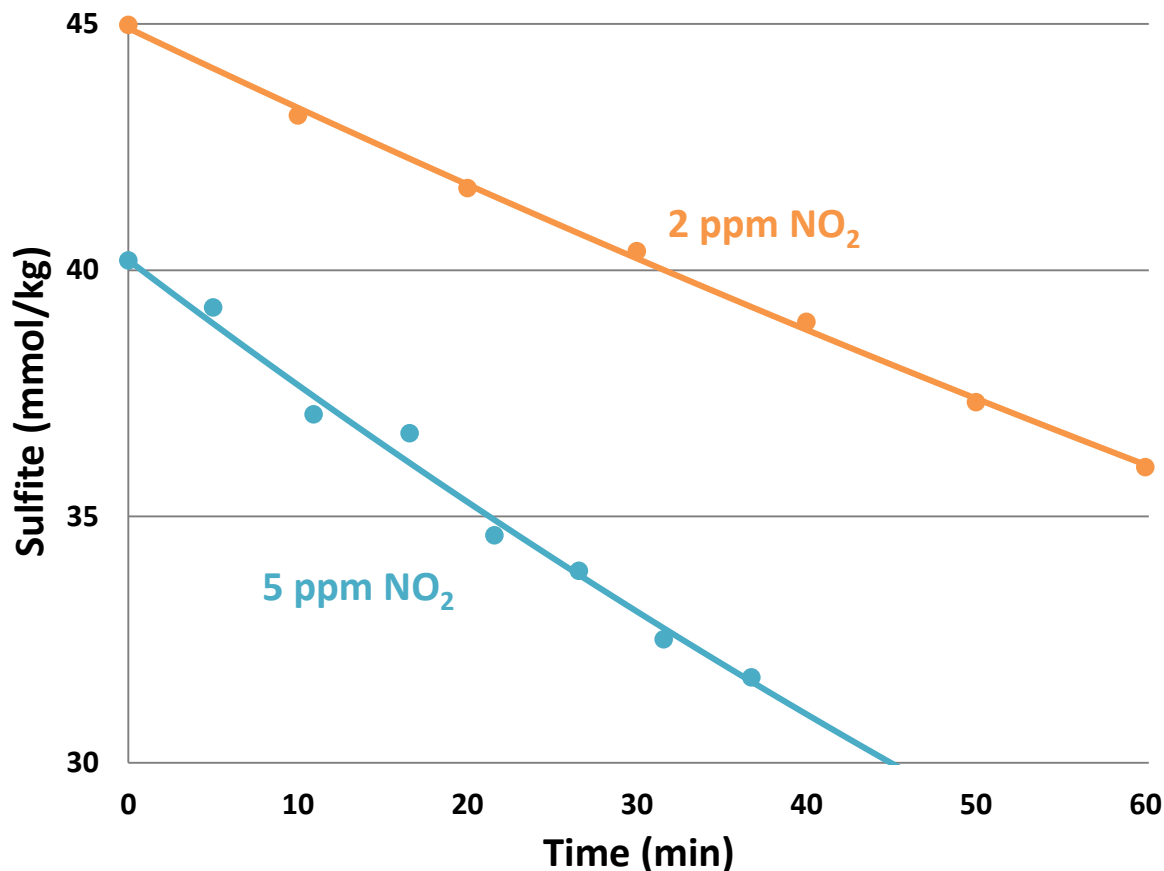


Figure 6.5: Inhibited SO_3^{2-} oxidation with varying NO_2 concentration: 0.5 M NaHCO_3 , pH = 9.2, 20 °C, 21 kPa O_2 , 25 mM $\text{S}_2\text{O}_3^{2-}$ (Experiments 6.1, 6.9)

6.3.7 Inhibited Aerobic NO_2 Absorption with Added Iron

Work done by Ulrich et al. indicated that Fe^{2+} is a powerful oxidation catalyst that is effective at concentrations as low as 0.003 mM (Ulrich, Rochelle, and Prada 1986). To test this effect, sulfite oxidation rates were quantified with 0.01 mM Fe^{2+} and compared to the base case, which had 0.02 mM EDTA to chelate any background Fe^{2+} . Thiosulfate, sulfite, temperature, pH, and gas flow and composition were kept constant at base case conditions. The addition of 0.01 mM Fe^{2+} increased $k_{l \text{ obs}}$ by a factor of 2.83, which contradicts earlier conclusions that metals did not have a significant effect on NO_2 -catalyzed sulfite oxidation (Shen 1997). Shen reported that

metals such as Fe^{2+} are insignificant catalysts of sulfite oxidation in the presence of NO_2 , however, his experiments were conducted with 200–1000 ppm NO_2 , which catalyzes far more sulfite oxidation than added metals do. The addition of iron, therefore, did not cause a significant increase in the oxidation rate in his experiments. The current results show the importance of adding chelating agents to the NaOH scrubber to limit sulfite oxidation when the flue gas contains less than 10 ppm NO_2 . Chelating Fe^{2+} is economically viable in NaOH scrubbing since most of the fly ash, a large source of metal ions, will effectively be captured upstream of the scrubber. Furthermore, the NaOH feed is expected to have much lower levels of dissolved metal compared to the limestone feed for traditional flue gas desulfurization.

6.3.8 Inhibited Aerobic NO_2 Absorption with Varying Temperature

Sulfite oxidation rates were quantified at 20–65 °C (Figure 6.6) with thiosulfate, sulfite, pH, and gas flow and composition constant at base case conditions. The k_g for NO_2 absorption has almost no temperature dependence due to competing effects on NO_2 solubility and reaction rates in this temperature range, (Shen 1997) so NO_2 flux was assumed to be constant. Since all other dependent variables for f were held constant, an apparent activation energy of 24.1 kJ/mol was regressed using Equation 6.15.

$$f = A * \exp \left[\frac{-E_a}{R} \left(\frac{1}{293K} - \frac{1}{T} \right) \right] \quad (6.15)$$

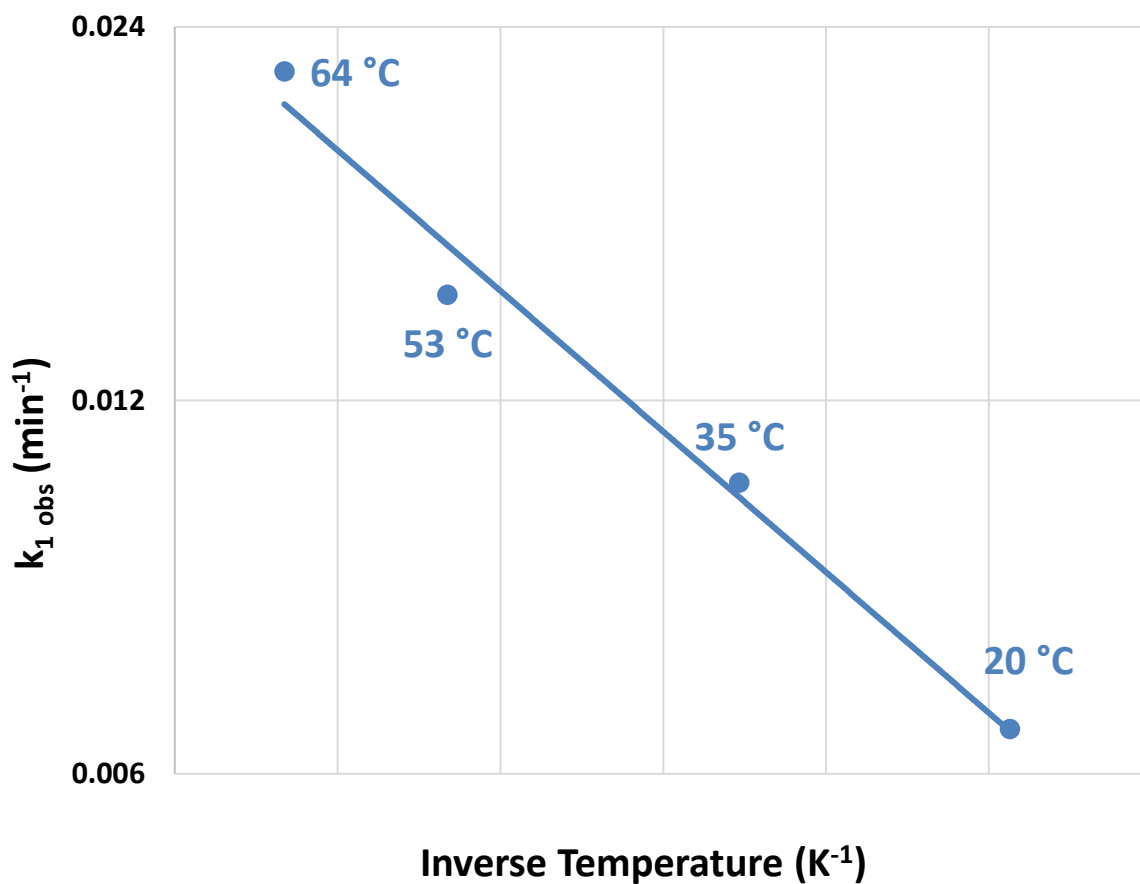


Figure 6.6: SO_3^{2-} oxidation with varying temperature: 0.5 M NaHCO_3 , pH = 9.2, 21 kPa O_2 , 5 ppm NO_2 , 25 mM $\text{S}_2\text{O}_3^{2-}$, 40 mM initial SO_3^{2-} (Experiments 6.1 & 6.11–6.13)

6.3.9 Inhibited Aerobic NO_2 Absorption with Varying Oxygen Flow

Sulfite oxidation rates were quantified with at 2 to 21% oxygen while thiosulfate, sulfite, temperature, pH, and total gas flow were kept constant at base case conditions. Total gas flow was kept constant by blending air and N_2 to the desired O_2 concentration (Figure 6.7).

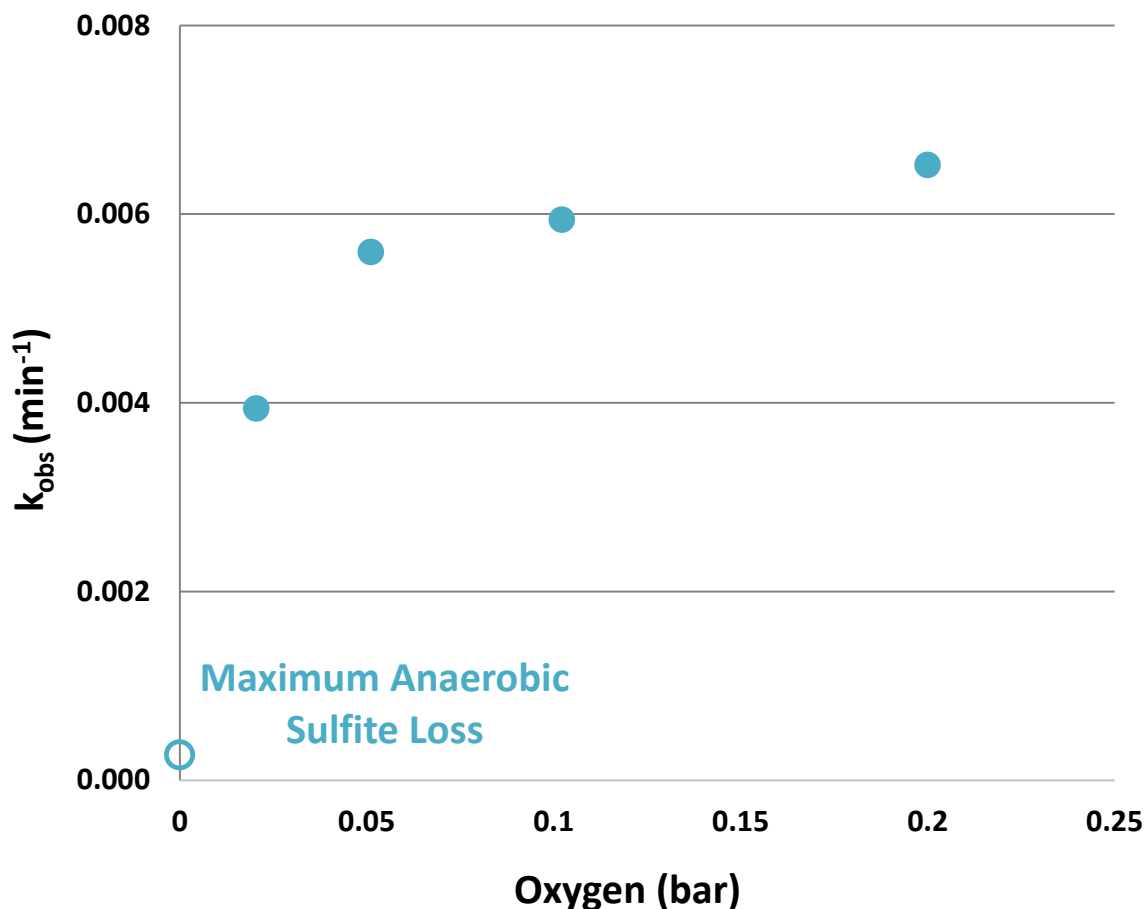
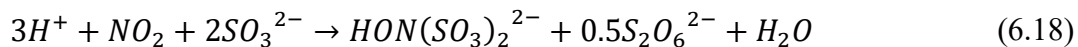
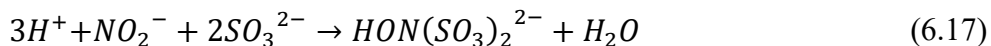


Figure 6.7: SO_3^{2-} oxidation with varying oxygen: 0.5 M NaHCO_3 , pH = 9.2, 5 ppm NO_2 , 25 mM $\text{S}_2\text{O}_3^{2-}$, 40 mM initial SO_3^{2-} (Experiments 6.1, 6.14–6.16)

In disagreement with the strong dependence on O_2 partial pressure that Shen reported, (Shen 1997) O_2 does not have a significant effect on $k_{l\text{ obs}}$ until O_2 partial pressure decreases below 5 kPa. This is due to the free-radical species in the rate-limiting step of the propagation. At high O_2 partial pressure, $\text{SO}_3^{\cdot -}$ oxidizes instantaneously in the boundary layer to form $\text{SO}_5^{\cdot -}$ (Equation 6.2). The $\text{SO}_5^{\cdot -}$ then catalyzes oxidation until thiosulfate terminates the mechanism. At low O_2 partial pressure, the rate-limiting step occurs when $\text{SO}_3^{\cdot -}$ reacts with dissolved oxygen. Since $\text{SO}_3^{\cdot -}$ is present in the bulk solution, thiosulfate can directly react with $\text{SO}_3^{\cdot -}$. The relative concentrations of thiosulfate and dissolved oxygen then become determining factors in the overall oxidation rate. The O_2 partial pressure in power generation applications will not affect sulfite oxidation since coal flue gas usually contains over 5% O_2 due to the excess air used during

combustion. The stronger dependence on O₂ partial pressure that Shen reported was most likely due to the lack of thiosulfate and the relatively high NO₂ partial pressures (3.5–8 Pa) used in this set of oxidation experiments, which depleted sulfite concentration at the gas-liquid interface.

The maximum anaerobic sulfite loss solely from the NO₂ absorption rate was calculated using the stoichiometry for NO₂ absorption as nitrite followed by the reaction of nitrite with sulfite to form hydroxylamine disulfonate (HADS) (Equations 6.1 & 6.16–6.18). Neither nitrite nor HADS accumulated to quantifiable concentrations during these experiments, but they are expected major products from anaerobic absorption of NO₂ into sulfite (Shen 1997; Oblath et al. 1981; Susianto et al. 2005). Even at 2 kPa oxygen, sulfite loss is dominated by NO₂-catalyzed oxidation with less than 10% of sulfite loss attributable to NO₂/NO₂⁻ reactions.



6.4 INDUSTRIAL APPLICATION FOR SULFITE OXIDATION RESULTS

The f value can be used to determine the thiosulfate makeup rate necessary to maintain a given sulfite concentration in the NaOH scrubber. The NaOH polishing scrubber can be modeled as a semi-batch reactor with the flue gas countercurrently contacting the circulating solvent (Figure 6.8). NaOH is fed to the system to maintain a basic pH while NaS₂O₃ can be fed to inhibit sulfite oxidation. The unpolished flue gas from coal-fired power plants contains approximately 30–300 ppm SO₂ and 0.5–5 ppm NO₂ depending on the coal type, burner technology, and upstream treatment; natural gas-fired power plants have very little inlet SO₂, making them poor candidates for NO₂ scrubbing with sulfite. Almost all of the SO₂ will be absorbed in the scrubber, while NO₂ absorption depends on the sulfite concentration in the solvent. The circulating solvent is bled to maintain sulfate concentration below its approximately 2 M solid solubility limit. Inside the

polishing scrubber SO_2 reacts with OH^- to form SO_3^{2-} , NO_2 reacts with SO_3^{2-} to form $SO_3^{\cdot -}$, and $SO_3^{\cdot -}$ catalyzes SO_3^{2-} oxidation until terminated by reacting with thiosulfate or another radical (Equations 6.1–6.8).

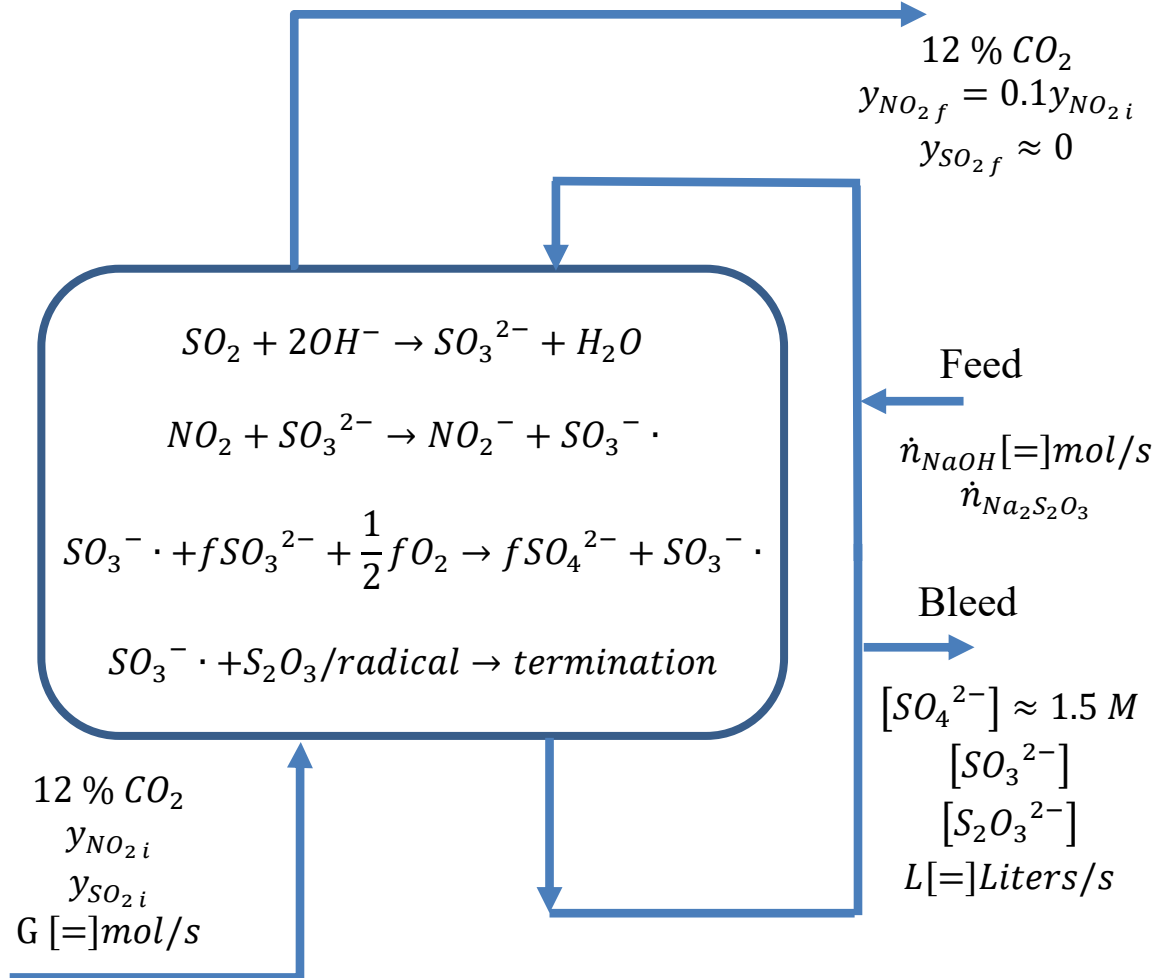


Figure 6.8: Schematic for simultaneous NO_2 and SO_2 absorption in a NaOH scrubber using $Na_2S_2O_3$ inhibition.

The mass balances for sulfite, sulfate, and thiosulfate accumulation can be solved assuming that sulfite loss is dominated by NO_2 -catalyzed oxidation and the NaOH scrubber is large enough to absorb 90 % of the inlet NO_2 and practically all of the SO_2 (Equations 6.19–6.21).

$$\frac{d[SO_4^{2-}]}{dt} = G y_{SO_2 i} - L [SO_4^{2-}] \quad (6.19)$$

$$\frac{d[SO_3^{2-}]}{dt} = Gy_{SO_2 i} - f * 0.9Gy_{NO_2 i} \quad (6.20)$$

$$\frac{d[S_2O_3^{2-}]}{dt} = \dot{n}_{Na_2S_2O_3} - L[S_2O_3^{2-}] \quad (6.21)$$

At steady state and a conservative sulfate concentration of 1.5 M in the bleed, the f value from Equation 6.12 and the molar feed rate for $Na_2S_2O_3$ can be written in terms of inlet gas conditions (Equations 6.22 & 6.23).

$$f = \frac{y_{SO_2 i}}{0.9y_{NO_2 i}} = 233 \sqrt{\frac{5 * 10^{-6}}{0.9y_{NO_2 i}}} * \frac{[SO_3^{2-}]}{\sqrt{[S_2O_3^{2-}] * \sqrt{1.0 M}}} * \exp \left[\frac{-24.1}{R} \left(\frac{1}{293 K} - \frac{1}{T} \right) \right] \quad (6.22)$$

$$\dot{n}_{Na_2S_2O_3} = Gy_{SO_2 i} * \frac{[S_2O_3^{2-}]}{1.5 M} \quad (6.23)$$

For an inlet concentration of 100 ppm SO_2 and 2.5 ppm NO_2 with a NaOH scrubber operating at 55 °C, 0.050 M thiosulfate would be needed to keep SO_3^{2-} concentration at 0.010 M in the solvent (Equation 6.24). Assuming 90% CO_2 capture from the flue gas and substituting 50 mM $Na_2S_2O_3$ into Equation 6.23, the polisher requires a feed of $3.1 * 10^{-5}$ mole $Na_2S_2O_3$ per mole of CO_2 captured (Equation 6.25). The economics of the process, as discussed further in Chapter 7, are a balance between the cost of $Na_2S_2O_3$ feedstock and the size of the polishing scrubber.

$$f = 44.4 = 994 * \frac{[SO_3^{2-}]}{\sqrt{[S_2O_3^{2-}]}} \quad (6.24a)$$

$$[S_2O_3^{2-}] = \left(\frac{994 * 0.01 M}{44.4} \right)^2 = 0.050 M \quad (6.24b)$$

$$\dot{n}_{CO_2 \text{ captured}} = 0.9 * 0.12 * G \quad (6.25a)$$

$$\frac{\dot{n}_{Na_2S_2O_3}}{\dot{n}_{CO_2 \text{ captured}}} = \frac{100 * 10^{-6}}{0.9 * 0.12} * \frac{0.050 M}{1.5 M} = \frac{3.1 * 10^{-5} \text{ mol}_{Na_2S_2O_3}}{\text{mol}_{CO_2 \text{ captured}}} \quad (6.25b)$$

6.5 CONCLUSIONS

- NO₂ catalyzed sulfite oxidation was measured at conditions relevant to a NaOH polishing scrubber with: 7–135 mM sulfite, 0–100 mM thiosulfate, 2–10 ppm NO₂, Fe²⁺/EDTA, 2–20 % O₂, and 20–65 °C.
- Sulfite oxidizes to sulfate at high yields via free-radical mechanisms initiated by NO₂ absorption.
- With 5 ppm NO₂ absorbing into 40 mM sulfite and no thiosulfate inhibition, approximately 1000 moles of sulfite will oxidize for each mole of NO₂ absorbed.
- 25 mM thiosulfate reduced sulfite oxidation by a factor of 30; oxidation rates are inverse-half-order with respect to thiosulfate concentration.
- Sulfite oxidation is first-order in sulfite when normalized for the amount of NO₂ absorbed at varying sulfite concentrations.
- Sulfite oxidation is half-order in NO₂ absorption for both inhibited and uninhibited systems.
- Sulfite oxidation increases by a factor of 2.8 when 0.01 mM Fe²⁺ is present instead of EDTA.
- Oxidation follows an Arrhenius temperature dependence with an activation energy of 24.1 kJ/mole
- Oxygen partial pressures do not affect the oxidation rate until below roughly 5 kPa O₂. For common industrial applications, oxygen concentrations will not affect sulfite oxidation.
- With no metals in solution and 20 % O₂ in the sparge gas, the ratio of sulfite oxidized per mole of NO₂ absorbed (f) was regressed with Equation 6.12.

$$f = f_o \sqrt{\frac{5 * 10^{-6}}{(1 - e^{-N_{og}})y_{NO_2}}} * \frac{[SO_3^{2-}]}{\sqrt{[S_2O_3^{2-}] * \sqrt{1.0 M}}} * \exp\left[\frac{-E_a}{R}\left(\frac{1}{293 K} - \frac{1}{T}\right)\right] \quad (6.12)$$

$$f_o [=] \frac{mol SO_3^{2-}}{mol NO_{2Abs}^{ox}} = 233 \quad E_a = 24.1 kJ/mol$$

- A NaOH polishing scrubber was modeled at steady-state to show how the f value determines thiosulfate concentration.
- For an inlet concentration of 100 ppm SO_2 and 2.5 ppm NO_2 with a NaOH scrubber operating at 55 °C, 0.050 M thiosulfate would be needed to keep sulfite concentration at 0.010 M.
- The corresponding feed rate would be 3.1×10^{-5} mole $\text{Na}_2\text{S}_2\text{O}_3$ per mole of CO_2 captured.

Chapter 7: Modeling Nitrosamine Accumulation in the Amine Scrubber

Chapters 3–6 showed detailed results for NO_x absorption, nitrosation from nitrite, nitrosamine decomposition, and NO_2 prescrubbing. These results can be combined to determine nitrosamine accumulation in the amine scrubber under normal operating conditions. Furthermore, NO_2 prescrubbing parameters can be optimized to economically lower nitrosamines in the amine scrubber if the nitrosamine level is unacceptable. Section 7.1 defines an environmental basis for nitrosamine accumulation in the amine scrubber using current emission limits and industrial standards. Section 7.2 derives the nitrosamine mole balance based on the results from Chapter 3–5. The balances are then solved for MEA, PZ, and MDEA/PZ solvents under steady-state and transient conditions to give the steady-state nitrosamine concentration as well as the relevant time constant to reach steady-state. Section 7.3 shows how NO_2 prescrubbing with triethanolamine or sulfite can be a cost-effective way to control nitrosamines when the inlet flue gas contains relatively high NO_2 .

7.1 RELEVANT NITROSAMINE LIMITS IN THE AMINE SCRUBBER

7.1.1 Nitrosamine limits in Drinking Water and Air

There are currently no limits set for nitrosamine levels in the amine scrubber itself. Instead nitrosamine levels are regulated only by their emission rates into the atmosphere and the water supply. The first major demonstration-size carbon capture pilot plant was built at the Technology Center in Mongstad (TCM) as part of the Norwegian “moonshot” project. Under this project, the Norwegian Institute of Public Health (NIPH) set nitrosamine and nitramine emission levels to minimize risk of exposure to the general Norwegian public (Låg et al. 2011). Total nitrosamine and nitramine were limited to 0.3 ng/m^3 in air and 4 ng/l in water, corresponding to an increase in cancer risk of 10^{-6} after lifetime exposure to these levels of nitrosodimethylamine (NDMA). NDMA is the second most carcinogenic nitrosamine screened by the NIPH, demonstrating the

appropriately conservative approach to nitrosamine emission limits for this first-of-a-kind demonstration plant. While total nitrosamine emissions are currently not controlled through the EPA or the WHO, this work assumes that similar nitrosamine limits will be adopted worldwide as amine scrubbing becomes more prevalent.

7.1.2 Connecting Point Source Emissions to Environmental Regulations

Nitrosamines from the amine scrubber will be continuously emitted to the environment from two main streams: the reclaimer waste and the scrubbed flue gas. As discussed in Chapter 5, nitrosamines decompose rapidly in the basic, high-temperature conditions of the thermal reclaimer. Furthermore, reclaimer waste usually contains high levels of metals, which could already make reclaimer waste hazardous (Sexton et al. 2014). Therefore, nitrosamine emissions through reclaimer waste will not be the environmental driver in reclaimer waste handling. Nitrosamines have also been found in the scrubbed flue gas after the water wash (Koeijer and Talstad 2013; da Silva et al. 2013). These emissions will enter the atmosphere where they could exceed nitrosamine limits set by the NIPH. Thus, nitrosamines may be the environmental driver for emissions reductions from the scrubbed flue gas.

The steady-state concentration of nitrosamines in the atmosphere and water is based on five main mechanisms (Koeijer and Talstad 2013):

1. The emissions rate of the nitrosamine and amine from the absorber
2. The atmospheric reaction rate of amine with $\text{NO}\bullet$ to make nitrosamine
3. The photolytic decomposition of nitrosamines under sunlight
4. The dispersion of nitrosamines and amines as the plume expands
5. The partitioning of nitrosamines into water

Koeijer et al. evaluated these effects for nitrosamine levels based off of emissions from the TCM pilot plant running an MEA solvent. Using “The Air Pollution Model” (TAPM) (Hurley, Physick, and Luhar 2005) as well as the topography and wind speed around the Mongstad area, the worst

case emissions estimates were more than thirty times lower than environmental regulations in the path of least dispersion (Figure 7.1).

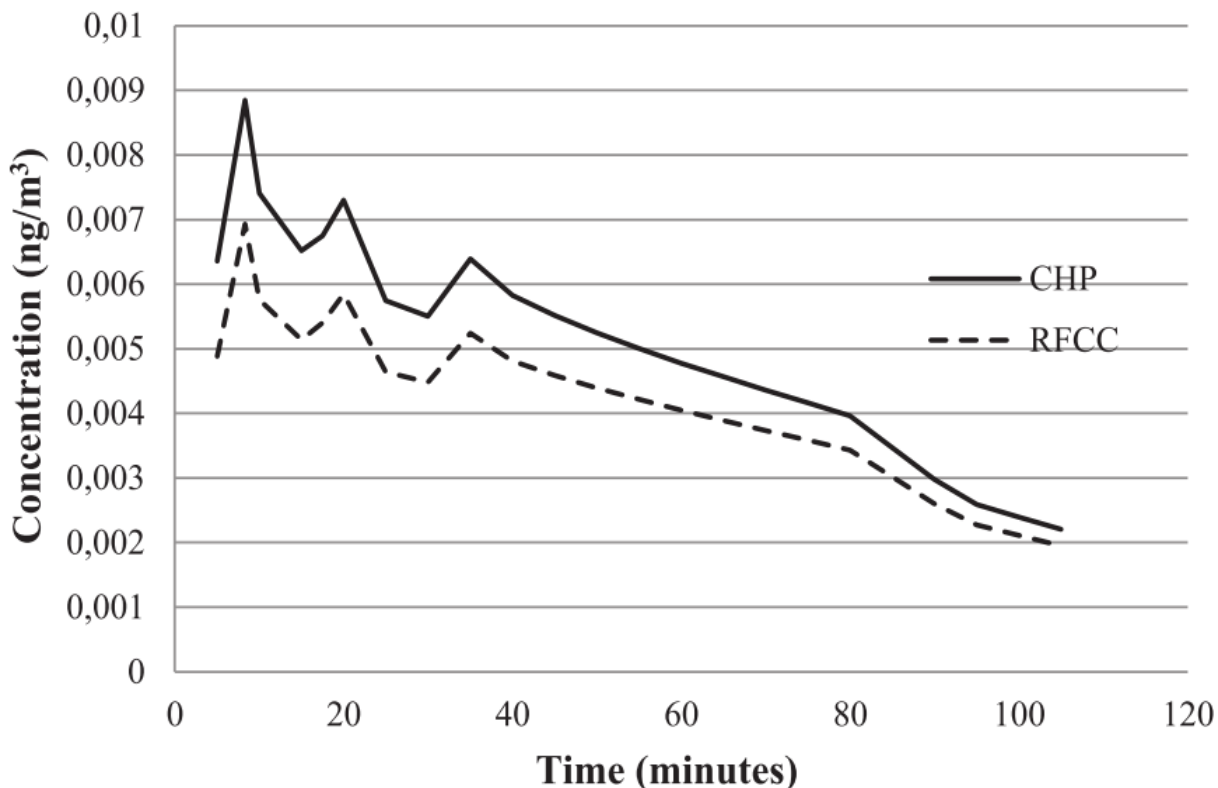


Figure 7.1: Nitrosamine concentrations for worst case along the paths of minimum dispersion as function of time spent after emission along the south-east path (Koeijer and Talstad 2013) (CHP is the flue gas from natural gas combustion, RFCC is the flue gas from catalytic cracking).

TCM emissions were remodeled using AERSCREEN to validate the AERSCREEN model compared to the more rigorous TAPM model and to further understand the factors that govern the maximum atmospheric nitrosamine concentration. The AERSCREEN software is a screening tool based on the EPA AERMOD model (US EPA, 2011). The model uses Gaussian plume dispersion over a range of atmospheric conditions to determine the maximum concentration profile for given flue stack dimensions and emissions. Since AERSCREEN is designed to over-estimate emissions, the model is used to determine if emissions *could* be a concern and if further modeling should be

conducted. As expected, the AERSCREEN model over-predicted TCM nitrosamine concentrations by a factor of 3.5 compared to the TAPM inert model (Figure 7.2). However, the dispersion time after emission determined by plume speed and distance downwind of the point source (Equation 7.1) was roughly equivalent for the maximum nitrosamine concentration in both the TAPM and the AERSCREEN model.

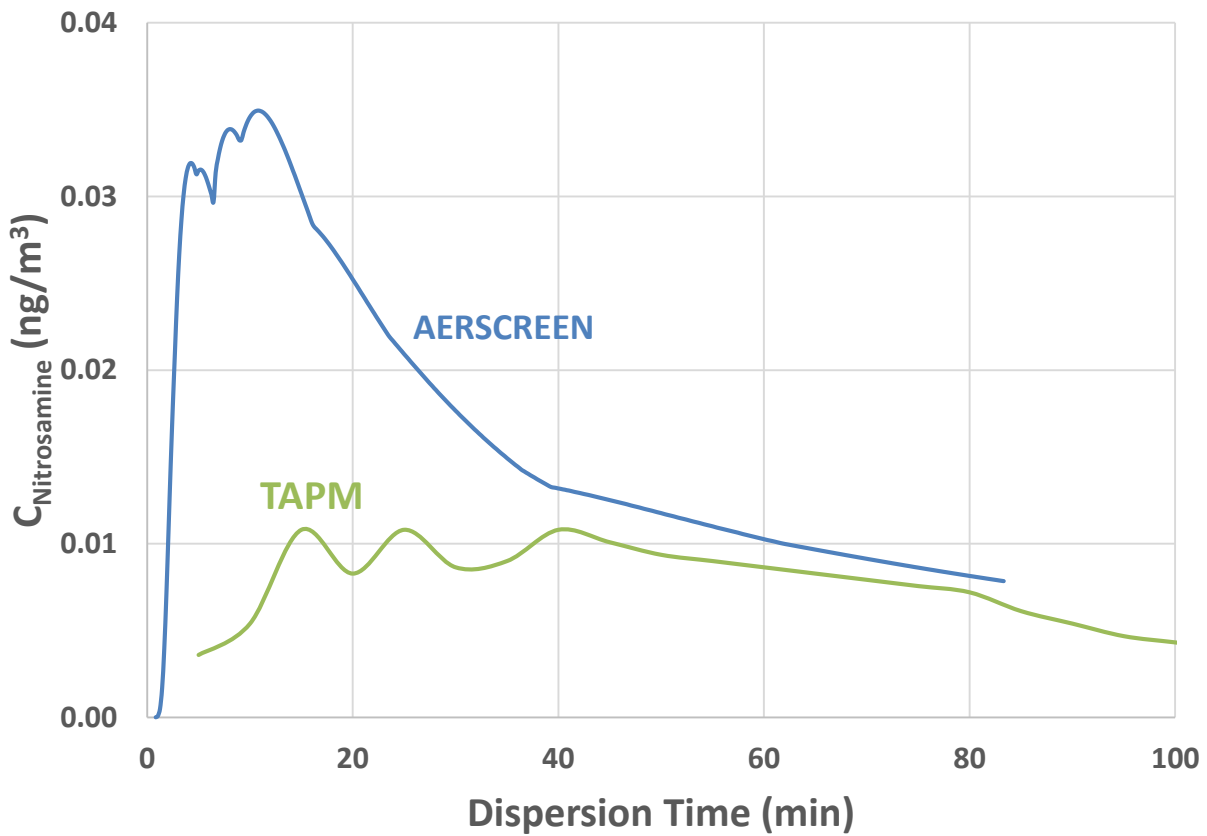


Figure 7.2: Nitrosamine maximum concentration for TAPM (Koeijer and Talstad 2013) and AERSCREEN model; 100 m stack height, 3.6×10^{-4} g/s nitrosamine emissions, dispersion time from Equation 7.1, emissions treated as inert, full AERSCREEN specifications in Appendix D.

$$t_{disp} = \sum_{i=0}^n \frac{d_{i+1} - d_i}{plume\ speed_i} \quad (7.1)$$

The nitrosamine photolytic decomposition chemistry was then overlaid on top of the inert emissions using Equation 7.2. As Koeijer et al. concluded, the maximum nitrosamine levels are

very close to the point source, less than 10 minutes downwind. Because of the proximity to the point source, the nitrosamines do not have time to decompose; assuming a half-life of 60 minutes, photolytic nitrosamine decomposition only decreases the maximum nitrosamine concentration by 15 %. Sørensen et al. found that under summer conditions photolytic decomposition will have a half-life on the order of 10 minutes (Sørensen et al. 2015), which would lower the maximum nitrosamine concentration by 30 % and shift the peak within 5 minutes downwind of the stack (Figure 7.3). Even under ideal conditions, nitrosamine photolytic decomposition will not solve the nitrosamine emissions issue close to the amine scrubber point source.

$$C_{\text{Nitrosamine}} = C_{\text{Inert}} * 0.5^{\frac{t_{\text{disp}}}{\tau_{1/2}}} \quad (7.2)$$

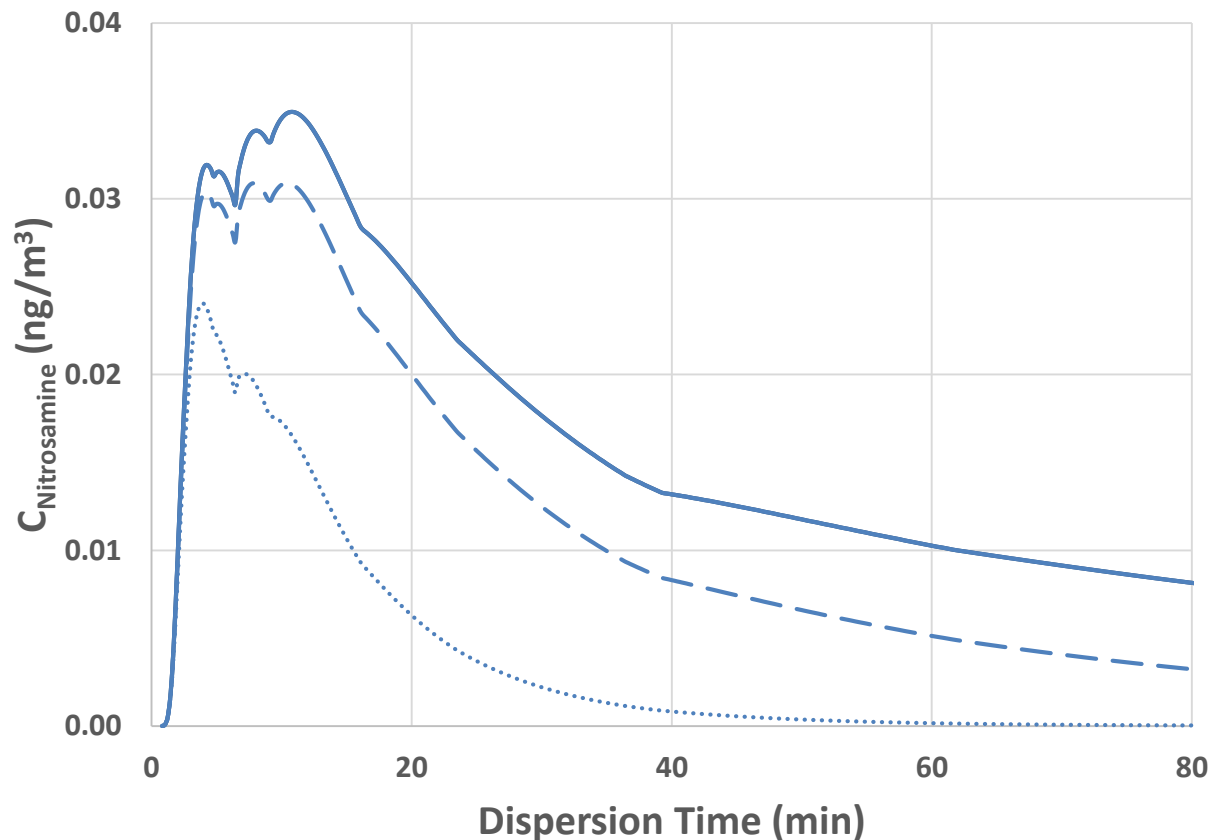


Figure 7.3: Nitrosamine maximum concentration assuming nitrosamine is: inert (solid), photolytically degrades with a half-life of 60 minutes (dashed), and photolytically degrades with a half-life of 10 minutes (dotted).

Finally, emissions were scaled up from the TCM pilot plant (20 m³/s flue gas flow, 10 MW equivalent) to a full-sized capture plant (1000 m³/s flue gas flow, 500 MW equivalent). The absolute emission rate and stack cross-sectional area were scaled proportionally to overall gas flow in order to give comparable emissions, and a conservative nitrosamine decomposition half-life of 60 minutes was assumed. The AERSCREEN results for the maximum nitrosamine concentration of the scaled-up amine scrubber did exceed NIPH regulations, proving that nitrosamine might be an emissions issue if left unchecked. A gas reheat to 150 °C to promote flue gas buoyancy could be one method to reduce the maximum nitrosamine concentration (Figure 7.4).

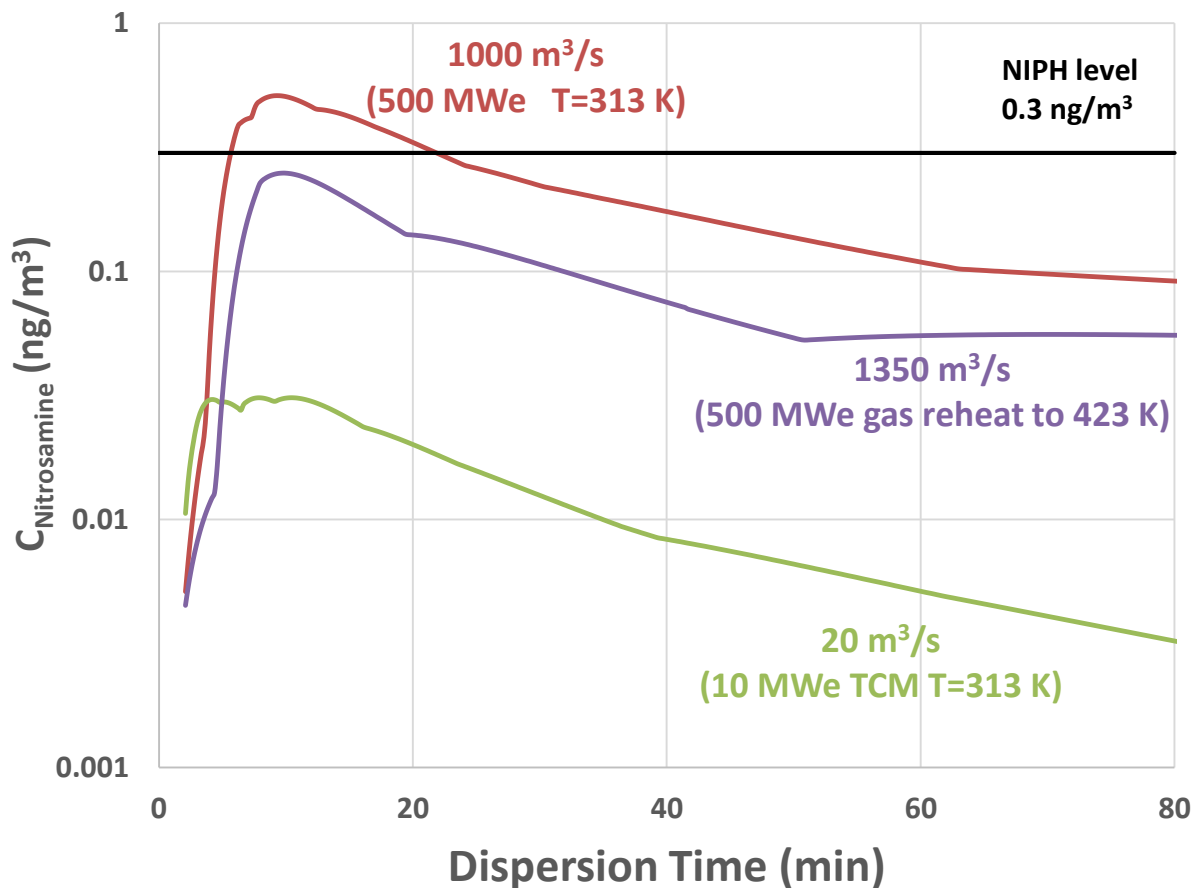


Figure 7.4: Nitrosamine maximum concentration from AERSCREEN model; dispersion time from Equation 7.1, 60 minute nitrosamine half-life, nitrosamine emissions are 0.018 g/s for 500 MW size and 3.6×10^{-4} g/s for 10 MW size, full AERSCREEN specifications in Appendix D.

The maximum absolute emission rate from the point source that results in concentrations below NIPH limits can be calculated using the AERSCREEN results from Figure 7.4 along with the underlying Gaussian plume dispersion model (Equation 7.3).

$$C_{\text{Nitrosamine}}(x, y, z) = \frac{Q_{\text{Nitrosamine}}}{\bar{u}_x} \phi_y \phi_z \quad (7.3)$$

$Q_{\text{Nitrosamine}}$ is the point source emission rate of nitrosamines in grams per second, \bar{u}_x is the average plume velocity in the direction of the wind, and ϕ_y/ϕ_z are functions of dispersion coefficients in the y and z direction based on atmospheric and plume conditions (Figure 7.5).

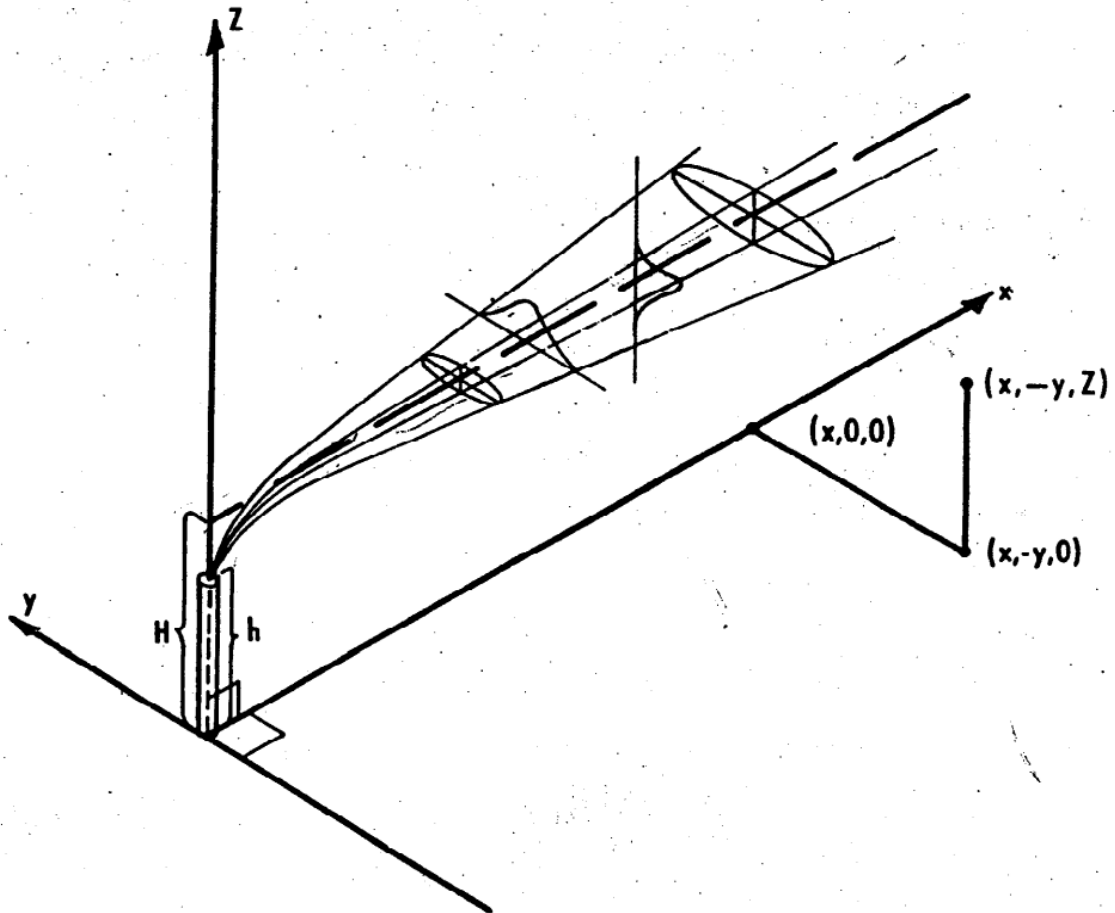


Figure 7.5: Coordinate system for the Gaussian Plume Equation (Allen and Durrenberger 2014)

AERSCREEN automatically calculates \bar{u}_x , ϕ_y , and ϕ_z for the maximum nitrosamine concentration at given stack dimensions, so the nitrosamine concentration is directly proportional to the absolute emissions rate (Equation 7.4). Substituting the full-scale results from Figure 7.4 without the gas reheat and a maximum nitrosamine concentration equivalent to the NIPH standard (0.3 ng/m^3) yields a maximum emission rate of 0.011 g/s (Equation 7.5). Assuming a nitrosamine molecular weight of 100 g/mol , the emission rate is equivalent to $2.8 \times 10^{-6} \text{ m}^3/\text{s}$ or approximately 2.8 ppbv (Equations 7.6 & 7.7). Since AERSCREEN is a conservative modeling tool used for screening, nitrosamine emissions below 2.8 ppbv from a 500 MW equivalent amine scrubber with should not exceed NIPH regulations. More rigorous modeling on emissions higher than 2.8 ppbv would need to be performed under specific atmospheric and topographic conditions to determine if NIPH regulations would be exceeded.

$$\frac{C_{\text{Nitrosamine } 1}}{C_{\text{Nitrosamine } 2}} = \frac{Q_{\text{Nitrosamine } 1}}{Q_{\text{Nitrosamine } 2}} \quad (7.4)$$

$$Q_{\text{Nitrosamine Max}} = 0.018 \frac{\text{g}}{\text{s}} * \frac{0.3 \text{ ng/m}^3}{0.51 \text{ ng/m}^3} = 0.011 \frac{\text{g}}{\text{s}} \quad (7.5)$$

$$G_{\text{Nitrosamine Max}} = 0.011 \frac{\text{g}}{\text{s}} * 0.01 \frac{\text{mol}}{\text{g}} * 0.0224 \frac{\text{n m}^3}{\text{g}} * \frac{313 \text{ K}}{273 \text{ K}} = 2.8 * 10^{-6} \frac{\text{m}^3}{\text{s}} \quad (7.6)$$

$$y_{\text{Nitrosamine Max}} = \frac{G_{\text{Nitrosamine Max}}}{G_{\text{Flue Gas}}} = 2.8 \text{ ppbv} \quad (7.7)$$

7.1.3 Connecting Nitrosamine Concentration in the Scrubber to Point Source Emissions

Nitrosamines can be emitted in the flue gas either through mechanical entrainment, aerosols, or the gas phase. Aerosols and mechanical entrainment emissions must be minimized in any carbon capture system regardless of the nitrosamine issue, and several technologies have been developed recently to address these issues (Khakharia et al. 2013; Bade et al. 2013; Khakharia et al. 2014; Moser et al. 2013). Gaseous emissions of the amines have been traditionally controlled using a water wash. The water wash absorbs the gaseous amine until amine emissions are lower than approximately 1 ppm (Sexton et al. 2014); the volatile nitrosamine will simultaneously be

absorbed in the water wash based on its volatility. Total amine and nitrosamine emissions can thus be related based on their relative volatilities and concentrations in the amine scrubber (Equation 7.8).

$$\frac{y_{\text{Nitrosamine}}}{y_{\text{Amine}}} = \frac{C_{\text{Nitrosamine}} H_{\text{Nitrosamine}}}{C_{\text{Amine}} H_{\text{Amine}}} \quad (7.8)$$

For primary amine solvents, the nitrosamine will be formed from the amine degradation products. Volatilities for these nitrosamines will vary based on the substituent groups of the specific secondary amine and need to be evaluated individually to determine the extent of gaseous emissions. Nitrosamines in secondary amine solvents will form from the solvent itself. These nitrosamines are expected to be approximately 10 times less volatile than their parent amine (C. J. Nielsen and Hoffmann 2010; Cousins et al. 2015). However, amines may absorb CO₂ in the scrubber and the water wash, lowering the concentration of free amine and the apparent volatility of the amine at operating conditions (Nguyen 2013; Hilliard 2008). Voice found that MNPZ volatility was roughly equivalent to PZ volatility at absorber conditions, with the ratio of MNPZ to PZ remaining constant in both the absorber and absorber condensate (Table 7.1). The absence of K⁺ in the absorber condensate proved there was no entrainment carryover into the condensate.

Table 7.1: Relative MNPZ and PZ volatility from the absorber condensate (Voice 2013).

| Species | Rich solution | Absorber condensate | Solvent / Condensate Ratio |
|----------------------|---------------|---------------------|----------------------------|
| PZ (mmol/kg) | 1157 | 12.52 | 92.45 |
| MNPZ (mmol/kg) | 4.973 | 0.0528 | 94.20 |
| K ⁺ (ppm) | 150.5 | 0.04* | 3761.5 |
| PZ/MNPZ Ratio | 232.7 | 237.1 | |

*K⁺ in absorber condensate is at detection limit

Assuming that the volatility of nitrosamines and amines are equivalent at absorber and water wash conditions, Equation 7.8 simplifies to Equation 7.9. Substituting in 1 ppm emissions for amines, a maximum 2.8 ppb emissions for nitrosamines and a 5 M concentration for the solvent

yields a maximum nitrosamine concentration in the amine scrubber of 14 mM. Above 14 mM nitrosamine in the solvent, gaseous nitrosamine emissions *may* become the environmental driver for flue gas emissions control. Several techniques such as flue gas reheat, multiple water wash loops (Gorset et al. 2014), and UV treatment (Dai and Mitch 2015) could be used to lower gaseous nitrosamine emissions if necessary.

$$\frac{y_{\text{Nitrosamine}}}{y_{\text{Amine}}} = \frac{C_{\text{Nitrosamine}}}{C_{\text{Amine}}} \quad (7.9a)$$

$$C_{\text{Nitrosamine}} = \frac{y_{\text{Nitrosamine}}}{y_{\text{Amine}}} * C_{\text{Amine}} = \frac{2.8 \text{ ppb}}{1000 \text{ ppb}} * 5000 \text{ mM} = 14 \text{ mM} \quad (7.9b)$$

7.1.4 Nitrosamine Limits Based on Solvent Spills

While nitrosamine accumulation up to 14 mM in the solvent should pose no problem for continuous gaseous emissions, there will still be some risk attached to accidental solvent spill. Determining the inherent risk of spill and environmental impact for a First-of-a-Kind process is outside the scope of this work, but has been previously discussed in literature (Sugiyama and Fischer 2008; Koller, Fischer, and Hungerbühler 2000; Hassim et al. 2013). The risk of spilling the solvent will be determined by process conditions, but any promising solvent can also be compared to currently published nitrosamine levels for the first generation MEA solvent and the low nitrosamine-forming ACCTM S26 solvent. Nitrosamines have accumulated to a maximum 2.9 mM and 0.15 mM for MEA and ACCTM S26 respectively (Strazisar, Anderson, and White 2003; Gorset et al. 2014).

7.2 MODELING NITROSAMINE ACCUMULATION IN THE AMINE SCRUBBER

7.2.1 Description of the Nitrosamine Accumulation Process

Figure 7.6 gives the proposed sequence of processes that determine nitrosamine accumulation in amine scrubbing based on Chapters 3–6. Flue gas containing NO_x enters a polishing scrubber where a fraction (α_{pre}) of the NO₂ can be removed via reaction with sulfite or

tertiary amine. The remaining NO_x then enters the absorber where a portion of the NO_2 (β_{abs}) can absorb into the amine solution as nitrite. A fraction of the NO (γ_{abs}) can directly form nitrosamines by reacting with the amine radical formed during NO_2 absorption. The rest of the NO_x will vent from the absorber along with the scrubbed flue gas. A fraction of amine oxidation (ϵ) also yields nitrite in amine solvents that are not oxidatively stable. Nitrite from NO_x absorption and amine oxidation will then travel to the stripper where it can nitrosate a secondary amine with a yield of δ_{str} . The yield is determined by the concentration of secondary amines in the solvent and their relative nitrosation rates compared to the primary amine solvent. After nitrosation, the nitrosamine will thermally decompose in the stripper according to a pseudo-first order nitrosamine decomposition rate constant (k_{str}). In many amine scrubbing systems, a slipstream (x_{recl}) of the solvent is passed through a distillation reclaimer to remove any nonvolatile impurities. Efficiency of nitrosamine removal through thermal reclaiming will be determined by nitrosamine volatility ($k_{\text{H NNO}}$) and the thermal decomposition rate in the reclaimer (k_{Recl}). Finally, nitrosamines will exit the amine scrubber through gaseous emissions (y_{NNO}) or accidental spills (x_{spill}).

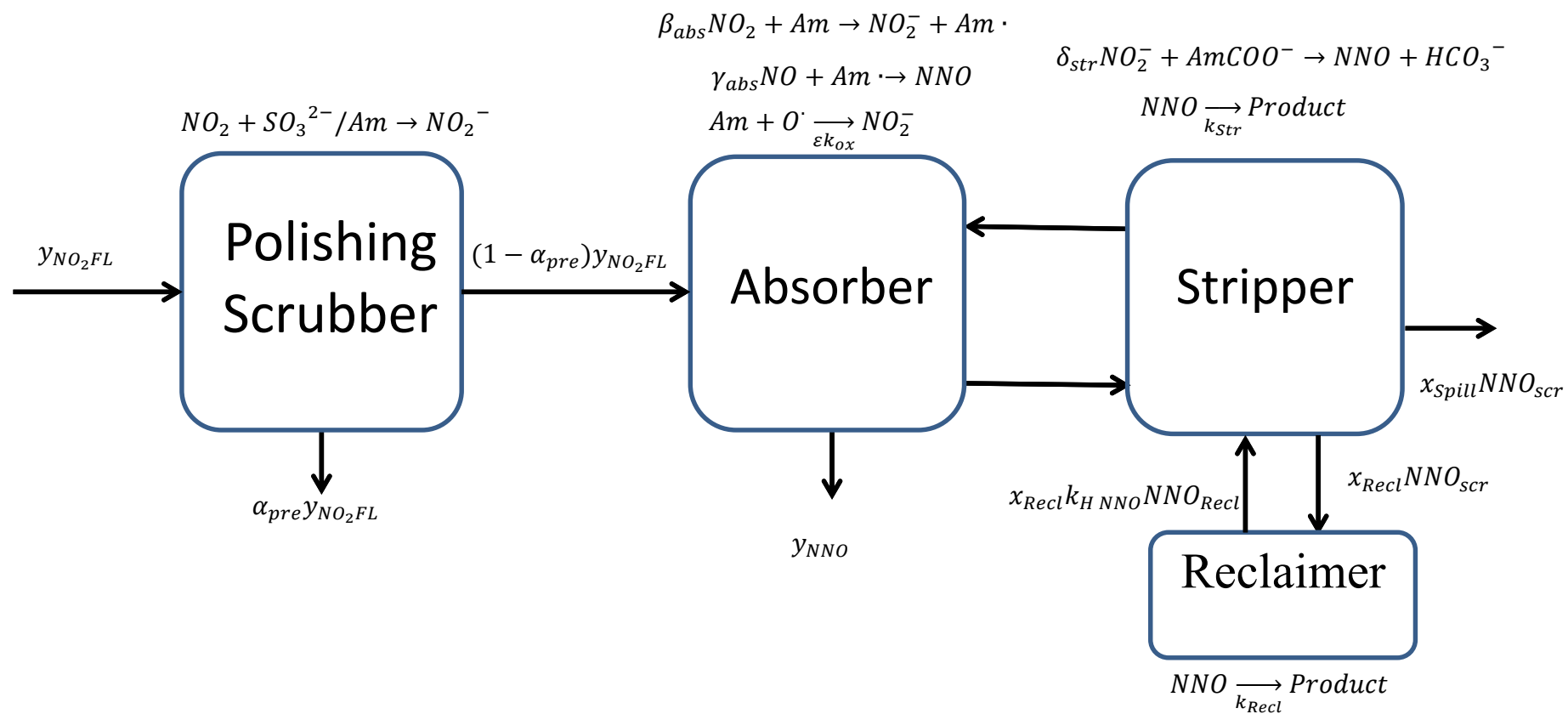


Figure 7.6: Nitrosamine accumulation in amine scrubbing

7.2.2 Mass Balances for Nitrosamine Accumulation

A total mole balance over the accumulation of nitrosamine in the amine scrubber yields Equation 7.10. Dividing by the volumetric solvent flow rate (L) and assuming a 95 % reclaimer removal efficiency (Chapter 5) leads to Equation 7.11. Assuming all variables except nitrosamine concentration are constant with respect to time, the first order differential equation can be solved to give Equations 7.12 and 7.13.

$$\begin{aligned} \frac{dn_{NNO}}{dt} = & \delta_{str}[(1 - \alpha_{pre})(\beta_{abs} + \gamma_{abs})y_{NO_2FL}G + \varepsilon k_{ox}V_{Tot}] - V_{str}k_{str}C_{NNO} \\ & - x_{Recl}LC_{NNO} + x_{Recl}Lk_{HNNO}C_{NNO} - Lx_{spill}C_{NNO} - Gy_{NNO} \end{aligned} \quad (7.10)$$

$$\begin{aligned} \tau_{Tot} \frac{dC_{NNO}}{dt} = & \delta_{str} \left[(1 - \alpha_{pre})(\beta_{abs} + \gamma_{abs})y_{NO_2FL} \frac{G}{L} + \varepsilon k_{ox}\tau_{Tot} \right] \\ & - \left(\tau_{str}k_{str} + 0.95 * x_{Recl} + x_{spill} + \frac{G}{L} \frac{y_{amine}}{C_{amine}} \right) C_{NNO} \end{aligned} \quad (7.11)$$

$$\text{Where: } \tau_{Tot} = \frac{V_{Tot}}{L}, C_{NNO} = \frac{n_{NNO}}{V_{Tot}}, \text{ and } \frac{y_{amine}}{C_{amine}} = \frac{y_{NNO}}{C_{NNO}}$$

$$\frac{C_{NNO} t - C_{NNO} i}{C_{NNO} SS - C_{NNO} i} = 1 - e^{-\left(\tau_{str}k_{str} + 0.95 * x_{Recl} + x_{spill} + \frac{G}{L} \frac{y_{amine}}{C_{amine}}\right) \frac{t}{\tau_{Tot}}} \quad (7.12)$$

$$C_{NNO} SS = \frac{\delta_{str} \left[(1 - \alpha_{pre})(\beta_{abs} + \gamma_{abs})y_{NO_2FL} \frac{G}{L} + \varepsilon k_{ox}\tau_{Tot} \right]}{\tau_{str}k_{str} + 0.95 * x_{Recl} + x_{spill} + \frac{G}{L} \frac{y_{amine}}{C_{amine}}} \quad (7.13)$$

As expected, the steady-state nitrosamine concentration is proportional to mechanisms for nitrosamine formation and inversely proportional to the mechanisms for nitrosamine removal. Using Equation 7.12, the time to reach 95% of the final steady-state concentration can be found (Equation 7.14).

$$0.95 = 1 - e^{-\left(\tau_{str}k_{str} + 0.95x_{Recl} + x_{spill} + \frac{Gy_{amine}}{L C_{amine}}\right) \frac{t_{ss}}{\tau_{Tot}}} \quad (7.14a)$$

$$t_{ss} \approx \frac{3\tau_{Tot}}{\tau_{str}k_{str} + x_{Recl} + x_{spill} + \frac{G}{L} \frac{y_{amine}}{C_{amine}}} \quad (7.14b)$$

7.2.3 Evaluating Generic Parameters for Nitrosamine Accumulation Model

All of the parameters in Equations 7.13 & 7.14 must be evaluated to determine the steady-state nitrosamine concentration in a given amine scrubber. These parameters can change drastically based on the flue gas composition, solvent, process configuration, and operating conditions. To simplify the analysis, all the parameters that do not change significantly with solvent choice were kept constant (Table 7.2), simplifying Equations 7.13 & 7.14 to Equations 7.15 & 7.16. Gaseous emissions do not significantly impact total nitrosamine losses, comprising less than 0.3 % of the total nitrosamine sink.

Table 7.2: Parameter values for steady-state nitrosamine concentration based on a flue gas from a coal-fired power plant

| Parameter | Description | Range | Base Value |
|----------------|---|------------|-------------------|
| α_{pre} | Fraction of NO ₂ absorbed in prescrubber | 0–1 | 0 |
| y_{NO_2FL} | Mole fraction of NO ₂ in inlet flue gas | 0.5–5.5 | 1.5 ppm* |
| G/L | Ratio of flue gas flow rate to solvent flow rate | 5–15 | 10 mol/Liter |
| ϵ | Yield of nitrite from oxidation | 0.002–0.02 | 0.01 ⁺ |
| τ_{Tot} | Total residence time of the amine scrubber | 1200–2400 | 1800 s* |
| τ_{str} | Total residence time in the stripper | 120–600 | 300 s* |

Table 7.2 Cont.

| | | | |
|-------------------------------|---|---|-------------------------------------|
| x_{Recl} | Fraction of overall solvent flow sent to reclaimer | 0.0003–0.001 | 0.001* |
| x_{spill} | Average fraction of flow going to solvent spills | N/A | 0 |
| $\frac{y_{amine}}{C_{amine}}$ | Ratio of amine in outlet flue gas amine in the scrubber | $\frac{0 - 3 \text{ ppm}}{5 \text{ M}}$ | $\frac{1 \text{ ppm}}{5 \text{ M}}$ |

*(Sexton et al., 2014) ⁺Appendix B

$$C_{NNOSS} = \frac{\delta_{str}[(\beta_{abs} + \gamma_{abs})1.5 * 10^{-5} \text{ M} + 18 \text{ s} * k_{ox}]}{300 \text{ s} * k_{str} + 9.5 * 10^{-4} + 2 * 10^{-6}} \quad (7.15)$$

$$t_{ss} \approx \frac{5400 \text{ s}}{300 \text{ s} * k_{str} + 9.5 * 10^{-4} + 2 * 10^{-6}} \quad (7.16)$$

7.2.4 Evaluating Solvent-Specific Parameters for Nitrosamine Accumulation Model

The remaining parameters (δ_{str} , β_{abs} , γ_{abs} , k_{ox} , and k_{str}) must be evaluated individually based on solvent properties; Table 7.3 gives parameter values for 9 m MEA, 8 m PZ, and 7 m MDEA/ 2m PZ. Nitrosamine yield from nitrite (δ_{str}) is determined by the relative reaction rates of nitrite with primary and secondary amines. Since tertiary and hindered amines do not readily form carbamates, they do not nitrosate competitively with secondary amines. For the MEA solvent, HeGly is considered to be the dominant secondary amine for nitrosamine formation while PZ is the dominant secondary amine for nitrosamine formation in the PZ and MDEA/PZ solvents. HeGly nitrosates approximately 6 times faster than MEA at stripper conditions with total nitrosamine yield proportional to HeGly concentration (Chapter 4). The fraction of NO₂ absorbed as nitrite (β_{abs}) is calculated in Chapter 3 based on NO₂ absorption rates, absorber packing height; the corresponding NO absorption (γ_{abs}) is assumed to be 20 % of β_{abs} based on NO_x absorption in PZ. Overall

oxidation rates (k_{ox}) were taken from the degradation model built by Nielsen (Sexton et al. 2014) based on data from Voice (Voice 2013). The thermal decomposition rate in the stripper (k_{str}) is determined from Chapter 4 results and the maximum stripper temperatures corresponding to amine thermal degradation rate of $k_1=2.91 \cdot 10^{-8} \text{ s}^{-1}$ (Freeman 2011; Davis 2009).

Table 7.3: Solvent specific parameters for determining steady-state nitrosamine concentration

| Solvent | δ | γ | β | T_{str} (°C) | $k_{ox} \cdot 10^7$ (M/s) | $k_{str} \cdot 10^6$ (s ⁻¹) | $C_{NNO SS} \cdot 10^3$ (M) | t_{ss} (Days) |
|---------------------|----------|----------|---------|-------------------|------------------------------|--|--------------------------------|--------------------|
| MEA+50 mM HeGly | 0.05 | 0.73 | 0.15 | 121 | 5.5 | 1.2 | 0.9 | 48 |
| MEA+200 mM HeGly | 0.19 | 0.73 | 0.15 | 121 | 5.5 | 1.2 | 3.4 | 48 |
| PZ | 1 | 0.92 | 0.18 | 163 | 1.5 | 60 | 1.0 | 3 |
| MDEA/PZ | 1 | 1 | 0.20 | 127 | 2.4 | 1.1 | 20.5 | 49 |

The results for MEA are on the same order of magnitude as several pilot plant campaigns where nitrosamines have built up to between 0.8 mM and 2.9 mM (da Silva et al. 2012; Einbu et al. 2013; Strazisar, Anderson, and White 2003; Gorset et al. 2014). The main difference in nitrosamine content is attributable to differences in total degradation of the MEA solvent, which effects HeGly levels. Despite directly forming nitrosamines, the PZ solvent has a similar steady-state nitrosamine concentration due to high stripper operating temperature. Thus, the higher nitrosamine decomposition rate counterbalances the higher nitrosamine formation rate. Similar nitrosamine levels in PZ solvents have been observed at two pilot plants operating with real flue gas (Cousins et al. 2015; P. T. Nielsen, Li, and Rochelle 2013). The MDEA/PZ blend suffers from the highest steady-state

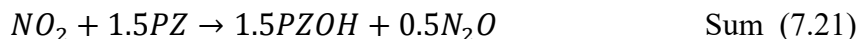
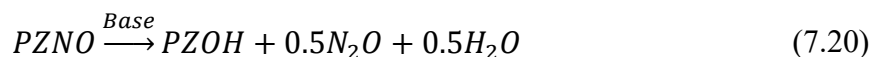
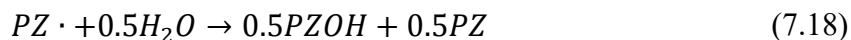
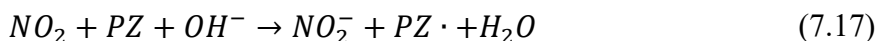
nitrosamine at 20.5 mM since MDEA does not compete with PZ for nitrite and the nitrosamine decomposition rate is low. Of the three solvents tested, only nitrosamines in the MDEA/PZ could necessitate further emissions control on the scrubbed flue gas. While steady-state is reached within a few days for the PZ solvent, both MEA and MDEA/PZ solvents continue to accumulate nitrosamines for 50 days. Thus, preliminary pilot plant results showing low nitrosamines should be treated with caution if the nitrosamine is relatively stable at stripper temperature.

7.3 PRESCRUBBING WITH TRIETHANOLAMINE AND SULFITE

7.3.1 Economic Benefit of Polishing Scrubbers for PZ

In carbon capture from coal-fired power plants, a sodium hydroxide polishing scrubber is economically favorable to remove SO_2 before it reaches the main amine scrubber. A NaOH polishing scrubber works by absorbing SO_2 into NaOH to make sulfite. Under uninhibited conditions, SO_3^{2-} oxidizes immediately to sulfate, which is then purged from the system. NaOH scrubbing is economical because SO_2 absorption is k_g limited, NaOH is much cheaper than the amine, and the waste is non-hazardous. Any SO_2 that does make it through the polishing scrubber will react with the amine and form a sulfate salt, which will eventually cost \$0.10–\$0.30/MT CO_2 /ppm SO_2 for a PZ solvent depending on reclaiming efficiency and cost of disposal (Sexton et al. 2014). Previous studies based on upgrading an existing limestone slurry scrubber before an MEA scrubber have reported an optimum removal to 10 ppm of SO_2 (Rao and Rubin 2002); more recent work based on a NaOH polishing scrubber before a proprietary solvent has targeted removal to 0–2 ppm of SO_2 (Gorset et al. 2013).

A similar economic analysis can be done with NO₂ pre-scrubbing to prevent amine nitrosation in the CO₂ absorption loop. NO₂ reacts with PZ with a final stoichiometry of 1:1.5 (Equations 7.17–7.21), costing \$0.15–\$0.45/MT CO₂/ppm NO₂ based on PZ losses and reclaiming costs. Depending on the rate of NO₂ absorption in the polishing scrubber and the cost of the sacrificial solvent, it may therefore be economical to remove NO₂ upstream of the absorber. NO₂ removal also lowers steady-state MNPZ providing further incentive for NO₂ pre-scrubbing.



7.3.2 Kinetics and Material Balances for NO₂ Scrubbing with TEA

In Chapter 3, TEA was shown to rapidly absorb NO₂ at the pH and temperature in a polishing scrubber. The material balance for absorption is shown in Figure 7.7. NaOH and TEA are fed to the polishing scrubber at a constant rate. The NaOH reacts with SO₂ to form sulfate, and it also reacts with a small amount of CO₂ to form a sodium bicarbonate (NaHCO₃) buffer at pH = 7.0–8.0. The TEA will speciate to protonated TEA (TEAH⁺) and free TEA depending on the pH; only the free TEA is active in absorbing NO₂. The free TEA absorbs NO₂ forming nitrite (NO₂⁻) and a TEA radical (TEA•), which then oxidizes

to byproducts. Unlike NO_2 absorption into SO_2 , the $\text{TEA}\cdot$ does not propagate oxidation, and the overall stoichiometry of NO_2 absorption with TEA is approximately 1:1. The solvent is continuously purged so that the exit sodium sulfate will not precipitate out of solution. For this work, the sulfate concentration was set to a conservative 1.5 M since the effects of nitrite and TEA on the solid solubility of sodium sulfate have not been determined. The steady-state material balances for NaOH and TEA are given in Equations 7.22–7.23.

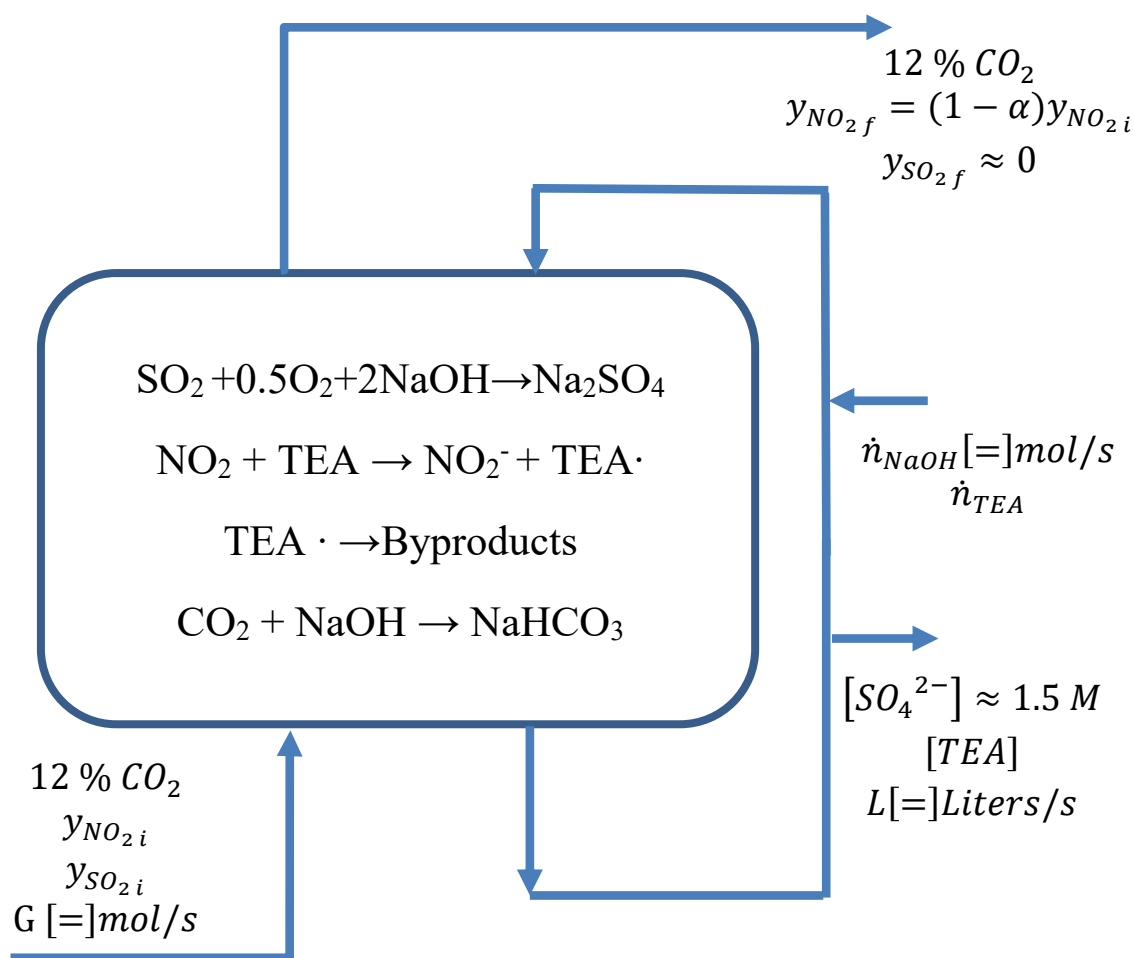


Figure 7.7: Material balance for SO₂ and NO₂ absorption in a polishing scrubber with TEA

$$\frac{dC_{Na_2SO_4}}{dt} = 0 = Gy_{SO_2 i} - LC_{Na_2SO_4} \quad (7.22)$$

$$\frac{dC_{Na}}{dt} = 0 = n_{NaOH feed} - 2Gy_{SO_2} - LC_{NaHCO_3} \quad (7.23)$$

$$\frac{dC_{TEA}}{dt} = 0 = n_{TEA feed} - G\alpha y_{NO_2 i} - LC_{TEA} \quad (7.24)$$

Since the purge is set to 1.5 M Na₂SO₄, the ratio of purge flow to gas flow can be directly determined from Equation 7.22 to yield Equation 7.25. Any excess NaOH not used to neutralize the SO₂ will react with CO₂ and fix the pH (Equation 7.26). The steady-state concentration of TEA in solution is given by Equation 7.27 with the concentration of free TEA determined using Henderson-Hasselbalch (Equation 7.28).

$$\frac{L}{G} = \frac{y_{SO_2 i}}{C_{Na_2SO_4}} = \frac{y_{SO_2 i}}{1.5 M} \quad (7.25)$$

$$pH = 6.1 + \log \frac{HCO_3^-}{p_{CO_2} * H_{CO_2}} = 6.1 + \log \frac{HCO_3^-}{0.12 atm * 0.018 M/atm} \quad (7.26)$$

$$[TEA] = \alpha y_{NO_2} * \frac{G}{L} - \frac{n_{TEA feed}}{L} \quad (7.27)$$

$$[TEA]_{free} = [TEA] * \frac{10^{pH - pK_{a TEA}}}{1 + 10^{pH - pK_{a TEA}}} \quad (7.28)$$

The fraction of NO₂ absorbed (α) into the solvent is determined by the number of mass transfer units in the polishing scrubber (Equation 7.29), which is a function of the overall mass transfer coefficient for NO₂ absorption, the effective wetted area in the polishing scrubber, and the volumetric gas flow rate. An $\frac{a_e}{G}$ of $1.52 * 10^6$ s Pa m² mol⁻¹ was used, representing a gas at 55 °C travelling through 7 m of Mellapak 250X with a

superficial velocity of 1.5 m/s. The gas side mass transfer coefficient (k_g) was taken to be $5 \times 10^{-6} \text{ mol s}^{-1} \text{ Pa}^{-1} \text{ m}^{-2}$ and the overall liquid side mass transfer coefficient (k_g') is assumed to be in the mass transfer with fast reaction regime as determined in Chapter 3 (Equation 7.31).

$$\alpha = 1 - e^{-N_{OG}} = 1 - e^{-K_g \frac{a_g}{G}} \quad (7.29)$$

$$\frac{1}{K_g} = \frac{1}{k_g} + \frac{1}{k_g'} \quad (7.30)$$

$$k_g' [=] \frac{\text{mol}}{\text{s Pa m}^2} = 5.4 \times 10^{-6} * \sqrt{[TEA]_{free}} \quad (7.31)$$

7.3.3 Effect of Varying TEA

The economic benefit of removing NO_2 upstream of the absorber using TEA was analyzed for a flue gas containing 50 ppm SO_2 and 5 ppm NO_2 . Any NO_2 not absorbed in the polishing scrubber is captured in the main absorber, costing a nominal \$0.23/MT CO_2 /ppm NO_2 . The polishing scrubber is assumed to be built for SO_2 absorption, so there is negligible additional capital cost associated with using TEA as an additive. The only additional cost is the cost of the TEA (\$0.30/mol) added to the polishing scrubber; the savings are given by Equation 7.32.

$$\text{Savings} = \frac{\$0.23}{\text{MT CO}_2 \cdot \text{ppm NO}_2} (1 - \alpha) 5 \text{ ppm NO}_2 - \frac{\$0.30}{\text{mol TEA MT CO}_2} \frac{n_{TEA_{feed}}}{\text{mol TEA MT CO}_2} \quad (7.32)$$

Figure 7.8 shows the performance of the scrubber as the concentration of total TEA varies. At low concentrations of TEA, NO_2 penetration is high, which limits the possible savings on PZ nitrosation. At high circulating TEA concentration, the feed rate of TEA is dominated by the purge rate with diminishing additional savings from NO_2 removal. The

economic optimum occurs when these two effects are balanced. However, the best operating condition is at higher concentrations of TEA due to the additional benefit of lower nitrosamine concentration in the PZ loop.

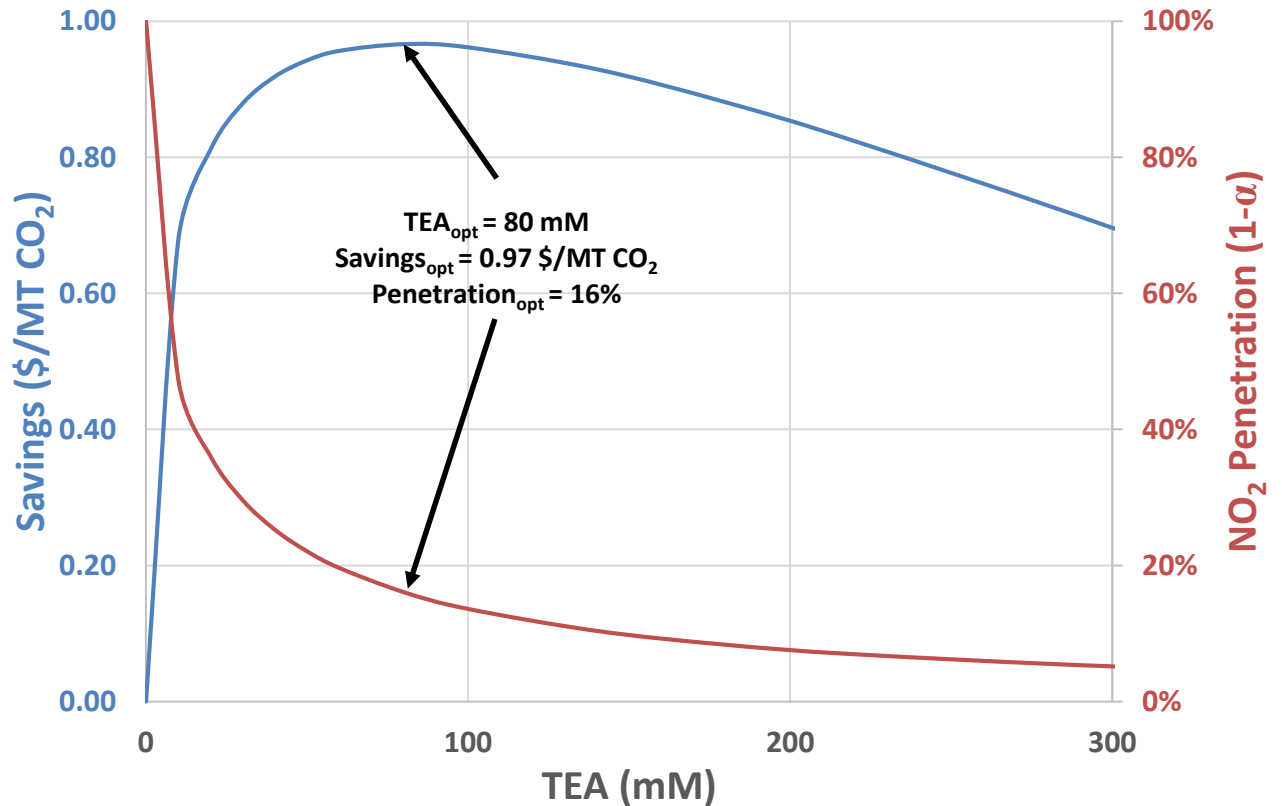


Figure 7.8: Polishing scrubber performance with varying TEA; pH = 8.0, T = 55 °C, $y_{\text{NO}_2 \text{ i}} = 5 \text{ ppm}$, $y_{\text{SO}_2 \text{ i}} = 50 \text{ ppm}$, $\frac{a_e}{G} = 1.52 \cdot 10^6 \text{ s Pa m}^2 \text{ mol}^{-1}$ (roughly 7 m Mellapak 250X, $u_{\text{gas}} = 1.5 \text{ m/s}$)

7.3.4 Effect of Varying SO₂

The optimal TEA concentration was found for 10–300 ppm inlet SO₂ (Figure 7.9). As SO₂ increases, the purge rate must increase to keep a constant outlet concentration of Na₂SO₄. This decreases the possible savings since the TEA feed rate must increase to keep the same concentration of TEA in the scrubber. In response, the optimal TEA decreases

with increasing SO_2 since the purge rate begins to dominate the economics at lower TEA. Predictably, NO_2 penetration at optimal savings increases with increasing SO_2 due to lower circulating TEA. The economics could be improved further by upgrading the existing limestone slurry scrubber to lower inlet SO_2 to the polishing scrubber, decreasing the purge rate needed to keep NaSO_4 soluble.

The analysis was repeated for a packing height of 3 meters instead of 7 meters, reflecting assumptions made in recent amine scrubbing techno-economic evaluations (Frailie 2014). Overall savings decrease by approximately \$0.40/MT CO_2 , and NO_2 penetration increases by 30%, as the packing height decreases from 7 meters to 3 meters (Figure 7.9). High NO_2 penetration in the 3 m column shows that more packing is needed to effectively remove NO_2 in the pre-scrubber. Thus, the height of the polishing scrubber will be determined by the target NO_2 removal (k_g ' limited) instead of the target SO_2 removal (k_g limited).

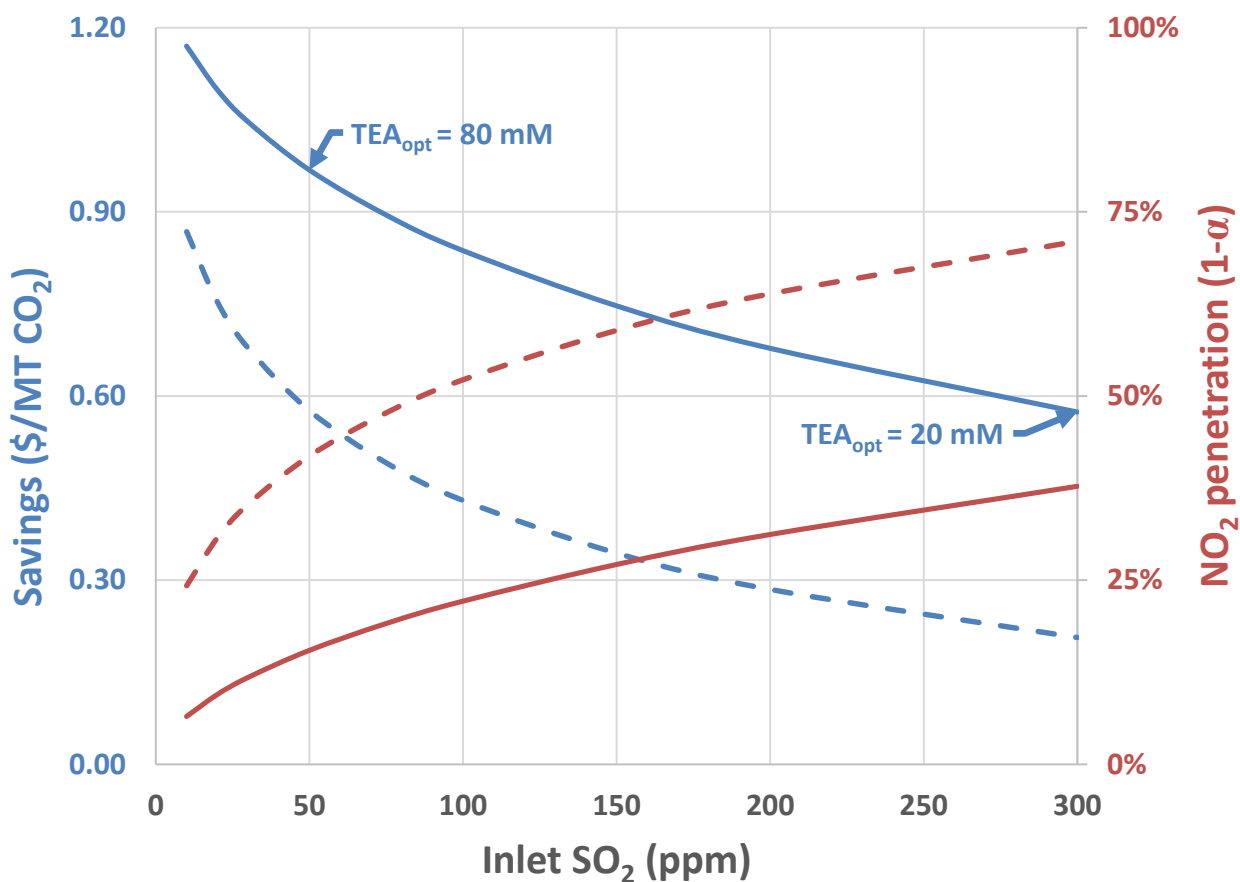


Figure 7.9: Savings and NO₂ penetration for 7 m (Solid) and 3 m (dashed) of packing; pH = 8.0, T = 55 °C, $y_{\text{NO}_2 \text{ i}} = 5\text{ppm}$, $u_{\text{gas}} = 1.5 \text{ m/s}$, optimal TEA

7.3.5 Effect of Varying Inlet NO₂

The economics of the 7 m polishing scrubber were evaluated as both NO₂ and SO₂ varied, with TEA optimized at each condition. As inlet NO₂ decreases, there is less overall PZ degradation through nitrosation, so there is less opportunity for saving through TEA scrubbing (Figure 7.10). Furthermore, amine oxidation to nitrite becomes the dominant mechanism for nitrosamine formation at low NO₂ levels (Figure 7.11). Thus, NO₂ scrubbing will have diminishing returns as inlet NO₂ decreases and should only be pursued when NO₂ is greater than approximately 1 ppm.

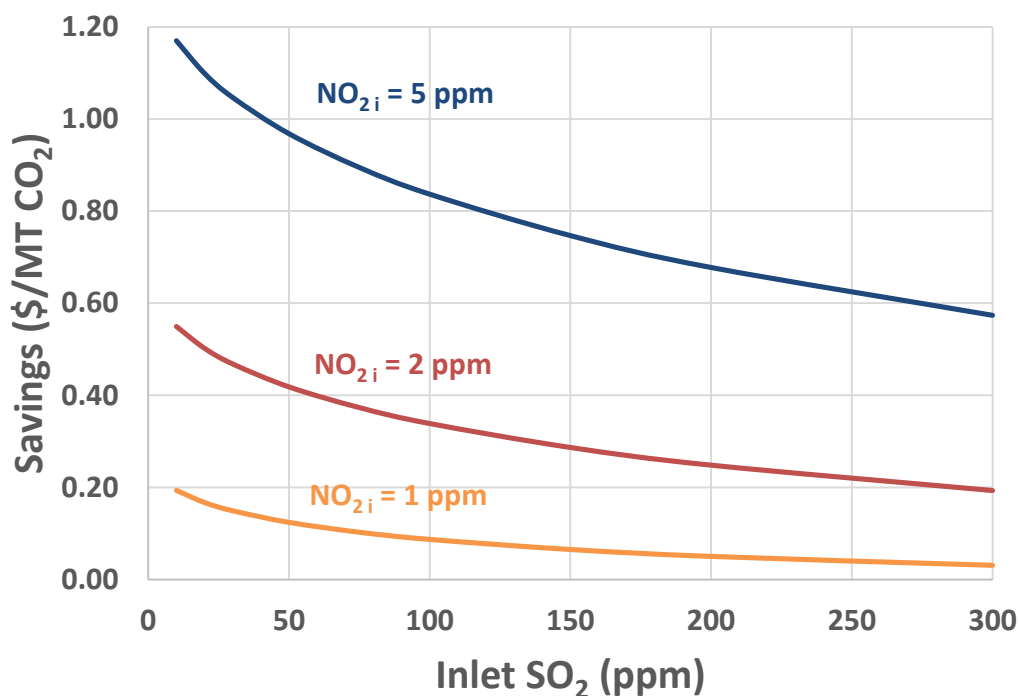


Figure 7.10: Savings from NO₂ scrubbing with varying inlet NO₂; pH = 8.0, T = 55 °C, 7 m Mellapak 250X, u_{gas} = 1.5m/s, optimal TEA

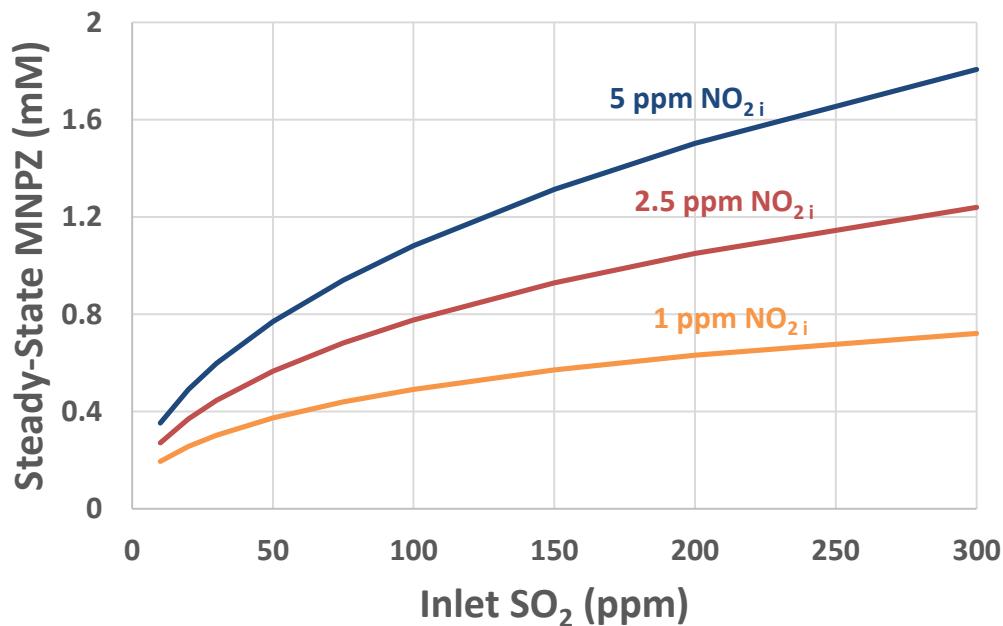


Figure 7.11: MNPZ accumulation in PZ scrubber after economic optimal NO₂ prescrubbing using Equation 7.13 with parameters from Tables 7.2 & 7.3

7.3.6 Packing Height and TEA Optimization at Constant NO₂ Penetration

The previous optimizations have focused on solvent management through NO₂ pre-scrubbing, but the more important goal is to economically limit nitrosamine accumulation in the main scrubber. TEA and packing height were both optimized to find the lowest-cost option for prescrubbing 5 ppm NO₂ to 0.5 ppm NO₂. The cost for NO₂ scrubbing is the additional height over the 3 meters already needed for SO₂ polishing and the cost of the TEA additive. Packing cost for Mellapak 250X constructed from 304 stainless steel is approximately \$2000/m³ (Equation 7.33). Given a gas velocity of 1.5 m/s and 12% inlet CO₂, packing costs can be directly converted to an amortized capital cost (Equations 7.34–7.36) (Frailie 2014). The additional height needed to remove 90 % of NO₂ was found by neglecting end effects of the column and assuming packing area was proportional to packing height (Equation 7.37).

$$Packing\ Cost\ [=]\frac{\$}{m^3} = 7.31 * a_p + 203.05 = 2031 \frac{\$}{m^3} \quad (7.33)$$

$$Amortized\ Cost[=]\frac{\$}{MT\ CO_2} = \frac{Packing\ Cost * (V_{pack\ add}) * (\alpha\beta)}{MT\ CO_{2\ captured}/year} \quad (7.34)$$

$$Amort.\ Cost = \frac{2031 \frac{\$}{m^3} * \pi r_{col}^2 * (h_{add}) * 0.2 * 5}{1.5 \frac{m}{s} * \pi r_{col}^2 * 0.00019 \frac{MT\ CO_{2\ captured}}{m^3_{Flue\ Gas}} * 2.8E7 \frac{s}{oper\ year}} \quad (7.35)$$

$$Amortized\ Cost = \frac{\$0.25}{MT\ CO_2 \cdot m} * (h_{add}) \quad (7.36)$$

$$\frac{a_e}{G} = 1.52 * 10^6 \frac{s\ Pa\ m^2}{mol} * \frac{h_{add} + 3m}{7m} \quad (7.37)$$

Additional blower, pump, and shell costs associated with the extra NO₂ scrubbing height were neglected in the analysis, but could add 0.10–0.20 \$/MT CO₂. No additional

distributors or collectors are needed since NO_2 absorbs simultaneously with SO_2 . Figure 7.12 shows how optimal savings and packing height vary as inlet SO_2 increases. The maximum savings occurs at the lowest inlet SO_2 and requires an additional 1 m of packing to reach 90% NO_2 removal. Under these conditions, the purge rate is very low, allowing a high TEA concentration (750 mM) before the purge rate dominates TEA losses. As inlet SO_2 increases, optimal TEA decreases and packing must increase to remove 90% NO_2 . At 50 ppm inlet SO_2 and 5 ppm inlet NO_2 , the cost of the additional TEA feedstock and extra packing balances out with the savings from not nitrosating PZ. Thus under these conditions, MNPZ concentration in the absorber can be reduced from 3.0 mM to 0.4 mM (Equation 7.13, inputs from Tables 7.1 & 7.2) without increasing the overall cost for CO_2 removal.

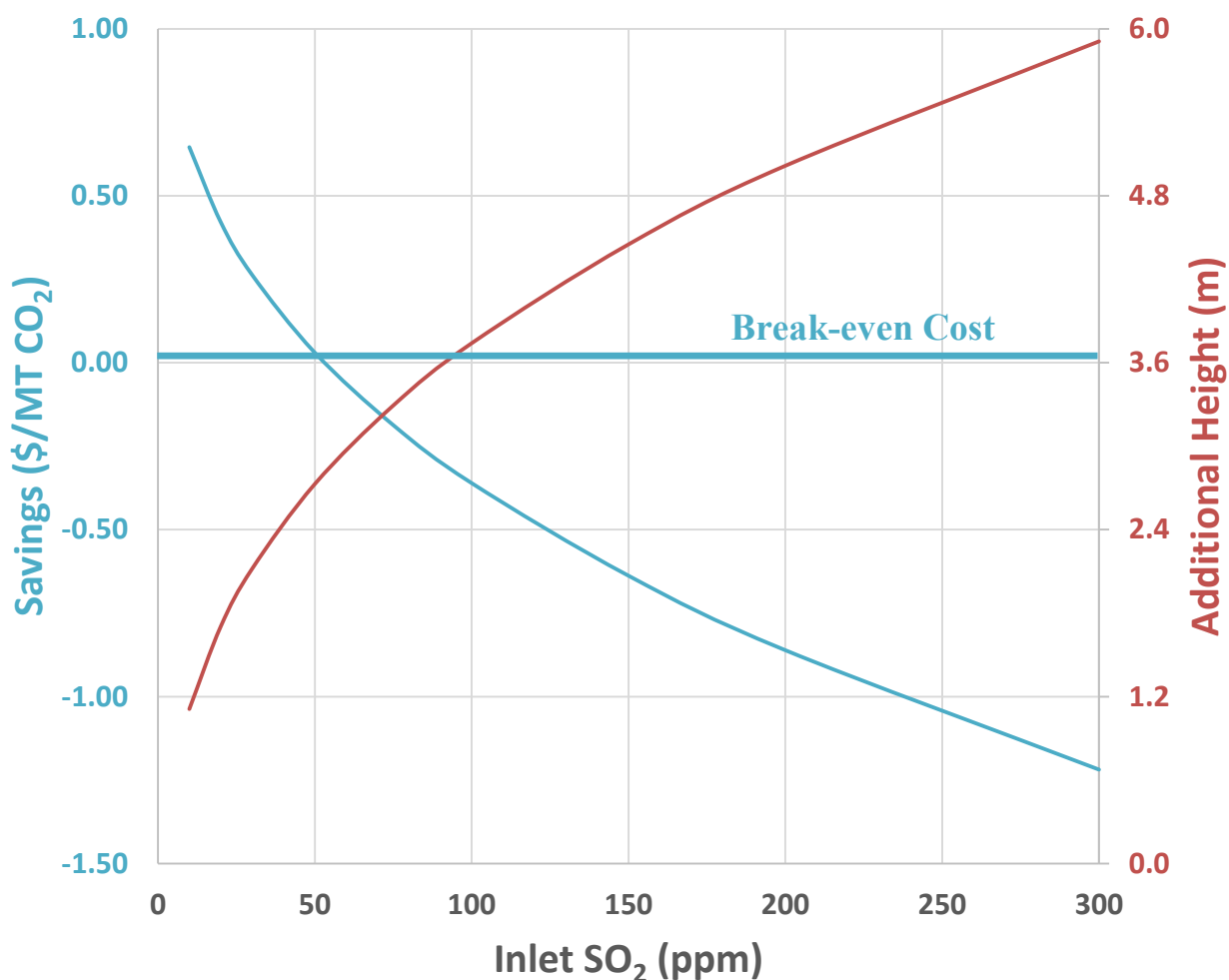


Figure 7.12: Savings for 90% NO₂ removal; pH = 8.0, $y_{\text{NO}_2\text{i}} = 5\text{ppm}$, $T = 55\text{ }^{\circ}\text{C}$, $u_{\text{gas}} = 1.5\text{m/s}$, optimal TEA, optimal packing height

7.3.7 Prescrubbing with Sulfite Using Thiosulfate Inhibition

At high inlet SO₂, the cost of NO₂ prescrubbing with TEA becomes prohibitive due to the high purge rate. In contrast, the cost of NO₂ prescrubbing using sulfite decreases with increasing inlet SO₂ since the SO₂ serves as the sulfite feedstock. Sulfite scrubbing was economically optimized for variable sulfite concentration and scrubber height while keeping 90 % NO₂ removal constant (Figure 7.13). Sulfite does not need to be added to the

scrubber since it forms during SO₂ absorption. However, since sulfite oxidizes rapidly with NO₂ absorption, thiosulfate must be added to inhibit oxidation (Chapter 6). The savings from NO₂ prescrubbing are defined by the balance between unrealized PZ losses and the cost of thiosulfate feed and additional packing (Equation 7.38). The feed cost was assumed to be \$0.03/mol Na₂S₂O₃, but Na₂S₂O₃ could be even cheaper if made on site using emulsified sulfur (Lee and Benson 1990). The thiosulfate needed per metric ton of CO₂ can be simplified from Equations 6.22 & 6.25 in Chapter 6 to yield Equation 7.39. Finally, the height needed for 90 % NO₂ removal was found assuming the overall liquid side mass transfer was reaction limited which gives a half-order dependence on sulfite (Equation 7.40–7.42) (Shen 1997).

$$Savings = \frac{\$0.23 * 4.5 \text{ ppm } NO_2}{MT \text{ } CO_2 \cdot \text{ ppm } NO_2} - \frac{\$ 0.03}{mol \text{ } Na_2S_2O_3} \frac{n_{Na_2S_2O_3}}{n_{CO_2 \text{ captured}}} - \frac{\$0.25}{MT \text{ } CO_2 \cdot m} h_{add} \quad (7.38)$$

$$\frac{n_{Na_2S_2O_3}}{n_{CO_2 \text{ captured}}} = \left(994 * [SO_3^{2-}] \frac{0.9y_{NO_2i}}{y_{SO_2i}} \right)^2 * \frac{y_{SO_2i}}{[SO_4^{2-}] * 0.9y_{CO_2}} \quad (7.39)$$

$$k_g' [=] \frac{mol}{s \text{ Pa } m^2} = 18.5 * 10^{-6} * \sqrt{[SO_3^{2-}]} \quad (7.31)$$

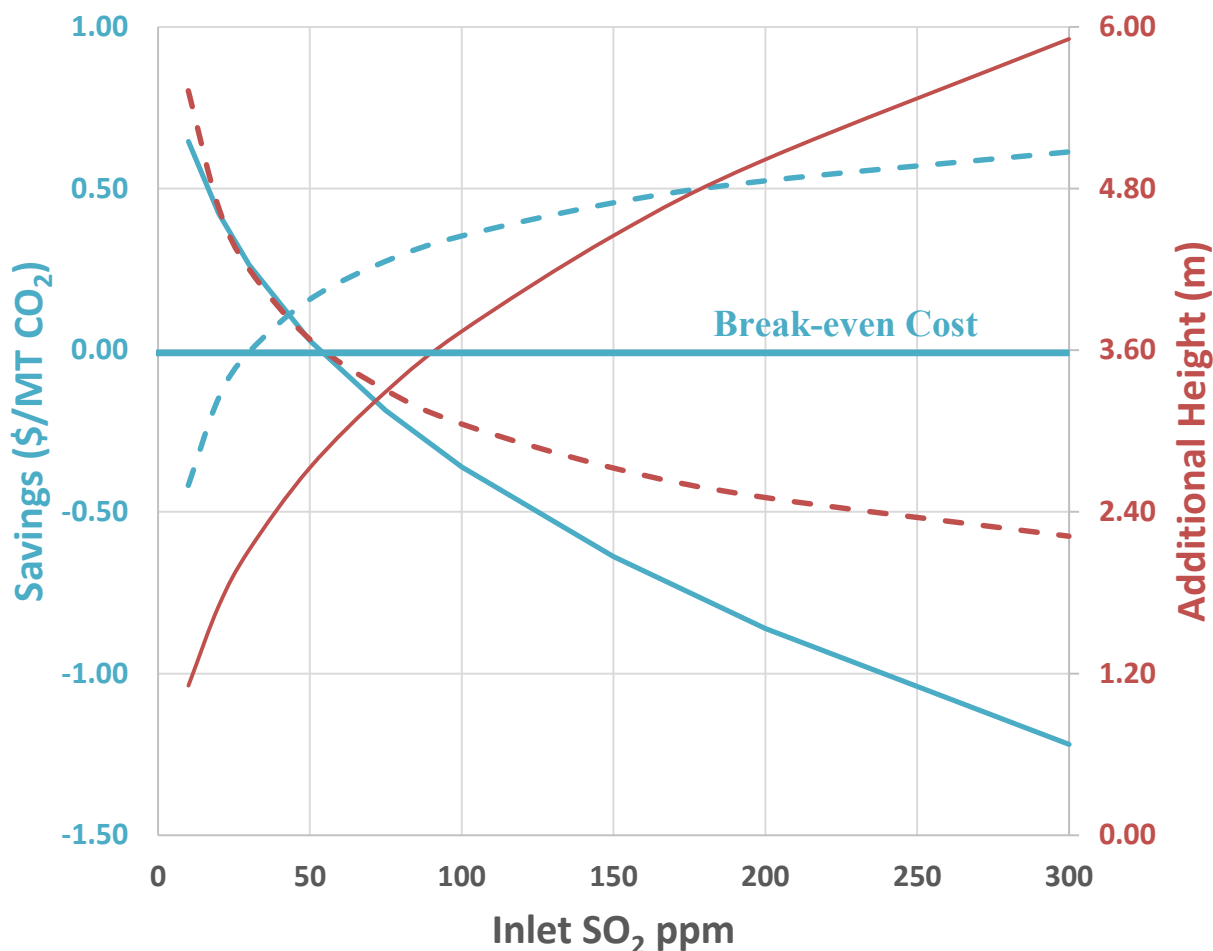


Figure 7.13: Savings for 90% NO₂ removal using either sulfite or TEA as the prescrubbing solvent; pH = 8.0, $y_{\text{NO}_2 i} = 5\text{ppm}$, $T = 55\text{ }^\circ\text{C}$, $u_{\text{gas}} = 1.5\text{m/s}$, optimal TEA (—) or sulfite (---), optimal additional packing height above 3 m.

As predicted, NO₂ scrubbing with sulfite shows the opposite trend compared to NO₂ scrubbing with TEA. At inlet SO₂ below 40 ppm, thiosulfate addition is unfavorable compared to TEA addition due to the low replenishment rate of sulfite and the high thiosulfate feed needed to keep sulfite in solution. At higher than 40 ppm SO₂, NO₂ scrubbing with sulfite is economically favorable; savings continue to increase to a final

value of \$0.61/MT CO₂ at 300 ppm inlet SO₂, and a relatively short column of 5.2 m height is needed to reach 90 % removal. At all inlet SO₂ conditions, NO₂ scrubbing with either TEA or sulfite makes economic sense when PZ degradation from nitrosation is taken into account. Therefore from an economic and environmental standpoint, flue gases with high levels of NO₂ (above approximately 5 ppm) should be pre-scrubbed prior to the main absorber.

7.4 CONCLUSIONS

7.4.1 Relevant Nitrosamine Limits in the Amine Scrubber

- There are currently no limitations for nitrosamines in the amine scrubber itself, but the Norwegian Institute of Public Health has limited total nitrosamine emissions to 0.3 ng/m³ in air and 4 ng/L in water.
- The rigorous TAPM emissions model built for the TCM 10 MWe pilot plant using an MEA solvent predicts peak air concentrations of less than 0.01 ng/m³, which is 30 times lower than nitrosamine emission limits (Koeijer and Talstad 2013).
- The AERSCREEN model used for screening emissions limits over-predicts the TAPM model by a factor of 3.5, but correctly predicts that the maximum concentration would be 10 minutes downwind of the point source.
- The maximum nitrosamine concentration is too close to the point source for nitrosamine photolysis to be an effective emissions control. Under ideal conditions with a photolysis half-life of 10 minutes, the maximum nitrosamine concentration only decreases 35 % over the inert case.

- TCM emissions modeled using AERSCREEN exceed NIPH air emissions regulations when scaled from a 10 MWe point source to a 500 MWe point source.
- For a 500 MWe point source, nitrosamine emissions would need to be less than 2.8 ppbv for nitrosamine gaseous emissions to be a non-issue.
- Assuming that nitrosamines are as volatile as their parent amines at process conditions, nitrosamines must be less than approximately 14 mM in the amine scrubber for nitrosamine gaseous emissions to be a non-issue.

7.4.2 Mass Balance for Nitrosamine Accumulation

- The mass balance for nitrosamine accumulation can be solved to give its transient behavior in the amine scrubber (Equations 7.12 & 7.13)

$$\frac{C_{NNO\ t} - C_{NNO\ i}}{C_{NNO\ SS} - C_{NNO\ i}} = 1 - e^{-\left(\tau_{str}k_{str} + 0.95x_{Recl} + x_{spill} + \frac{Gy_{amine}}{LC_{amine}}\right)\frac{t}{\tau_{Tot}}} \quad (7.12)$$

$$C_{NNO\ SS} = \frac{\delta \left[(1 - \alpha)(\beta + \gamma)y_{NO_2FL} \frac{G}{L} + \varepsilon k_{ox}\tau_{Tot} \right]}{\tau_{str}k_{str} + 0.95 * x_{Recl} + x_{spill} + \frac{G}{L} \frac{y_{amine}}{C_{amine}}} \quad (7.13)$$

- Substituting in values for a generic amine scrubber (Table 7.2) gives the steady-state nitrosamine concentration based on solvent-specific parameters (Equation 7.15).

$$C_{NNO\ SS} = \frac{\delta[(\beta + \gamma)1.5 * 10^{-5} M + 18 s * k_{ox}]}{300 s * k_{str} + 9.5 * 10^{-4} + 2 * 10^{-6}} \quad (7.15)$$

- When the stripper is operated at T_{max} , nitrosamines in MEA will accumulate to approximately 1–3 mM, nitrosamines in PZ will accumulate to 1 mM, and

nitrosamines in MDEA/PZ will accumulate to 21 mM; only MDEA/PZ could surpass gaseous emissions limits if no advanced nitrosamine emissions control is installed.

7.4.3 Prescrubbing with Triethanolamine and Sulfite

- NO₂ absorption into PZ will cost \$0.15–45/MT CO₂/ppm NO₂ due to amine degradation and the cost of reclaiming.
- NO₂ and SO₂ can be simultaneously removed in a NaOH prescrubber with the addition of triethanolamine or sulfite.
- NO₂ prescrubbing is cost-effective since it requires no additional equipment, the additives are relatively inexpensive, and the waste is non-hazardous.
- Scrubbing with TEA is most effective with low inlet SO₂; optimal savings for a 7 m tall column range from 1.10–0.57 \$/MT CO₂ when scrubbing 5 ppm NO₂ and 10–300 ppm SO₂.
- Including the cost of additional packing for NO₂ absorption, 90 % of NO₂ can be removed from an inlet gas of 50 ppm SO₂ and 5 ppm NO₂ without increasing the total cost of CO₂ capture.
- Sulfite scrubbing with thiosulfate inhibition is most effect with high inlet SO₂; scrubbing with sulfite instead of TEA becomes more economical when inlet SO₂ is greater than about 40 ppm.

Chapter 8: Conclusions and Recommendations

Section 8.1 gives the major conclusions from Chapters 3–6 for nitrosamine management in amine scrubbing, focusing on the results in PZ, MEA, and MDEA/PZ solvents. While MEA, PZ, and MDEA/PZ are highly competitive solvents for industrial carbon capture, there are many other competitive solvents that will also form nitrosamines. Different amine-based solvents will likely follow the same general method for nitrosamine accumulation, but they may have significantly different properties that affect their specific proclivity to accumulate nitrosamines. Section 8.2 outlines a method for estimating the steady-state nitrosamine concentration in a solvent with the results in Chapters 3–5 and a minimum number of screening experiments. Finally, Section 8.3 gives recommendations for future research on nitrosamine management in amine scrubbing.

8.1 CONCLUSIONS

8.1.1 Absorption of Nitrogen Oxides in Aqueous Amines

- NO_x absorption initiates through the free-radical absorption of NO_2 to form nitrite and an amine radical; less than 5 % of NO_x absorption can be attributed to hydrolysis.
- The overall liquid side mass transfer coefficient (k_g') for NO_2 at absorber conditions is approximately 3×10^{-7} , 10×10^{-7} , and $>40 \times 10^{-7}$ mol/m² s Pa for 9m MEA, 8m PZ and 7m MDEA/2m PZ, respectively.
- Total NO_2 absorbed will be approximately 75 %, 95 %, and >99% for 9m MEA, 8m PZ, and 7m MDEA/ 2m PZ respectively for an absorber designed for 90 % CO_2 capture.

- Tertiary amines absorb NO_2 the fastest; MDEA absorbs NO_2 30% faster than TEA at $\text{pH} > 10$, but TEA absorbs NO_2 approximately 40 % faster than MDEA at conditions relevant to NaOH prescrubbing ($\text{pH} = 7\text{--}8$).
- The amine radical from NO_2 absorption can react with NO to directly form nitrosamines at absorber conditions.
- In PZ solutions at absorber conditions, about 15 % of NO_x absorption will directly form MNPZ; the balance is almost all nitrite.
- 200 mM of Inhibitor A lowers the direct formation of MNPZ by 50 %, but has no effect on NO_2 absorption as nitrite.
- Most nitrosamine formation will occur at stripper conditions with nitrosation from nitrite.

8.1.2 High Temperature Nitrosation of Amines

- Nitrosation at high temperature occurs through nitrite attack on amine carbamic acid.
- Primary and secondary amine high temperature nitrosation is first order in nitrite and carbamate concentration and in H^+ activity.
- All primary amines screened nitrosated slower than the secondary amines, possibly due to steric hindrance effects on the nitroso-carbamic acid leaving group.
- PZ nitrosation kinetics fit an Arrhenius temperature dependence; the third-order rate constant is $8500 \text{ L mol}^{-1} \text{ s}^{-1}$ at 100°C with an activation energy of 84 kJ/mol.
- Nitrosamine yield in primary amine solvents is proportional to the concentration of secondary amine in solution, increasing with the accumulation of degradation products.

- With 70 mM HeGly in solution, approximately 7 % of nitrite will nitrosate to NHeGly.

8.1.3 Nitrosamine Control in the Stripper and Thermal Reclaimer

- Nitrosamines thermally decompose at stripper conditions in amine solutions; the pseudo-first order decomposition rate of MNPZ in 4.9 M PZ at $\alpha = 0.31$ and 150 °C is $2.7 \times 10^{-5} \text{ s}^{-1}$.
- Decomposition for MNPZ, NDELA, and NHeGly was modeled with an Arrhenius temperature dependence with an activation energy around 100 kJ/mol.
- Decomposition is half-order in total base concentration and is base-catalyzed with a Brønsted slope of approximately 0.5.
- MNPZ decomposition forms 2PZOH with an approximate yield of 0.5 moles 2PZOH per mole of MNPZ decomposed; the nitrogen on the nitroso-group decomposes into a gaseous product predicted to be N_2O .
- The hypothesized, base-catalyzed MNPZ decomposition mechanism goes through an E2 elimination, forming an imine and N_2O ; the imine equilibrates in aqueous solution with 2PZOH.
- Nitrosamine volatility in the thermal reclaimer is 30–70 times less than MEA or PZ.
- 95 % of MNPZ in a PZ solvent entering the thermal reclaimer will be removed assuming a reclaimer temperature of 150 °C, a reclaimer residence time of 10 minutes, and 1 M excess NaOH added to catalyze nitrosamine decomposition.

8.1.4 NO_2 -Catalyzed Sulfite Oxidation

- Sulfite oxidizes to sulfate via free-radical mechanisms initiated by NO_2 absorption.

- With 5 ppm NO₂ absorbing into 40 mM sulfite and no thiosulfate inhibition, approximately 1000 moles of sulfite will oxidize for each mole of NO₂ absorbed.
- 25 mM thiosulfate reduced sulfite oxidation by a factor of 30; oxidation rates are inverse-half-order with respect to thiosulfate concentration.
- With no metals in solution and 20 % O₂ in the sparge gas, the ratio of sulfite oxidized per mole of NO₂ absorbed (f) is given by Equation 8.1.

$$f = f_o \sqrt{\frac{5 * 10^{-6}}{(1 - e^{-N_{og}})y_{NO_2}}} * \frac{[SO_3^{2-}]}{\sqrt{[S_2O_3^{2-}] * \sqrt{1.0 M}}} * \exp\left[\frac{-E_a}{R}\left(\frac{1}{293 K} - \frac{1}{T}\right)\right] \quad (8.1)$$

$$\text{Where: } f_o = 233 \frac{\text{mol } SO_3^{2-} \text{ ox}}{\text{mol } NO_2 \text{ Abs}} \quad E_a = 24.1 \text{ kJ/mol}$$

- The presence of 0.1 mM Fe²⁺ increased oxidation rates by three-fold; Iron can be chelated out of solution with the addition of EDTA.
- For an inlet concentration of 100 ppm SO₂ and 2.5 ppm NO₂ with a NaOH scrubber operating at 55 °C, 0.050 M thiosulfate would be needed to keep sulfite at 0.010 M.

8.1.5 Modeling Nitrosamine Accumulation in the Amine Scrubber

- There are currently no limitations for nitrosamines in the amine scrubber itself, but the Norwegian Institute of Public Health has limited total nitrosamine emissions to 0.3 ng/m³ in air and 4 ng/L in water.
- For a 500 MWe point source, nitrosamine emissions would need to be less than 2.8 ppbv for nitrosamine gaseous emissions to be a non-issue.

- Assuming that nitrosamines are as volatile as their parent amines at process conditions, nitrosamines must be less than approximately 14 mM in the amine scrubber for nitrosamine gaseous emissions to be a non-issue.
- The mass balance for nitrosamine accumulation can be solved to give its transient behavior in the amine scrubber (Equations 8.2 & 8.3)

$$\frac{C_{NNO\ t} - C_{NNO\ i}}{C_{NNO\ SS} - C_{NNO\ i}} = 1 - e^{-\left(\tau_{str}k_{str} + 0.95 * x_{Recl} + x_{spill} + \frac{G y_{amine}}{L C_{amine}}\right) \frac{t}{\tau_{Tot}}} \quad (8.2)$$

$$C_{NNO\ SS} = \frac{\delta_{str} \left[(1 - \alpha_{pre})(\beta_{abs} + \gamma_{abs}) y_{NO_2 FL} \frac{G}{L} + \varepsilon k_{ox} \tau_{Tot} \right]}{\tau_{str}k_{str} + 0.95 * x_{Recl} + x_{spill} + \frac{G y_{amine}}{L C_{amine}}} \quad (8.3)$$

- When the stripper is operated at T_{max} , nitrosamines in MEA will accumulate to approximately 1–3 mM, nitrosamines in PZ will accumulate to 1 mM, and nitrosamines in MDEA/PZ will accumulate to 21 mM; only MDEA/PZ could surpass gaseous emissions limits if no advanced nitrosamine emissions control is installed.
- NO_2 absorption into PZ will cost \$0.15–45/MT CO_2 /ppm NO_2 due to PZ degradation and the cost of reclaiming.
- Scrubbing with TEA is most effective with low inlet SO_2 ; optimal savings for a 7 m tall column range from 1.10–0.57 \$/MT CO_2 when scrubbing 5 ppm NO_2 and 10–300 ppm SO_2 .
- Sulfite scrubbing with thiosulfate inhibition is most effective with high inlet SO_2 ; scrubbing with sulfite instead of TEA becomes more economical when inlet SO_2 is greater than about 40 ppm.

8.2 RECOMMENDATIONS FOR SCREENING NITROSAMINES IN AMINE-BASED SOLVENTS

Nitrosamines will accumulate in solvents containing amines based on the framework presented in Chapter 7. However, the rate of accumulation and the rate of decomposition is dependent on solvent specific properties, which could vary drastically. This section outlines an experimental screening process to estimate nitrosamine accumulation in a solvent before pilot plant testing and commercialization. The method starts by estimating the most conservative nitrosamine levels without any knowledge of the solvent and then outlines the experiments needed to refine those estimations if the estimated nitrosamines levels are unacceptable.

With some simplifying assumptions made in Section 7.2.2, the steady state nitrosamine concentration can be calculated from Equation 8.4; δ_{str} represents the yield of nitrosamine from nitrite, β_{abs} represents the fraction of NO_2 absorbed, γ_{abs} represents the fraction of amine radical reacting with NO , k_{ox} is the oxidation rate of the amine, and k_{str} is the thermal decomposition rate of the amine at stripper conditions. The range of parameter values are given in Table 8.1. Assuming the most conservative base value, the maximum nitrosamine concentration predicted is approximately 23 mM, which is over the threshold for possible gaseous emissions issues. The analysis assumes that thermal reclaiming will operate continuously at a rate of 0.1 % the solvent circulation rate. For non-volatile solvents, other reclaiming techniques must be used that will not necessarily remove nitrosamines.

$$C_{NNO\ SS} = \frac{\delta_{str}[(\beta_{abs} + \gamma_{abs})1.5 * 10^{-5} M + 18 s * k_{ox}]}{300 s * k_{str} + 9.5 * 10^{-4} + 2 * 10^{-6}} \quad (8.4)$$

Table 8.1: Range and base values for solvent-specific parameters in Equation 8.4

| Parameter | Range | Base Value |
|--|-------|------------|
| δ_{str} | 0–1 | 1 |
| β_{abs} | 0–1 | 1 |
| γ_{abs} | 0–0.2 | 0.2 |
| $k_{ox} * 10^7$ (M/s) | 1–6 | 6 |
| $k_{str} * 10^6$ (s ⁻¹) | 1–60 | 1 |

The thermal decomposition rate (k_{str}) has the largest effect on nitrosamine accumulation, varying over an order of magnitude. The rate of decomposition can be roughly estimated based on the stripper operating temperature and results for NDELA decomposition, the most thermally stable nitrosamine measured (Equation 8.5). The thermal cylinder experiment described in Section 5.2 can be implemented to get an exact thermal decomposition rate at operating conditions.

$$k_{str} = 5.0 * 10^{-6} s^{-1} * e^{\frac{100 \text{ kJ/mol}}{R} (\frac{1}{423K} - \frac{1}{T})} \quad (8.5)$$

The yield of nitrosamine from nitrite (δ_{str}) can also vary drastically depending on the choice of solvent and its major degradation products. Table 8.2 outlines recommendations for estimating high temperature nitrosamine yield in generic solvents. For primary amines, the estimates for nitrosamine yield become more conservative as the knowledge about the amine decreases. Therefore, the first category with complete knowledge should be used to safely and accurately estimate nitrosamine yield. The thermal

cylinder experiments described in Section 4.3 can be implemented to get the exact nitrosamine yield from nitrite at operating conditions.

Table 8.2: Method for estimating nitrosamine yield from nitrite in different amine blends based on available information

| Solvent | Nitrosamine Yield (δ_{str}) |
|--|--|
| Primary Amine and Primary/Tertiary Blend | |
| a. Reactivity and steady state concentration of secondary amine byproducts known* | $\frac{r_{2^\circ Am}[2^\circ Am]}{r_{2^\circ Am}[2^\circ Am] + [1^\circ Am]}$ |
| b. Steady state concentration of secondary amine byproducts known | $\frac{8 * [2^\circ Am]}{8 * [2^\circ Am] + [1^\circ Am]}$ |
| c. Steady state concentration of secondary amine byproducts unknown | 0.36 |
| Secondary Amine | 1 |
| Secondary/Tertiary Blend | 1 |

*Relative reactivity (r) as defined in Section 4.3

The uptake of NO₂ and NO ($\beta_{abs} + \gamma_{abs}$) by the amine can vary substantially as well. Given the range of absorber configurations and since the absorber could be over-designed, it is advisable to set β_{abs} equal to 1 and γ_{abs} equal to 0.2. The wetted wall column experiments described in Section 3.2 can be implemented to get an exact value for NO₂ uptake; NO uptake will be approximately 20 % of that value.

Finally, the overall oxidation rate of the solvent (k_{ox}) varies across amines and operating conditions. However, nitrite from amine oxidation is approximately equivalent to 0.2–1 ppm of inlet NO₂, so it will not dominate nitrosamine formation unless amine oxidation is very high or inlet NO₂ is very low. Furthermore, amine oxidation is important

to control in order to minimize solvent loss and ammonia emissions. Therefore, lower levels of amine oxidation may be realized in the near future with better oxidation inhibitors and corrosion control.

8.3 RECOMMENDATIONS FOR FUTURE RESEARCH

- Expand the work on NO_2 absorption kinetics to a wider variety of amines, amino acids, and imidazoles.
- Confirm that nitramine formation from NO_2 absorption at absorber conditions is minimal.
- Model the absorption of NO_2 and NO in the liquid boundary layer as mass transfer with fast reactions in series to predict yields of nitrosamine from NO reaction with the amine radical.
- Expand the research on nitrosation from nitrite and nitrosamine thermal decomposition to non-aqueous amine solvents.
- Confirm N_2O as the gaseous Nitrogen product from nitrosamine thermal decomposition.
- Measure MNPZ volatility at the vacuum thermally reclaiming conditions needed to reclaim MDEA/PZ blends.
- Measure nitrosamine volatility at absorber and water wash conditions.
- Examine the efficacy of UV photolytic decomposition for nitrosamine control in water wash solution.
- Examine the efficacy of NO_2 prescrubbing from a real flue gas using sulfite or tertiary amines.
- Measure NO_2 absorption rates in the presence of concentrated ($\approx 1.5 \text{ M}$) sulfate solution.

Appendix A: List of Abbreviations and Symbols

Table A.1 contains all of the uncommon abbreviations and symbols listed alphabetically. Greek symbols are placed at the end of the list.

Table A.1: List of uncommon abbreviations and symbols

| Abbreviation | Description | Unit |
|------------------------------------|--|---|
| $\frac{a_{e \text{ scrubber}}}{G}$ | Wetted area per gas flow rate in the CO ₂ scrubber | m ² s Pa/mol |
| A_{HGF} | Gas-liquid interfacial area of the high gas flow apparatus | m ² |
| $C_{NNO \ t}$ | Concentration of nitrosamine in the scrubber at time=t | M |
| $C_{NNO \ i}$ | Initial concentration of nitrosamine in the scrubber | M |
| $C_{NNO \ SS}$ | Steady state concentration of nitrosamine in the scrubber | M |
| d | Distance of the plume from the point source | M |
| f | Amount of SO ₃ ²⁻ oxidized per mol of NO ₂ absorbed | mol SO ₃ ²⁻ / mol NO ₂ |
| G_{HGF} | Molar gas flow rate through the high gas flow apparatus | mol/s |
| G_{WWC} | Molar flow rate of gas in the wetted wall column | mol/s |

| | | |
|-------------------|--|---------------------------------|
| h_{add} | Additional height above 3 m the SO ₂ prescrubber needed to simultaneously scrub NO ₂ | m |
| H_{Amine} | Volatility of amine from the water wash | M ⁻¹ |
| $H_{Nitrosamine}$ | Volatility of nitrosamine from the water wash | M ⁻¹ |
| k_2 | Second order rate constant | s ⁻¹ M ⁻¹ |
| k_3 | Third order rate constant | s ⁻¹ M ⁻² |
| k_g' | Overall liquid side mass transfer coefficient expressed with NO ₂ partial pressure unit | mol/m ² s Pa |
| K_g | Overall mass transfer coefficient | mol/m ² s Pa |
| $k_{H\ NNO}$ | Henry's coefficient for nitrosamine volatility | - |
| k_{obs} | Observed pseudo-first order rate constant | s ⁻¹ |
| k_{ox} | Zeroth order rate constant for amine oxidation in the scrubber | M/s |
| k_{Recl} | Thermal decomposition rate of nitrosamine in the thermal reclaimer | s ⁻¹ |
| k_{Str} | Thermal decomposition rate of nitrosamine in the stripper | s ⁻¹ |
| L_{slip} | Volumetric flow rate of the slipstream fed to the thermal reclaimer | L/s |
| L_{purge} | Volumetric flow rate of the purge stream from the thermal reclaimer | L/s |

| | | |
|-------------------|--|-----------------------------------|
| L_{return} | Volumetric flow rate of the slipstream returned to the scrubber from the thermal reclaimer | L/s |
| NNO_{scr} | Steady state nitrosamine concentration in the amine scrubber | mmol/kg |
| N_{NO_2} | Molar flux of NO ₂ in the wetted wall column or the high gas flow apparatus | mol/m ² /s |
| $P_{NO_2 LM}$ | Log mean partial pressure of NO ₂ in the wetted wall column | Pa |
| $Q_{Nitrosamine}$ | Absolute mass emission rate of nitrosamine from the flue source | g/s |
| r | Relative reactivity of nitrite with a secondary amine compared to a primary amine | - |
| t_{disp} | Dispersion time of the plume from the point source | min |
| \bar{u}_x | Wind velocity in the plume direction | m/s |
| V_{recl} | Volume of the reclaimer | L |
| x_{Recl} | Fraction of solvent sent to thermal reclaimer | - |
| x_{Spill} | Fraction of solvent lost to spills | - |
| y_{NNO} | Mole fraction of nitrosamine in the exit flue gas | - |
| $y_{NO_2 FL}$ | Inlet NO ₂ mole fraction to the amine scrubber | mol NO ₂ /mol flue gas |

| | | |
|-----------------------|---|-------------------------------------|
| α | Total CO ₂ loading in amine solutions | mol CO ₂ /mol alkalinity |
| α_{pre} | Fraction of NO ₂ absorbed in the prescrubber | - |
| β_{abs} | Fraction of NO ₂ absorbed in the absorber | - |
| γ_{abs} | Amount of NO absorbed in the absorber | - |
| δ_{str} | Nitrosamine yield from nitrite in the stripper | - |
| ε | Fraction of total amine oxidation that forms nitrite | - |
| ζ | Ratio of nitrite formation to formate formation in H ₂ O ₂ addition experiments | - |
| φ_y/φ_z | Plume dispersion coefficients in the y/z direction | m ⁻¹ |
| τ_{Recl} | Residence time in the thermal reclaimer based on the volumetric flow rate of the feed | s |
| τ_{str} | Residence time of the stripper based on the volumetric flow rate of the solvent | s |
| τ_{Tot} | Residence time of the amine scrubber based on the volumetric flow rate of the solvent | s |

Appendix B: Nitrite Formation from Amine Oxidation

The main mechanism for nitrosamine formation is the absorption of NO_2 as nitrite followed by high temperature, carbamate-catalyzed nitrosation. However, even with low or no inlet NO_2 , nitrosamines may still form in amine solutions. Nitrosamines have been found in the pilot plant at the Separations Research Program (SRP), which runs synthetic flue gas consisting of only air and CO_2 . Maximum MNPZ levels at SRP were measured at 0.09 mmol/kg, approximately 10–20 times less than MNPZ levels measured at Pilot Plant 2 (PP2), a pilot plant operating with a real flue gas (P. T. Nielsen, Li, and Rochelle 2013). MNPZ was also quantified in PZ solvents run on the bench scale “Integrated Solvent Degradation Apparatus” (ISDA), which operates with a synthetic flue gas (Voice 2013). MNPZ accumulated linearly at a rate of 3.5 $\mu\text{mol/kg/hr}$ over a five day experiment when the ISDA operated between 55 °C and 120 °C; experimental time was not long enough to measure nitrosamine thermal degradation.

While nitrosamines have been measured during high temperature cycling experiments without inlet NO_2 , they have not been measured in low temperature oxidation experiments. Freeman did find nitrite and nitrate as minor products from amine oxidation, accounting for approximately 0.1 % of PZ loss (Freeman 2011). However, since nitrite is not an important oxidation product from a nitrogen loss perspective, it has been ignored by most experimentalists. The proposed mechanism for nitrosamine formation in the absence of inlet NO_x is the initial oxidation of amine to nitrite. The nitrite then cycles to the stripper where it nitrosates any primary or secondary amine. The accumulation rate of nitrosamines from oxidation depends on the oxidation rate and the yield of nitrite. Section B.1 gives a

summary of nitrite yields in MEA and PZ solvents. Section B.2 shows screening results for nitrite yield in a range of other amines using the formate to nitrite ratio.

B.1 NITRITE YIELD IN PZ AND MEA SOLUTIONS

Table B.1 show nitrite yield from MEA oxidation measured by Sexton (2008) (Equation B.1). Nitrite yield was highest in the low gas flow (LGF) experiments with high oxygen content (Sexton 2008). The high gas flow (HGF) experiments run closer to oxygen partial pressures found in a flue gas and are likely to be more indicative of nitrite yields with a real flue gas.

$$\varepsilon_{Nitrite} = \frac{k_{nitrite}}{k_{ox}} = \frac{[Nitrite]_t}{[MEA]_i - [MEA]_t} \quad (B.1)$$

Table B.1: Nitrite yield form MEA oxidation at 55 °C in the LGF and HGF apparatuses (Sexton 2008)

| Gas Conditions | Additives | Nitrite Yield (%) |
|--|--------------------|-------------------|
| 98% O ₂ , 2% CO ₂ in LGF | 1 mM Fe | 5.5 |
| 94% O ₂ , 6% CO ₂ in LGF | 1 mM Fe | 5.0 |
| 98% O ₂ , 2% CO ₂ in LGF | 0.1 mM Fe, 5 mM Cu | 2.8 |
| 21% O ₂ , 2% CO ₂ in HGF | 1 mM Fe | 0.6 |
| 21% O ₂ , 2% CO ₂ in HGF | 0.1 mM Fe, 5 mM Cu | 0.6 |

Freeman measured nitrite formation in only one LGF oxidation experiment for PZ decomposition. Nitrite accounted for only 0.1 % of total nitrogen loss in PZ; nitrite concentrations were close to the detection limit (Figure B.1).

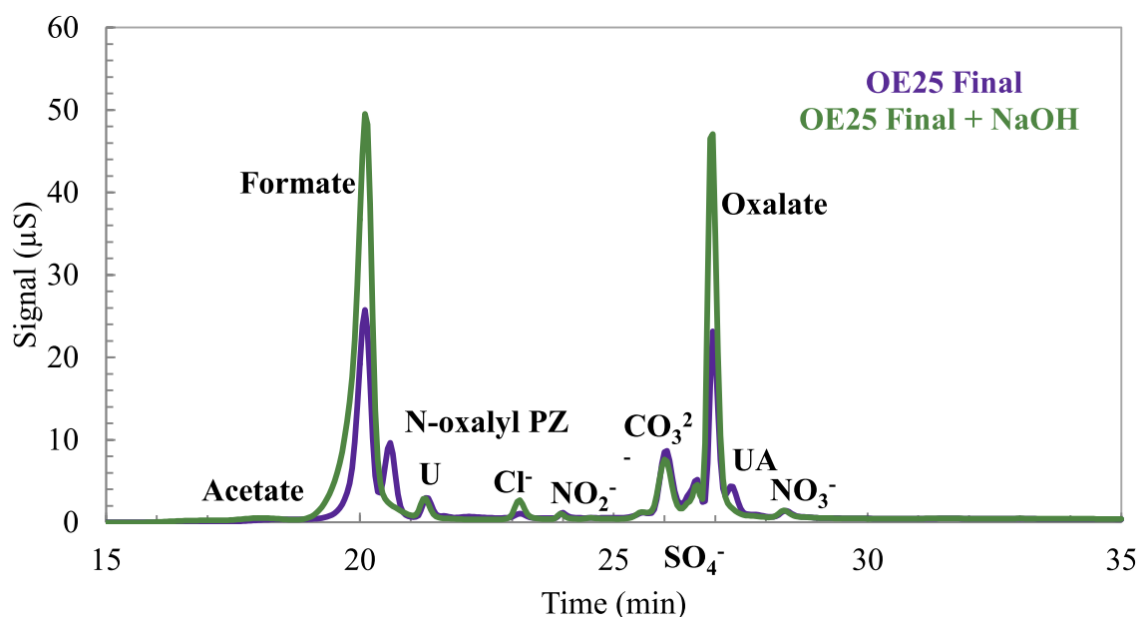


Figure B.1: Comparison of anion IC chromatograms for the final sample of OE25 before and after NaOH treatment; abbreviations: U, unidentified; UA, unidentified amide (8 m PZ, 70 °C, 1400 rpm, 100 mL/min, 94% O₂, 4 mM Cu²⁺, 14 days) (Freeman 2011)

Voice measured nitrite and nitrosamine formation in high temperature cycling apparatuses for both MEA and PZ solvent. Nitrite accumulated to a steady-state of 2 mmol/kg after approximately half a day of MEA oxidation. The initial nitrite formation rate was 0.13 mmol/kg/hr (Figure B.2) while the MEA oxidation rate was 5.3 mmol/kg/hr. Nitrite yield was therefore approximately 2.5 % of the total oxidation rate, in line with results from Sexton. Inh. A did not inhibit MEA oxidation, but stopped nitrate and nitrite from forming. Since Inh. A is a free-radical scavenger, it is likely that nitrite/nitrate formation must form through a free-radical mechanism that cannot occur with Inh. A in solution. In cases where nitrite from oxidation is the dominant mechanism for nitrosamine formation, free-radical scavengers could be an effective solution for limiting nitrosamines.

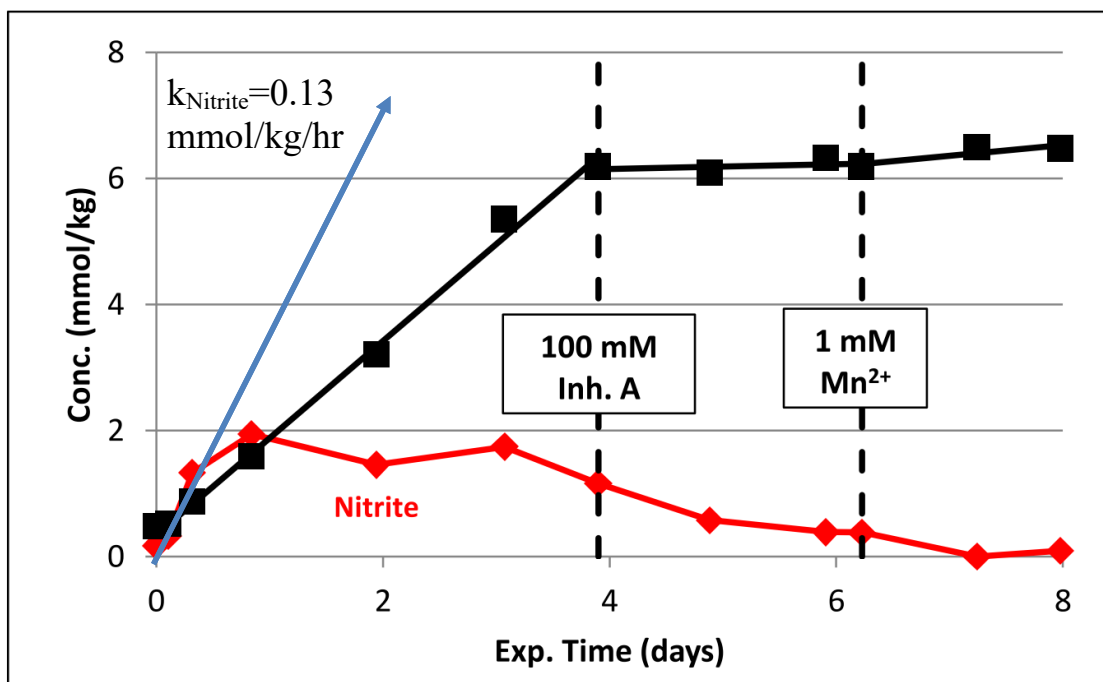


Figure B.2: Nitrate and nitrite production during oxidation of 7 m MEA in the ISDA with 2% CO_2 in oxygen cycling from 55 to 120 °C at 0.2 L/min. Initial metals added (mM): 0.4 Fe^{2+} , 0.1 Mn^{2+} , 0.1 Ni^{2+} , 0.04 Cr^{3+} (Voice, 2013)

Nitrite did not accumulate in PZ solution most likely due to the relatively fast nitrosation of PZ to MNPZ. MNPZ accumulated in PZ at a rate of 3.5 $\mu\text{mol/kg/hr}$ in the ISDA over a period of 5 days (Figure B.3). At the same time PZ degraded at a rate of 2.1 mmol/kg/hr, corresponding to a nitrite yield of approximately 0.2 % the total oxidation rate.

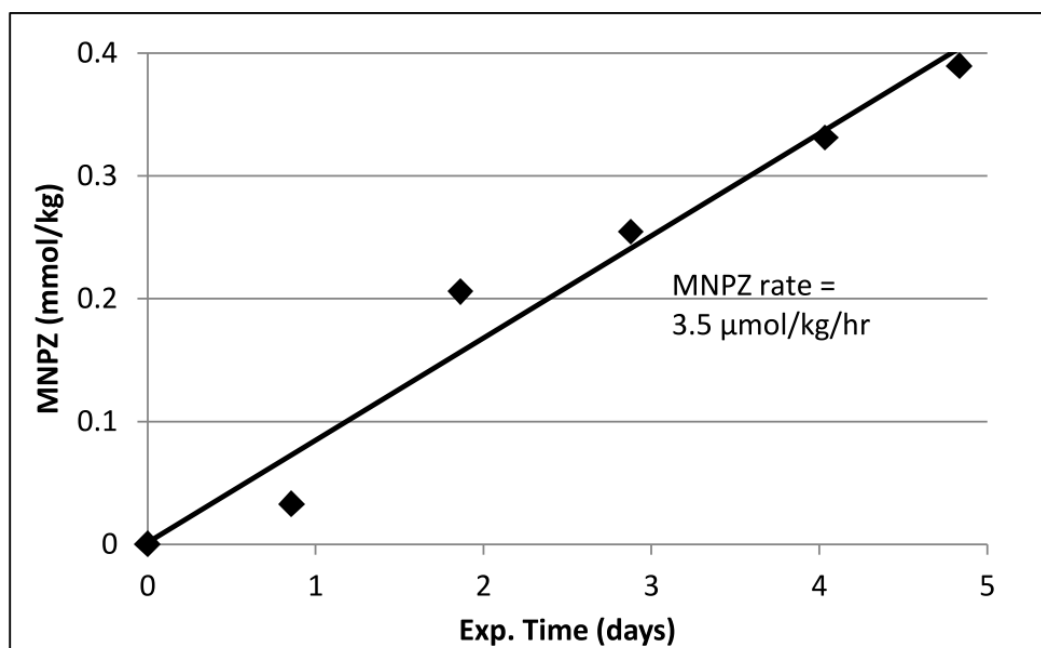


Figure B.3: Formation of MNPZ from endogenous nitrite during oxidation of 8 m PZ in the ISDA cycling from 55 to 120 °C at 0.2 L/min (Voice 2013)

B.2 NITRITE YIELD SCREENING USING LGF AND PEROXIDE ADDITION

The yield of nitrite from oxidation of hexamethylenediamine (HMDA), tetramethylenediamine (TMDA), and bisaminoethylether (BAE) was measured using the LGF apparatus (Liu, Namjoshi, and Rochelle 2014). As the amines oxidized, they formed formate and nitrite at a constant ratio (Figure B.4). Nitrite yields were 0.7 %, 0.9 %, and 1.3 % for HMDA, BAE, and TMDA respectively.

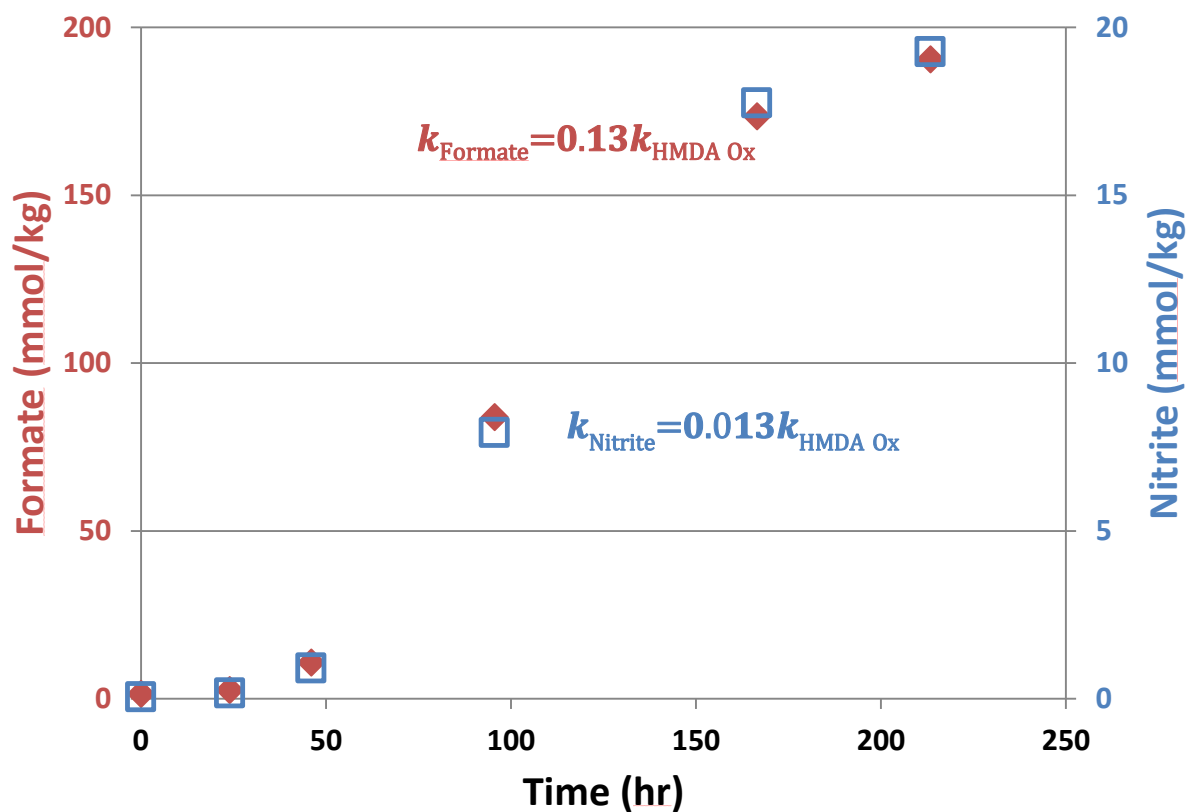


Figure B.4: Nitrite and formate formation from HMDA oxidation; LGF apparatus with 98 % O₂ and 2 % CO₂; Metals added (mM): 0.4 Fe²⁺, 0.1 Mn²⁺, 0.1 Ni²⁺, 0.04 Cr³⁺

Finally, a series of amines were screened for nitrite formation rate by adding hydrogen peroxide (H₂O₂) to CO₂-loaded amine solutions (10 m alkalinity, $\alpha = 0.2$) and measuring the resulting nitrite and formate (Section 2.2.4). Since H₂O₂ is a strong oxidizing agent, the reaction finished within 5 minutes, cutting down the week-long experimental time needed for accumulating nitrite in the LGF. Instead of analyzing individual amine loss for each experiment, formate formation was used as a surrogate. Since formate usually accounts for 10–20 % of the total oxidation rate (Voice, Closmann, and Rochelle 2013),

the ratio of nitrite to formate (ζ) should be 5–10 times higher than nitrite yield from amine oxidation (Equation B.2).

$$\zeta = \frac{[Nitrite]}{[Formate]} \approx 5 - 10 * \varepsilon_{Nitrite} \quad (B.2)$$

The value for ζ was 0.09, in MEA oxidation with H₂O₂ addition, translating to a nitrite yield from overall oxidation of approximately 1–2 %. Thus nitrite yield in MEA using H₂O₂ as the oxidant matched oxidation results from the HGF and ISDA experiments. The ζ in PZ was 0.07, which is over 3 times greater than the nitrite to formate ratio measured using the LGF and ISDA. Nitrite accumulated to 11 %, 21 %, and 29 % of formate in HMDA, BAE, and TMDA respectively. While these ratios were 2–3 times greater than those measured in the LGF, the ζ value followed the same trend in both experiments (HMDA < BAE < TMDA) (Figure B.5).

Nitrite formed in all amines tested; ζ equaled 0.001–0.42 with the notable exception of MAE. During MAE oxidation, nitrite accumulated to a concentration 3.3 times higher than formate, showing that solvents containing MAE might be pre-disposed to form nitrite from oxidation. However, since the H₂O₂ screening was done at conditions far different than normal oxidation, nitrite formation with MAE oxidation would need to be re-evaluated in the ISDA, LGF, or another oxidation apparatus closer to standard operating conditions.

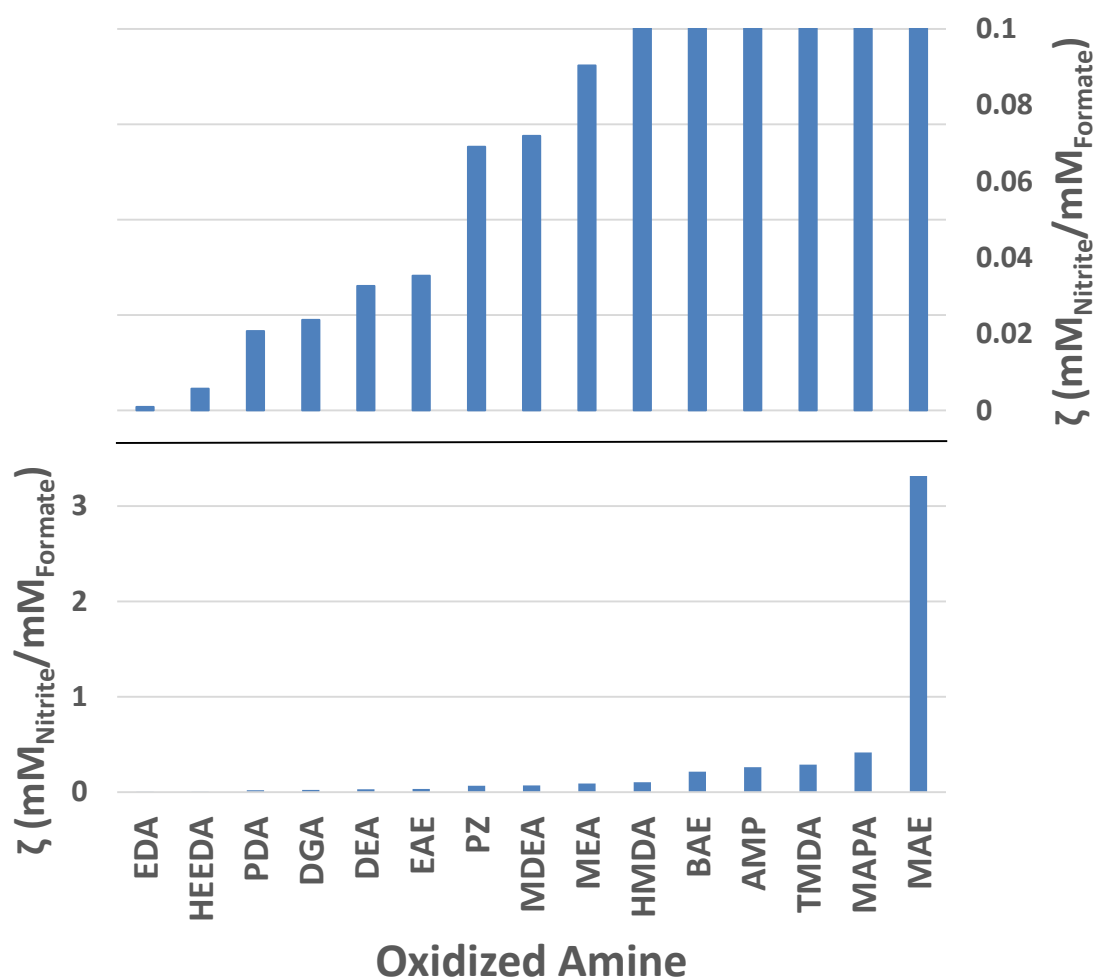


Figure B.5: The ratio of nitrite to formate (ζ) from amine oxidation with H_2O_2 addition; 10 m alkalinity amine, 0.2 CO_2 loading, 0.2 mM Mn^{2+} , 1 M 30 wt % H_2O_2 added. Full y-axis on bottom, close-up on top. Abbreviations in Table B.2

Table B.2: Amine name abbreviations for Figure B.5

| Amine Name | Common Name |
|------------------------|-------------|
| Trimethylenediamine | PDA |
| 2-(Ethylamino)ethanol | EAE |
| 2-(Methylamino)ethanol | MAE |

| | |
|-------------------------------------|-------|
| bisaminoethylether | BAE |
| 3-Amino-1-Propanol | AMP |
| Hydroxyethyl-ethylenediamine | HEEDA |
| Ethanolamine | MEA |
| Piperazine | PZ |
| Diethanolamine | DEA |
| Diglycolamine | DGA |
| Ethylenediamine | EDA |
| Hexamethylenediamine | HMDA |
| N-Methyldiethanolamine | MDEA |
| N-Methyl-1,3-propranediamine | MAPA |
| Tetramethylenediamine | TMDA |

With the exception of MAE, 0–8 % of the oxidized amine can be expected to form nitrite. All amines except MAPA and MAE formed less nitrite than TMDA, which had a nitrite yield of 1.3 % in the LGF. The base value for nitrite yield from oxidation can thus be set at 1 % for an arbitrary amine, but could vary an order of magnitude in either direction. Nitrosamine formation through amine oxidation can always be controlled by lowering the overall oxidation rate of the amine.

Appendix C: Experimental Raw Data

Table C.1: Raw data for Table 3.2

| Exp 3.1 | | Exp 3.2 | | Exp 3.3 | | Exp 3.4 | |
|------------------------------------|--|------------------------------------|--|------------------------------------|--|------------------------------------|--|
| $P_{\text{NO}_2 \text{ LM}}$ Pa | $N_{\text{NO}_2} * 10^7$ mol/s/m ² | $P_{\text{NO}_2 \text{ LM}}$ Pa | $N_{\text{NO}_2} * 10^7$ mol/s/m ² | $P_{\text{NO}_2 \text{ LM}}$ Pa | $N_{\text{NO}_2} * 10^7$ mol/s/m ² | $P_{\text{NO}_2 \text{ LM}}$ Pa | $N_{\text{NO}_2} * 10^7$ mol/s/m ² |
| 18.8 | 26.9 | 31.4 | 61.7 | 23.9 | 39.7 | 3.5 | 7.0 |
| 14.8 | 20.2 | 25.6 | 45.5 | 20.7 | 35.4 | 10.0 | 18.6 |
| 6.9 | 6.2 | 16.6 | 24.0 | 16.3 | 29.1 | 14.8 | 27.2 |
| 1.7 | 3.2 | 8.1 | 13.6 | 9.9 | 18.2 | 20.9 | 38.2 |
| 20.8 | 31.2 | 3.6 | 5.0 | 3.5 | 10.1 | 25.1 | 44.5 |
| 0.8 | 1.5 | | | 40.0 | 76.9 | | |
| | | | | | | | |
| Exp 3.5 | | Exp 3.6 | | Exp 3.7 | | Exp 3.8 | |
| $P_{\text{NO}_2 \text{ LM}}$ Pa | $N_{\text{NO}_2} * 10^7$ mol/s/m ² | $P_{\text{NO}_2 \text{ LM}}$ Pa | $N_{\text{NO}_2} * 10^7$ mol/s/m ² | $P_{\text{NO}_2 \text{ LM}}$ Pa | $N_{\text{NO}_2} * 10^7$ mol/s/m ² | $P_{\text{NO}_2 \text{ LM}}$ Pa | $N_{\text{NO}_2} * 10^7$ mol/s/m ² |
| 3.4 | 9.3 | 19.9 | 38.0 | 4.5 | 8.8 | 47.5 | 332.1 |
| 1.9 | 4.8 | 17.4 | 35.9 | 8.6 | 16.4 | 33.9 | 220.1 |
| 9.3 | 21.9 | 13.9 | 23.8 | 13.0 | 23.4 | 23.4 | 150.6 |
| 19.3 | 43.9 | 10.3 | 18.5 | 17.1 | 30.5 | 75.4 | 502.0 |
| 23.9 | 54.2 | 4.6 | 9.0 | 20.0 | 43.5 | 109.4 | 710.5 |
| 14.3 | 33.2 | 9.2 | 15.0 | | | | |

| | | | | | | | |
|--------------------------------------|--|--------------------------------------|--|--------------------------------------|--|--------------------------------------|--|
| | | | | | | | |
| Exp 3.9 | | Exp 3.10 | | Exp 3.11 | | Exp 3.12 | |
| $P_{\text{NO}_2 \text{ LM}}$ Pa | $N_{\text{NO}_2} * 10^7$ mol/s/m ² | $P_{\text{NO}_2 \text{ LM}}$ Pa | $N_{\text{NO}_2} * 10^7$ mol/s/m ² | $P_{\text{NO}_2 \text{ LM}}$ Pa | $N_{\text{NO}_2} * 10^7$ mol/s/m ² | $P_{\text{NO}_2 \text{ LM}}$ Pa | $N_{\text{NO}_2} * 10^7$ mol/s/m ² |
| 45.3 | 212.4 | 47.1 | 289.6 | 77.7 | 397.5 | 4.2 | 63.1 |
| 70.1 | 308.9 | 51.3 | 305.1 | 60.3 | 280.0 | 3.6 | 52.9 |
| 94.3 | 440.2 | 25.3 | 139.0 | 46.0 | 218.4 | 2.1 | 32.6 |
| 119.9 | 552.2 | 73.5 | 405.5 | 31.7 | 145.6 | 1.5 | 21.4 |
| 24.5 | 115.8 | 101.1 | 559.9 | 17.3 | 89.6 | | |
| | | 118.8 | 629.4 | | | | |
| | | | | | | | |
| Exp 3.13 | | Exp 3.14 | | Exp 3.15 | | Exp 3.16 | |
| $P_{\text{NO}_2 \text{ LM}}$ (Pa) | $N_{\text{NO}_2} * 10^7$ mol/s/m ² | $P_{\text{NO}_2 \text{ LM}}$ (Pa) | $N_{\text{NO}_2} * 10^7$ mol/s/m ² | $P_{\text{NO}_2 \text{ LM}}$ (Pa) | $N_{\text{NO}_2} * 10^7$ mol/s/m ² | $P_{\text{NO}_2 \text{ LM}}$ (Pa) | $N_{\text{NO}_2} * 10^7$ mol/s/m ² |
| 4.2 | 65.5 | 8.0 | 66.4 | 7.6 | 93.4 | 9.0 | 52.2 |
| 3.8 | 60.1 | 3.7 | 25.8 | 6.1 | 70.4 | 7.1 | 41.8 |
| 2.2 | 34.2 | 2.2 | 17.5 | 4.6 | 59.5 | 4.9 | 28.2 |
| 1.4 | 23.8 | 1.1 | 7.4 | 3.3 | 34.2 | 2.3 | 13.9 |
| | | | | 1.6 | 21.6 | | |
| | | | | | | | |
| Exp 3.17 | | | | | | | |
| $P_{\text{NO}_2 \text{ LM}}$ Pa | $N_{\text{NO}_2} * 10^7$ mol/s/m ² | | | | | | |

| | | | | | | | |
|-----|------|--|--|--|--|--|--|
| 8.6 | 61.3 | | | | | | |
| 7.8 | 55.5 | | | | | | |
| 4.9 | 31.5 | | | | | | |
| 2.2 | 14.7 | | | | | | |
| 6.7 | 49.6 | | | | | | |

Table C.2: Raw data for Table 4.1

| Exp 4.1 | | | Exp 4.2 | | | Exp 4.3 | | |
|-----------|-----------------|--------------|-----------|-----------------|--------------|-----------|-----------------|--------------|
| Time days | Nitrite mmol/kg | MNPZ mmol/kg | Time days | Nitrite mmol/kg | MNPZ mmol/kg | Time days | Nitrite mmol/kg | MNPZ mmol/kg |
| 0.00 | 0.78 | 0.00 | 0.00 | 0.78 | 0.00 | 0.00 | 0.64 | 0.00 |
| 0.05 | 0.36 | 0.46 | 0.06 | 0.52 | 0.31 | 0.05 | 0.54 | 0.13 |
| 0.07 | 0.34 | 0.52 | 0.12 | 0.37 | 0.49 | 0.12 | 0.37 | 0.30 |
| 0.09 | 0.25 | 0.60 | 0.17 | 0.25 | 0.59 | 0.19 | 0.29 | 0.41 |
| 0.11 | 0.19 | 0.67 | 0.21 | 0.21 | 0.65 | 0.24 | 0.08 | 0.39 |
| 0.14 | 0.15 | 0.71 | 0.25 | 0.16 | 0.66 | | | |
| | | | | | | | | |
| Exp 4.4 | | | Exp 4.5 | | | Exp 4.6 | | |
| Time days | Nitrite mmol/kg | MNPZ mmol/kg | Time days | Nitrite mmol/kg | MNPZ mmol/kg | Time days | Nitrite mmol/kg | MNPZ mmol/kg |
| 0.00 | 0.74 | 0.02 | 0.00 | 52.09 | 0.00 | 0.00 | 74.90 | 0.07 |
| 0.06 | 0.66 | 0.13 | 0.01 | 49.35 | 0.00 | 0.05 | 60.27 | 1.16 |
| 0.13 | 0.54 | 0.25 | 0.01 | 48.88 | 0.00 | 0.13 | 48.66 | 9.69 |

| | | | | | | | | |
|----------------|--------------------|-----------------|----------------|--------------------|-----------------|----------------|--------------------|-----------------|
| 0.20 | 0.45 | 0.37 | 0.03 | 49.87 | 0.16 | 0.24 | 37.44 | 17.51 |
| 0.00 | 0.76 | 0.00 | 0.06 | 46.88 | 0.93 | 0.33 | 30.83 | 21.47 |
| 0.20 | 0.48 | 0.35 | 0.10 | 46.65 | 1.98 | 0.65 | 13.63 | 27.36 |
| 0.25 | 0.39 | 0.37 | 0.18 | 44.24 | 2.47 | 0.89 | 6.30 | 36.41 |
| 0.28 | 0.37 | 0.44 | 0.26 | 42.48 | 6.09 | 1.18 | 2.44 | 38.11 |
| | | | 0.59 | 35.70 | 12.39 | | | |
| | | | 0.85 | 27.49 | 17.99 | | | |
| | | | 2.02 | 14.91 | 29.43 | | | |
| | | | 2.94 | 10.50 | 32.30 | | | |
| | | | 4.22 | 3.30 | 28.51 | | | |
| | | | | | | | | |
| Exp 4.7 | | | Exp 4.8 | | | Exp 4.9 | | |
| Time days | Nitrite mmol/kg | MNPZ mmol/kg | Time days | Nitrite mmol/kg | MNPZ mmol/kg | Time days | Nitrite mmol/kg | MNPZ mmol/kg |
| 0.00 | 52.88 | 0.00 | 0.00 | 48.19 | 0.71 | 0.00 | 220.98 | 0.00 |
| 0.03 | 45.14 | 5.29 | 0.03 | 34.26 | 11.64 | 0.04 | 178.79 | 0.45 |
| 0.09 | 24.54 | 23.14 | 0.05 | 6.56 | 39.61 | 0.15 | 143.62 | 53.55 |
| 0.18 | 7.69 | 40.84 | 0.07 | 1.79 | 44.44 | 0.25 | 26.31 | 346.28 |
| 0.37 | 1.66 | 40.47 | 0.09 | 0.64 | 45.54 | 0.35 | 10.02 | 178.39 |
| 0.65 | 0.10 | 41.33 | 0.13 | 0.09 | 46.38 | 0.61 | 0.00 | 188.56 |
| | | | 0.17 | 0.01 | 46.42 | | | |
| | | | | | | | | |

| Exp 4.10 | | | Exp 4.11 | | | Exp 4.12 | | |
|-----------|-----------------|--------------|-----------|-----------------|--------------|-----------|-----------------|--------------|
| Time days | Nitrite mmol/kg | MNPZ mmol/kg | Time days | Nitrite mmol/kg | MNPZ mmol/kg | Time days | Nitrite mmol/kg | MNPZ mmol/kg |
| 0.00 | 41.03 | 0.11 | 0.00 | 16.14 | 0.06 | 0.00 | 33.05 | 0.00 |
| 0.06 | 25.79 | 14.99 | 0.06 | 11.79 | 4.67 | 0.18 | 32.13 | 1.14 |
| 0.08 | 20.99 | 20.81 | 0.17 | 5.71 | 10.58 | 0.91 | 27.17 | 5.55 |
| 0.11 | 13.46 | 28.13 | 0.27 | 3.76 | 12.79 | 1.24 | 24.50 | 7.76 |
| 0.14 | 8.65 | 32.05 | 0.35 | 1.93 | 14.12 | 1.86 | 20.17 | 10.38 |
| 0.17 | 6.32 | 35.00 | 0.64 | 0.34 | 15.39 | 2.20 | 18.79 | 11.68 |
| | | | | | | | | |
| Exp 4.13 | | | Exp 4.14 | | | | | |
| Time days | Nitrite mmol/kg | MNPZ mmol/kg | Time days | Nitrite mmol/kg | MNPZ mmol/kg | | | |
| 0.00 | 54.18 | 0.00 | 0.00 | 48.99 | 0.00 | | | |
| 0.18 | 43.74 | 8.63 | 4.79 | 41.11 | 8.15 | | | |
| 0.37 | 35.22 | 15.83 | 8.79 | 33.66 | 13.01 | | | |
| 0.67 | 24.81 | 23.89 | 14.00 | 29.06 | 19.60 | | | |
| 1.04 | 16.46 | 31.48 | 18.75 | 24.30 | 24.28 | | | |
| 1.31 | 12.43 | 33.08 | 22.88 | 21.22 | 27.99 | | | |
| 1.66 | 7.36 | 37.07 | | | | | | |
| 2.04 | 5.76 | 38.91 | | | | | | |
| 2.70 | 2.29 | 41.35 | | | | | | |

Table C.3: Raw data for Table 4.2

| Exp 4.15 | | Exp 4.16 | | Exp 4.17 | | Exp 4.18 | | Exp 4.19 | |
|-----------|-----------------|-----------|-----------------|-----------|-----------------|-----------|-----------------|-----------|-----------------|
| Time days | Nitrite mmol/kg | Time days | Nitrite mmol/kg | Time days | Nitrite mmol/kg | Time days | Nitrite mmol/kg | Time days | Nitrite mmol/kg |
| 0.05 | 31.52 | 0.05 | 36.90 | 0.06 | 20.98 | 0.06 | 38.88 | 0.05 | 13.34 |
| 0.12 | 19.78 | 0.26 | 30.63 | 0.32 | 10.77 | 0.32 | 29.22 | 0.09 | 5.71 |
| 0.19 | 13.41 | 0.75 | 19.84 | 0.67 | 4.02 | 0.81 | 18.97 | 0.14 | 1.56 |
| 0.24 | 11.51 | 1.04 | 15.71 | 1.06 | 1.09 | 1.66 | 8.50 | 0.19 | 0.64 |
| 0.24 | 8.34 | 1.29 | 13.09 | 1.66 | 0.17 | 2.01 | 5.58 | 0.24 | 0.35 |
| | | | | | | | | | |
| Exp 4.20 | | Exp 4.21 | | Exp 4.22 | | Exp 4.23 | | Exp 4.24 | |
| Time days | Nitrite mmol/kg | Time days | Nitrite mmol/kg | Time days | Nitrite mmol/kg | Time days | Nitrite mmol/kg | Time days | Nitrite mmol/kg |
| 0.04 | 21.19 | 0.06 | 20.98 | 0.06 | 38.88 | 0.04 | 18.78 | 0.05 | 12.97 |
| 0.15 | 13.66 | 0.32 | 10.77 | 0.32 | 29.22 | 0.07 | 13.00 | 0.07 | 4.06 |
| 0.21 | 10.66 | 0.67 | 4.02 | 0.81 | 18.97 | 0.12 | 9.08 | 0.11 | 0.80 |
| 0.28 | 8.30 | 1.06 | 1.09 | 1.66 | 8.50 | 0.19 | 5.06 | 0.15 | 0.11 |
| 0.67 | 1.87 | 1.66 | 0.17 | 2.01 | 5.58 | 0.28 | 2.37 | 0.18 | 0.01 |
| | | | | | | | | | |
| Exp 4.25 | | Exp 4.26 | | Exp 4.27 | | Exp 4.28 | | Exp 4.29 | |

| Time days | Nitrite mmol/kg | Time days | Nitrite mmol/kg | Time days | Nitrite mmol/kg | Time days | Nitrite mmol/kg | Time days | Nitrite mmol/kg |
|-----------------|-----------------|-----------------|-----------------|-----------------|-----------------|-----------------|-----------------|-----------------|-----------------|
| 0.04 | 42.05 | 0.08 | 33.95 | 0.16 | 44.65 | 0.04 | 21.06 | 0.04 | 30.42 |
| 0.16 | 11.08 | 0.17 | 20.47 | 1.00 | 19.99 | 0.15 | 2.85 | 0.16 | 20.90 |
| 0.20 | 14.03 | 0.36 | 5.92 | 1.89 | 9.06 | 0.23 | 0.61 | 0.31 | 12.78 |
| 0.31 | 5.96 | 0.75 | 0.38 | 2.81 | 3.63 | 0.31 | 0.12 | 0.59 | 5.69 |
| 0.34 | 1.10 | | | | | 0.34 | 0.09 | 0.90 | 2.21 |
| | | | | | | | | | |
| Exp 4.32 | | Exp 4.33 | | Exp 4.34 | | Exp 4.35 | | Exp 4.34 | |
| Time days | Nitrite mmol/kg | Time days | Nitrite mmol/kg | Time days | Nitrite mmol/kg | Time days | Nitrite mmol/kg | Time days | Nitrite mmol/kg |
| 0.05 | 31.02 | 0.05 | 27.75 | 0.08 | 5.08 | 0.05 | 50.27 | 0.11 | 30.45 |
| 0.95 | 0.77 | 2.00 | 8.81 | 0.15 | 0.90 | 0.32 | 40.16 | 1.21 | 24.06 |
| 1.86 | 0.02 | 2.79 | 4.69 | 0.20 | 0.36 | 0.66 | 33.14 | 2.23 | 19.42 |
| | | 4.18 | 3.07 | 0.26 | 0.07 | 1.02 | 26.12 | 3.23 | 15.55 |
| | | 5.90 | 0.81 | 0.32 | 0.00 | 1.32 | 16.54 | 4.09 | 12.90 |
| | | | | | | | | | |
| Exp 4.35 | | Exp 4.36 | | Exp 4.37 | | Exp 4.38 | | Exp 4.39 | |
| Time days | Nitrite mmol/kg | Time days | Nitrite mmol/kg | Time days | Nitrite mmol/kg | Time days | Nitrite mmol/kg | Time days | Nitrite mmol/kg |
| 0.00 | 32.86 | 0.11 | 7.22 | 0.05 | 6.50 | 0.05 | 6.40 | 0.05 | 6.12 |
| 0.04 | 30.45 | 1.21 | 5.65 | 0.10 | 5.97 | 1.07 | 5.21 | 0.10 | 5.46 |

| | | | | | | | | | |
|-----------------|------------------------|-----------------|------------------------|------|------|------|------|------|------|
| 0.10 | 28.61 | 2.23 | 4.29 | 0.21 | 5.24 | 4.01 | 1.07 | 0.21 | 4.15 |
| 0.21 | 25.40 | 3.23 | 3.28 | 0.35 | 4.43 | 4.83 | 1.10 | 0.35 | 2.96 |
| 0.35 | 21.20 | 4.09 | 2.78 | | | 3.05 | 2.16 | 0.74 | 1.40 |
| 0.69 | 13.30 | | | | | | | | |
| | | | | | | | | | |
| Exp 4.40 | | Exp 4.41 | | | | | | | |
| Time days | Nitrite mmol/ kg | Time days | Nitrite mmol/ kg | | | | | | |
| 0.04 | 18.92 | 0.04 | 14.68 | | | | | | |
| 0.08 | 14.72 | 0.08 | 7.29 | | | | | | |
| 0.12 | 12.30 | 0.12 | 3.60 | | | | | | |
| 0.15 | 10.62 | 0.15 | 2.04 | | | | | | |
| 0.23 | 6.02 | 0.23 | 0.67 | | | | | | |

Table C.4: Raw data for Table 4.5

| Exp 4.42 | | Exp 4.43 | | Exp 4.44 | | Exp 4.45 | | Exp 4.46 | |
|-----------------|-------|-----------------|-------|-----------------|-------|-----------------|-------|-----------------|-------|
| DEA mmol/kg | Yield | DEA mmol/kg | Yield | DEA mmol/kg | Yield | DEA mmol/kg | Yield | DEA mmol/kg | Yield |
| 0.0 | 2.6% | 0.0 | 0.8% | 0.0 | 0.4% | 0.0 | 0.3% | 0.0 | 0.4% |
| 26.4 | 4.4% | 27.5 | 7.1% | 16.9 | 2.2% | 17.6 | 2.3% | 27.7 | 2.1% |
| 50.3 | 10.4% | 51.0 | 9.9% | 23.5 | 2.9% | 32.1 | 2.4% | 66.5 | 4.5% |
| 60.0 | 14.4% | 105.2 | 18.5% | 46.1 | 5.3% | 59.6 | 5.2% | 75.6 | 5.2% |
| | | | | | | | | | |

| Exp 4.47 | | Exp 4.48 | | Exp 4.49 | | Exp 4.50 | | Exp 4.51 | |
|------------------|-------|------------------|-------|------------------|-------|------------------|-------|------------------|-------|
| DEA mmol/kg | Yield | DEA mmol/kg | Yield | DEA mmol/kg | Yield | HEEDA mmol/kg | Yield | HEEDA mmol/kg | Yield |
| 0.0 | 0.1% | 0.0 | 0.4% | 0.0 | 0.3% | 18.9 | 0.9% | 21.4 | 2.8% |
| 21.1 | 2.1% | 27.5 | 3.4% | 15.6 | 1.1% | 39.3 | 2.3% | 39.0 | 3.9% |
| 33.5 | 2.6% | 51.0 | 5.5% | 66.5 | 3.7% | 83.6 | 5.6% | 91.3 | 7.2% |
| 47.2 | 3.5% | 105.2 | 11.4% | 75.6 | 4.1% | 218.1 | 12.0% | 195.0 | 12.4% |
| | | | | | | | | | |
| Exp 4.52 | | Exp 4.53 | | Exp 4.54 | | Exp 4.55 | | Exp 4.56 | |
| HEEDA mmol/kg | Yield | HEEDA mmol/kg | Yield | HeGly mmol/kg | Yield | HeGly mmol/kg | Yield | HeGly mmol/kg | Yield |
| 18.9 | 0.8% | 21.4 | 0.8% | 9.8 | 1.2% | 2.7 | 0.2% | 2.7 | 0.3% |
| 39.3 | 1.5% | 39.0 | 1.4% | 23.4 | 2.0% | 5.6 | 0.5% | 5.6 | 0.6% |
| 83.6 | 3.8% | 91.3 | 4.1% | 44.8 | 4.3% | 10.8 | 1.3% | 10.8 | 0.9% |
| 218.1 | 9.4% | 195.0 | 8.5% | 52.8 | 5.4% | 26.6 | 2.0% | 26.6 | 1.9% |
| | | | | | | | | | |
| Exp 4.57 | | | | | | | | | |
| HeGly mmol/kg | Yield | | | | | | | | |
| 0.0 | 0.0% | | | | | | | | |
| 2.5 | 0.2% | | | | | | | | |
| 5.3 | 0.4% | | | | | | | | |
| 10.5 | 0.9% | | | | | | | | |

Table C.5: Raw data for Table 4.8

| Exp 4.63 | | Exp 4.64 | | Exp 4.65 | | Exp 4.66 | | Exp 4.67 | |
|-----------|-----------------|-----------|-----------------|-----------|-----------------|-----------|-----------------|-----------|-----------------|
| Time days | Nitrite mmol/kg | Time days | Nitrite mmol/kg | Time days | Nitrite mmol/kg | Time days | Nitrite mmol/kg | Time days | Nitrite mmol/kg |
| 0.000 | 0.570 | 0.000 | 0.570 | 0.000 | 0.570 | 0.000 | 0.541 | 0.000 | 0.519 |
| 0.220 | 0.571 | 0.257 | 0.540 | 0.711 | 0.571 | 0.257 | 0.476 | 0.689 | 0.418 |
| 0.711 | 0.571 | 1.031 | 0.474 | 0.220 | 0.571 | 1.031 | 0.123 | 1.005 | 0.355 |
| 0.990 | 0.550 | 1.175 | 0.330 | 0.990 | 0.550 | 1.175 | 0.097 | 4.027 | 0.113 |
| 4.106 | 0.324 | 3.074 | 0.018 | 4.106 | 0.324 | | | | |
| 5.049 | 0.263 | 4.017 | 0.004 | 5.049 | 0.263 | | | | |
| | | | | | | | | | |
| Exp 4.68 | | Exp 4.69 | | Exp 4.70 | | Exp 4.71 | | Exp 4.72 | |
| Time days | Nitrite mmol/kg | Time days | Nitrite mmol/kg | Time days | Nitrite mmol/kg | Time days | Nitrite mmol/kg | Time days | Nitrite mmol/kg |
| 0.000 | 0.588 | 0.000 | 0.637 | 0.000 | 0.637 | 0.000 | 0.646 | 0.000 | 0.646 |
| 1.131 | 0.002 | 2.752 | 0.493 | 0.041 | 0.685 | 0.188 | 0.613 | 0.281 | 0.470 |
| 0.953 | 0.003 | 0.188 | 0.627 | 0.127 | 0.635 | 0.827 | 0.482 | 0.090 | 0.637 |
| 0.106 | 0.557 | 1.238 | 0.621 | 0.168 | 0.632 | 1.238 | 0.611 | 0.192 | 0.641 |
| 0.318 | 0.228 | 2.181 | 0.617 | 0.322 | 0.291 | 2.181 | 0.584 | 0.979 | 0.030 |
| | | | | | | | | | |
| Exp 4.73 | | Exp 4.74 | | Exp 4.75 | | Exp 4.76 | | Exp 4.77 | |
| Time days | Nitrite mmol/kg | Time days | Nitrite mmol/kg | Time days | Nitrite mmol/kg | Time days | Nitrite mmol/kg | Time days | Nitrite mmol/kg |

| | | | | | | | | | |
|-----------------|-----------------|-----------------|-----------------|-----------------|-----------------|-----------------|-----------------|-----------------|-----------------|
| 0.000 | 0.716 | 0.000 | 0.716 | 0.000 | 0.626 | 0.000 | 0.522 | 0.000 | 0.522 |
| 0.699 | 0.589 | 0.210 | 0.357 | 0.827 | 0.468 | 0.041 | 0.502 | 0.689 | 0.230 |
| 1.681 | 0.460 | 0.699 | 0.120 | 0.188 | 0.223 | 0.127 | 0.426 | 0.262 | 0.446 |
| 2.955 | 0.296 | 1.681 | 0.008 | 1.238 | 0.651 | 0.168 | 0.361 | 1.002 | 0.158 |
| 3.781 | 0.207 | | | 2.752 | 0.422 | 0.322 | 0.231 | 1.540 | 0.084 |
| 3.781 | 0.198 | | | | | | | | |
| | | | | | | | | | |
| Exp 4.78 | | Exp 4.79 | | Exp 4.80 | | Exp 4.81 | | Exp 4.82 | |
| Time days | Nitrite mmol/kg | Time days | Nitrite mmol/kg | Time days | Nitrite mmol/kg | Time days | Nitrite mmol/kg | Time days | Nitrite mmol/kg |
| 0.000 | 0.522 | 0.000 | 0.641 | 0.000 | 0.641 | 0.000 | 0.595 | 0.000 | 0.595 |
| 0.041 | 0.502 | 0.188 | 0.576 | 0.153 | 0.467 | 1.110 | 0.312 | 0.257 | 0.372 |
| 0.127 | 0.426 | 0.827 | 0.343 | 0.047 | 0.621 | 0.220 | 0.562 | 1.031 | 0.045 |
| 0.168 | 0.361 | 1.238 | 0.142 | 0.260 | 0.247 | 0.990 | 0.306 | 3.074 | 0.003 |
| 0.322 | 0.231 | 2.181 | 0.030 | 0.260 | 0.284 | | | 4.017 | 0.001 |
| | | | | | | | | | |
| Exp 4.83 | | Exp 4.84 | | Exp 4.85 | | Exp 4.86 | | Exp 4.87 | |
| Time days | Nitrite mmol/kg | Time days | Nitrite mmol/kg | Time days | Nitrite mmol/kg | Time days | Nitrite mmol/kg | Time days | Nitrite mmol/kg |
| 0.000 | 0.604 | 0.000 | 0.604 | 0.000 | 0.629 | 0.000 | 0.629 | 0.000 | 0.627 |
| 0.198 | 0.560 | 0.210 | 0.479 | 0.198 | 0.574 | 0.210 | 0.512 | 0.198 | 0.605 |
| 1.014 | 0.355 | 0.894 | 0.090 | 1.014 | 0.440 | 0.894 | 0.279 | 1.014 | 0.503 |
| 2.179 | 0.155 | 1.104 | 0.039 | 2.179 | 0.274 | 1.104 | 0.219 | 2.179 | 0.338 |

| | | | | | | | | | |
|-----------------|-----------------|-------|-------|-------|-------|-------|-------|-------|-------|
| 3.219 | 0.082 | 2.067 | 0.002 | 3.219 | 0.176 | 1.178 | 0.180 | 3.219 | 0.168 |
| 4.059 | 0.035 | | | 4.059 | 0.000 | 2.067 | 0.001 | 4.059 | 0.105 |
| | | | | | | | | | |
| Exp 4.88 | | | | | | | | | |
| Time days | Nitrite mmol/kg | | | | | | | | |
| 0.000 | 0.627 | | | | | | | | |
| 0.210 | 0.557 | | | | | | | | |
| 0.894 | 0.142 | | | | | | | | |
| 1.104 | 0.104 | | | | | | | | |

Table C.6: Raw data for Table 5.1

| Exp 5.1 | | Exp 5.2 | | Exp 5.2 (cont.) | | Exp 5.3 | | Exp 5.4 | |
|----------------|--------------|----------------|--------------|------------------------|--------------|----------------|--------------|----------------|--------------|
| Time days | MNPZ mmol/kg | Time days | MNPZ mmol/kg | Time days | MNPZ mmol/kg | Time days | MNPZ mmol/kg | Time days | MNPZ mmol/kg |
| 0.89 | 39.82 | 0.13 | 41.52 | 1.28 | 28.04 | 0.06 | 47.80 | 0.15 | 24.97 |
| 2.06 | 37.21 | 0.13 | 41.02 | 2.00 | 22.64 | 0.14 | 44.32 | 0.19 | 23.83 |
| 8.27 | 24.72 | 0.19 | 38.28 | 2.00 | 23.67 | 0.21 | 36.48 | 0.28 | 19.99 |
| 16.96 | 14.78 | 0.19 | 39.49 | 2.15 | 19.77 | 0.27 | 37.05 | 0.72 | 5.49 |
| 23.79 | 9.68 | 0.26 | 40.12 | 2.15 | 22.40 | 0.85 | 21.59 | 1.00 | 2.83 |
| | | 0.26 | 40.80 | 2.30 | 20.16 | 1.11 | 16.86 | 1.27 | 1.80 |
| | | 0.31 | 39.24 | 2.71 | 19.51 | 1.75 | 9.61 | 1.64 | 0.50 |

| | | | | | | | | | |
|-----------------|--------------|-----------------|--------------|-----------------|--------------|-----------------|--------------|-----------------|--------------|
| | | 0.31 | 40.99 | 3.00 | 18.27 | 2.07 | 7.20 | 2.19 | 0.28 |
| | | 1.00 | 31.97 | 3.73 | 14.28 | 2.21 | 5.76 | | |
| | | 1.00 | 32.24 | 4.00 | 11.81 | 2.91 | 2.88 | | |
| | | 1.11 | 29.91 | 8.25 | 2.89 | | | | |
| | | 1.11 | 29.68 | | | | | | |
| | | | | | | | | | |
| Exp 5.5 | | Exp 5.6 | | Exp 5.7 | | Exp 5.8 | | Exp 5.9 | |
| Time days | MNPZ mmol/kg | Time days | MNPZ mmol/kg | Time days | MNPZ mmol/kg | Time days | MNPZ mmol/kg | Time days | MNPZ mmol/kg |
| 0.13 | 24.12 | 0.03 | 52.98 | 0.04 | 51.74 | 0.05 | 40.39 | 0.00 | 27.25 |
| 0.22 | 14.55 | 0.16 | 35.06 | 0.26 | 31.48 | 0.12 | 34.62 | 0.33 | 14.87 |
| 0.66 | 1.16 | 0.25 | 30.26 | 0.69 | 7.21 | 0.20 | 25.04 | 0.69 | 7.45 |
| 1.00 | 0.21 | 0.33 | 31.75 | 0.97 | 2.42 | 0.28 | 25.60 | 1.01 | 3.90 |
| | | 0.57 | 14.69 | 1.67 | 0.23 | 0.35 | 19.52 | 1.70 | 1.11 |
| | | 0.65 | 12.54 | 1.86 | 0.18 | 0.68 | 14.89 | | |
| | | 0.76 | 10.25 | | | 1.03 | 6.27 | | |
| | | 0.84 | 5.63 | | | | | | |
| | | 1.02 | 2.67 | | | | | | |
| | | | | | | | | | |
| Exp 5.10 | | Exp 5.11 | | Exp 5.12 | | Exp 5.13 | | Exp 5.14 | |
| Time days | MNPZ mmol/kg | Time days | MNPZ mmol/kg | Time days | MNPZ mmol/kg | Time days | MNPZ mmol/kg | Time days | MNPZ mmol/kg |
| 0.00 | 16.48 | 0.00 | 8.91 | 0.00 | 4.83 | 0.00 | 1.95 | 0.14 | 10.59 |

| | | | | | | | | | |
|-----------------|--------------|-----------------|--------------|-----------------|--------------|-----------------|--------------|-----------------|--------------|
| 0.33 | 10.62 | 0.69 | 4.70 | 0.29 | 4.09 | 2.61 | 0.64 | 0.28 | 7.46 |
| 0.69 | 6.63 | 1.29 | 2.73 | 0.71 | 3.01 | 1.29 | 1.03 | 0.72 | 3.31 |
| 1.01 | 4.28 | 1.98 | 1.41 | 1.00 | 2.46 | 1.98 | 0.81 | 1.16 | 1.44 |
| 1.70 | 1.70 | 3.95 | 0.23 | 1.14 | 2.48 | 3.95 | 0.43 | 1.80 | 0.33 |
| | | | | 1.92 | 1.62 | | | | |
| | | | | 2.76 | 1.01 | | | | |
| | | | | 3.77 | 0.60 | | | | |
| | | | | | | | | | |
| Exp 5.15 | | Exp 5.16 | | Exp 5.17 | | Exp 5.18 | | Exp 5.19 | |
| Time days | MNPZ mmol/kg | Time days | MNPZ mmol/kg | Time days | MNPZ mmol/kg | Time days | MNPZ mmol/kg | Time days | MNPZ mmol/kg |
| 0.04 | 1.43 | 0.05 | 68.17 | 0.23 | 39.52 | 0.03 | 0.04 | 0.00 | 1.15 |
| 0.15 | 0.75 | 0.67 | 12.90 | 0.95 | 11.83 | 0.04 | 0.04 | 0.03 | 0.30 |
| 0.34 | 0.83 | 1.08 | 4.66 | 1.95 | 2.52 | 0.04 | 0.03 | 0.04 | 0.27 |
| 0.55 | 0.27 | 1.84 | 0.78 | 3.01 | 0.49 | 0.05 | 0.03 | 0.05 | 0.20 |
| 0.89 | 0.27 | | | | | | | 0.06 | 0.19 |
| | | | | | | | | 0.06 | 0.13 |
| | | | | | | | | | |
| Exp 5.20 | | Exp 5.21 | | Exp 5.22 | | Exp 5.23 | | Exp 5.24 | |
| Time days | MNPZ mmol/kg | Time days | MNPZ mmol/kg | Time days | MNPZ mmol/kg | Time days | MNPZ mmol/kg | Time days | MNPZ mmol/kg |
| 0.03 | 0.06 | 0.00 | 1.99 | 0.00 | 8.97 | 0.00 | 3.46 | 0.00 | 1.52 |
| 0.04 | 0.04 | 0.15 | 1.89 | 1.81 | 4.39 | 0.96 | 2.66 | 1.17 | 1.25 |

| | | | | | | | | | |
|-----------------|--------------|-----------------|--------------|-----------------|--------------|-----------------|--------------|-----------------|--------------|
| 0.04 | 0.02 | 0.33 | 1.82 | 2.06 | 4.04 | 1.97 | 1.94 | 2.10 | 1.06 |
| 0.05 | 0.01 | 0.78 | 1.78 | 5.74 | 1.18 | 2.98 | 1.51 | 4.94 | 0.75 |
| | | 1.02 | 1.76 | 7.93 | 0.38 | 4.05 | 1.16 | 4.94 | 0.70 |
| | | 1.20 | 1.74 | | | 5.97 | 0.03 | | |
| | | | | | | | | | |
| Exp 5.25 | | Exp 5.26 | | Exp 5.27 | | Exp 5.28 | | Exp 5.29 | |
| Time days | MNPZ mmol/kg | Time days | MNPZ mmol/kg | Time days | MNPZ mmol/kg | Time days | MNPZ mmol/kg | Time days | MNPZ mmol/kg |
| 0.00 | 1.92 | 0.00 | 3.46 | 0.00 | 1.52 | 0.00 | 3.68 | 0.00 | 0.78 |
| 2.09 | 1.83 | 0.99 | 3.25 | 2.09 | 1.49 | 0.98 | 2.67 | 0.07 | 0.40 |
| 5.98 | 1.52 | 5.94 | 2.75 | 5.98 | 1.39 | 1.93 | 2.09 | 0.20 | 0.17 |
| 7.99 | 1.39 | 7.95 | 2.50 | | | 3.11 | 1.43 | 0.25 | 0.10 |
| 11.95 | 1.18 | 15.90 | 2.16 | | | 4.01 | 0.97 | 0.33 | 0.04 |
| | | | | | | | | | |
| Exp 5.30 | | Exp 5.31 | | Exp 5.32 | | Exp 5.33 | | Exp 5.34 | |
| Time days | MNPZ mmol/kg | Time days | MNPZ mmol/kg | Time days | MNPZ mmol/kg | Time days | MNPZ mmol/kg | Time days | MNPZ mmol/kg |
| 0.00 | 7.79 | 0.00 | 3.12 | 0.00 | 17.48 | 0.00 | 5.44 | 0.07 | 0.41 |
| 2.00 | 5.30 | 0.24 | 2.78 | 0.94 | 13.82 | 1.11 | 4.88 | 0.00 | 0.49 |
| 6.99 | 3.20 | 0.70 | 2.16 | 2.96 | 8.97 | 4.14 | 3.48 | 0.21 | 0.36 |
| 9.13 | 2.91 | 0.94 | 1.93 | 4.85 | 5.34 | 7.05 | 2.68 | 0.06 | 0.43 |
| 10.08 | 2.51 | | | 7.23 | 3.07 | | | | |
| | | | | | | | | | |

Table C.7: Raw data for Table 6.1

| Exp 6.1 | | Exp 6.2 | | Exp 6.3 | | Exp 6.4 | | Exp 6.5 | |
|----------|-----------------|----------|-----------------|----------|-----------------|----------|-----------------|----------|-----------------|
| Time min | Sulfite mmol/kg | Time min | Sulfite mmol/kg | Time min | Sulfite mmol/kg | Time min | Sulfite mmol/kg | Time min | Sulfite mmol/kg |
| 16.6 | 36.7 | 17.8 | 31.8 | 8.6 | 39.2 | 0.0 | 33.8 | 0.0 | 39.6 |
| 21.6 | 34.6 | 22.3 | 21.7 | 14.3 | 25.4 | 2.3 | 25.4 | 5.0 | 39.1 |
| 26.6 | 33.9 | 27.3 | 16.0 | 19.4 | 11.9 | 4.6 | 19.2 | 10.0 | 37.4 |
| 31.6 | 32.5 | 32.4 | 10.3 | 24.4 | 5.6 | 6.9 | 13.0 | 15.0 | 37.1 |
| 36.7 | 31.7 | 37.5 | 6.4 | 29.8 | 2.4 | 9.2 | 7.0 | 20.0 | 36.4 |
| | | 42.5 | 4.2 | 34.8 | 0.9 | 11.2 | 4.6 | 25.0 | 35.8 |
| | | | | 39.7 | 0.0 | | | 29.7 | 35.4 |
| | | | | | | | | 34.6 | 35.3 |
| | | | | | | | | | |
| Exp 6.6 | | Exp 6.7 | | Exp 6.8 | | Exp 6.9 | | Exp 6.10 | |
| Time min | Sulfite mmol/kg | Time min | Sulfite mmol/kg | Time min | Sulfite mmol/kg | Time min | Sulfite mmol/kg | Time min | Sulfite mmol/kg |
| 0.0 | 7.9 | 0.0 | 70.6 | 5.0 | 127.9 | 0.0 | 45.0 | 0.0 | 37.2 |
| 5.1 | 7.1 | 5.0 | 64.4 | 10.0 | 123.7 | 10.0 | 43.1 | 2.0 | 36.1 |
| 10.2 | 6.9 | 10.3 | 61.7 | 15.0 | 122.0 | 20.0 | 41.7 | 4.0 | 32.7 |
| 15.2 | 6.7 | 15.3 | 58.8 | 20.6 | 117.5 | 30.0 | 40.4 | 6.0 | 32.1 |
| 20.2 | 6.7 | 20.2 | 57.1 | 25.6 | 113.1 | 40.0 | 38.9 | 8.0 | 31.0 |
| 25.6 | 6.5 | 25.2 | 55.5 | 31.3 | 109.7 | 50.0 | 37.3 | 10.0 | 30.7 |
| 76.4 | 5.3 | 30.4 | 53.4 | 36.7 | 105.9 | 60.0 | 36.0 | 12.0 | 29.9 |

| | | | | | | | | | |
|-----------------|--------------------|-----------------|--------------------|-----------------|--------------------|-----------------|--------------------|-----------------|--------------------|
| 126.4 | 4.4 | 35.4 | 51.7 | | | | | | |
| | | 40.4 | 50.1 | | | | | | |
| | | | | | | | | | |
| Exp 6.11 | | Exp 6.12 | | Exp 6.13 | | Exp 6.14 | | Exp 6.15 | |
| Time min | Sulfite mmol/kg | Time min | Sulfite mmol/kg | Time min | Sulfite mmol/kg | Time min | Sulfite mmol/kg | Time min | Sulfite mmol/kg |
| 0.0 | 45.2 | 0.0 | 7.4 | 36.5 | 30.2 | 0.0 | 41.6 | 0.0 | 48.2 |
| 5.0 | 40.4 | 5.8 | 6.7 | 41.7 | 26.2 | 5.0 | 40.7 | 10.0 | 46.6 |
| 10.0 | 38.1 | 10.8 | 6.3 | 46.8 | 23.2 | 10.0 | 37.8 | 20.0 | 43.5 |
| 15.0 | 35.4 | 16.3 | 5.9 | 51.8 | 21.8 | 15.0 | 35.7 | 30.2 | 41.2 |
| 20.0 | 34.8 | 21.3 | 5.5 | 56.8 | 18.7 | 20.0 | 33.6 | 40.2 | 39.0 |
| 25.0 | 32.9 | 26.3 | 5.1 | 61.8 | 17.2 | 25.0 | 31.9 | 50.2 | 36.9 |
| 30.0 | 30.9 | 31.3 | 4.7 | | | 30.1 | 30.1 | 60.2 | 34.6 |
| | | 36.7 | 4.1 | | | | | | |
| | | 42.7 | 3.9 | | | | | | |
| | | 47.7 | 3.8 | | | | | | |
| | | | | | | | | | |
| Exp 6.16 | | | | | | | | | |
| Time min | Sulfite mmol/kg | | | | | | | | |
| 0.0 | 49.1 | | | | | | | | |
| 10.0 | 46.2 | | | | | | | | |
| 20.0 | 44.4 | | | | | | | | |

| | | | | | | | | | |
|------|------|--|--|--|--|--|--|--|--|
| 30.0 | 42.1 | | | | | | | | |
| 40.0 | 41.0 | | | | | | | | |
| 50.5 | 39.9 | | | | | | | | |
| 60.5 | 38.3 | | | | | | | | |

Appendix D: Raw Input for AERSCREEN Results

D.1 AERSCREEN INPUTS FOR PILOT PLANT AT THE TECHNOLOGY CENTER IN MONGSTAD

AERSCREEN 11126 / AERMOD 09292

05/06/14

16:43:25

TITLE: TCM 1 WS 100 M

***** STACK PARAMETERS

| | | |
|-------------------------|---------------|-----------------|
| SOURCE EMISSION RATE: | 0.360E-03 g/s | 0.286E-02 lb/hr |
| STACK HEIGHT: | 100.00 meters | 328.08 feet |
| STACK INNER DIAMETER: | 1.420 meters | 55.91 inches |
| PLUME EXIT TEMPERATURE: | 313.0 K | 103.7 Deg F |
| PLUME EXIT VELOCITY: | 98.769 m/s | 324.04 ft/s |
| STACK AIR FLOW RATE: | 164368 ACFM | |
| RURAL OR URBAN: | RURAL | |

INITIAL PROBE DISTANCE = 10000. meters 32808. feet

***** BUILDING DOWNWASH PARAMETERS

NO BUILDING DOWNWASH HAS BEEN REQUESTED FOR THIS ANALYSIS

***** PROBE ANALYSIS

25 meter receptor spacing: 100. meters - 5000. meters
50 meter receptor spacing: 5050. meters - 10000.
meters

| Zo | ROUGHNESS | 1-HR CONC | DIST | TEMPORAL |
|--------|-----------|------------|--------|----------|
| SECTOR | LENGTH | (ug/m3) | (m) | PERIOD |
| 1* | 1.300 | 0.3494E-03 | 1300.0 | WIN |

* = worst case flow sector

***** MAKEMET METEOROLOGY PARAMETERS *****

MIN/MAX TEMPERATURE: 273.0 / 303.0 (K)

MINIMUM WIND SPEED: 2.0 m/s

ANEMOMETER HEIGHT: 10.000
meters

SURFACE CHARACTERISTICS INPUT: AERMET SEASONAL TABLES

DOMINANT SURFACE PROFILE: Coniferous Forest
DOMINANT CLIMATE TYPE: Average Moisture
DOMINANT SEASON: Winter

ALBEDO: 0.35
BOWEN RATIO: 1.50
ROUGHNESS LENGTH: 1.300
(meters)

METEOROLOGY CONDITIONS USED TO PREDICT OVERALL MAXIMUM
IMPACT

YR MO DY JDY HR

10 01 24 24 01

H0 U* W* DT/DZ ZICNV ZIMCH M-O LEN ZO BOWEN ALBEDO REF WS

-2.58 0.487 -9.000 0.020 -999.782.4180.4 1.300 1.50 0.35 2.50

HT REF TA HT

10.0 303.0 2.0

ESTIMATED FINAL PLUME HEIGHT (non-downwash): 173.5 meters

METEOROLOGY CONDITIONS USED TO PREDICT AMBIENT BOUNDARY
IMPACT

YR MO DY JDY HR

10 02 08 24 12

H0 U* W* DT/DZ ZICNV ZIMCH M-O LEN ZO BOWEN ALBEDO REF WS

269.77 0.497 1.800 0.020 725.806. -38.2 1.300 0.80 0.12 2.00

HT REF TA HT

10.0 273.0 2.0

ESTIMATED FINAL PLUME HEIGHT (non-downwash): 261.4 meters

D.2 AERSCREEN INPUTS FOR FULL-SCALE 500 MWE PLANT

AERSCREEN 11126 / AERMOD 09292

05/12/14

14:23:44

TITLE: TCM 1 WS 100 M

***** STACK PARAMETERS *****

SOURCE EMISSION RATE: 0.0180 g/s 0.143 lb/hr
STACK HEIGHT: 100.00 meters 328.08 feet
STACK INNER DIAMETER: 10.000 meters 393.70 inches
PLUME EXIT TEMPERATURE: 313.0 K 103.7 Deg F
PLUME EXIT VELOCITY: 98.000 m/s 321.52 ft/s
STACK AIR FLOW RATE: 16308872 ACFM
RURAL OR URBAN: RURAL

INITIAL PROBE DISTANCE = 10000. meters 32808. feet

***** BUILDING DOWNWASH PARAMETERS *****

NO BUILDING DOWNWASH HAS BEEN REQUESTED FOR THIS ANALYSIS

***** PROBE ANALYSIS *****

25 meter receptor spacing: 100. meters - 5000. meters
50 meter receptor spacing: 5050. meters - 10000. meters

| Zo | ROUGHNESS | 1-HR CONC | DIST | TEMPORAL |
|--------|-----------|-----------|------|----------|
| SECTOR | LENGTH | (ug/m3) | (m) | PERIOD |

| | | | | |
|----|-------|------------|--------|-----|
| 1* | 1.300 | 0.5113E-02 | 1125.0 | WIN |
|----|-------|------------|--------|-----|

* = worst case flow sector

 ***** MAKEMET METEOROLOGY PARAMETERS

MIN/MAX TEMPERATURE: 273.0 / 303.0 (K)

MINIMUM WIND SPEED: 2.0 m/s

ANEMOMETER HEIGHT: 10.000
meters

SURFACE CHARACTERISTICS INPUT: AERMET SEASONAL TABLES

DOMINANT SURFACE PROFILE: Coniferous Forest

DOMINANT CLIMATE TYPE: Average Moisture

DOMINANT SEASON: Winter

ALBEDO: 0.35

BOWEN RATIO: 1.50

ROUGHNESS LENGTH: 1.300
(meters)

METEOROLOGY CONDITIONS USED TO PREDICT OVERALL MAXIMUM IMPACT

YR MO DY JDY HR

10 02 23 23 01

H0 U* W* DT/DZ ZICNV ZIMCH M-O LEN ZO BOWEN ALBEDO REF WS

-10.36 1.960 -9.000 0.020 -999. 4000. 8888.0 1.300 1.50 0.35 10.00

HT REF TA HT

10.0 303.0 2.0

ESTIMATED FINAL PLUME HEIGHT (non-downwash): 300.0 meters

METEOROLOGY CONDITIONS USED TO PREDICT AMBIENT BOUNDARY IMPACT

YR MO DY JDY HR

10 02 27 23 12

H0 U* W* DT/DZ ZICNV ZIMCH M-O LEN ZO BOWEN ALBEDO REF WS

208.89 0.479 1.800 0.020 1039.763. -49.0 1.300 0.70 0.12 2.00

HT REF TA HT

10.0 303.0 2.0

ESTIMATED FINAL PLUME HEIGHT (non-downwash): 883.1 meters

***** AERSCREEN AUTOMATED DISTANCES

OVERALL MAXIMUM CONCENTRATIONS BY DISTANCE

Appendix E: Procedure for Handling Toxic Gas Cylinders

Updated: 14 Jan 2014

The following steps must be taken to minimize the inherent risk of accidental release of toxic gas while replacing a cylinder:

1. Two people are required to change a toxic gas cylinder – one will physically remove the regulator and install it on the full cylinder, while the other will stand by the door to the utility corridor in case something goes wrong.
2. First, check that the gas regulator is not plugged and the gauge is functioning correctly by turning on the mass flow controller connected to the toxic gas. Watch the display and ensure the number (percent open) increases when the knob is turned.
3. Leaving the mass flow controller on, shut off the toxic gas at the tank by closing the valve on top of the tank. Watch the pressure reading on the gauge drop to zero. If the gauge does not drop to zero, abort the procedure – the valve on the tank may have a leak. Check the mass flow controller to ensure the flow has also dropped to zero.
4. Disconnect the depressurized line from the tank gauge while keeping the vented cabinet door closed.
5. Flush the disconnected lines that contain toxic gas with either nitrogen or air. The easiest way to do this is to attach the exit line to the compressed air in the fume hood and reverse the flow back to the vented cabinet. Flushing should last for two minutes at 0.5 SLPM.

6. Disconnect the regulator from the empty bottle. Remove the empty bottle from the ventilated gas cabinet and put the full bottle in its place. Uncap the full bottle and connect the regulator. Tighten the regulator with a wrench as much as possible.
7. Connect the tank end of the line to the full tank and disconnect the vent end of the line from the compressed air.
8. Turn the mass flow controller to off and open the regulator valve while keeping the vented cabinet door closed. Observe the pressure increase on the tank gauge.
9. Listen for any hissing coming from the tank and check for a leak around the regulator using soap bubbles.
10. Turn on the mass flow controller and observe the flow change.
11. Close the valve on top of the tank and watch as the gauge depressurizes and the mass flow controller returns to zero.

The following steps must be taken to minimize the inherent risk of accidental release of toxic gas while starting up and running an experiment:

1. All toxic gas lines should be appropriate materials for their respective toxic gas. Only Teflon and stainless steel lines may be used for NO₂ and NO.
2. Turn off the toxic gas valve and make sure all lines from the toxic gases are depressurized.
3. Disconnect the gas lines from the toxic gas tanks and flush all depressurized lines into the vented cabinet.
4. Reconnect the gas line to the closed toxic gas tank, and connect the exit gas line to the compressed air located inside the fume hood.
5. Connect all gas lines for your experimental set up and turn on the compressed air.

6. Check for leaks at all connections using the soap bubble test.
7. After all leaks are sealed, turn off the compressed air and wait for thirty minutes.
8. Open the compressed air line and check that it did not depressurize in the thirty minutes.
9. If the line is leaking, repeat steps 5-8 until the line maintains pressure over the thirty minutes.
10. Disconnect the compressed air line and keep the exit line safely inside the fume hood.
11. Open the toxic gas valve and check that it is flowing properly through the mass flow controller and into the fume hood.
12. Experiments with toxic gases should not be run overnight. Before leaving each night, turn off the toxic gas valve and depressurize the gas lines.

| Gas Type/ Conc. (ppm) | OSHA LEL/ SEL (mg/m³) | Odor | Hazard | NFPA (Health/Fire/RX/O x) |
|--------------------------------------|---|---------------------------------|---|--|
| NO₂ (5000) | 5/9 | Sharp, biting | Mutagen, reproductive | 3/0/0/Oxidizing |
| NO (5000) | 45/30 | Odorless | Mutagen | 3/0/0/Oxidizing |
| NH₃ (1000) | 27/18 | Sharp (cleaning products) | Tumorigen, mutagen | 3/1/0 |
| SO₂ (1000) | 5/13 | Pungent, penetrating | Tumorigen, mutagen, reproductive effector, primary irritant | 3/0/0 |

Bibliography

- Allen, David T., and Cyril J. Durrenberger. 2014. "Gaussian Plume Modeling." http://www.utexas.edu/research/ceer/che357/PDF/Lectures/gaussian_plume_modeling.pdf
- Ashouripashaki, Mandana. 2012. "Formation and Decomposition of 1-Nitrosopiperazine in the CO₂ Capture Process." University of Texas at Austin. Master Thesis.
- Atkins, P W, and J de Paula. 2006. "The Response of Equilibria to Temperature." In *Physical Chemistry*, 8th ed. New York: Oxford University Press.
- Bade, Otto Morten, Jacob Nygaard Knudsen, Oddvar Gorset, and Inga Askestad. 2013. "Controlling Amine Mist Formation in CO₂ Capture from Residual Catalytic Cracker (RCC) Flue Gas" *Energy Procedia* 63: 791–802. doi:10.1016/j.egypro.2014.11.091.
- Bishnoi, Sanjay. 2000. "Carbon Dioxide Absorption and Solution Equilibrium in Piperazine Activated Methyldiethanolamine." University of Texas at Austin. PhD Dissertation.
- Blauwhoff, Peter M, and Martinus Bos. 1981. "Dissociation Constants of Diethanolamine and Diisopropanolamine in an Aqueous 1.00 M Potassium Chloride Solution." *Journal of Chemical Engineering Data* 26 (1): 7–8. doi:10.1021/jc00023a004.
- Buchholz, Jerry R., and Richard E. Powell. 1963. "The Decomposition of Hyponitrous Acid. I. The Non-Chain Reaction." *Journal of the American Chemical Society* 1 (5): 509–11.
- Cachaza, J M, Julia Casado, Enrique A Castro, and Santiago De Compostela. 1978. "Kinetic Studies on the Formation of Nitrosamines I Formation of Dimethylnitrosamine in Aqueous Solution of Perchloric Acid." *Zeitschrift für Krebsforschung Und Klinische Onkologie* 91: 279–90.
- Casado, Julia, Manuel Mosquera, Carlos Paz, Flor Rodriguez-Prieto, and Jose Vázquez-Tat. 1984. "Nitrite Ion as a Nitrosating Reagent. Nitrosation of Morpholine and Diethylamine in the Presence of Formaldehyde." *Journal of the Chemical Society. Perkin Transactions II*, no. 12: 1963–66. <http://pubs.rsc.org/en/content/articlelanding/1984/p2/p29840001963>.

- Castro, Enrique A, Andrea Hormazabal, and Jose G Santos. 1997. "Concerted Mechanism of 4-Cyanobenzoate with Secondary Alicyclic Amines in Aqueous Ethanol." *International Journal of Chemical Kinetics* 30 (4): 267–72.
- Challis, Brian C., and Soterios A. Kyrtopoulos. 1976. "Nitrosation under Alkaline Conditions." *Journal of the Chemical Society, Chemical Communications* 21: 877. doi:10.1039/c39760000877.
- Challis, Brian C., and Soterios A. Kyrtopoulos. 1979. "The Chemistry of Nitroso-Compounds. Part 11. Nitrosation of Amines by the Two-Phase Interaction of Amines in Solution with Gaseous Oxides of Nitrogen." *Journal of the Chemical Society, Perkin* 203: 299–304. <http://pubs.rsc.org/en/content/articlepdf/1979/p1/p19790000299>.
- Challis, Brian C., and JR Outram. 1979. "The Chemistry of Nitroso-Compounds. Part 15. Formation of N-Nitrosamines in Solution from Gaseous Nitric Oxide in the Presence of Iodine." *Journal of the Chemical Society, Perkin* 2768–75. <http://pubs.rsc.org/en/content/articlelanding/1979/p110.1039/p19790002768>.
- Chandan, Payal A, Emily Harrison, Sarah Honchul, Jiren Li, Jesse Thompson, and Kunlei Liu. 2014. "Destroying Nitrosamines in Post-Combustion CO₂ Capture." *Energy Procedia* 63 : 808–13. doi:10.1016/j.egypro.2014.11.091.
- Chandan, Payal A, Joseph E Remias, and Kunlei Liu. 2014. "International Journal of Greenhouse Gas Control Possible Ways to Minimize Nitrosation Reactions during Post-Combustion CO₂ Capture Process." *International Journal of Greenhouse Gas Control* 31. 61–66. doi:10.1016/j.ijggc.2014.09.028.
- Chandan, Payal A, Joseph E Remias, James K Neathery, and Kunlei Liu. 2013. "Morpholine Nitrosation To Better Understand Potential Solvent Based CO₂ Capture Process Reactions." *Environmental Science & Technology* 47 (10): 5481–87. doi:10.1021/es4003108.
- Closmann, Frederick Bynum. 2011. "Oxidation and Thermal Degradation of Methyl-diethanolamine / Piperazine in CO₂ Capture." The University of Texas at Austin. PhD Dissertation.
- Cousins, Ashleigh, Paul T. Nielsen, Sanger Huang, Rob Rowland, Bill Edwards, Aaron Cottrell, Eric Chen, Gary T. Rochelle, and Paul H.M. Feron. 2015. "Pilot-Scale Evaluation of Concentrated Piperazine for CO₂ Capture at an Australian Coal-Fired Power Station: Nitrosamine Measurements." *International Journal of Greenhouse Gas Control* 37. 256–63. doi:10.1016/j.ijggc.2015.03.007.

- Da Silva, Eirik Falck, Andreas Grimstvedt, Solrun Johanne Vevelstad, Aslak Einbu, Kai Vernstad, Hallvard F Svendsen, and Kolbjørn Zahlsen. 2012. "Understanding 2-Ethanolamine Degradation in Postcombustion CO₂ Capture." *Industrial & Engineering Chemistry Research* 51: 13329–38.
- Da Silva, Eirik Falck, Herman Kolderup, Earl Goetheer, Kai W Hjarbo, Arjen Huizinga, Purvil Khakharia, Ilse Tuinman, et al. 2013. "Emission Studies from a CO₂ Capture Pilot Plant." *Energy Procedia* 37: 778–83. doi:10.1016/j.egypro.2013.05.167.
- Dai, Ning, and William A Mitch. 2013. "Influence of Amine Structural Characteristics on N-Nitrosamine Formation Potential Relevant to Postcombustion CO₂ Capture Systems." *Environmental Science and Technology*. doi:10.1021/es4035396.
- Dai, Ning, and William A Mitch. 2013. 2014b. "Effects of Flue Gas Compositions on Nitrosamine and Nitramine Formation in Postcombustion CO₂ Capture Systems." *Environmental Science and Technology* 48: 7519–26. doi:10.1021/es501864a.
- Dai, Ning, Amisha D Shah, Lanhua Hu, Michael J Plewa, Bruce Mckague, and William A Mitch. 2012. "Measurement of Nitrosamine and Nitramine Formation from NO_x Reactions with Amines during Amine-Based Carbon Dioxide Capture for Postcombustion Carbon Sequestration." *Environmental Science and Technology* 46: 9793–9801.
- Danckwerts, PV. 1950. "Absorption by Simultaneous Diffusion and Chemical Reaction." *Transactions of the Faraday Society*.
<http://pubs.rsc.org/en/content/articlepdf/1950/tf/tf9504600300>.
- Davis, Jason. 2009. "Thermal Degradation of Aqueous Amines Used for Carbon Dioxide Capture." University of Texas at Austin. PhD Dissertation.
- Douglass, ML, and BL Kabacoff. 1978. "The Chemistry of Nitrosamine Formation, Inhibition and Destruction." *J. Soc. Cosmet. Chem.* 606 (September): 581–606.
<http://journal.sconline.org/abstracts/cc1978/cc029n09/p00581-p00606.html>.
- Drescher, G S, and C W Frank. 1978. "Estimation of Extractable N-Nitroso Compounds at the Parts- per- Billion Level." *Analytical Chemistry* 50 (14): 2118–21.
- Dugas, Ross. 2009. "Carbon Dioxide Absorption, Desorption, and Diffusion in Aqueous Piperazine and Monoethanolamine." University of Texas at Austin. PhD Dissertation.

- Einbu, Aslak, Eirik Falck da Silva, Geir Haugen, Andreas Grimstvedt, Kristin Giske Lauritsen, Kolbjørn Zahlén, and Terje Vassbotn. 2013. “A New Test Rig for Studies of Degradation of CO₂ Absorption Solvents at Process Conditions ; Comparison of Test Rig Results and Pilot Plant Data for Degradation of MEA.” *Energy Procedia* 37: 717–26.
- Energy Information Administration. Emissions of Greenhouse Gases in the United States 2009 http://www.eia.gov/environment/emissions/ghg_report/pdf/tbl6.pdf.
- Environmental Protection Agency. 2012. “Standards of Performance for Greenhouse Gas Emissions for New Stationary Sources: Electric Utility Generating Units.” *Federal Register* 77 (72): 22392–441.
- Fan, T Y, and S R Tannenbaum. 1972. “Stability of N-Nitroso Compounds.” *Journal of Food Science* 37 (2): 274–76.
- Fernandes, Debra, William Conway, Robert Burns, Geoffrey Lawrance, Marcel Maeder, and Graeme Puxty. 2012. “Investigations of Primary and Secondary Amine Carbamate Stability by 1H NMR Spectroscopy for Post Combustion Capture of Carbon Dioxide.” *The Journal of Chemical Thermodynamics* 54 (November). Elsevier Ltd: 183–91. doi:10.1016/j.jct.2012.03.030.
- Fine, Nathan A, Mark J Goldman, and Gary T Rochelle. 2014. “Nitrosamine Formation in Amine Scrubbing at Desorber Temperature.” *Environmental Science & Technology* 48 (15): 8777–83. doi:10.1021/es501484w.
- Fine, Nathan A, Paul T Nielsen, and Gary T Rochelle. 2014. “Decomposition of Nitrosamines in CO₂ Capture by Aqueous Piperazine or Monoethanolamine.” *Environmental Science & Technology* 48 (10): 5996–6002. doi:10.1021/es404949v.
- Fine, Nathan A, and Gary T Rochelle. 2013. “Thermal Decomposition of N-Nitrosopiperazine.” *Energy Procedia* 37: 1678–86.
- Fine, Nathan A, and Gary T Rochelle. 2014. “Absorption of Nitrogen Oxides in Aqueous Amines.” *Energy Procedia* 63: 830–47.
- Frailie, Peter. 2014. “Modeling of Carbon Dioxide Absorption / Stripping by Aqueous Methyldiethanolamine / Piperazine.” The University of Texas at Austin. PhD Dissertation.
- Freeman, Stephanie. 2011. “Thermal Degradation and Oxidation of Aqueous Piperazine for Carbon Dioxide Capture.” The University of Texas at Austin. PhD Dissertation.

- Freeman, Stephanie, Ross Dugas, David H. Van Wagener, Thu Nguyen, and Gary T Rochelle. 2010. "Carbon Dioxide Capture with Concentrated, Aqueous Piperazine." *International Journal of Greenhouse Gas Control* 4 (2): 119–24. doi:10.1016/j.ijggc.2009.10.008.
- Garcia, Humberto, Larry Keefer, and William Lijinsky. 1970. "Carcinogenicity of Nitrosothiomorpholine and 1-Nitrosopiperazine in Rats." *Z. Krebsforsch* 74: 179–84.
- Goldberg, Robert N, Nand Kishore, and Rebecca M Lennen. 2002. "Thermodynamic Quantities for the Ionization Reactions of Buffers." *Journal of Physical Chemistry Reference Data* 31 (2): 231–370.
- Goldman, Mark J, Nathan A Fine, and Gary T Rochelle. 2013. "Kinetics of N-Nitrosopiperazine Formation from Nitrite and Piperazine in CO₂ Capture." *Environmental Science and Technology* 47 (7): 3528–34.
- Gorset, Oddvar, Jacob Nygaard Knudsen, Otto Morten Bade, and Inga Askestad. 2014. "Results from Testing of Aker Solutions Advanced Amine Solvents at CO₂ Technology Centre Mongstad." *Energy Procedia* 63: 6267–80. doi:10.1016/j.egypro.2014.11.658.
- Grzybowski, A K, and S P Datta. 1958. "The Second Acid Dissociations of Glycine, Sarcosine and N-Dimethylglycine." *Transactions of the Faraday Society*, 1188–94.
- Hamborg, Espen S, and Geert F Versteeg. 2009. "Dissociation Constants and Thermodynamic Properties of Amines and Alkanolamines from (293 to 353) K." *Journal of Chemical Engineering Data* 54.
- Hassim, Mimi H., Markku Hurme, David W. Edwards, Nik Aziz, and Fariha L.M. Rahim. 2013. "Simple Graphical Method for Inherent Occupational Health Assessment." *Process Safety and Environmental Protection* 91 (6): 438–51. doi:10.1016/j.psep.2012.09.003.
- Hilliard, Marcus Douglas. 2008. "A Predictive Thermodynamic Model for an Aqueous Blend of Potassium Carbonate, Piperazine, and Monoethanolamine for Carbon Dioxide." University of Texas at Austin. PhD Dissertation.
- Honikel, Karl Otto. 2008. "The Use and Control of Nitrate and Nitrite for the Processing of Meat Products." *Meat Science* 78: 68–76. doi:10.1016/j.meatsci.2007.05.030.

- Huie, Robert E., and P Neta. 1984. "Chemical Behavior of Sulfur Trioxide (1^-)(SO_3^-) and Sulfur Pentoxide (1^-)(SO_5^-) Radicals in Aqueous Solutions." *The Journal of Physical Chemistry* 88 (23): 5665–69.
- Hummer, Gerhard, Lawrence R. Pratt, and Angel E. Garcia. 1995. "Hydration Free Energy of Water." *The Journal of Physical Chemistry* 99 (38): 14188–94. doi:10.1021/j100038a062.
- Hurley, Peter J., William L. Physick, and Ashok K. Luhar. 2005. "TAPM: A Practical Approach to Prognostic Meteorological and Air Pollution Modelling." *Environmental Modelling and Software* 20 (6): 737–52. doi:10.1016/j.envsoft.2004.04.006.
- Inami, Keiko, Satoko Ishikawa, and Masataka Mochizuki. 2009. "Activation Mechanism of N -Nitrosodialkylamines as Environmental Mutagens and Its Application to." *Genes and Environment* 31 (4): 97–104.
- Jackson, Phil, and M. Attalla. 2010. "N-Nitrosopiperazines Form at High pH in Post-combustion Capture Solutions Containing Piperazine: A Low-energy Collisional Behaviour Study." *Rapid Communications in Mass* 24: 3567–77. doi:10.1002/rcm.
- Jackson, Phil, and M. Attalla. 2011. "Environmental Impacts of Post-Combustion capture—New Insights." *Energy Procedia* 4: 2277–84. doi:10.1016/j.egypro.2011.02.117.
- Jenks, William P. 1972. "General Acid-Base Catalysis of Complex Reactions in Water." *Chemical Reviews* 72 (6): 705–18.
- Kameoka, Yohji, and Robert L Pigford. 1977. "Absorption of Nitrogen Dioxide into Water, Sulfuric Acid, Sodium Hydroxide, and Alkaline Sodium Sulfite Aqueous Solutions." *Industrial Engineering Chemistry Fundamentals* 16 (1): 163–69.
- Khakharia, Purvil, Hanne M. Kvamsdal, Eirik Falck da Silva, Thijs J H Vlugt, and Earl Goetheer. 2014. "Field Study of a Brownian Demister Unit to Reduce Aerosol Based Emission from a Post Combustion CO₂ Capture Plant." *International Journal of Greenhouse Gas Control* 28: 57–64. doi:10.1016/j.ijggc.2014.06.022.
- Kim, Inna, Christian M. Jens, Andreas Grimstvedt, and Hallvard F Svendsen. 2011. "Thermodynamics of Protonation of Amines in Aqueous Solutions at Elevated Temperatures." *The Journal of Chemical Thermodynamics* 43 (11). 1754–62. doi:10.1016/j.jct.2011.06.004.

- Kirsch, M, H G Korth, R Sustmann, and H de Groot. 2000. "Carbon Dioxide but Not Bicarbonate Inhibits N-Nitrosation of Secondary Amines. Evidence for Amine Carbamates as Protecting Entities." *Chemical Research in Toxicology* 13 (6): 451–61. <http://www.ncbi.nlm.nih.gov/pubmed/10858318>.
- Knudsen, Jacob Nygaard, Otto Morten Bade, Inga Askestad, and Oddvar Gorset. 2014. "Pilot Plant Demonstration of CO₂ Capture from Cement Plant with Advanced Amine Technology." *Energy Procedia* 63: 6464–75. doi:10.1016/j.egypro.2014.11.682.
- Koeijer, Geleijn De, and V. R. Talstad. 2013. "Health Risk Analysis for Emissions to Air from CO₂ Technology Centre Mongstad." *International Journal of Greenhouse Gas Control* 18: 200–207. <http://www.sciencedirect.com/science/article/pii/S1750583613002788>.
- Koller, Guntram, Ulrich Fischer, and Konrad Hungerbühler. 2000. "Assessing Safety, Health, and Environmental Impact Early during Process Development." *Industrial & Engineering Chemistry Research*, 960–72. <http://pubs.acs.org/doi/abs/10.1021/ie990669i>.
- Kulshrestha, Pankaj, Katherine C McKinstry, Bernadette O Fernandez, Martin Feelisch, and William a Mitch. 2010. "Application of an Optimized Total N-Nitrosamine (TONO) Assay to Pools: Placing N-Nitrosodimethylamine (NDMA) Determinations into Perspective." *Environmental Science & Technology* 44 (9): 3369–75. doi:10.1021/es100361f.
- Låg, M., B. Lindeman, C. Instanes, G. Brunborg, and P. Schwarze. 2011. *Health Effects of Amines and Derivatives Associated with CO₂ Capture. The Norwegian Institute of Public Health*. http://www.fhi.no/eway/default.aspx?pid=239&trg=Content_6510&Main_6157=6263:0:25,6287&MainContent_6263=6510:0:25,6293&Content_6510=6259:89915:25,6293:0:6250:1:::0:0.
- Lambert, Joseph B, Gerhard Binsch, and John D. Roberts. 1964. "Nitrogen-15 Magnetic Resonance Spectroscopy, I. Chemical Shifts." *Proceedings of the National Academy of Sciences USA* 51 (5): 735–37.
- Lashof, Daniel A., and Dilip R. Ahuja. 1990. "Relative Contributions of Greenhouse Gas Emissions to Global Warming." *Letters to Nature* 344: 529–521.
- Lee, Yung J, and Lewis B. Benson. 1990. "Sulfur Dioxide Removal from Flue Gases with Sulfite Oxidation Inhibition." United States: United States Patent Office.

- Liu, Hanbi, Omkar A. Namjoshi, and Gary T. Rochelle. 2014. "Oxidative Degradation of Amine Solvents for CO₂ Capture." *Energy Procedia* 63: 1546–57. doi:10.1016/j.egypro.2014.11.164.
- Lv, Chun Lin, Yong Dong Liu, and Ru-Gang Zhong. 2009. "Theoretical Investigation of N-Nitrosodimethylamine Formation from Dimethylamine Nitrosation Catalyzed by Carbonyl Compounds." *The Journal of Physical Chemistry. A* 113 (4): 713–18. doi:10.1021/jp8061674.
- Lv, Chun Lin, Yong Dong Liu, Ru-Gang Zhong, and Yunhai Wang. 2007. "Theoretical Studies on the Formation of N-Nitrosodimethylamine." *Journal of Molecular Structure* 802 (1-3): 1–6. doi:10.1016/j.theochem.2006.08.045.
- McCann, Nichola, Duong Phan, Xiaoguang Wang, William Conway, Robert Burns, M. Attalla, Graeme Puxty, and Marcel Maeder. 2009. "Kinetics and Mechanism of Carbamate Formation from CO₂(aq), Carbonate Species, and Monoethanolamine in Aqueous Solution." *The Journal of Physical Chemistry. A* 113 (17): 5022–29. doi:10.1021/jp810564z.
- Miguel, Ferran De, Alexander K Voice, and Henk Trap. 2013. "Nitrosamine Degradation by UV Light in Post-Combustion CO₂ Capture : Effect of Solvent Matrix." *Energy Procedia* 37: 701–16.
- Mimura, Tomio, Shigeru Shimojo, and Shigeaki Mitsuoka. 1997. "Process for Removing Carbon Dioxide and Nitrogen Oxides from Combustion Gases." United States: United States Patent Office.
- Mirvish, S S. 1975. "Blocking the Formation of N-Nitroso Compounds with Ascorbic Acid in Vitro and in Vivo." *Annals of the New York Academy of Sciences*. <http://www.ncbi.nlm.nih.gov/pubmed/1106296>.
- Mitch, William A. 2011. "Critical Literature Review of Nitrosation/Nitration Pathways." *Gassnova*. http://www.gassnova.no/frontend/files/CONTENT/Rapporter/NitrosamineandNitramineformationchemistry_YALE.pdf.
- Moser, Peter, Sandra Schmidt, Knut Stahl, Gerald Vorberg, Gustavo A Lozano, Torsten Stoffregen, and Frank Rösler. 2013. "Demonstrating Emission Reduction – Results from the Post-Combustion Capture Pilot Plant at Niederaussem" *Energy Procedia* 37: 2377–88.

- Nash, T. 1979. "The Effect of Nitrogen Dioxide and of Some Transition Metals on the Oxidation of Dilute Bisulphite Solutions." *Atmospheric Environment* 13 (8): 1149–54.
- Neta, P, Robert E. Huie, and Alberta B. Ross. 1988. "Rate Constants for Reactions of Inorganic Radicals in Aqueous Solution." *Journal of Physical and Chemical Reference Data* 17 (3): 1027. doi:10.1063/1.555808.
- NETL. 2010. "Cost and Performance Baseline for Fossil Energy Plants Volume 1 : Bituminous Coal and Natural Gas to Electricity" DOE/2010/1397
- Nguyen, Thu. 2013. "Amine Volatility in CO₂ Capture Committee." The University of Texas at Austin. PhD Dissertation.
- Nielsen, Claus J, and Dirk Hoffmann. 2010. "Theoretical Evaluation of the Fate of Harmful Compounds Post Emission," no. September 2010: 1–69.
- Nielsen, Paul T., Le Li, and Gary T Rochelle. 2013. "Piperazine Degradation in Pilot Plants." *Energy Procedia* 37: 1912–23.
- Namjoshi, Omkar A. 2015. "Thermal Degradation of PZ-Promoted Tertiary Amines for CO₂ Capture." University of Texas, Austin. PhD Dissertation.
- Oblath, S.B., S.S. Markowitz, T. Novakov, and S.G. Chang. 1981. "Kinetics of the Formation of Hydroxylamine Disulfonate by Reaction of Nitrite with Sulfites." *Journal of Physical Chemistry* 85: 1017–21.
- Pacheco, Manuel A. 1998. "Mass Transfer, Kinetics and Rate-Based Modeling of Reactive Absorption." Univeristy of Texas Austin. PhD Dissertation.
- Pai, S. R., A. J.; Shirke, and S. V. Gothoskar. 1981. "Long-Term Feeding Study in C17 Mice Administered Saccharin Coated Betel Nut and 1,4-Dinitrosopiperazine in Combination." *Carcinogenesis* 2 (3): 175–77.
- Patwardhan, Janaki A., and Jyeshtharaj B. Joshi. 2003. "Unified Model for NO_x Absorption in Aqueous Alkaline and Dilute Acidic Solutions." *AIChE Journal* 49 (11): 2728–48. doi:10.1002/aic.690491106.
- Plaza, Jorge M. 2011. "Modeling of Carbon Dioxide Absorption Using Aqueous Monoethanolamine , Piperazine and Promoted Potassium Carbonate." University of Texas at Austin. PhD Dissertation.

- Pradhan, M.P., and Jyeshtharaj B. Joshi. 2000. "Absorption of NO_x Gases in Plate Column: Selective Manufacture of Sodium Nitrite." *Chemical Engineering Science* 55 (7): 1269–82. doi:10.1016/S0009-2509(99)00397-8.
- Price, Ilene, and Brian Smith. 2008. *Carbon Capture and Storage, Meeting the Challenge of Climate Change*. IEA Greenhouse Gas R&D Programme: Cheltenham, U.K.
- Rao, Anand B, and Edward S Rubin. 2002. "A Technical , Economic , and Environmental Assessment of Amine-Based CO₂ Capture Technology for Power Plant Greenhouse Gas Control," no. 412: 4467–75.
- Ridd, J. H. 1961. "Nitrosation, Diazotisation, and Deamination." *Quarterly Reviews, Chemical Society* 15 (418-441). doi:10.1039/QR9611500418.
- Rochelle, Gary T, Sanjay Bishnoi, Susan Chi, Hongyi Dang, and Jesse Santos. 2001. *Research Needs for CO₂ Capture from Flue Gas by Aqueous Absorption/Stripping*. Austin, Texas. US DOE Report No. DE-AF26-99FT01029
- Rochelle, Gary T, Eric Chen, Stephanie Freeman, David H. Van Wagener, Qing Xu, and Alexander K Voice. 2011. "Aqueous Piperazine as the New Standard for CO₂ Capture Technology." *Chemical Engineering Journal* 171 (3) : 725–33. doi:10.1016/j.cej.2011.02.011.
- Sapkota, Virbin Nath A, Nathan A Fine, and Gary T Rochelle. 2015. "NO₂ Catalyzed Sulfite Oxidation." *Industrial & Engineering Chemistry Research*. doi:10.1021/ie504767w.
- Sartori, Guido, and David W. Savage. 1983. "Sterically Hindered Amines for Carbon Dioxide Removal from Gases." *Industrial & Engineering Chemistry Fundamentals* 22 (2): 239–49. doi:10.1021/i100010a016.
- Schwetlick, Klaus, Rainer Noack, and Fanziska Stebner. 1994. "Three Fundamental Mechanisms of Base-Catalysed Reactions of Isocyanates with Hydrogen-Acidic Components." *J. Chem. Soc. Perkin Trans. 2*, 599–609.
- Sexton, Andrew James. 2008. "Amine Oxidation in CO₂ Capture Processes." University of Texas at Austin. PhD Dissertation.
- Sexton, Andrew James, Kevin S Fisher, Anne I Ryan, Paul T. Nielsen, Gary T Rochelle, Eric Chen, Katherine Dombrowski, Jean Youngerman, William A Steen, and Douglas Orr. 2014. "Evaluation of Reclaimer Sludge Disposal from Post-Combustion CO₂ Capture." IEA Environmental Projects LTD.

- Shen, Chen H. 1997. "Nitrogen Dioxide Absorption in Aqueous Sodium Sulfite." The University of Texas Austin. PhD Dissertation.
- Shen, Chen H., and Gary T Rochelle. 1998. "Nitrogen Dioxide Absorption and Sulfite Oxidation in Aqueous Sulfite." *Environmental Science & Technology* 32 (2): 1994–2003.
- Sørensen, Lisbet, Eirik Falck da Silva, Odd Gunnar Brakstad, Kolbjørn Zahlén, and Andy Booth. 2013. "Preliminary Studies into the Environmental Fate of Nitrosamine and Nitramine Compounds in Aquatic Systems." *Energy Procedia* 37: 683–90.
- Sørensen, Lisbet, Kolbjørn Zahlén, Astrid Hyldbakk, Eirik Falck Da Silva, and Andy M. Booth. 2015. "Photodegradation in Natural Waters of Nitrosamines and Nitramines Derived from CO₂ Capture Plant Operation." *International Journal of Greenhouse Gas Control* 32. Elsevier Ltd: 106–14. doi:10.1016/j.ijggc.2014.11.004.
- Sorenson, E.C, J.L Price, B.R McRae, and E.M Woolley. 2003. "Thermodynamics of Proton Dissociations from Aqueous L-Proline: Apparent Molar Volumes and Apparent Molar Heat Capacities of the Protonated Cationic, Zwitterionic, and Deprotonated Anionic Forms at Temperatures from 278.15K to 393.15K and at the Pressure 0." *The Journal of Chemical Thermodynamics* 35 (3): 529–53. doi:10.1016/S0021-9614(02)00375-0.
- Strazisar, Brian R, Richard R Anderson, and Curt M White. 2003. "Degradation Pathways for Monoethanolamine in a CO₂ Capture Facility." *Energy & Fuels* 17: 1034–39.
- Sugiyama, Hirokazu, and Ulrich Fischer. 2008. "Decision Framework for Chemical Process Design Including Different Stages of Environmental, Health, and Safety Assessment." *AIChE* 54 (4): 1037–53. doi:10.1002/aic.
- Sun, Zhi, Yong Dong Liu, and Ru-Gang Zhong. 2011. "Carbon Dioxide in the Nitrosation of Amine: Catalyst or Inhibitor?" *The Journal of Physical Chemistry. A* 115 (26): 7753–64. doi:10.1021/jp202002m.
- Susianto, Mathieu Pétrissans, Anélie Pétrissans, and André Zoulalian. 2005. "Experimental Study and Modelling of Mass Transfer during Simultaneous Absorption of SO₂ and NO₂ with Chemical Reaction." *Chemical Engineering and Processing: Process Intensification* 44 (2): 1075–81. doi:10.1016/j.cep.2005.03.001.

- Takeuchi, Hiroshi., Makoto. Ando, and Nobuo. Kizawa. 1977. "Absorption of Nitrogen Oxides in Aqueous Sodium Sulfite and Bisulfite Solutions." *Industrial & Engineering Chemistry* 16 (3): 303–8. doi:10.1021/i260063a010.
- Tsurko, E.N., and Yu.S. Kuchtenko. 2014. "Thermodynamics of the Dissociation Processes of Beta-Alanine in Ethanol–water Mixtures at Temperatures from 293.15K to 318.15K." *Journal of Molecular Liquids* 189 (January) : 95–99. doi:10.1016/j.molliq.2013.03.023.
- Ulrich, Richard Kevin, Gary T Rochelle, and Roberto E. Prada. 1986. "Enhanced Oxygen Absorption Into Bisulfite Solutions Containing Transition Metal Ion Catalysts." *Chemical Engineering Science* 41 (8): 2183–91.
- Voice, Alexander K. 2013. "Amine Oxidation in Carbon Dioxide Capture by Aqueous Scrubbing." University of Texas, Austin. PhD Dissertation
- Voice, Alexander K, Frederick Bynum Cloosmann, and Gary T Rochelle. 2013. "Oxidative Degradation of Amines with High-Temperature Cycling." *Energy Procedia* 37: 2118–32.
- Williams, Lyn H. 1994. "Quantitative Aspects of Nitrosamine Denitrosation." In *Nitrosamines and Related N-Nitroso Compounds*, 66–73.

Vita

Nathan Andrew Fine was born in Lawrence, Kansas on January 5, 1989. He graduated from Pattonville High School in 2007 and attended Washington University in Saint Louis where he earned a B.S. in Chemical Engineering with a Minor in Spanish. During his undergraduate career, he researched platinum nanocluster catalysis with Dr. Cynthia Lo. After graduating in 2011, he began research under the supervision of Dr. Gary T. Rochelle at the University of Texas at Austin. Nathan has accepted a position with New Sky Energy in Boulder, Colorado.

Permanent email: nafine1@gmail.com

This dissertation was typed by the author.